UNIVERSITY OF QUEBEC AT CHICOUTIMI

DISSERTATION PRESENTED TO THE
UNIVERSITY OF QUEBEC AT CHICOUTIMI

IN PARTIAL FULFILMENT OF THE REQUIREMENT FOR THE
DEGREE OF DOCTOR OF PHILOSOPHY IN ENGINEERING

BY
OMID LASHKARI

THE RHEOLOGICAL BEHAVIOR OF
SEMI-SOLID A356 ALLOY

JULY 2006

UNIVERSITÉ DU QUÉBEC Á CHICOUTIMI

THÉSE PRÉSENTÉE Á
L'UNIVERSITÉ DU QUÉBEC Á CHICOUTIMI

COMME EXIGENCE PARTIELLE
DU DOCTORAT EN INGÉNIERIE

PAR
OMID LASHKARI

LE COMPORTEMENT RHÉOLOGIQUE
DE L'ALLIAGE A356 SEMI-SOLIDE

JUILLET 2006

Dedicated to

Mama for her emotional and spiritual supports

ABSTRACT

The semi-solid-metal, SSM, processing deals with semi solid slurries, in which non dendritic solid particles are dispersed in a liquid matrix with apparent viscosity values near to that of liquid. It is able to flow easily under pressure and fills complicated die cavities to manufacture sound as-cast products with high integrity. The SSM slurry is prepared through different methods. In the current study conventional casting and the SEED process were employed to produce SSM billets with different morphologies of primary α-Al phase in A356 Al-Si alloy. For conventional casting, a range of solid particle morphologies, microstructure, were realized through variation of pouring temperature while for the SEED billets, as a new patent of ALCAN international for semi solid casting, changes in the morphology were achieved by control of process parameters during solidification of the melt.

In order to investigate the morphological evolution due to the effect of different process parameters, pouring temperature and swirling intensities, the SSM billets prepared by both methods were studied using quantitative metallography. The microstructure of SSM A356 alloy has also been characterized using an innovative method, parallel plate compression viscometry, where a correlation was made between the morphology and viscosity. The main objective of the current research was the implication of rheological principles to study the deformation behavior of A356 alloy at different morphologies and fraction of solid, while treating the SSM billets as Newtonian and Non-Newtonian fluids respectively. Furthermore, two empirical relationships were proposed to underline the correlation among the viscosity, and fraction solid and its morphology. In order to further confirm the reliability of the tests results in this research and to highlight that the sample size has no effect on the final deformation and viscosity values, a new series of tests were performed using two sets of specimens with aspect ratio (height/diameter) of 0.4 and 1.8.

It was found that conventional billets cast at low pouring temperature of 615°C comprise fine and equiaxed grains while the billets cast at high pouring temperature of 695°C have dendritic structure. For SEED billets, swirling refined the primary α-Al dendrites and promoted the formation of rosette and/or globular α-Al particles with increasing swirling speed. The effectiveness of swirling speed may be due to reduction in segregation of alloying elements at the solidification front and better heat transfer between the mold and bulk of liquid to establish a shallow temperature gradient resulting in refining and formation of equiaxed as-cast structure. There was no evidence of entrapped eutectic within the primary α-Al particles as one of the advantages of SEED slurry-on-demand technology.

The reduction of pouring temperature down to liquidus point, 615°C, improved the flow characteristics of the billets. The calculated viscosity for the billets with globular primary α-Al particles are almost three orders of magnitude smaller than that for the fully dendritic structure. The difference reduces to one order of the magnitude in the case of rosette morphology compared to that of globular. Application of swirling during solidification has an obvious effect on the deformability and viscosity of the SEED prepared SSM billets. For the billets cast at 695°C, the results show superior deformation and lower viscosity at high swirling intensity due to the globular structure of the billet. Decreasing the swirling intensity brings some degree of resistance against deformation due to presence of rosette or dendritic morphology. For the

billets cast at 645°C, once the swirling is applied the engineering strain increases. In the case of 630°C, swirling is important to induce uniform temperature distribution across the bulk liquid where the resulting globular structure renders better deformability. The magnitude of applied pressure is also an important parameter in differentiating between the structures. The refinement of the grains has been identified as the main factor for better deformability of the billets. Modification also plays an important role on alloy deformability through reduction of the residual liquid surface tension which reduces the apparent viscosity of the billets.

Two empirical equations were presented for rheological behavior of the SSM billets using viscosity as the principal parameter;

$$\log \eta = 5.56 - 1.39 f_s - (1.56 f_s + 0.14) \log \overset{o}{\gamma}$$

$$\log \eta = -1.85 + 4.9 \overline{AR} - (0.255 \overline{AR} + 0.03) \log \overset{o}{\gamma}$$

The empirical relationships express the direct effect of fraction solid and morphology on the viscosity of semi solid billets. The validity of these equations was further confirmed with plotting log viscosity against shear rate for different fractions solid and morphology and a good agreement was found between the predicted values and the previously reported results in the literature.

The irrelevance of sample size effect on the viscosity of SSM billets was also confirmed, where the same engineering strain and viscosity values were obtained for both large scale billets and small size disks. The current thesis reported that using large scale samples, the axial movement of the billets could be neglected against the radial flow during the steady state deformation stage, where the magnitude of viscosity values, are within the same range for both the sets of samples; ($\frac{h}{d} > 1$) and ($h \langle\langle d$) respectively.

RÉSUMÉ

Le traitement du métal semi-solide, MSS, fait référence a des gelées semi-solides contenant des particules non dendritiques qui sont dispersées dans une matrice liquide, le tout ayant une viscosité apparente voisine de celle du liquide. Cette masse peut s'écouler facilement sous pression et remplir les cavités complexes d'un moule pour fabriquer des produits de qualité et de haute-intégrité. La gelée de MSS peut être préparée par différentes méthodes. Dans la présente étude la coulée conventionnelle et la procédure SEED ont été utilisées pour produire des billettes de MSS avec différentes morphologies de la phase primaire α-Al dans l'alliage Al-Si A356. Pour la coulée conventionnelle, une gamme de morphologies de particules solides et de microstructures, ont été obtenues en variant température d'alimentation. Pour les billettes SEED, nouveau brevet d'ALCAN international pour la coulée semi-solide, les changements de morphologies ont été réalisés en contrôlant les paramètres du procédé pendant la solidification de la masse.

Afin d'étudier l'évolution morphologique due à l'effet des différents paramètres du procédé, la température d'alimentation et les intensités de brassage, les billettes MSS préparées par les deux méthodes ont été étudiées en utilisant la métallographie quantitative. La microstructure de l'alliage de MSS A356 a été également caractérisée en utilisant une méthode innovatrice, soit la viscométrie par la compression entre plaques parallèles, ce qui a permis d'obtenir une corrélation entre la morphologie et la viscosité. L'objectif principal de la présente recherche était de tirer partie de principes rhéologiques pour étudier le comportement à la déformation de l'alliage A356 pour différentes morphologies et fractions solides, en traitent des billettes de MSS comme des fluides newtoniens et non newtoniens, respectivement. En outre, deux relations empiriques ont été proposées pour mettre en évidence le lien entre la viscosité, la fraction solide et la morphologie. Afin de confirmer d'avantage la fiabilité des résultats des tests et de montrer que la dimension de l'échantillon n'a aucun effet sur les valeurs finales de la déformation et de la viscosité, une nouvelle série d'essais a été réalisée en utilisant deux types de spécimens ayant un rapport d'aspect (hauteur/diamètre) de 0.4 et de 1.8.

On a constaté que la coulée conventionnelle des billettes à basse température d'alimentation (soit 615°C), donne des grains très fins et equiaxes tandis que les billettes façonnées à haute température d'alimentation (695°C) ont une structure dendritique. Pour les billettes SEED, on a noté que le brassage a raffiné les dendrites primaires et a favorisé la formation de particules α-Al en rosettes et/ou globulaires. L'efficacité de l'augmentation du brassage peut être due à la réduction de la ségrégation des éléments d'alliage au front de solidification et à un meilleur transfert thermique entre le moule et le liquide conduisant ainsi à un faible gradient de température pour résultat d'un meilleur raffinage et la formation d'une structure equiaxe. On n'a noté aucune évidence d'eutectique emprisonnée dans les particules primaires d'α - Al, un des avantages la technologie SEED.

Les résultats ont montré qu'une diminution de la température d'alimentation jusqu'au liquidus (615°C) améliore les caractéristiques d'écoulement des billettes. Les valeurs de viscosité calculées pour les billettes comportant des particules primaires globulaires de α-Al sont presque trois ordres de grandeur inférieures a celles obtenues pour les billettes possédant une structure entièrement dendritique. La différence des valeurs est réduite à un ordre de

grandeur dans le cas d'une morphologie de rosette comparé à celui d'une morphologie globulaire. L'application d'un brassage pendant la solidification a un effet évident sur la déformabilité et la viscosité des billettes de MSS préparées par la méthode SEED. Pour les billettes produites à 695°C, les résultats montrent une déformation supérieure et une valeur de viscosité à la laisse lorsque l'intensité de brassage s'accent, ceci étant du à la structure globulaire de la billette. Une diminution de l'intensité de brassage amène un certain degré de résistance à la déformation due à la morphologie rosette ou dendritique. Pour les billettes coulées à 645°C, la mise en œuvre du brassage augmente la déformation. Dans le cas d'une coulée à 630°C, le brassage est important pour induire une distribution uniforme de la température à travers le liquide ce qui conduit à une structure globulaire et une meilleure déformabilité. L'intensité de la pression appliquée est également un paramètre important pour différencier les structures. L'affinage des grains a été identifié comme facteur principal pour une meilleure déformabilité des billettes. La modification joue également un rôle important sur la déformabilité des alliages en réduisant de la tension superficielle du liquide résiduel, ce qui réduit la viscosité apparente des billettes.

Deux équations empiriques ont été présentées pour le comportement rhéologique des billettes de MSS en utilisant la viscosité comme paramètre principal;

$$\log \eta = 5.56 - 1.39 f_s - (1.56 f_s + 0.14) \log \overset{o}{\gamma}$$

$$\log \eta = -1.85 + 4.9 \overline{AR} - (0.255 \overline{AR} + 0.03) \log \overset{o}{\gamma}$$

Les relations empiriques expriment l'effet direct de la fraction solide et de la morphologie sur la viscosité des billettes semi solides. La validité de ces équations a été confirmée en portant en graphique le logarithme de la viscosité en fonction du taux de cisaillement pour différentes fractions solides et morphologies. Une bonne concordance a été trouvée entre les valeurs prédites et les résultats précédemment rapportés dans la littérature.

L'effet négligeable de la dimension de l'échantillon sur la viscosité des billettes de MSS a été également confirmée, où les mêmes valeurs déformation et de viscosité ayant été obtenues pour des billettes de grande échelle et des disques de petite taille. Les résultats montrent qu'en utilisant des échantillons à grande échelle, le mouvement axial des billettes pourrait être négligée par rapport a l'écoulement radial pendant l'étape de déformation a l'état d'équilibre, où la grandeur de viscosité évalue, sont dans la même gamme pour les deux ensembles d'échantillons; ($\dfrac{h}{d} > 1$) et (h⟨⟨d) respectivement.

ACKNOWLEDGMENTS

I express sincerely all my especial thanks to my supervisors, Professor Reza Ghomashchi for his continual supports, technical discussions and advice, and of course the time that he took to read and edit the current thesis, Professor Andre Charette, for his kind accompany, encouragement, and advice along this work, and Professor Frank Ajersch, for his availability during the work at École poly techniques de Montréal and very helpful advices on the concept of rheology and viscosity.

I also appreciate the close collaboration of Mr. Joseph Langlais from ALCAN Arvida Research and Development Center, and the industrial support of Dr. B. Kulunk from Société des Technologies de l'Aluminium du Saguenay Inc., STAS.

I should mention all my gratitude to Mr. G. Lemire and Mr. M. Bouchard, technicians of the NSERC-ALCAN-UQAC Industrial Research Chair, for their assistance in casting operations, and all the efforts that they made to construct the in-house designed parallel plate compression test machine.

At the end I should greatly thank my friend Dr. Sh. Nafisi, for his support and constant encouragements, his close collaboration and pursuing spirit, who accompanied me for three years during this Ph.D. project.

LIST OF PUBLICATIONS

JOURNAL PAPERS

Due to the innovative nature of the current project and the fact that a comprehensive study was carried out, there are ample opportunities for numerous publications. However due to confidentiality issues with ALCAN international limited and prolonged submission time for journal publication to date three (3) journal articles proposed for publication. In addition there have been seven (7) conference (refereed) publications. The list of those is as follows:

1. O. Lashkari, R. Ghomashchi, "The Implication of Rheological principles for Characterization of Semi-Solid Aluminum Cast billets" *Accepted for publication*, Journal of Materials Science, October 2005

2. Sh. Nafisi, O. Lashkari, R. Ghomashchi, F. Ajersch, A. Charette, "Microstructure and Rheological Behavior of Grain Refined and Modified Semi-Solid A356 Al-Si Slurries", *Accepted for publication*, Acta Materialia, March 2006

3. O. Lashkari, R. Ghomashchi, "A New Machine to Characterize Microstructural Evolution of Semi Solid Metal Billets through Viscometry", *Accepted for publication*, Materials & Design, January 2006

CONFERENCE PROCEEDINGS

1. Sh. Nafisi, O. Lashkari, R. Ghomashchi, A. Charette, "Effect of different fraction solids on the fluidity of rheocast 356 Al-Si Alloy", multi phase phenomena and CFD modeling and solidification in materials processes. Edited Ben Q. Li, TMS publication, 2004 charlotte, North Carolina, 14-18 March, pp. 119-128, ISBN no. 0-87339-570-0

2. O. Lashkari, Sh. Nafisi, R. Ghomashchi, A. Charette, "Impact of superheat on microstructural evolution of 356 alloy in SEED slurry-on-demand process", Light Metal Conf. CIM, 2004, Hamilton, Ontario, pp. 315-321, ISBN no. 1-894475-53-4

3. O. Lashkari, R. Ghomashchi, F. Ajersch, "Rheological Study of 356 Al-Si Foundry alloy prepared by a new innovative SSM process", EPD Congress, Edited by M. Schlinger, TMS 2005, San Francisco, USA

4. O. Lashkari, R. Ghomashchi, A. Charette, "Application of Rheological study to characterize the microstructure of SSM Rheo-Cast Billets", Light Metal Conf., edited by J. P. Martin, CIM, 2005, Calgary, Alberta, pp. 235-243

5. S. Nafisi, O. Lashkari, R. Ghomashchi, J. Langlais, B. Kulunk, " The SEED Technology: A New Generation in Rheocasting", Light Metal Conf., edited by J. P. Martin, CIM, 2005, Calgary, Alberta, pp. 359-371

6. O. Lashkari, R. Ghomashchi, A. Charette, F. Ajersch, "Effect of fraction solid and shear rate on the viscosity of conventionally cast semi-solid A356 Al-Si alloys", Light Metal Conf., CIM 2006, Montreal, Quebec

7. Sh. Nafisi, O. Lashkari, J. Langlais, R. Ghomashchi, "The Impact of Partial Drainage on Chemical Composition of A356 Al-Si Alloy", ICAA 10, 2006, Vancouver, British Colombia

TABLE OF CONTENTS

CHAPTER 6
RESULTS AND DISCUSSION
MICROSTRUCTURAL CHARACTERIZATION – VISCOMETRY

CHAPTER 7
RESULTS AND DISCUSSION
RHEOLOGICAL STUDIES

LIST OF FIGURES

LIST OF TABLES

NOMENCLATURE

A Area (mm^2)

AR Aspect Ratio

C_o Composition (wt %)

C_s Solid composition (wt %)

C_L Liquid composition (wt %)

d Diameter(mm), Secondary dendrite arm spacing (μm)

$\bar{d}$ Average particle size (μm)

D_f Fractal dimension

D_L Liquid diffusivity (m^{2}s^{-1})

E Young's modulus (GPa)

f_L Fraction liquid

f_s Fraction solid

$f_s^{\,eff}$ Effective fraction solid

F Force (N), Shape factor

G Shear modulus (GPa)

h Height (mm), material history

k Equilibrium partition ratio

K Bulk modulus (GPa)

k_c Kinetics rate constant

L Length (mm)

M_L Liquidus line slope (wt %/°C)

m Consistency constant, mass (kg)

n Power law index

N_A Particles density (mm^{-2})

P Pressure (Pa), Perimeter (mm)

r Radius (mm)

R Growth rate (Cm^{2}s), Gas constant (J/k.mol)

RQI Rheocast quality index

S Structural parameter

S_v Surface area per unit volume (mm)

t time (s)

T Temperature (°C), Torque (N.m)

T_M Melting point of pure solvent (°C)

T_L liquidus temperature (°C)

$\overset{o}{T}$ Cooling rate (°C/s)

v Velocity (m/s)

V Volume (mm^3)

α, β Numerical values

γ Shear strain

$\overset{o}{\gamma}$ Shear rate (s^{-1})

γ_B Bulk strain

Γ Capillary constant (mK)

ΔE Activation energy (J)

ε Tensile strain

$\overset{o}{\varepsilon}$ Strain rate (s^{-1})

η Viscosity (Pa s)

v Kinematic viscosity ((Pa s)m^3/kg)

π Pi number

ρ Density (m^3/kg)

σ Tensile stress (Pa)

σ_B Bulk stress (Pa)

σ_f Friction stress (Pa)

σ_y Yield stress (Pa)

τ Shear stress (Pa)

υ Poisson's ratio

Φ Dimensionless temperature

Ω Angular speed (t^{-1})

CHAPTER 1

RATIONALE AND OBJECTIVES

CHAPTER 1
RATIONALE AND OBJECTIVES

1.1 Overview

Semi Solid Metal (SSM) processing is a relatively new technology for metal forming, different from the conventional metal forming technologies where the starting metal is either solid or liquid. The SSM processing deals with semi solid slurries, in which non dendritic solid particles are dispersed in a liquid matrix. The "slurry" contains solid volume fractions ranging from 0.1 to 0.6 with apparent viscosity near to that of liquid state viscosity at room temperature. It is able to flow easily under pressure and fills complicated die cavities to manufacture sound as-cast products with high integrity. The slurry is prepared by different means including direct or indirect mechanical stirring, chemical treatments of the melt, manipulation of pouring temperature, to mention just a few.

All methods are based on inducing shear forces into the melt to cause vigorous agitation and to induce a homogenous temperature gradient, resulting in homogenous microstructure and fine distribution of solids in liquid. Stirring can break up the primary dendrites and prevent the formation of solid skeleton structure. The implementation of, low pouring temperature can directly affect the nucleation and growth of primary crystals, α-Al for hypo-eutectic Al-Si alloys, within the melt, where nucleation controls the size of grains formed and growth determines the grain morphology and the distribution of alloying elements within the matrix. The final structure is therefore dependent on the nucleation density, growth morphology, temperature gradient, fluid flow and diffusion of solutes resulting in low viscosity mush having better mold filling capability. The shaping of a component directly from such slurry is named "Rheocasting". In contrast to rheocasting, the reheating of pre-solidified feedstock to the solidification range and maintaining it isothermally for a suitable time is the basis of another SSM processing route known as thixocasting/thixoforming. The resulting

material which is shaped easier and faster than solid material has a spherical microstructure instead of as-cast dendritic structure and can be formed with less force and lower problems in forming process such as forging, extrusion or high pressure die casting. High quality raw material and globular microstructure are the first pre-requisites of successful in Thixoforming. The feed materials for thixocasting/thixoforming are prepared by a variety of methods including rheocasting. The role of rheocasting and rheological behavior of materials in shaping final components or as feedstock for other processes are therefore critical and the main reasons for many research currently underway in different laboratories across the world.

1.2 Objectives

The current research concerns with a newly patented rheo route semi-solid metal (SSM) processing by ALCAN international; the "Swirled Enthalpy Equilibration Device", SEED. The SEED process is based on the development of thermal equilibrium within the solidified melt brought about by off center swirling of the mold, to homogenize the distribution of heat content (enthalpy) in the liquid metal. The uniform distribution of the heat within the melt removes the steep temperature gradient within bulk liquid and encourages the multi directional heat flow i.e. equiaxed growth of the primary phase instead of unidirectional, columnar growth. The swirling of the liquid is applied on the continuously solidifying melt through solid-liquid zone, mushy zone, for certain duration of time to reach the desired fraction solid. In order to fabricate a self standing semi solid billet, the remaining liquid within the slurry is drained out for a certain time and the final billet is then transferred into the shot sleeve of a high pressure die casting machine to be injected into the die. The SEED process is mainly intended for Al foundry alloys and since A356 alloy has been used widely in foundry industry, this alloy was the selected one for semi solid billets preparation.

There are several process parameters that directly affect the final billet microstructure prepared by the SEED process. These are the swirling speed or intensity of swirling, pouring temperature or superheat and SEED process time sequences like swirling time (t_s), resting time (t_r) and draining time (t_d). The manipulation of these

parameters could change the final microstructure of the semi solid billets. Finding the optimum parameters to achieve desirable microstructure with homogeneous distribution of the primary α-Al phase within the billets was the primary aspect of the current research. This part that was performed in collaboration with another Ph.D. student of the NSERC-ALCAN-UQAC industrial chair, Shahrooz Nafisi and concerns with microstructural evolution of the SEED prepared billets due to application of different process parameters. The work was carried out using image analysis to study the microstructural evolution. The main objective of the preliminary experiments was the fabrication of billets having uniformly distributed fine globular primary α–Al particles by optimizing the parameters of the SEED process. The final results of the first part are presented in the form of micrographs and image analysis graphs. The image analysis results due to different process variables correspond well to the changes of the resulting microstructures. This is a good confirmation that image analysis is a reliable method to study and characterize the features of α-Al phase.

In the second part of this program, conventional casting was employed to produce semi solid aluminum billets. In this method the effect of pouring temperature as an effective parameter to fabricate the optimum microstructure was considered. The application of pouring temperature as an effective means to develop the desired microstructure is a well known concept in the semi solid literature, as briefly reviewed in chapter 2. The liquid metal was poured into a metallic mold at different temperatures and the microstructural evolution was studied at specific fraction solid. The final results of the conventional casting also presented in terms of micrographs and image analysis data. This part was again carried out in collaboration with Mr. Sh. Nafisi, and has shown that the low pouring temperature method is the simplest and the fastest method of producing semi solid slurries.

In addition to the preliminary studies on the interrelationships between the SSM process parameters and the resulting microstructure, the main objective of the current research is to study the rheological behavior of SSM billets prepared by the SEED and Conventional casting processes.

Rheology is the science of deformation and flow of materials. One of the main parameters to characterize rheological behavior of semi-solid metal, SSM, slurries is the apparent viscosity. The viscosity is an indication of materials' capability in filling die cavity during casting operation. It is also a measure of the magnitude of force required for deformation of materials. The lower viscosity causes better movement of material through the die and allows intricate thin wall components to be cast at low injection pressure and low scrap amounts. From a commercial point of view, knowledge of viscosity is helpful in predicting die filling properties of commercial alloys. Since the viscosity of semi solid slurries is dependent on the microstructure, the objectives were to study such interrelationships and to establish possible mathematical correlations.

Rheology tests have been performed by many researchers within different branches of science, particularly in chemistry and polymer applications, and have only found use in metallurgical applications since 1970s. In fact the innovation of semi solid metals processing in early 70's has opened the ways for such experiments in the metallurgical field. Up to now, almost all researchers have shown the ability of rheological tests to characterize the mechanical properties or the viscoplastic behavior of SSM slurries. There are different rheological tests applicable for SSM slurries of different fraction solids. Rotational viscometry and capillary test are the two most widely employed techniques for measuring the viscosity and rheological behavior of low fraction solid slurries. Such tests have generally been applied for continuously cooled SSM slurries.

The most practical way to examine the rheological behavior of materials with high solid fraction, such as a self standing metal billet, is by parallel plate compression test. In this method a dead weight is simply applied on the top surface of SSM slug and its deformation behavior is investigated by analyzing strain variation with time. The resulting strain-time graph is further treated mathematically to calculate the viscosity. Since the mathematical treatment is different for Newtonian or non-Newtonian fluids, the other objective is to establish the appropriate procedure for calculation of viscosity in conjunction with parallel plate compression test method.

Furthermore since parallel plate compression test was normally applied on thixocast small samples for h<<R (an indication of long time test), within several published literatures, the objective of this study was to apply this test for large feedstocks with comparison to the conventional geometry of samples.

This method for the commercial billets, i.e. large scale samples, has been applied for the first time during the current research. Engineering strain-time graphs and calculated viscosity values should be attributed to the microstructural features which themselves are an indication of process parameters effects on the microstructural evolution.

1.3 Outlines

In conclusion, the objectives of the current research program may be summarized as;

- Conventional Casting; Microstructural evolution due to manipulation of superheat

- SEED; microstructural evolution due to different process parameters such as swirling speed, pouring temperature and process times

- Introduction of large scale compression parallel plate test machine to be fabricated in our labs

- Application of parallel plate test viscometry to establish the interrelationship between the superheat and the resulting microstructure of the conventionally cast billets

- Application of parallel plate test viscometry to establish the interrelationships between different SEED process parameters and the resulting microstructure of as-cast billets

- Confirming rheological tests as a reliable method to characterize the microstructure

- Introducing empirical equations to relate fraction solid, morphology and viscosity of as-cast SSM prepared billets

- Confirming the negligible effect of sample size by comparing the viscosity values for the large size billets and the small size discs

CHAPTER 2
LITERATURE REVIEW

SEMI SOLID METAL PROCESSING

CHAPTER 2
LITERATURE REVIEW
SEMI SOLID METAL PROCESSING

2.1 Introduction

Semi Solid Metal (SSM) processing is a relatively new technology for metal forming, different from the conventional metal forming technologies which use either solid or liquid metals as the starting materials. SSM processing deals with semi solid slurries, in which non dendritic solid particles are dispersed in a liquid matrix.

SSM processing can be divided into rheo and thixo routes; the former is based on direct shaping of slurry while solidification is taking place within two phase region, and the latter deals with reheating of feedstock materials to the solidification range and shaping the reheated material within close die, i.e. Thixocasting, or open die, i.e. Thixoforging. Some advantages and potential benefits of SSM technology are listed in Table 2-1. [1]

SSM processing is usually applied by introducing the agitation into the melts within solidification range, where the agitation changes the distribution of chemical composition, removes the constitutional supercooling effect, and promotes dendrite break down and globularization of the primary phases. Degeneration of the primary phases, eventuates some opportunities which are interested in commercial viewpoints. Low viscosity of alloy in the mushy state, capability of shape forming with lower force than forging, longer die life because of lower temperature of slurry than melt, superior mechanical properties, less shrinkage porosity and less oxide layers are some of these advantages [2-3].

Table 2-1: Some advantages of semi solid processing of metals [1]

CAPACITIES	POTENTIAL BENEFITS AND APPLICATION
Lower heat content than liquid metal	Higher speed part forming Higher speed continuous casting Lower mold erosion Ferrous part forming Forming of high melting point materials Forming of reactive materials
Solid present at time of mold filling	Less shrinkage voids Less feeding required Less macrosegregation Fine grain structure
Viscosity higher than liquid metals and controllable	Less entrapped mold gases Reduced oxides Improved machinability Less mold attack Higher speed part forming Improved surface finishing Automation and new processes
Flow stress lower than solid metals	Forming of intricate parts High speed part forming Lower cost part forming High speed forming of continuous shapes New processes
Ability to incorporate other materials	Composites
Ability to separate liquid and solid	Purification

2.1.1 Definition

SSM slurry is a mixture of solid particles in a liquid matrix, slurry, with solid volume fractions of 0.1-0.5 and apparent viscosity close to that of liquid state. The slurry flows easily under pressure and makes complicated shapes with high degree of die filling and integrity. There are different ways to prepare SSM slurries including the application of direct or indirect mechanical stirring, chemical treatments of the melt and manipulation of pouring temperature. The outcome is to introduce shear forces within the melt to cause vigorous agitation and impose uniform temperature distribution. This solidification process encourages the formation of a homogenous microstructure having fine distribution of solids in the liquid. Stirring can break the primary dendrites and prevents a solid skeleton structure formation, while low pouring temperature directly affects the nucleation and growth of primary crystals, α-Al for hypo-eutectic Al-Si alloys, within the melt, where nucleation controls the size of grains formed and growth

determines the grain morphology and the distribution of alloying elements within the matrix. The final structure is therefore dependent on the nucleation density, growth morphology, temperature gradient, fluid flow and diffusion of solutes. The structure itself controls the SSM viscosity. Shaping of a component directly from such slurry is named "Rheocasting". In addition, reheating of rheocast structures to the solidification range and maintaining it for suitable time can produce raw materials with good viscosity and high die filling properties. The material so prepared is shaped easier and faster than solid material because of the spherical primary phase particles instead of as-cast dendritic structure. It can be formed with less force and lower problems are encountered during forming processes such as forging, extrusion or high pressure die casting. The procedure explained is termed "Thixoforming" process [4]. High quality raw materials having globular microstructure are the pre-requisites for successful Thixoforming.

Therefore understanding the evolution of SSM microstructure and resulting rheological behavior are critically important and comprise the main theme of researches on SSM alloys [5].

2.1.2 Fundamentals of solidification

During dendritic solidification of castings and ingots, a number of processes take place simultaneously within the mushy region. These include crystallization, solute redistribution, ripening, interdendritic fluid flow, and solid movement. The dendritic structure is greatly affected by convection during the early stages of solidification. In the range of vigorous convection and slow cooling, grains become spheroidal [1]. Alloys with this microstructure possess rheological properties in the semisolid state which are quite different from those of dendritic alloys. They behave thixotropically, and viscosity can be varied over a wide range, depending on processing conditions. The metal structure and its rheological properties are retained after solidification and partial remelting [1]. The rheological behavior of partially solidified metallic alloys has relied on some basic behaviors of dendritic and non-dendritic solidification of alloys. It is known that in fine grained alloys, shrinkage in the early stages of solidification is compensated by simultaneous movement of liquid and solid. This is termed "mass feeding". At later stages of solidification the growing dendrites form a continuous skeleton within the

liquid-solid zone. As cooling continues, this skeleton is subjected to strain from thermal contraction. The strain can be highly localized. Within local regions of high strain, bonds between dendrites or dendrite arms are broken, the dendrites separate, and if sufficient fluid is not available to fill the space, open "hot tears" result. If fluid fills the space, segregated regions, sometimes termed "filled hot tears" are produced [1]. Depending somewhat on grain size, the continuous solid skeleton forms at fractions solid greater than a few tenths, and thereafter tensile strength increases rapidly. In an aluminum alloy, for example, strengths of the order of 100 psi were found when fraction solid reached 0.5 [1]. But the vigorous agitation of a metal alloy postpones the formation of continuous solid network to much higher fractions solid. With this agitation an alloy can behave as thixotropic slurry to fractions solid in excess of 0.5 [5]. The semisolid alloys can be formed in new ways, broadly termed "semisolid metal (SSM) forming processes". Some of these are now employed commercially to produce metal components and are also used to produce metal-matrix composites [1, 2]. Using the semi solid processing was also used for purification of the alloys from the undesirable solutes [6] but this has not been studied to great extent.

2.1.2.1 Dendritic solidification

Nearly all metal alloys of commercial importance solidify dendritically, either with a columnar or with an equiaxed dendritic structure, as illustrated in Figure 2-1 [7]. The presence of a wide solidification range, temperature gradient, solute distribution, curvature effect and higher superheat in commercial melts causes dendritic solidification. This manner of solidification is a developed cellular solidification that the secondary dendrite arms form on primary dendrites. Columnar solidification takes place in a narrow solidification range or for high conductivity materials but equiaxed solidification takes place in wide solidification range or low conductivity alloys.
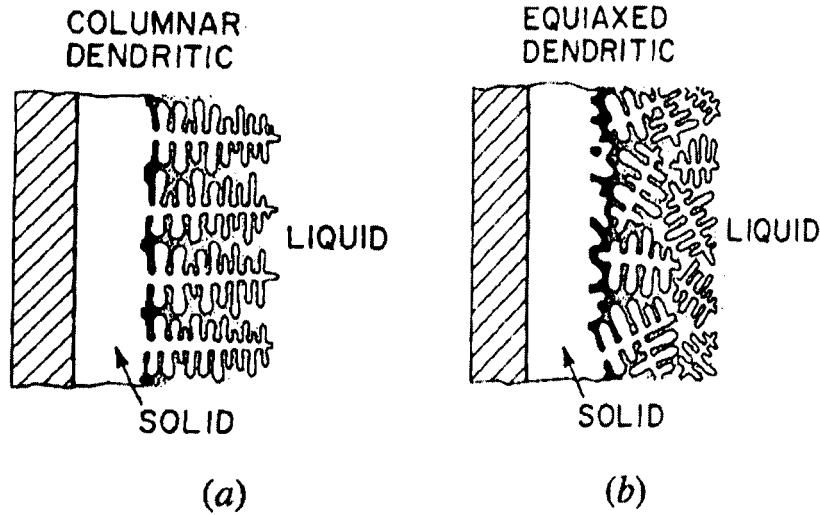
Fig. 2-1: Solidification of an alloy against a cold chill wall (a) columnar solidification and (b) equiaxed solidification [7]

The fraction solid at given location in the solid-liquid zone is given by a mass balance which in a simplest case neglects ripening and diffusion in the solid. For this case the relation between weight fraction liquid in mushy zone, f_L, and liquid composition at a given location, C_L, is given by the Scheil equation which may be written in the following form for the constant partition ratio, k:

$$f_L = (\frac{C_L}{C_o})^{-1/1-k} \qquad (2\text{-}1)$$

Where C_o is initial composition. Since temperature, T, in the solid-liquid zone and C_L are related by the equilibrium liquidus line, equation 2-1 may also be written as:

$$f_L = \Phi^{-1/1-k} \qquad (2\text{-}2)$$

Where Φ is dimensionless temperature, $(T_M\text{-}T)/(T_M\text{-}T_L)$, and T_M and T_L are the melting point of pure solvent and liquidus temperature of the alloy of composition C_o, respectively. Equation 2-2 illustrates the direct relationship of local weight fraction solid to temperature in mushy zone. It is often employed in experimental studies to calculate directly the local fraction solid from temperature measurements. The relationship is also often employed in mathematical models of solidification processes [1]. Refinements of the Scheil equation are used to calculate local fraction solid with greater precision. For example both solid diffusion and ripening occur to some extent in metal alloys during solidification, resulting in a somewhat higher fraction solid at a given temperature than

that calculated from equation 2-2. Investigation of fraction solid has been the matter which is concerned also in the thermal analysis studies [8] and several researchers have used such means to predict the fraction of solid within different compositions and temperatures [9]. Some efforts have also been made to evaluate the fraction of solid by ultrasonic method which seems not to be a reliable method [10].

After commencing the dendrite formation, the solid and liquid phases can pass over together easily and compensate the lack of liquid due to contraction of liquid during solidification which is called mass feeding stage. At the later stage, the formed dendrites grow up and connect together which causes the formation of a solid skeleton structure. Since commencing dendrites connection in the melt, resistance to deformation is started and the melt shows yield stress against deformation. This point is called dendrite coherency point, DCP [11]. Figure 2-2 shows schematically formation of dendrites in mass feeding and coherency point stages. After coherency point, dendrites continue growing up and the solid network in melt shows greater yield stress. Increasing of yield stress continues till 0.5-0.6 fractions solid which after that the melt shows the yield stress near to solid state. After connection of dendrites the moving of liquid is restricted and changes to interdendritic move. Coarsening of dendrites causes entrapment of liquid between dendrite arms and these regions would be the sensitive points to crack and hot tear initiation. Suction of liquid due to contraction or presence of strain induced regions in these parts cause shrinkage porosity or hot tear problems [1, 7]. Behavior of yield stress in a dendritic solidified alloy with increasing of solid fraction is shown in Figure 2-3. [5]

(a)   (b)
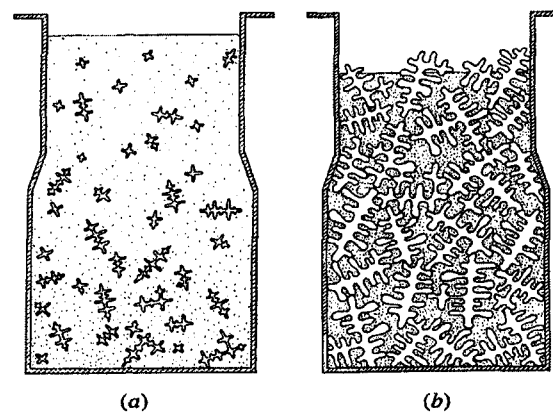
Fig. 2-2: Feeding of a mushy freezing alloy (schematic): (a) mass feeding stage and (b) interdendritic feeding stage [7]

In both equiaxed and columnar structures, the dendrites themselves evolve greatly during solidification as a result of ripening due to surface energy. The structure becomes gradually coarser during solidification as a result of the remelting of dendrite arms of smaller radius. The parameter usually chosen to measure this change is secondary dendrite arm spacing, *d*, in accordance with expected ripening kinetics, it is found that final secondary dendrite arm spacing bears an approximately cube root relation ship to the local solidification time or inversely to the cooling rate. The increase of dendrite arm spacing takes place only during the initial portion of the solidification time. In later stages of solidification, liquid-solid area can be most effectively reduced by the filling of spaces between rodlike arms to form plates; such plates are commonly observed in alloys which solidify without too high a fraction eutectic.

2.1.2.2 Non-dendritic solidification

Vigorous agitation: During the course of his doctoral thesis in early 1971, Spencer was conducting the hot tearing tests on Sn-15%Pb alloy [5]. He decided to use the same apparatus to conduct a quite different type of test. Instead of partially solidifying the alloy before beginning shear, he began the shear above the liquidus and slowly cooled the alloy into the solidification range while it was being sheared.
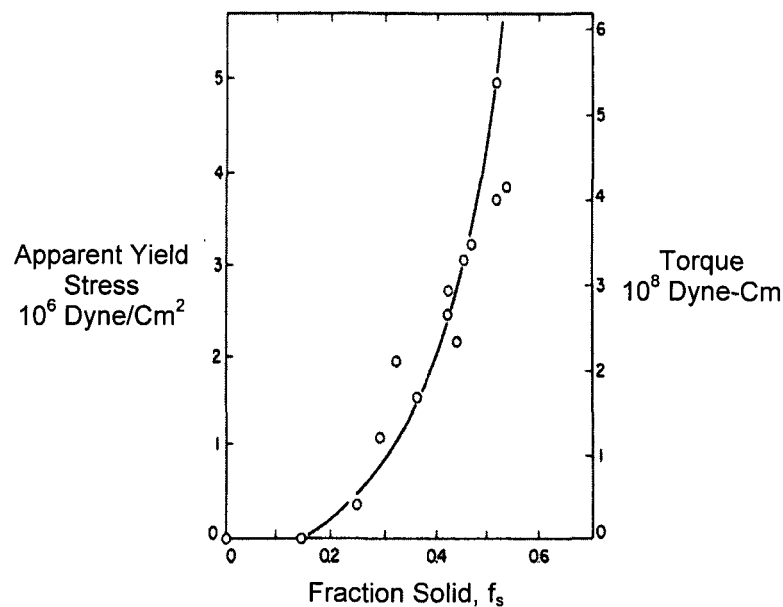
Fig. 2-3: The effect of fraction solid on the yield strength of Sn-15%Pb alloy continuously cooled without shearing [5]

The results were surprising. Shear stress increased only very slowly as temperature was decreased below the liquidus. The stress measured at a given temperature was orders of magnitude less than when the samples were cooled to the given temperature before shear. Comparison of Figures 2-3 and 2-4 shows this remarkable reduction in shear stress. For example in the dendritic material, maximum shear stress at a little over fs=0.4 is 200 kPa. For the non-dendritic material at the same fraction solid, it is three orders of magnitude less, 0.2 kPa. In both of these Figures, fraction solid, fs, is calculated from the Scheil equation based on actual temperature measurements [5]. Since the initial finding of Spencer, many studies have been conducted on fundamental and engineering aspects of vigorously agitated SSM's [1-3]. Nonetheless there is still much that is not understood about the detailed mechanisms of structure formation or about the rheology behavior of the material [3]. Non-dendritic solidification can be achieved by vigorous agitation in the melt by different stirring methods. The forced convection which exists after vigorous agitation promotes ripening and globularization mechanisms and changes dendrites formation to rosette or globular structure. In fact, forced convection causes fast migration of rejected solutes from the front of solidification plane to the bulk of melt and removes the constitutional undercooling in front of dendrites tips. Also forced convection accelerates ripening mechanism in dendritic growth, and then secondary arms are separated easier from their roots on primary dendrite. These two main mechanisms which are promoted by vigorous agitation change the dendritic growth to rosette growth or globular growth [5]. The microstructure tends to be more globular with the agitation increase. Figure 2-5 shows the effect of agitation intensity and solidification progress on microstructure evolution in a dendritic solidified alloy [2].
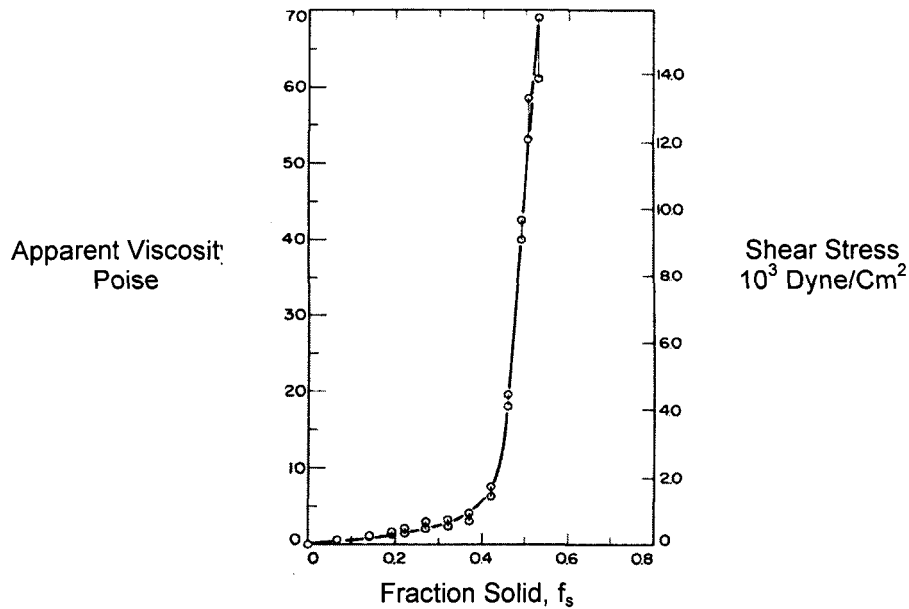
Fig. 2-4: Experimentally determined viscosity and shear stress vs. fraction solid for Sn-15%Pb alloy continuously cooled and sheared [5]
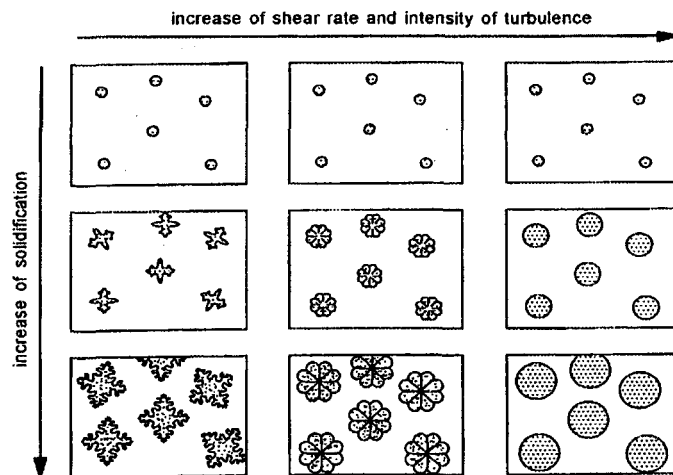
Fig. 2-5: Microstructure evolution in dendritic and non-dendritic solidification [2]

Agitation also appears to refine primary dendrites and promote the formation of rosette and/or globular particles through the reduction in segregation of alloying elements at the solidification front and promotes better heat transfer between the mold and bulk of liquid to establish a lower temperature gradient. A low temperature gradient coupled with lack of directional heat transfer due to agitation, are the main recipe for refining and formation of equiaxed as-cast structure [1]. Agitation also results in the formation of

more low-angle grain boundaries or twin boundaries between neighboring particles and thus promotes the higher degree of agglomeration than unstirred alloys [12]. Such characteristic yields the thixotropic behavior of non dendritic alloys which will be explained in chapter 3.

In some cases the rotation or applied agitation seems to be the operant of higher cooling rate within the solidified melt which increases the primary nuclei or refine the final microstructure of phases, especially intermetallics. K. Ishikawa et al. [13] have shown the approximate 90 percent decreasing of the size for the intermetallics within Cu-37% Al due to applied rotation in stirring synthesis method. Such variation has also been seen for silicon crystal size within 70-80 percent for Al-17%Si [13]. S. Mohan et al. [14] have shown the same results for the size of primary silicon within two hypereutectic aluminum-silicon alloys, while Nafisi et al. reported such effects for A356 alloy for both Fe-based intermetallics and eutectic silicon particles [15, 16].

A. Das et al. [17] have interpreted the effect of fluid flow either laminar or turbulent using Monte-Carlo simulation. As per their discussion, a laminar type fluid flow appears to destabilize the solid-liquid interface for particles growing from a fixed substrate and promote dendritic morphology through abundant supply of solvent atoms to the growing dendrite tips. Particle suspended in the melt experiences a rotational motion under laminar flow. Periodic stabilizing and destabilizing of the solid-liquid interface consequently promotes rosette type morphology. The turbulent type fluid flow that penetrates into the interdendritic region supplying solvent atoms (in other words, depleting the interdendritic solute boundary layer) seems to prevent dendritic growth and stabilize the solid-liquid interface such that compact solidification morphology develops.

Amongst different techniques for SSM processing, low pouring temperature casting has been developed for production of thixo/rheo billets. Foundrymen and ingot casters from long time ago have understood that low pouring temperature causes not only equiaxed grains but also reduces casting defects by lowering gas porosity and shrinkage. Low pouring temperature has not only a great interest in the research field [18-22] but also commercial processes took benefits of this concept [23-26].

Pouring temperature directly affects the nucleation and growth of primary crystals, α-Al for hypo-eutectic Al-Si alloys, within the melt, where nucleation controls the size of grains formed and growth determines the grain morphology and the distribution of alloying elements within the matrix. The driving force for nucleation is the degree of undercooling created during solidification and growth is controlled by the temperature gradient and solute concentration in liquid. Both are however affected by the rate of heat extraction from the melt. The final structure is therefore dependent on the nucleation density, growth morphology, fluid flow and diffusion of solutes. Therefore close control of casting conditions, such as pouring temperature, cooling rate, nucleation sites and temperature gradient, may result in formation of the desired globular as-cast structure [27].

Grain refinement causes smaller particle size and better distribution of α-Al primary phases within SSM slurry, thus the obtained material may show lower viscosity and better flow behavior [28]. Small size of primary phases reduces the collision rate amongst the particles and extends the free moving time of α-Al phase within samples, which is seen as the lower viscosity of slurry during rheological test. Although grain refining has not a great effect on the morphology of primary α-Al phases it is somehow used to fabricate the suitable feedstock for thixocasting processes. It seems that the feedstock which are prepared by grain refiner additions have shown better globularity in microstructure after reheating of the billets than non grain refined billets [28].

As a conclusion, it could be mentioned that all innovated SSM processes are concerned with producing non-dendritic structure within the semi solid materials. Non-dendritic structure, as described before, shows low viscosity and better die filling ability than dendritic microstructure. From commercial viewpoint SSM alloys are interesting since they can be used in casting and forming processes where the cost of die materials is less with longer die life. The following section discusses different methods developed to produce SSM materials both commercially and at laboratory scales.

2.2 SSM Processing

Since the innovation of SSM concept in early 1970s [5], there have been many processes patented to cast SSM feed stocks. These processes may be classified based on the starting materials from which SSM billets or ingots are produced

2.2.1 Liquid processing

2.2.1.1 Agitation processes

The original method for producing non-dendritic slurries developed at MIT involved vigorous stirring during solidification from the liquid state [4-5]. This was developed from a batch process to a continuous process illustrated in Figure 2-6, in which the superheated liquid in the holding vessel flows down into an annulus between a stirring rod and outer cylinder where it is simultaneously stirred and cooled. Slurry flows from the bottom of the rheocaster either to be cast directly to shape, as in a die casting operation (rheocasting), or to be solidified and at a later date to be cut into slugs, partially remelted back to the slurry state, and then shaped (thixocasting). Efforts have been made to scale up the continuous rheocaster to industrial level but apparently without success. The reasons are the unacceptable erosion of the ceramic stirrer (particularly with high melting point alloys), the contamination of the slurry by dross and gas entrapment, low productivity, and difficulty in process control [4].
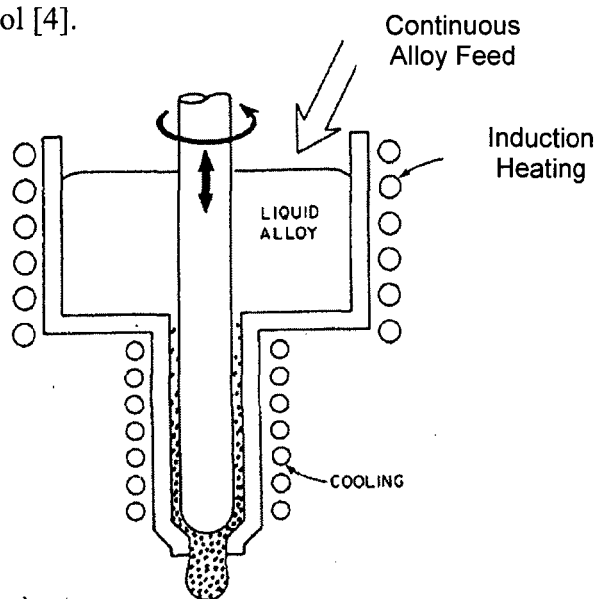
Fig. 2-6: schematic of high temperature continuous rheocaster [4]

D. Brabazon et al. [8, 11] also designed stir caster machine which operates like a rheometer and has almost the same form as Figure 2-6. The schematic diagram in Figure 2-7 shows another apparatus designed for continuous mechanical stirring process [29]. The researchers have obtained better deformation ability either for wrought or cast aluminum alloys, using such SSM preparation method for primary extrudeable billets [29].

The application of mechanical stirring is not restricted to billet production and is applicable for component shaping through high pressure die casting processes. Screw stirring and double screw stirring, see Figure 2-8, are two methods for preparation of melt before high pressure die casting. In these two methods, mechanical stirring is induced directly into the melt and turbulent agitation, which is raised by an impeller, can develop spherical microstructures in the melt. Figure 2-8 shows two machines which use mechanical stirring for preparation of slurry before component shaping by high pressure die casting. Higher intensity of agitation in these machines which causes better final microstructure coupled with low cost have attracted industry to employ mechanical stirring processes instead of other expensive routes, for direct rheocasting and component shaping [30].
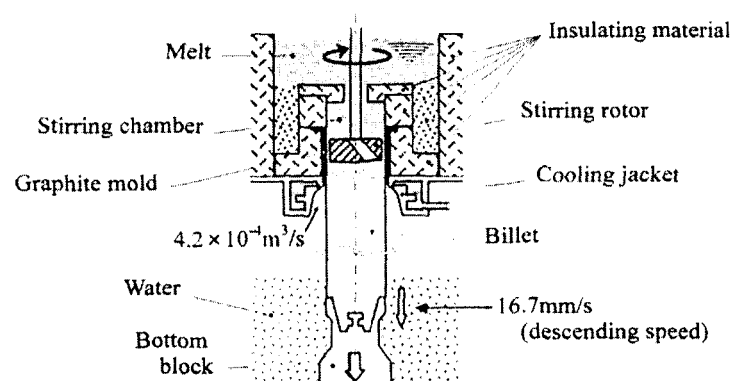
Fig 2-7: Schematic illustration of mechanically stirred continuous casting method [29]

However all the mechanical methods have the same shortcomings resulting from direct touching of stirrers and semi solid materials, as briefly noted before.

Other researchers [31] have proposed a new continuous rheocaster which using the same concept of having mechanical stirrer to produce degenerated dendrite followed

by two rolling cylinder to perform the forming of the alloy within semi solid condition. The final particle size achieved through this method is reported to be 7 µm which is ten times smaller than the particle size obtained in batch type rheocasting.

A possible improvement in productivity of mechanical rheocaster is the introduction of SCR process (shearing-cooling roll) in which the slurry is generated by pouring liquid metal between a rotating roll and a stationary cooling shoe, Figure 2-9. The shearing of the solidifying melt within the gap produces fine slurry in lead and aluminium alloys, but how much contamination occurs from oxygen pickup is not reported [32].

(a)

(b)
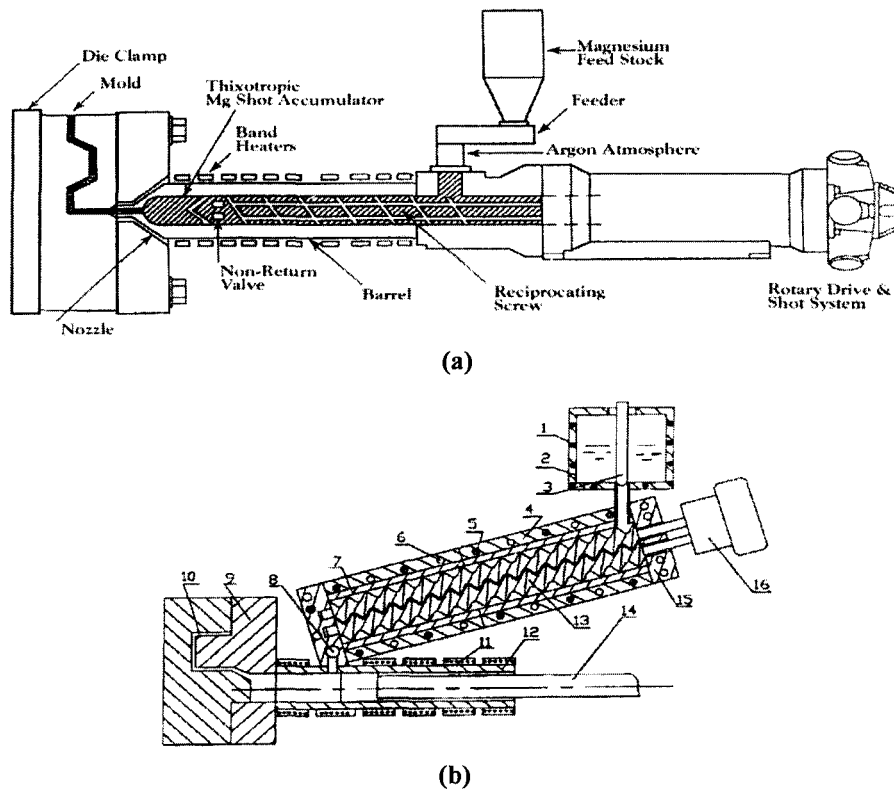
Fig 2-8: (a) Screw stirring and (b) Double screw stirring apparatuses which are used in commercial scales for direct component shaping and rheocasting [30]

stationary shoe

molten metal

rotating
roll

supporting
block

stripper

semisolid metal
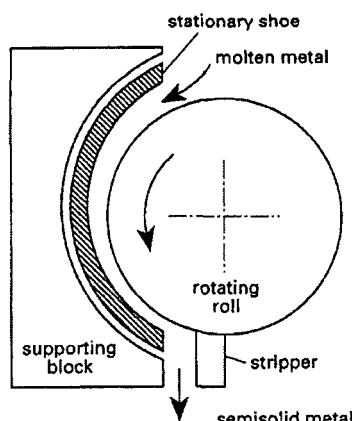
Fig. 2-9: Schematic of shear-cooling roll process [32]

A different approach to direct agitation of the melt is provided by the so called passive stirring techniques [3]; this is achieved by forcing the liquid through a static mixing devise whose geometry ensures high shear in the fluid while heat is being removed and solidification is occurring. The alloy may be forced through a static mixer under gas pressure or driven by an electromagnetic pomp. One such device involves passing the liquid through a series of helical paths which alternate between left hand and right hand screws, providing very high shearing of the alloy without turbulence. Under these conditions slurries containing 80% solid may be formed with the viscosity of 1 Nsm^{-2} and particle size of around 100 μm. Another design of static mixer consists of a metal tube packed with refractory spheres, Figurer 2-10, through which the liquid alloy is forced under pressure and cooled [3]. Other more efficient mixers have also been developed. All these mixers are cooled from the outside by an atomized water spray and the alloy may be filtered before entering the static mixer to provide clean inclusion free slurry. Industrial plants using this technology are currently operating, producing billets of 100 mm diameter, and it is claimed that the production rate of 1000 kg/day of Al-alloy is achieved [3].

molten
metal

heat
removal

semisolid
alloy
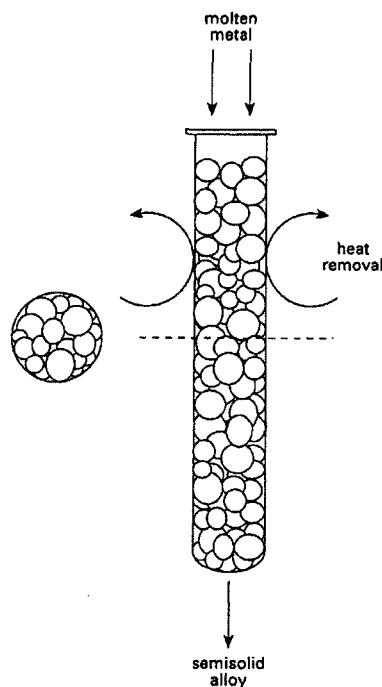
Fig. 2-10: Schematic of passive stirring process [3]

In order to overcome the problems associated with direct mechanical stirring methods, Magneto-hydrodynamic (MHD) method has been developed. MHD stirring of melt is the most interested method in continuous and semi continuous SSM billets production. In this process, application of strong magnetic field around water-cooled die of continuous caster induces vigorous agitation to the melt and causes degeneration of dendritic structures into rosette structure. The MHD route has attracted industries which produce feedstock such as billets or slabs. This is because of faster production speed, reduction of contamination in melt and better controlling of continuous line with computer programming [33]. One important disadvantage of this process is the shortage of spheroidal microstructure, although the rosette microstructure achievable through this method is suitable for partial remelting processes such as thixocasting or thixoforging [34-35]. Not to be cost effective is another disadvantage of MHD method. Figure 2-11 shows schematic of this process for billet production [36-39]. The researchers [36] have presented the simultaneous effects of stirring and strontium modification on the size of primary α-Al phase and the silicon particles. They have shown a direct effect of stirring

on the size of α-Al phase but the variation of the size within silicon particles is attributed to the homogenous modification due to stirring within the melt.
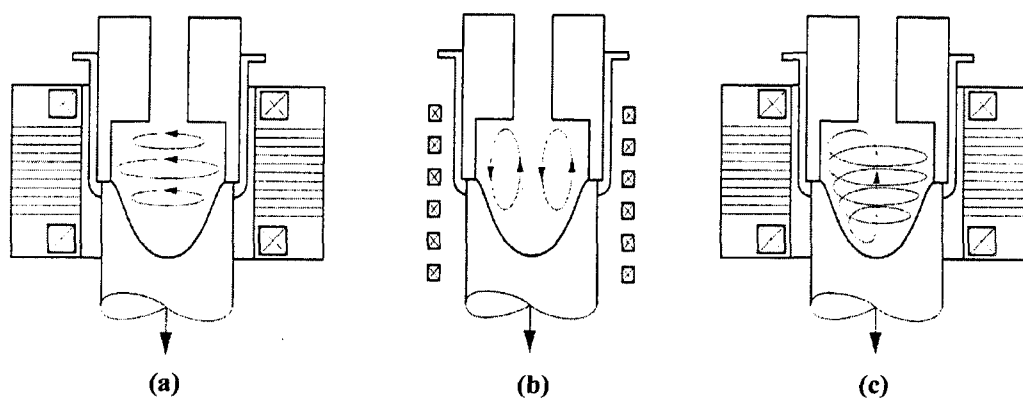
Fig. 2-11: Schematic diagram of the semi continuous caster with MHD system (a) Horizontal agitation (b) Vertical agitation (c) Helicoidal agitation [39]

It is well established that application of ultrasonic treatment of a cooling melt at a starting temperature just above its liquidus can produce effectively a fine and non dendritic microstructure, which is suitable for subsequent reheating and thixoforming operations [38, 40]. Regarding mechanism for the formation of such fine and non dendritic structure, it is now believed that the introduction of high power ultrasonic vibration into a liquid alloy can lead to two basic physical phenomena: cavitation and acoustic streaming. Cavitation involves the formation, growth, pulsation and collapsing of tiny bubbles in the melt. The compression rate of these unsteady bubbles can be so high that their collapsing generates hydraulic waves, thus producing artificial sources of nuclei. The propagation of high intensity ultrasonic wave involves the initiation of steady state acoustic streaming in the melt. The overall effect of various types of stream is to vigorously mix and homogenize the melt. Therefore, hydraulic shock waves generated by the collapse of cavitation bubbles fragment dendrite arms, and acoustic streams will distribute the dendritic arm fragments homogenously throughout the melt. When ultrasonic vibration is coupled to the solidifying metal, the structural changes include grain refinement, suppression of the columnar grain structure, increased homogeneity, and reduced segregation.

Swirled Enthalpy Equilibration Device, SEED, is a newly patented ALCAN international SSM process [41] with shorter processing time and superior billet structure [42-44]. It is based on achieving rapid thermal equilibrium between the mold and bulk metal by indirect off center mechanical swirling of the melt. In this Slurry on demand (SoD) process the alloy is poured into a cylindrical mold, stirred and residual liquid decanted before being cast into high pressure die casting machines. Figure 2-12 shows the SEED process schematically. After drainage, i.e. the end of process, the semi-solid slug could be transferred into high pressure die casting machine.
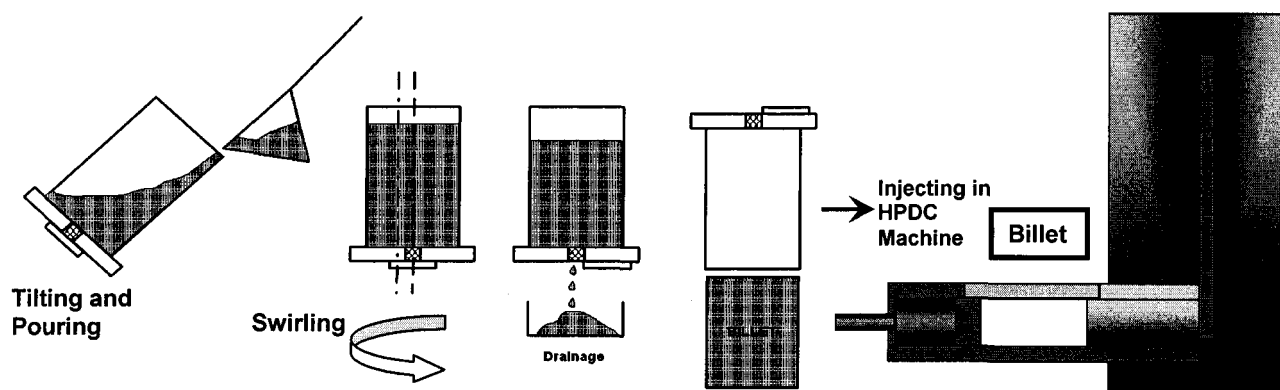
Fig. 2-12: Preparation procedure of billets in the SEED process [38]

This is pre process which will be used in the current research and therefore will be described in more details in the coming chapters of experimental and results.

A.C. Fonseca et al. have investigated the effect of different applied rotation on microstructural evolution such as, concentric rotation, eccentric rotation and torsional oscillation. They have shown the great effect of agitation on grain refinement of rheocast aluminum alloy without using the inoculants [45].

In conclusion the main parameter in the above mentioned processes is the stirring of the melt, either direct or indirect.

2.2.1.2 Non agitation processes:

There are a number of possibilities to produce non dendritic structure from liquid metals without agitation. In some alloy systems grain refiners added before casting (e.g.

Ti-B in aluminum alloys) can be so potent as to suppress dendrite growth and on reheating of such grain refined alloys to the semi solid state, thixo formable materials are generated. This could be an attractive route for the production of inexpensive starting materials for semi solid forming as investigated by several workers [28, 38]. Although suitable structures have been produced in aluminum alloys using standard grain refiners, it appears to be difficult to obtain grain sizes less than 100 µm and questions of recycleability of the alloys have been raised [38]. Another method is to introduce high melting point metal powders into a disimilar liquid metal to act as seeds for the formation of globular structure [38]. This may be regarded as a variation of the mixed powder route given below.

The spray casting of alloys [46-47] in which a stream of liquid metal is atomized by a gas jet and deposited in the semi solid state on to a cooled target produces a non dendritic structure. It has been demonstrated that on reheating spray formed alloy back to the semi solid state, a thixoforgable material is generated [47]. The spray forming process is in commercial operation and is able to deliver clean alloy with controllable grain size down to about 20 µm. One of the limitations of this route is the minimum size of billet that may be sprayed. In general this method could be more expensive if compared with agitation routes such as MHD; however, it may have particular advantages with high temperature alloys such as steels and superalloys.

Liquidus pouring temperature or low pouring temperature is another low cost alternative route to generate structures [19-26]. The ability of low superheats to bring temperature gradient homogeneity within Semi solid slugs results in equiaxed grain growth instead of columnar growth. This phenomenon is well researched by several investigators and has been developed to fabricate fully globular microstructure [19-27]. The advantage of the low pouring process is to neglect the contaminations and produce desirable microstructure with no supplementary accessories which reduce the total cost of process as well. Motegi et al [48] have used this route for continuous casting of semi solid aluminum alloys. They have put an inclined plate along the liquid way into the metallic mold and poured the alloy near liquidus temperature. Formation of seeds during the movement on the inclined plate just before entering into the mold fabricates a suitable microstructure for the rheocast material. Haga et al [49] have also proposed the new and

simple rheocasting method by using low superheat alloys. They poured the melt at low temperatures into a metallic die to produce a semi final shape which was ram extruded to its final shape while still at semi solid state.

The current research is also concerned with the effect of pouring temperature on the ability of semi solid slugs to plastic deformation as will be discussed later. Detailed information is presented in the result and discussion chapters.

2.2.2 Solid State Processing

Another technique proved to produce SSM slurries is to form a compact of fine powders of two alloys having different melting points [50]. On heating the components to temperatures above the lower melting point constituent slurry is produced with appropriate structure. This is clearly an expensive method but may have advantages in the production of special parts.

A production route which should show much greater commercial potential involves the heating and partial melting of recrystallised alloy. It has been explained that on the deformation of solid phase, high angle boundaries between solid grains will be penetrated causing fragmentation. If the material has been sufficiently deformed and recrystallised to generate a fine grained microstructure, partial melting will then cause it to fragment into ideal slurry composed of well rounded solid particles within a liquid matrix. The initial deformation may be carried out above the recrystallization temperature (hot working) followed by cold work at room temperature (Stress Induced Melt Activated, SIMA process), or alternatively below the recrystallization temperature (warm working) to ensure the maximum strain hardening is introduced into the particles [46, 47]. The particle can be as small as 30 μm depending on the degree of cold work and the rate of heating. However, it has been shown that heavy forging processes may also be used with success through this method and this may allow larger billet diameter to be available for thixoforming. The solid state production seems to be a good competitive method to the liquid MHD process, using simpler technology and equipment generally available.

2.2.3 Production of metal matrix composites

It was recognized early by the workers at MIT that metal slurries were ideal environments in which to incorporate ceramic particles to form composites [51]. The higher viscosity prevented settling or floating of reinforcement and allowed wetting and good bonding to occur between the particles and matrix. Furthermore these slurries of composites are proved to be forgeable and castable [51]. In fact there is evidence that for a given volume fraction of solids, the apparent viscosity of the composite slurry is lower than that of the equivalent alloy slurry containing no ceramic [4]. Unfortunately the early attempts to incorporate ceramic particles by mechanical mixing introduced as much as oxide and dross as particulate [1, 4]. With the development of other production routes, the situation has changed: for instance MHD and Osprey processes allow particulate materials to be introduced with no contamination [1]. It has been reported that reinforcing of aluminum alloy with angular particles such as SiC is restricted to about 20% after which the slurry becomes too thick to be die cast.

2.2.4 Semi Solid Metal Forming

The process of forming a partially remelted non dendritic alloy slug into a near net shape component within metal dies has been termed thixocasting, thixoforging, or more generally, thixoforming. "Thixocasting" usually refers to the operation of injecting the slug into the die by ram or plunger as in die casting, and the early works on SSM employed diecasting machines and dies [3]. Placing the slugs within open dies and squeezing the two halves together is often referred to as "thixoforging". However the deformation and flow of the semi solid alloy within the die is different from that of fully liquid or solid feedstocks [3].

There are two separate stages involved in thixoforming a slug of the appropriate non-dendritic structure into a shaped component within a die. The first step is the uniform reheating and partial remelting of the alloy before injection. In principle, a variety of heating methods might be used, for instance, radiation and convective heat transfer within a gas fired or electric resistance muffle furnace. However, it is difficult to avoid steep temperature gradients during rapid heating under such conditions since heat must be

transferred through the slug surface. Induction heating by contrast generates the heat within the slug with minimum gradients and is generally the preferred approach. Ideally, computer modelling of induction heating should be carried out to establish the optimum conditions (coil design, current frequency, power cycling, etc.) necessary for rapid and uniform partial remelting of the slug.

Once the slug is known to be in correct softened condition, either by adopting a heating program established experimentally, or by temperature measurement or some other non contacting device monitoring softness, the slug may be transferred into the die shot chamber by robot handling and injected into the die. In thixocasting, it is necessary to control the ram velocity which determines the flow rate of the slurry through the gate and into the die. The researches demonstrate that if the flow rate is too low, incomplete die filling results, whereas at too high rates, porosity in the component appears because the smooth slurry front breaks up and may atomize causing turbulence and air entrapment [4]. It is important to note that heat treatment cannot be carried out on conventional diecasting because air entrapment within the pores would cause blistering and distortion. This is not the case for thixocast components.

The main cause of die deterioration during diecasting arises from the formation of fine cracks on the die surface resulting from thermal cycling and fatigue, and from wear due to local welding and mechanical erosion. For thixocasting the lower die surface temperature results in less mechanical and chemical erosion and lower thermal gradient across the die reduces the formation of fine cracks. Therefore, the die life will be extended. This supports the case for the economic production of casting of high temperature alloys since die cost represents a large proportion of the production cost. Further work on using dies of high thermal conductivity has demonstrated that the thermal shock associated with injection of semi solid slurries can be reduced yet further and could provide a significantly enhanced die life in ferrous thixoforming [3].

As for rheocasting since it depends on the technologies being used to produce SSM structure, if the technology is capable to produce self standing billets such as SEED [41] and UBE [24] then close die forging may be utilized to produce near net shape components.

2.2.5 Liquid Segregation

The main short coming of SSM processing is the segregation of residual liquid during deformation or shaping within the die [9, 52]. This problem is due to separation of liquid and solid phases under pressure.

However several researchers [50, 53-56] have claimed no segregation of liquid at high shear rates, more than 10^2 (s^{-1}). Loong et al. [54] have reported such a phenomenon under the ram speed of 0.5-1 m/s, where there was little or no porosity and the segregation of residual liquid was negligible. Figure 2-13 shows the difference between the microstructures due to high and low shear rate deformations near the wall [54]. Segregation of liquid-solid has also been modeled [57] using an isothermal one-dimensional model of axisymmetric compression of solid-liquid mixture. The model predicts the mechanically induced macrosegregation.

(a)   (b)
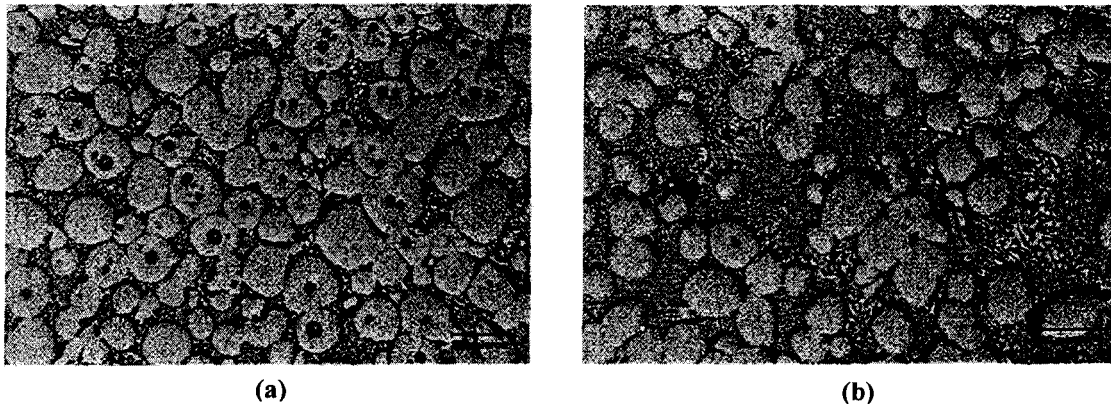
Fig. 2-13: Microstructures of compressed samples after (a) fast rate and (b) slow rate compression near the radial edge of the specimens [54]

Such reports are in controversy with others who have detected the segregation of liquid within high pressure die cast components [9, 58-59]. Kapranos et al. [58] proposed to use high ram speed, high shear rate before entrance of the slug into the gate and low ram speeds, low shear rates, during die filling stage to ensure lower viscosity during injection just before filling and lower segregation during die filling. Lee et al. [59] have reported the high injection speed of die casting as the main parameter responsible for

liquid segregation and proposed to find the optimum injection speed for fulfilling both the die filling and lower segregation.

2.2.6 Mechanical Properties

Only a small amount of work has been carried out to determine mechanical properties of SSM formed products and this has been confined mainly to aluminum foundry alloys, with less attention given to wrought alloys [8]. Some available data are given in Table 2-2 together with typical values from the literature relating primarily to permanent mold casting.

It is apparent that for the 356 aluminum alloy (Al-7Si-0.35Mg), the thixocastings in the fully heat treated state (T6 temper) have superior mechanical properties to those produced by permanent mold route, and approach those achieved in conventional close die forging (see Table 2-2); the ductility of thixoformed specimens is particularly noteworthy. Also, simple aging without solution treatment (T5 temper) provides a very useful improvement in the properties. The comparison of T6 treated parts is rather difficult due to different aging temperatures employed. Figure 2-14 shows a number of different routes and illustrates the general improvement to be expected by thixoforming as against other casting processes.

In another study, Parsad et al. [60] investigated mechanical properties of the mechanically stirred Al-Cu alloys and compared the resulting tensile strength for both conventional and rheocast conditions. They have reported almost no differences between tensile strengths of conventional and rheocast Al-10%Cu and just a slight improvement for Al-4.5% Cu. They have shown the tensile strength of Al-4.5%Cu alloy is an inverse function of square root of α-Al particle size. The proposed empirical equation is as following:

$$\text{Tensile Strength (MNm}^{-2}) \approx 159.3 + 81(\bar{d})^{-1/2} \qquad (2\text{-}3)$$

Where $\bar{d}$ is the average particle size.

Mohan et al. [61] have investigated the mechanical properties of mechanically stirred aluminum-silicon alloys and obtained superior yield and tensile strength for hypereutectic alloys with increasing the shear rate. They have claimed that the tensile

strength of Al-20.41%Si is increased from 147.68 MPa to 219.41 MPa with increasing of mechanical stirring speed from 1000 rpm to 1500 rpm.

Tab 2-2: Mechanical properties of some aluminum alloys in different condition [3]

Alloy	Process*	Temper	Yield stress, MN m^{-2}	Tensile strength, MN m^{-2}	Elongation, %	Hardness, HB
Casting alloys						
356	SSM	T6	193	296	12·0	90
(Al–7Si–0·5 Mg)	SSM	T6	256	300	11·4	...
	SSM	T6	240	320	12·0	105
	SSM	T7	260	310	9·0	100
	SSM	T5	172	234	11·0	89
	SSM	T5	180	225	5–10	80
	PM	T6	186	262	5·0	80
	CDF	T6	280	340	9·0	...
	PM	T51	138	186	2·0	...
357, A357	SSM	T6	290	358	10·0	100
(Al–7Si–0·3 Mg)	SSM	T6	260	330	9·0	115
	SSM	T7	290	330	7·0	110
	SSM	T5	207	296	11·0	90
	SSM	T5	200	285	5–10	90
	PM	T6	296	359	5·0	100
	PM	T51	145	200	4·0	...
Wrought alloys						
2017 (Al–4Cu–Mg)	SSM	T4	276	386	8·8	89
2017	W	T4	275	427	22	105
2024 (Al–4Cu–1Mg)	SSM	T6	277	366	9·2	...
2024	CDF	T6	230	420	8·0	...
2024	W	T6	393	476	10	...
2024	W	T4	324	469	19	120
2219 (Al–6Cu)	SSM	T8	310	352	5·0	89
2219	W	T6	260	400	8·0	...
6061 (Al–1Mg–Si)	SSM	T6	290	330	8·2	104
6061	W	T6	275	310	12	95
7075 (Al–6Zn–Mg–Cu)	SSM	T6	421	496	7·0	135
7075	SSM	T6	361	405	6·6	...
7075	CDF	T6	420	560	6·0	...
7075	W	T6	505	570	11·0	150

*CDF closed die forging; PM permanent mould casting; SSM semisolid metal processing; W wrought.
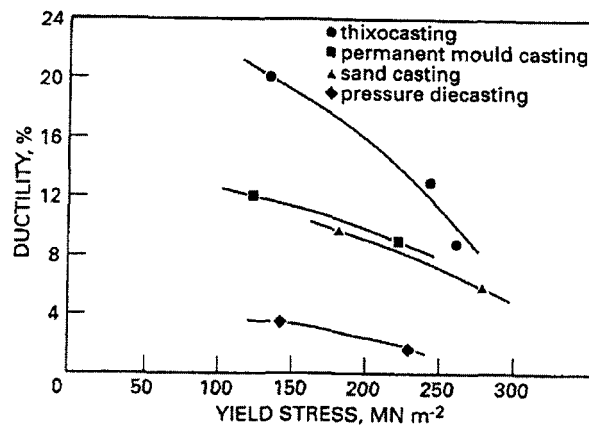
Fig. 2-14: Mechanical properties of thixocast parts of A356 alloy (Al-7Si-0.35Mg) compared with other production process [3]

Other researchers [18] have studied tensile properties of 319 aluminum alloy with globular microstructure and compared the obtained data with conventional sand cast alloy. They reported yield and U.T.S. strengths about 2 times greater for globular microstructures. Since they have not investigated the mechanical properties of conventional alloy prepared by high pressure die casting, such comparison may not be a reliable evidence to prove the advantages of semi solid processing. Cerri et al. [62] have also investigated the mechanical properties of thixocast 319 Al-alloy within different heat treatment conditions, T5 and T6, but they have also presented no evidence to prove the advantage of thixocast alloys.

K. Ichikawa et al. [31] developed a new continuous rheocaster to fabricate as-cast part with very fine structure. They reported tensile strength and elongation values of 248 MPa and 11% respectively for continuous rheocast Al-10%Cu in contrast to 192 MPa and 3.1% for die cast Al-10%Cu.

Mechanical properties of semi solid alloys have also been investigated at high temperature [63, 64]. The superior plasticity of rheocast materials in comparison with conventional alloy was of particular note [63], although the deteriorated tensile strength is also seen due to the agglomeration of solid particles [64]. De Freitas et al. [65] investigated mechanical properties of semi solid materials in mushy state at high fraction of solid. They reported upper yield strength for the slurries with smaller grain size, whilst lower viscoplastic strength for the same materials. Such properties were attributed to the larger contact surfaces of finer grains causing higher yield strength and easier movement of smaller particles in viscoplastic deformation, respectively.

Measurement of the fatigue properties of the A356 alloy in the T6 condition, Figure 2-15, also shows considerable improvement in fatigue strength of thixocastings over other conventional castings, which is attributed to the fine uniform microstructure. Other researchers have also shown the fatigue improvement for stir cast alloys [8]. They have claimed MHD route is capable of improving fatigue resistance when compared with specimens prepared by mechanical stirring and conventional casting.

N. Hayat et al. [66] have also reported the improvement of 11.3% in fatigue properties at 10^7 cycles for rheocast aluminum silicon alloy than squeeze cast materials, although the particles size of rheocast alloy was much smaller than the squeeze cast one

.
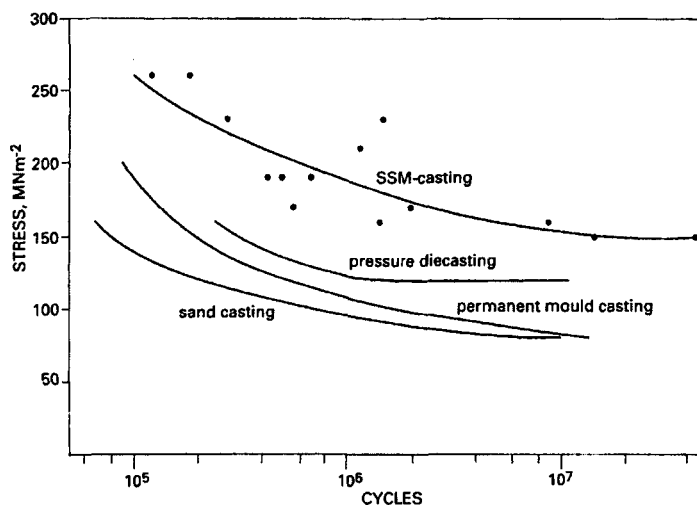
Fig. 2-15: Fatigue behavior of A356 alloy as thixocast, compared with other processes [3]

Wrought aluminum alloys have not been as extensively investigated in the thixoformed condition but the indications are that they do not quite achieve the highest strength and ductility that are typical of wrought alloys. This may reflect the presence of defects in the products, such as residual porosity or oxide film inclusions. Then improved processing control or component design may help to overcome such deterioration of properties. It is clearly an area of research worthy of more attention [3].

2.2.7 Metallography

Quantitative metallography has established itself as the reliable method to characterize the microstructural evolution in almost all metallurgical processes. Such method has also been used for characterization of semi solid materials [8, 34, 35, 53, 67]. There are several common parameters usually measured for SSM alloys including aspect ratio (longest / shortest feret diameters), equivalent circular diameter, density defined as the number of primary particles per unit area, Sphericity $= \dfrac{4\pi A}{P^2}$ where A is total area and

P is perimeter of liquid-solid interface (the closer the value of sphericity to one (1) is the higher the globularity of the particles), area to perimeter ratio which is proportional to inverse sphericity.

In addition there are other parameters proposed to precisely quantify the microstructures [39]. The surface area per unit volume, $S_V = \dfrac{4}{\pi} \dfrac{P_{sl}}{A_T}$, is the complementary parameter to evaluate the surface of the primary particles in 3D, where P_{sl} is the perimeter of the liquid-solid interface and A_T is the total area of primary particles.

Other researchers [28, 67] have used the equation 2-4 as a dimensionless parameter to indicate the sphericity of the grains

$$ F = \frac{S_v^2}{6\pi f_s N_A} \tag{2-4} $$

Where N_A is the density of particles.

For a perfectly spherical grains $F=1$ and higher values denote plate or needle-like morphologies. Zoqui et al. used the following equations to characterize the microstructural evolution of MHD prepared thixocast A356 alloy [34, 35]. They have also shown there is a direct relationship between grain size (macrostructure) and globule size (microstructure). The smaller the grain size the smaller are the globule size and shape factor [35]. Equation 2-5 shows the formula of shape factor applied by several authors [8, 34, 35, 53, 67].

$$ \text{Shape factor} = \frac{P_\alpha^2}{4\pi A_\alpha} \tag{2-5} $$

Where, A_α and P_α represent the area and perimeter of the primary phase in the microstructure.

Rheocast quality index (RQI) criteria (ideal=1):

$$ \text{RQI} = \text{globule size/(grain size x shape factor)} \tag{2-6} $$

Where the grain size was measured using polarized microscopy from the macrostructure characterisation. Should be noted that RQI=0.1 indicates rosette shape feature and

RQI=0.9 shows a perfect globular shape. The measured globule size is the size of the primary phase in the microstructure.

Aspect ratio of the primary α-Al phase, as an indication of equiaxed growth, is also a parameter which was studied by researchers [8].

$$\text{Aspect ratio } AR: L_j/L_n \qquad (2\text{-}7)$$

Where L_j is the length and L_n is the lateral wide of the primary particles.

CHAPTER 3
LITERATURE REVIEW

FUNDAMENTALS OF RHEOLOGY

CHAPTER 3
LITERATURE REVIEW
FUNDAMENTALS OF RHEOLOGY

3.1 Introduction

Rheology is the science of deformation and flow of matter. It is a branch of physics concerned with the mechanics of deformable bodies. Much of the theory of rheology relates to ideal cases based on first order differential equations (e.g. see equation 3-6) and on the concept that constants in these equations do not vary with changes in the main parameters. However, numerous exceptions to the ideal concepts which have been developed mathematically and indeed, non ideal systems appear to be even more than ideal systems.

Although most of the theory of rheology (either qualitative or quantitative) treats reversible phenomena, nonreversibility is often found. The rheological properties of substance sometimes exhibit considerable change with time or with continuing deformation, which occurring either reversibility or irreversibility.

Rheology is primarily concerned with the deformation of cohesive bodies. The breakup or rupture of solids and liquids into pieces or drops is included in rheology as is the reverse of these effects; sticking together or cohesion of particles or drops to make a continuous mass [68].

3.2 Deformation, Elasticity and Flow

The deformation of a body can be divided into two general types: (1) reversible deformation called elasticity and (2) irreversible deformation called flow. The work used in deforming a perfectly elastic body is recovered when the body is restored to its original undeformed shape, whereas the work used in sustaining flow is dissipated as heat and is not mechanically recoverable. Elasticity corresponds to mechanically recoverable energy and viscous flow to the conversion of mechanical energy into heat.

Shear is an important type of deformation in rheology. Simple shear can be considered as a process in which infinitely thin, parallel planes slide over each other, as

in a pack of rigid cards. Simple shear is a special case of laminar deformation. In simple shear the laminae are planes, but laminar deformation can be found in other geometries. Figure 3-1 shows simple or planar laminar deformation with three cases of cylindrical laminar deformation.

Case A, B and C are important for viscometry where A shows the basic pattern of flow in parallel plate compression viscometer, B represents the type of flow found in rotational viscometers and C is the flow pattern of capillary viscometers. Case D is commonly employed in determining the shear modulus of solids [68].
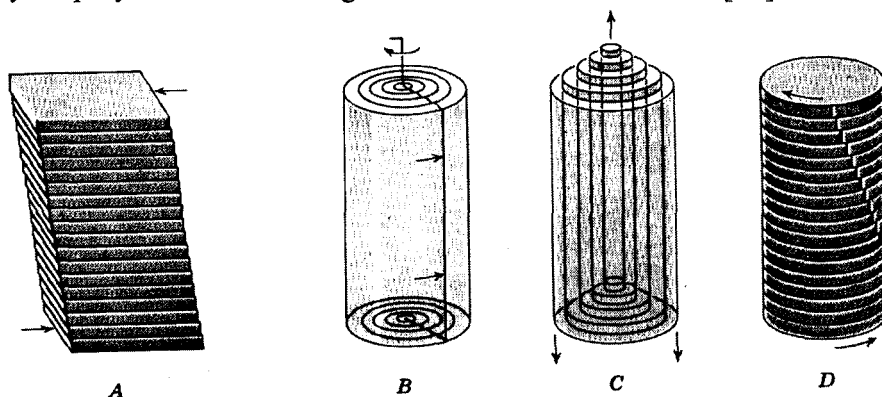
Fig. 3-1: Laminar deformation: (A) Simple shear (planar), (B) Rotational,
(C) Telescopic and (D) twisting shear.

It is clear from Figure 3-1 that deformation is the process of changing the relative positions of the parts of a body. As in case B, it is possible to have deformation without changing volume or shape, although many kinds of deformation involve such changes. Deformation resulting in change of shape of a body is called distortion.

Elastic deformation is always held to be a function of stress, whereas the rate of deformation for flow is a function of shear stress. Differential equations describing combined viscoelastic effects are generally set up with three basic terms: an elastic one involving deformation, a viscous one involving rate of deformation and an inertial term due to acceleration. If deformation is carried out very slowly there will be no viscous contribution and only elastic effects will show up. On the other hand, in continuous, steady state flow at a uniform rate there will be no elastic contribution and the entire effect will be viscous. From the view point of rheology, the mechanical properties of material bodies are describable in terms of elastic, viscous and inertial contributions. The word "viscous" is a generic term for flow phenomena and doesn't just refer to coefficient

of viscosity. The word "strain" can be used instead of elastic deformation as well. Thus in the case of body subjected to a uniform hydrostatic pressure, the strain is the relative change in volume ($\partial V/V$); or for a rod traction it would be the relative change in length ($\partial L/L$). Viscous deformation is expressed in terms of rate of shear, which is the change in velocity of flow with a distance measured at right angle to the direction of flow.

To produce flow or an elastic strain, a stress must be applied. The stress is defined as a force per unit area; and this force can be applied perpendicularly (compression/tensile stress), tangentially (shear stress) or at any other angle. Quantitative rheology is concerned with Stress-Strain-Time relationships and the influence on them of such factors as temperature, shear rate, type of material, etc [68].

3.2.1 Elasticity

An ideal elastic body is defined as a material that deforms reversibly and for which the strain is proportional to the stress, with recovery to the original volume and shape occurring immediately upon release of the stress. The ratio of stress over strain is called the elastic modulus or Young's modulus and it can be shown that a completely anisotropic homogenous solid exhibits neither more nor less than 21 independent elastic moduli [68] but for a completely isotropic body only 4 constants corresponding to the common types of deformation, are commonly employed. These are Young's modulus, E (change in normal stress divided by relative change in length), which describes the distortion of the materials under simple tension, Shear or rigidity modulus, G (change in tangential stress divided by change in resulting angle of extension), bulk modulus, K (change in hydrostatic pressure divided by relative change in volume) and Poisson's ratio, v (lateral contraction divided by extension in simple tension). Equations 3-1 to 3-4 show the mathematical relations amongst the material constants and the rate of deformation in bodies. The ideal theory of elasticity gives a good approximation to the rheological properties under small deformation of all materials except the softest ones.

Young's Modulus
$$E = \frac{\partial \sigma}{\partial \varepsilon} = \frac{(\partial f / A)}{(\partial L / L)} \tag{3-1}$$

Shear Modulus
$$G = \frac{\partial \tau}{\partial \gamma} = \frac{(\partial f / A)}{(\partial L_1 / L_2)} \tag{3-2}$$

Bulk Modulus $$K = \frac{\partial \sigma_B}{\partial \gamma_B} = \frac{(\partial f / A)}{(\partial V / V)}$$ (3-3)

Poisson's ratio $$v = -\frac{(\partial d / d)}{(\partial L / L)}$$ (3-4)

Where the σ, ε, τ, γ, σ_B, γ_B, f, A, L, d and V are simple stress, simple strain, shear stress, shear strain, bulk stress, bulk strain, force, area, length, diameter and volume respectively [68].

Regardless of 4 different constants mentioned above, the properties of an ideally elastic material, isotropic body, can be described just by two elastic constants. This means that there must be two simultaneous equations relating the four constants. These two equations are presented below in a single line:

$$E = 3K\ (1\text{-}2v) = 2G\ (1+\ v)$$ (3-5)

3.2.2 Viscous Flow

Ideal viscous bodies exhibit flow, with the rate of flow being a function of the stress [69-70]. An ideal viscous body cannot sustain strains for long, since these are relieved by flow. Of course, extremely viscous materials may exhibit elastic strain for considerable period of time. Periods which are short with respect to the time needed for appreciable flow. This means that a given material may be considered as an ideal elastic body for relatively short times and as an ideal viscous body for long time periods. Regardless of geometry of the body and deformation, the flow will always be in the form of laminar shear.

The ratio of applied shear stress to the gradient of velocity within ideal viscous bodies is called the coefficient of viscosity. Figure 3-2 shows a diagrammatic definition of such relationship as expressed mathematically in equation 3-6 [71].
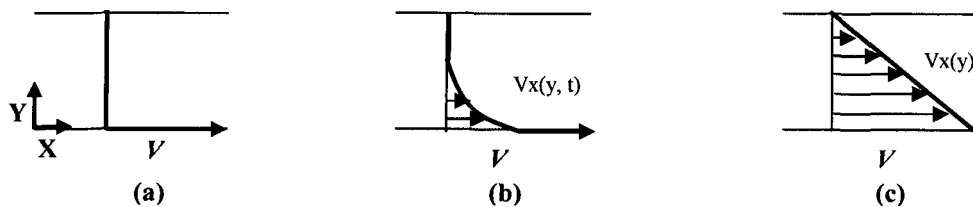
Fig. 3-2: Laminar flow of fluid between parallel plates where (a) at t=0 lower plate is set in motion at the constant velocity of v (b) at small t velocity is built up in unsteady flow and (c) at large t the fluid velocity is distributed in steady flow [71]

$$\tau_{yx} = -\eta \, \frac{dv_x}{dy} \qquad (3\text{-}6)$$

The best known ideal viscous body is the Newtonian fluid, for which the coefficient of viscosity, η, is a constant. The coefficient of viscosity is generally called simply viscosity. The so called kinematic viscosity, v, which is directly observed in capillary tube viscometers, equals the viscosity, η, divided by the density, equation 3-7. It is a measure of momentum diffusivity, analogous to thermal and mass diffusivity [71].

$$v = \frac{\eta}{\rho} \qquad (3\text{-}7)$$

Young's modulus and shear modulus are not always constant and may vary with strain or stress although for most rigid substances, this variation is small. On the other hand for several classes of fluid, the viscosity is found to vary by several orders of magnitude with changing rate of shear (or shear stress). Such materials are called non Newtonian fluids. Typical flow curves for non Newtonian fluids are presented for time independent fluids in Figure 3-3. Line A in this figure represents the Newtonian body for which, η is constant. When the shear rate increases more than in proportion to shear stress, curve B, the material is called "Pseudoplastic" or "shear thinning" liquid. To a first approximation, the flow curve of a pseudoplastic liquid can be represented by a power law; i.e., the rate of shear is roughly proportional to the power of the shearing stress or vice versa, equations 3-8& 3-9.

$$\tau_{yx} = \eta \, \overset{o}{\gamma}{}^{\,n} \qquad (3\text{-}8)$$

$$\eta = m \, \overset{o}{\gamma}{}^{\,n\text{-}1} \qquad (3\text{-}9)$$

m & n are the consistency constant and power index respectively, where $n<1$ for pseudoplastic fluid [71].

A material exhibiting a flow curve like C in Figure 3-3 where the shear rate increases less than in proportion to the shear stress is called the "dilatant" or "shear thickening" fluid. Although dilatant fluids have not been studied in so much detail as the pseudoplastic ones, the shape of their flow curves can also roughly be approximated by a power function as Eq. 3-8 with n>1. In other words, pseudoplastic and dilatant fluid may give straight lines when logarithm shear rate is plotted against logarithm shear stress.

There are also other type of fluids called Bingham fluids, Curve D, which requires a finite shear stress τ_0 (yield stress) to initiate flow. In other words, the fluid remains rigid when the shear rate is less than τ_0, but flows when the shear stress exceeds τ_0. The following relationship gives the rate of shear stress and shear strain:

$$\tau_{yx} = \pm \tau_0 + \eta \overset{o}{\gamma}, \qquad \tau_{yx} > \tau_0 \qquad (3\text{-}10)$$
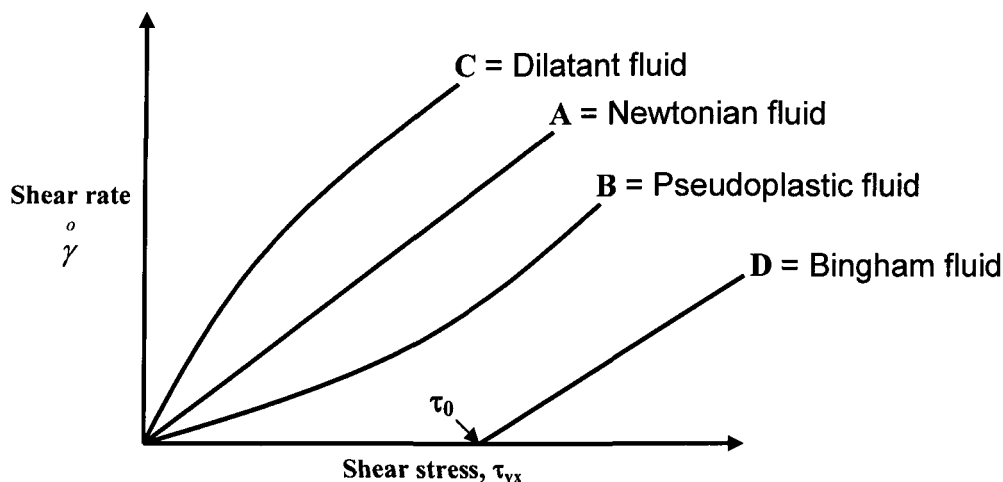
Fig. 3-3: stress-strain rate curves for time- independent fluids [71]

It has to be mentioned that some of non Newtonian fluids may exhibit dual behavior, where both, shear thinning, Pseudoplastic, and shear thickening, dilatant, may be observed at different loading condition. It has been reported [72, 73] that Al and Tin-lead alloys, using capillary die and rotational viscometer, have shown both the psuedoplasticity and dilatant behaviors depending on the applied shear rate. Such alloys behaves like pseudoplastic material at low shear rates, 2×10^3-2×10^4/s, and shows dilatant character when deformed at high shear rates, 10^6/s.

In addition, there are viscoelastic fluids which exhibit time dependent recovery from deformation, i.e. recoil. That is in contrast with the behavior of general Newtonian fluids which do not recoil. Such characteristic brings the time dependency of viscosity into the actual fluids. Different conditions create different type of time dependent fluid behavior. For example thixotropic fluids have a structure that breaks down with time under shear. At a constant shear-strain rate, the viscosity decreases with time and approaches an asymptotic value. Under steady state conditions, when the asymptotic value is maintained, thixotropic fluids may be treated as general Newtonian fluids, which

are presented in Figure 3-3. There are the fluids in which viscosity increases with time, i.e. rheopectic fluids, which behave quite differently from thixotropic fluids [71].

3.2.3 Creep Flow (High Temperature Flow)

The plastic deformation might be divided into two main categories of macroscopic and microscopic deformation. The above-mentioned deformations are classified as macroscopic, while the creep flow and its associated deformation mechanisms regarded as microscopic in nature. The creep deformation is divided into two subcategories of plastic deformation due to diffusion of atoms and that of the motion of dislocations. Each of them is further classified into sub groups depending on the deformation mechanisms [74].

"Grain boundary diffusion creep" is the deformation mechanism in which the plastic flow is brought about solely by the atomic diffusion along grain boundaries. The "volume diffusion creep" is the plastic flow produced by the diffusion flow of atoms within the grains. For "dislocation creep" and "dislocation glide", the plastic deformation mainly occurs due to the glide of dislocations. However the deformation rate is controlled by the atomic diffusion in the former while in latter is controlled mainly by dislocation glide. The "dislocation creep" is characteristics of high temperature deformation while the "dislocation glide" is responsible for plastic deformation at low temperature type. Generally the strain rate of a crystal can be expressed by the following equation:

$$\overset{o}{\varepsilon} = f(T, \sigma_{ij}, S_1, S_2 \ldots) \tag{3-11}$$

Where T is temperature, σ_{ij} is stress; S_i is the structural parameters such as grain size, dislocation density, etc.

In low temperature deformation, the structure parameters, S_i in Eq. 3-11 continuously change as the plastic deformation proceeds. The work hardening phenomenon is the result of this stage. In a constant stress test, the strain rate rapidly decreases and the deformation eventually stops. For high temperature deformation, the situation is different because the internal structure developed by plastic deformation can recover. An internal structure parameter like dislocation density increases on one hand with the increase of plastic strain and decreases on the other hand due to recovery process with the elapse of time. As a result an equilibrium state is realized at the particular S

value, and the strain rate becomes constant under creep condition. This state is called steady state creep. The occurrence of steady state deformation is one of the main features of high temperature plasticity. When an internal structural parameter S changes independently with strain and time, one can write:

$$dS = (\frac{\partial S}{\partial \varepsilon})_t \, d\varepsilon + (\frac{\partial S}{\partial t})_\varepsilon \, dt \qquad (3-12)$$

Since at the steady state $dS = 0$, the steady state creep rate is given by

$$\overset{o}{\varepsilon} = -(\frac{\partial S}{\partial t})_\varepsilon \, /(\frac{\partial S}{\partial \varepsilon})_t \qquad (3-13)$$

An accumulation of experimental data has established the general expression of the steady state creep as a function of temperature and stress. Under a constant creep stress, the creep rate changes with temperature, obeying an Arrhenius rate equation

$$\overset{o}{\varepsilon} \propto \exp(-\frac{\Delta E_c}{RT}) \qquad (3-14)$$

where ΔE_c is the activation energy of creep.

3.2.4 Types of fluids exhibiting various flow behaviors

All gases exhibit Newtonian flow curve, Figure 3-3. Single phase liquids which are composed of small or only moderately large molecules or ions are also Newtonian [71]. This includes all of the common solvents and their mixtures, as well as solution of such substances as sugar and salt. By going to more and more dilute solutions, larger and larger molecules will show Newtonian behavior at a given value of shear stress.

Melts and solution of substances exhibiting high molecular weight are, as far as is known, always pseudoplastic.

A true yield value is never found in a single phase liquid. It is always associated with emulsion and slurries, in which one or more phases are dispersed as particles or bubbles in a continuous phase. The yield value is due to the interference between the dispersed particles. As the concentration of the dispersed phase is reduced, the yield value decreases and eventually approaches to zero for true liquids. Slurries showing considerable settling upon standing will not exhibit a yield value. Semi solid metals have almost been treated as the slurry which contains primary phase particles within

continuous liquid phase. Such slurry shows Newtonian flow under the low applied shear rate and non Newtonian flow behavior due to the high applied shear rate [1].

It is generally found that the flow characteristics of the continuous phase determine the type of flow observed when the yield value is exceeded. Thus the concentrated slurry in a Newtonian liquid may exhibit Bingham body properties; but, when the continuous phase is pseudoplastic, formation of a dispersed poly phase system will lead to a pseudoplastic fluid.

Non Newtonian flow is found only in colloidal and other particulate systems [71]. The non linear flow curves observed from such systems can be explained by interaction amongst particles, interaction with the continuous phase and particle deformation.

Although the preceding paragraphs briefly explain different type of fluids in general term, the followings are intended to cover precisely the type of flow within semi solid metals, SSM, and reviews the rheological behavior of different SSM slurries. Useful machines for rheological study and viscometry are introduced and related equations are developed and discussed [71].

3.2.5 Flow behavior in the semi solid metals

As described in chapter 2, semi solid metals are prepared during solidification of molten metals or by reheating of primary stocks and remelting of alloys up to temperatures above solidus where both liquid and solid are stable, mushy zone. In both cases the final slug or slurry could be enumerated as a colloidal system which contains a suspension of primary phase particles within the liquid phase. Such system is shown to behave like Newtonian or non Newtonian fluids depending upon the applied process parameters [1-3].

Semisolid metal slurries having solid fraction less than 0.6 and globular solid morphology usually exhibit two unique rheological properties; thixotropy and pseudoplasticity [2]. Thixotropy describes the time dependence of transient state viscosity at a given shear rate, while pseudoplasticity refers to the shear rate dependence of steady state viscosity. All the SSM processing techniques rely on either one of these properties or both in a single process [5]. Therefore, successful development of SSM processing technologies requires a good understanding of the rheology of SSM slurries.

The rheological phenomena in stirred SSM slurries can be divided into three groups [5, 11, 73, 75]:

(i) Continuous cooling behavior, which describes the viscosity evolution during continuous cooling at constant cooling rate and shear rate.

(ii) Pseudoplastic behavior, which describes the shear rate dependence of steady state viscosity, or shear thinning behavior

(iii) Thixotropic behavior, which describes the time dependence of transient state viscosity.

The continuous cooling gives the first insight of the effects of solid fraction, shear rate, and cooling rate on the rheological behavior of SSM slurries. In particular, it is more relevant to the practical conditions set in SSM processing techniques such as rheocasting and rheomolding. However as has been pointed out by Surey et al. [39], such experiments are more relevant to exploiting the solidification behavior rather than studying the rheology of SSM slurries.

Isothermal steady state tests lead to a more precise rheological characterisation and are a first step towards the determination of a constitutive equation. It is now generally accepted that the steady state viscosity at a given shear rate depends on the degree of agglomeration between the solid particles, which in turn is the result of a dynamic equilibrium between agglomeration and deagglomeration processes [76].

The thixotropic behavior of SSM slurries was demonstrated by measuring the hysteresis loops during a cyclic shear deformation [77]. However, such procedure is not sufficient to quantify the kinetics of agglomeration and deagglomeration processes. To overcome this shortcoming, special experimental procedures involving an abrupt shear rate jump or a shear rate drop were developed to characterise the kinetics of structural evolution. It was found that the agglomeration process dominates after a shear rate drop, whereas a deagglomeration process dominates after a shear rate jump [76].

For the semi solid slugs with high fraction solid or self stand slugs, there are other type of rheological studies which are based on keeping the shear rate constant within the bulk of a preheated sample and measuring the velocity of deformation under a constant dead weight, parallel plate compression viscometry, or deals with constant stress applied on the semi solid slugs to develop the data of strain rate, extrusion methods. Such data

can provide useful information about the viscosity of SSM materials having high percentage of fraction solid.

3.3 Effective parameters on rheology

The most important parameter to show the rheological behavior of a material is its viscosity (η). The exact viscosity of a semi solid metal alloy is dependent on a number of parameters and may be represented by the following equation [11, 76, 78]:

$$\eta = f (\overset{o}{\gamma}, t_s, T_a, \overset{o}{T}, C_o, f_s, F, h_{istory}) \tag{3-15}$$

Where η represents the viscosity, $\overset{o}{\gamma}$ is the shear rate, t_s is shearing time, T_a is the temperature of semisolid alloy, $\overset{o}{T}$ is the cooling rate to T_a, C_o is the alloy composition, f_s is fraction solid, F is the shape factor and h_{istory} is history effect. Higher solute contents and cooling rates have been found to cause more dendritic morphology and hence higher viscosities for a given fraction solid [11]. The apparent viscosity of the slurry at a particular point in time depends on its previous internal state (the history effect, h_{istory}). The internal state, which is continually changing, is described in some way by microstructure size, morphology and distribution parameters. Developing an all-encompassing model for semisolid metals is therefore considered to be a difficult task and requires details knowledge of the effect of the above-mentioned parameters on the viscosity.

3.3.1 Fraction solid

One of the most important parameters affecting viscosity of the mush is the fraction solid of the primary phase, e.g. α-Al dendrites in case of Al-Si alloys [79-81], Figure 3-4. Fraction solid at a temperature T within mushy zone may be calculated by Scheil equation [7], equation 2-2;

Three different methods have been proposed to evaluate the solid fraction within semi solid alloys [81]. Equilibrium phase diagram, thermal analysis and quantitative metallography are the proposed methods where each routes has its advantages and disadvantages and could be used as per requirements of the research program.

Chen and Fan [76] developed a microstructural model to describe the relationship between viscosity and effective solid fraction, rheological behavior, of liquid-like SSM slurries under simple shear flow.

α-Al phase formation range
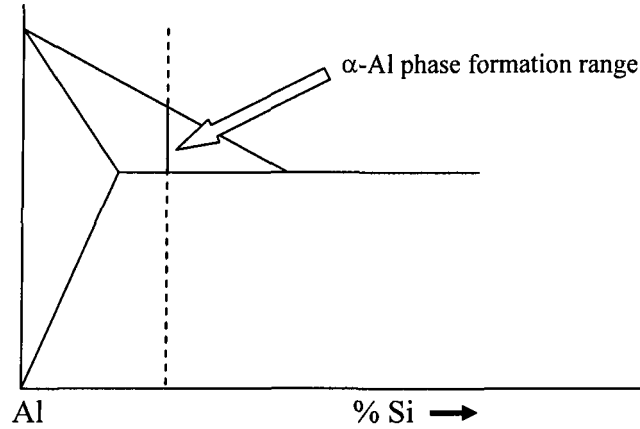
Al   % Si ➡

Fig. 3-4: Schematic representation of mushy zone and solidification range, formation of α phase, in binary Al-Si alloys

In this model, liquid-like SSM slurry is considered as a suspension in which interacting spherical solid particles of low cohesion are dispersed in a liquid matrix. In a simple shear flow field, the state of agglomeration and deagglomeration is described by a structural parameter, S, which is defined as the average number of particles in each agglomerated chunk. Through effective solid fraction, f_s^{eff}, viscosity can be expressed as a function of the structural parameter S.

$$\eta = \eta_o (1 - f_s^{eff})^{-\frac{5}{2}} \qquad (3\text{-}16)$$

The effective fraction solid is given as;

$$f_s^{eff} = (1 + \frac{S-1}{S} A) f_s \qquad (3\text{-}17)$$

where η is instantaneous viscosity, η_o is the viscosity of liquid matrix, A is a model parameter related to packing mode which decreases with increasing the packing density equal to $(3.395\text{-}4.96 f_s)$ in the Sn-15%Pb alloy case, S is a structural parameter and f_s^{eff}

is sum of the actual solid fraction and entrapped liquid fraction i.e. effective fraction solid.

Equation 3-17 indicates that the effective solid fraction is influenced by the actual solid fraction, agglomerate size, and the packing mode in the agglomerated chunks. It is interesting to note from equation 3-16 that the viscosity of semisolid slurry is a direct function of the viscosity of the liquid matrix and the effective solid fraction. The flow conditions affect viscosity only indirectly through changing the effective solid fraction.

Viscosity rises up steadily with increasing of solid fraction till the point where solid particles can no longer move easily and the already solidified segment have developed strength, i.e. a 3D solid skeleton is formed, dendrite coherency point (DCP). After DCP, viscosity increases abruptly [82]. The Dendrite Coherency Point marks the transition from mass feeding to interdendritic feeding during solidification.

In stir-based SSM processing, the DCP is postponed due to the forced convection and resulting shallow temperature gradient within the melt. The break down of dendrites due to stirring coupled with multi-directional growth of fragmented dendrites due to more uniform temperature distribution within the mold i.e. shallow temperature gradient, resulted from forced convection, encourage the formation of equiaxed grains, thus postpone the rapid rise of viscosity to higher fraction of solids.

3.3.2 Primary Phase morphology

The morphology of primary phase has a pronounced effect on the flow behavior of semi-solid-metal slurries [1-3]. It is found that dendritic structures at the same solid fraction exhibit approximately several orders of magnitude greater flow resistance than the equiaxed structures [83]. In fact the globular particles move easier over one another than dendritic ones which tend to interlock during the application of external force i.e. resistance against flow [5, 8, 84, 85]. In addition, since the beginning of SSM processing research, it was the non-dendritic structure which imparted the interesting and useful rheological characteristics, such as psuedoplastisity and thixotropy. Therefore a good understanding of the effect of particle morphology on the rheological behavior is not only

of scientific merits but also has great significance on the development of new SSM processes. At present there is neither an effective method to quantify the particle morphology nor a theoretical model to account for the effect of particle morphology on the flow behavior of metal slurries. However, there are simple models and defined parameters to describe rheological characteristics of slurries with different solid particles morphologies. Figure 3-5 shows variation of apparent viscosity for different fractal dimensions, D_f, which is defined as the parameter to characterise the morphology of solid particles where D=2.5 shows dendritic morphology and D=3 illustrate the fully globular particles in SSM slurries.

$$ f_s^{eff} = \frac{\pi}{6} \left(\frac{\pi^{\frac{D_f}{2}}}{2^{D_f} \times \left(\frac{D_f}{2} \right)} \right)^{-3/D_f} \left(\frac{V}{d^3} \right)^{(3-D_f)/D_f} f_s^{3/D_f} \tag{3-18} $$

Where f_s^{eff} is effective fraction solid, D_f is fractal dimension, V is the volume of an atom, d is the average grain size and f_s is fraction of solid. Substituting the f_s^{eff} values obtained from equation 3-18 in equation 3-16 should result the viscosity numbers based on variation of fractal dimension, as presented in Fig. 3-5. As can be seen for D_f value closer to 3, the apparent viscosity is lower [84].
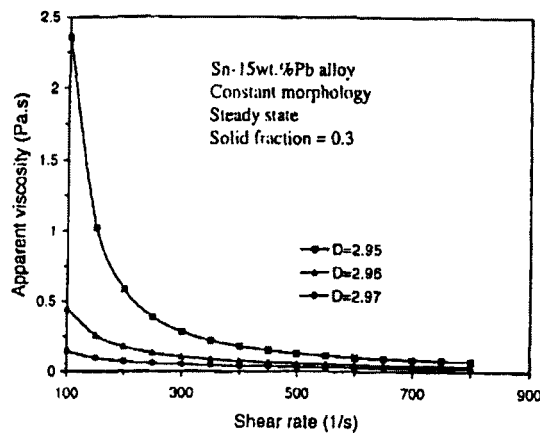
Fig 3-5: calculated steady state apparent viscosity for SSM slurries with different particle morphologies as a function of shear rate [84]

Zoqui et al. [34] also reported the effect of morphology on the rheology of SSM alloys, used rheocast quality index. Rheocast quality index, RQI, (see Eq. 2-6) indicates quasi rosette shape feature, where RQI=0.1 and shows a perfect globular shape for RQI=0.9.

3.3.3 Particle size and distribution

It is expected to have better flow in finer microstructure as there is easier movement and less collision amongst particles i.e. lower viscosity [1-3] Although Fan. et al [84, 86] believe larger size particles result in lower tendency to agglomeration and thus yields lower viscosity for SSM slurry, at least within particles size range of 10-200 μm. Uniform distribution of isolated particles within semi solid slurries was another important issue for researchers to lower viscosity and achieve the sound final components. There are always tendencies for the suspended particles in the liquid matrix to agglomerate. Such tendency could be decreased with application of external forces on the semi solid mush. The dynamic interaction amongst solid particles causes the formation of chunks, agglomerated particles, within semi solid slurries and makes the flow of mush harder. After a while under the influence of viscous forces, the equilibrium takes place between agglomeration and deagglomeration process, where the viscosity changes reach a steady state and uniform distribution of particles is observed [11, 12, 84-88]

3.3.4 Chemistry and pouring temperature

Effects of solute elements on reducing grain size and improving mechanical properties of as-cast products are well established facts [89]. The alloy chemical composition directly affects the percentage of primary phase solidifying within mushy zone.

It is generally believed that small addition of alloying elements interferes with grains growth and provides conditions required for new nuclei to form, i.e. to promote the formation of finer grains. The solutes form an enriched boundary layer ahead of the solidification front in which the actual temperature is lower than the solidification temperature, i.e., constitutional undercooling zone [7]. Constitutional undercooling is responsible for dendritic growth. In other words with controlling alloy chemical composition, i.e. the type and percentage of solute elements, constitutional undercooling

and thus the growth rate and morphology of primary phase, dendritic or equiaxed growth, may be controlled [11, 90].

Pouring temperature or superheat is one of the important parameters to affect the evolution of primary phase during solidification. Several Researchers have investigated the effect of pouring temperature on the microstructure of as-cast semi solid metals in recent years [19-22, 27, 91]. Low superheats are instrumental in establishing shallower temperature gradient within the slurry, thus encouraging equiaxed growth.

Shallow temperature gradient removes directional heat extraction from the melt and prevents the formation of dendrites within the mush [7]. This is an effective way to control the morphology of primary phase forms in the recently introduced SSM processes, since agitation of the slurry is no longer the principal factor in promoting globular morphology [23, 42-43]. Figure 3-6 shows the effect of pouring temperature on the microstructural evolution of 356 aluminum alloy [20].
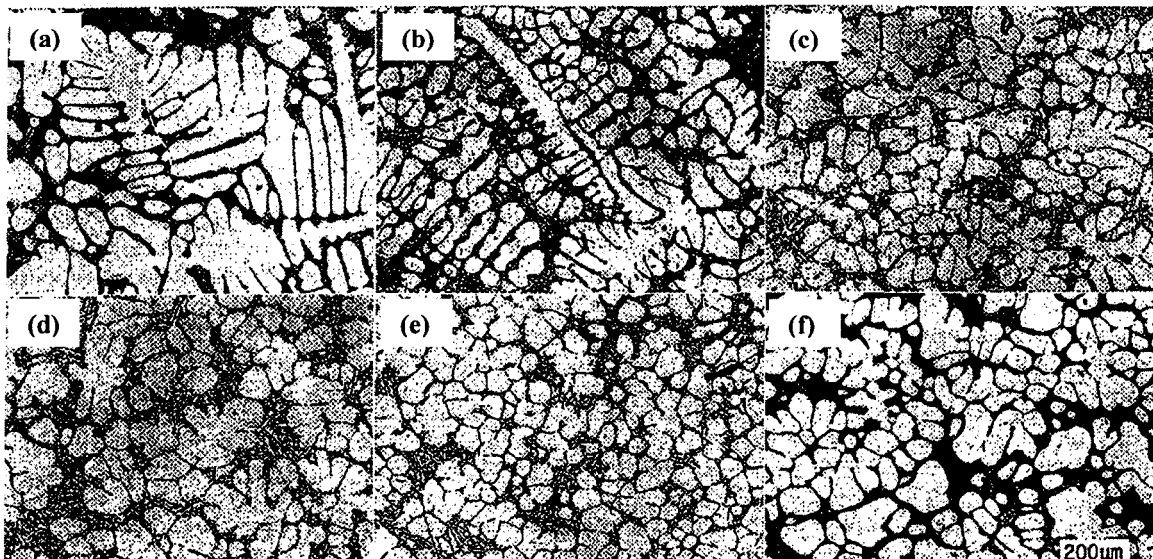
Fig. 3-6: Optical micrographs to show the effect of pouring temperature on the AlSi7Mg (a) 750, (b) 650, (c) 630, (d) 620, (e) 615, (f) 610°C [20]

3.3.5 Shear stress and shear rate (τ, $\overset{o}{\gamma}$)

One of the most important factors affecting the viscosity of SSM slurries is the applied shear force [78, 79]. It imposes laminar or turbulent flow within the slurry and induces disintegration of dendrites and the agglomeration or deagglomeration of the

dendrite fragments, i.e. the main drive for fine distribution of primary phase particles. The applied shear force could eventually establish some sort of equilibrium between agglomeration and deagglomeration phenomena within SSM slurries, "steady state", and prevent the formation of bulky particles; the main obstacle to SSM slurries flow within mold cavity. The great tendency for formation of agglomerated chunky parts due to presence of low energy grain boundaries within globular particles can be prevented by application of shear within the slurry [92]. The term "apparent viscosity" used for SSM slurries is to express the viscosity of steady sate flow and varies with shear rate and fraction of solid [5, 75], Figure 3-7.

Shear rate is a material related parameter which varies linearly with shear force in Newtonian fluids and non-linearly in non Newtonian fluids. Shear rate plays the same role as shear force where the increasing of shear rate decreases the viscosity within non Newtonian fluids. For ideal Newtonian fluids, the viscosity numbers are independent of shear rate [5, 75].

The implementation of shear force and the resulting agitation of the slurry is brought about by different means including mechanical stirring [5, 8, 51, 60, 75, 92-93], magneto hydrodynamic, (MHD), stirring [8, 33-36], ultrasonic vibration [40] or swirling of the melt as in "Swirled Enthalpy Equilibration Device-SEED" process [42, 43, 88, 94]. Application of Shear force also plays an important role during the course of preparing the primary feedstock for thixo- and rheo-casting processes, where the mechanical rheocaster or agitator, is the means by which the SSM billets are produced [35, 59].

O. Lashkari et al. [88, 94] have reported the effect of swirling on microstructural evolution of A356 aluminum alloy during SEED process. Swirling as an external applied force is believed to bring thermal homogeneity within the SSM slurry and establishes shallow temperature gradient to alleviate nucleation barrier within bulk liquid. In addition, swirling may assist in disintegration of secondary and tertiary dendrites. Such phenomenon resulted equiaxed grain growth in SSM cast billets with distinct deformation and flow characteristics [94].
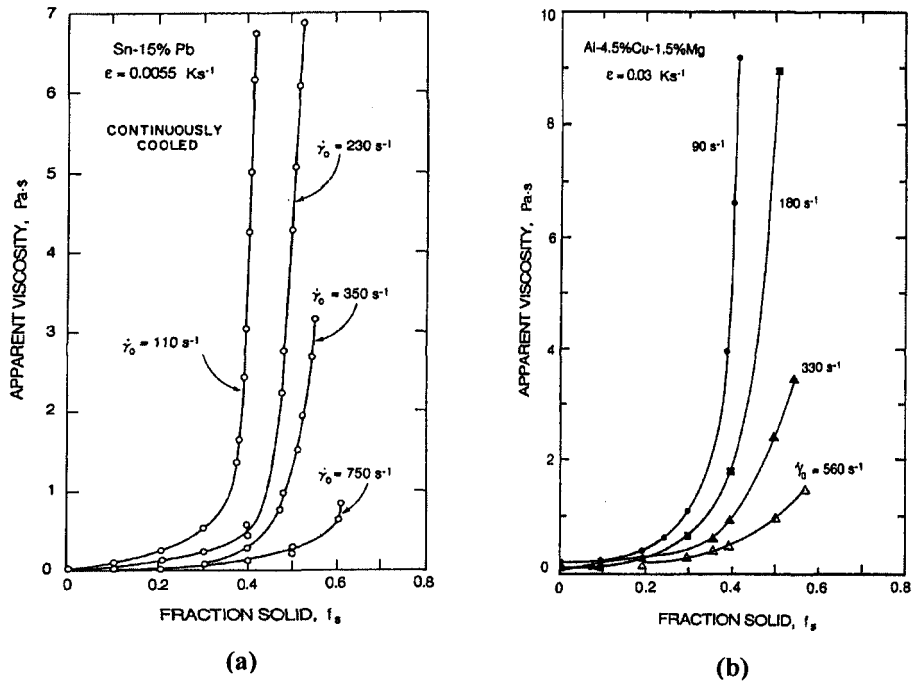
Fig. 3-7: Apparent viscosity versus fraction solid at different shear rate
(a) Pb-15%Sn [5] (b) Al-4.5%Cu-1.5%Mg [75]

P.R. Prasad et al. [95] have proposed a theoretical relationship, Eq. 3-19, between particle size and fraction solid, cooling rate and shear rate, which is in good agreement with experimental results. It is a useful tool to predict the effect of process parameters on the particle size.

$$d = \frac{0.119 D_L^{4/9}(T_L - T)^{1/3}}{C_o^{2/3} \overset{o}{T}^{1/3} \overset{o}{\gamma}^{1/3}} \left(\frac{-f_s}{(1-f_s)\ln(1-f_s)}\right)^{1/3} \left(\frac{C_L - C_o}{C_o - C_s}\right)^{2/3} \tag{3-19}$$

Where d is the particles diameter, D_L is liquid diffusivity, T_L is the liquidus temperature, T is the temperature in the semi solid region, C_o is the bulk liquid composition, C_L is liquid composition at the interface, C_S is the mean composition of the solid formed, $\overset{o}{T}$ is cooling rate, $\overset{o}{\gamma}$ is the shear rate and f_S is the fraction of solid,

3.3.6 Shear time (ts)

For constant shear rate tests, the changes of viscosity are dependent on the time of shearing. Based on the stirring time, the rheological behavior of SSM may be divided into two stages of transient and steady state. In the transient state, the viscosity is a function of time but in steady state condition, viscosity is constant and is only proportional to shear rate [71].

In more detail, the dynamic interactions amongst the solid particles result in the formation of agglomerates. Under viscous forces, collisions between agglomerates result in formation of new agglomerates of a larger size, and at the same time agglomerates also break up giving rise to agglomerates of a smaller size. At a particular time, the degree of agglomeration between solid particles depends on the nature of the system including particle size, volume fraction and the external flow conditions. At steady state, the degree of agglomeration is a direct result of the dynamic equilibrium between two opposing processes of structural build up and structural break down [86]. This condition is accessible after sufficient time from the beginning of shearing the slurry. But in transient state, which occurs at a time between the start of shearing and steady sate condition, there is not equilibrium between agglomeration and deagglomeration processes and the measured viscosity of slurry varies with time of stirring up to steady state condition. The amount of transient time is dependent on the amount of induced shear force and decreases with increasing shear force [87]. Other parameters such as solid fraction can affect steady state and transient state conditions as seen in Figure 3-8 in details.
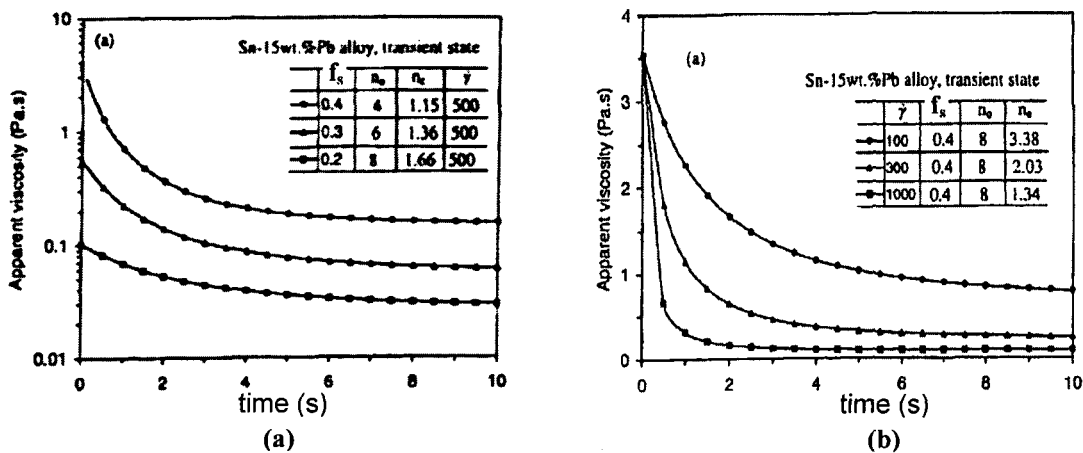
Fig. 3-8: : (a) Calculated transient state viscosity for Sn-15%Pb alloys with different solid fraction under shear rate 500/s as function of shearing time (b) with constant 0.4 fraction solid under different shear rates as function of shearing time ($\overset{o}{\gamma}$ is shear rate and f_s is fraction solid) [2]

3.3.7 Cooling rate and holding temperature and time

Cooling rate,$\overset{o}{T}$, shows the speed of heat extracted from slurry. It is well established now that the magnitude of cooling rate has direct effect on rate of solid formation or growth rate R. Increase of cooling rate causes increasing of growth rate and promotes dendritic solidification instead of cellular solidification. The formation of dendrites and subsequent dendritic skeleton increases the viscosity of slurry in comparison with the same fraction solid at lower cooling rate. Figure 3-9 shows the effect of cooling rate and temperature gradient on the solidification behavior of Sn-Pb alloy [7].

Holding temperature is the parameter to control the fraction solid in two phase region, mushy zone, of solidifying alloys. The relationship between the holding temperature and fraction solid may be determined by lever rule, Scheil's equation, thermal analysis or microscopic examination of quenched specimens. It is clear that higher fractions solid cause greater viscosity values [97] as shown in Fig. 3.7. It is also apparent that higher shear rate values are needed to compensate for greater fractions solid if the viscosity remains the same [5, 75]. Other researches have shown the fraction solids augmentation causes better spherical shaping in microstructure with better mechanical properties in final components [2].
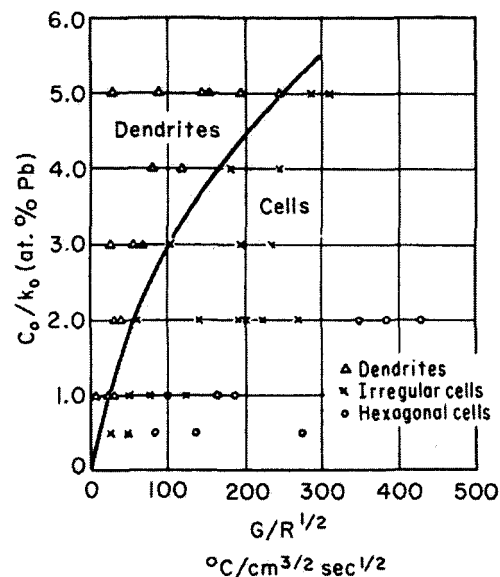
Fig 3-9: Effect of temperature gradient and growth rate in different composition of Pb on the solidification mode of Sn-Pb alloys [7]

It is not easy to differentiate between temperature and fraction solid effect on viscosity in semi solid situation due to their intertwined close relationship in mushy state. However there is an inverse relationship for temperature and viscosity, equation 3-20, where higher temperatures impart lower viscosity values. This equation is only valid for systems where there is not any phase changes due to temperature variation as for instance in polymeric materials.

$$\eta = \eta_o \exp\left(\frac{\Delta E}{RT}\right) \tag{3-20}$$

Where ΔE, η_o, R and T are the activation energy, initial viscosity, the gas constant and temperature respectively.

Holding time is another parameter which may affect viscosity due to particle growth. Particle growth in SSM slurries can take place by coalescence, Ostwald ripening or a combination of both mechanisms. The growth rate of Al-Si alloys in the SSM condition is almost invariably controlled by cube law of the type $R^3 = k_c t$ [98], where the kinetics rate constant is given as;

$$k_c = \frac{8}{9} \frac{\Gamma D}{M_L(C_S - C_L)} f(f_\alpha) \tag{3-21}$$

where $f(f_\alpha)$ is a function of the solid fraction (3.17 for globular α-Al particles in A356), Γ is the capillary constant (2×10^{-7} mK); D_L is the solute diffusivity in the liquid (3×10^{-9} m^{2}s^{-1}); M_L is the liquidus line slope (6.8K/at. %Si); C_S is the solute concentration in the solid phase (1.3 at. % Si) and C_L is the solute concentration in the liquid phase.

3.3.8 Composition (C$_0$)

As it is seen in Figure 3-9 composition of slurry has a direct effect on solidification morphology. Increasing solute elements concentration in the alloy causes enrichment of melt at the solidification front. The resulting constitutional supercooling breaks down planar interface to cellular morphology which eventually becomes dendritic with increasing constitutional supercooling at the solidification front. With the formation of dendrites, as mentioned before, the apparent viscosity of slurry increases and rheocasting in this condition becomes more difficult. In other words, rheocasting of alloys with lower solute concentration would be easier [90].

It is believed [90, 99] the higher concentration of solute in the alloy brings more rosette type feature and consequently the volume fraction of liquid trapped between the primary crystals increases. Such phenomenon brings higher viscosity within the slurry. An empirical equation has also been proposed to relate the viscosity and compositional factors [90, 99].

$$\eta = \eta_o \left\{ 1 + \frac{\alpha \rho C^{1/3} \overset{o}{\gamma}^{-4/3}}{2\left(\dfrac{1}{f_s} - \dfrac{1}{0.72 - \beta \overset{o}{T}^{1/3} \overset{o}{\gamma}^{-1/3}} \right)} \right\} \qquad \text{(Pa.s)} \qquad (3\text{-}22)$$

Where η_o is the apparent viscosity of liquid, ρ is the density of alloy, $\overset{o}{T}$ is the cooling rate, f_s is the fraction of solid, $\overset{o}{\gamma}$ is the shear rate and α and β are the values which are dependent on the chemical composition of alloy and become larger with increasing solute content.

Furthermore, alloy composition could affect dendrite coherency point, by postponing it with increasing solute concentration [82].

3.3.9 Sample size

Generally the sample size effect on viscosity is not a matter of concern if the homogeneity of temperature and shear rate distribution within the sample is maintained. Nonetheless it is preferred to perform tests on small size specimens to reduce the cost of testing, since for larger specimens more powerful machines are needed. In addition smaller specimens may render less diverse results. In rotational viscometry for example, the distance of the annular gap between outer cylinder (cup) and inner cylinder (bob). [5, 11, 75, 85] is always preferred to be as close as possible to make the shear rate distribution more homogenized within the slurry during rotation.

Parallel plate compression viscometry method [96, 100] also uses small size samples. Such matter refers back to mathematical calculation of viscosity for cylindrical samples under parallel plate compression test. Such calculation has been done for

Newtonian and non Newtonian fluid assumption. The mathematical solution is always based on the samples with h<<R to reduce mathematical complexity. In fact the term v_z, the velocity along z axis, is neglected against radial velocity, v_r and the continuity and momentum equations are solved, Appendix A. The current research project also studied the effect of sample size during parallel plate compression viscometry as given in the result and discussion, chapter 8.

3.4 Viscometry

There are several test procedures to study the visco-plastic behavior of SSM slurries. These methods are based on measuring the viscosity of slurries and are divided into two main categories depending on the fraction solid, i.e. low fraction solid up to 0.4, and high fraction solid, in excess of 0.4-0.5 [2].

3.4.1 Rotational viscometry

The simplest methods to measure the viscosity of low fraction solid slurries are the direct methods of rotational viscometry where the induced torque in the slurries is measured.

Since the introduction of viscosity concept by Newton, nearly 200 years elapsed before the first practical rotational viscometer was devised by Couette in 1890 [68]. Couette concentric cylinder viscometer consisted of a rotating cup and an inner cylinder which was supported by a torsion wire and rested in a point bearing in the bottom of the cup. This viscometer was a large device with an inner radius, R_{bob}, of 14.393 cm. and an outer radius, R_{cup}, of 14.630 cm. Couette design enabled him to calculate the apparent viscosities of non Newtonian fluids with only a small error because of the very small ratio of gap to inner radius. In Couette type viscometers, rotation of the cup while holding the bob stationary produces shear stress on the surface of the bob which are measured as torque. Figure 3-10 (a) shows the schematic of the apparatus which was used by several researchers [5, 75, 98]. There is another type of cylindrical viscometers, Searle type viscometer, which is slightly different where the cup is stationary and the bob or inner cylinder rotates and induces shear into the melt or slurry. In both apparatus, the temperature of slurry during stirring process is maintained almost constant by using

electric heating elements inside the body of the apparatus. Temperatures are controlled by using thermocouples which are embedded in different sections. Figure 3-10 (b) shows schematic of Searle type viscometer used by other researchers [8, 73, 85, 90, 99].
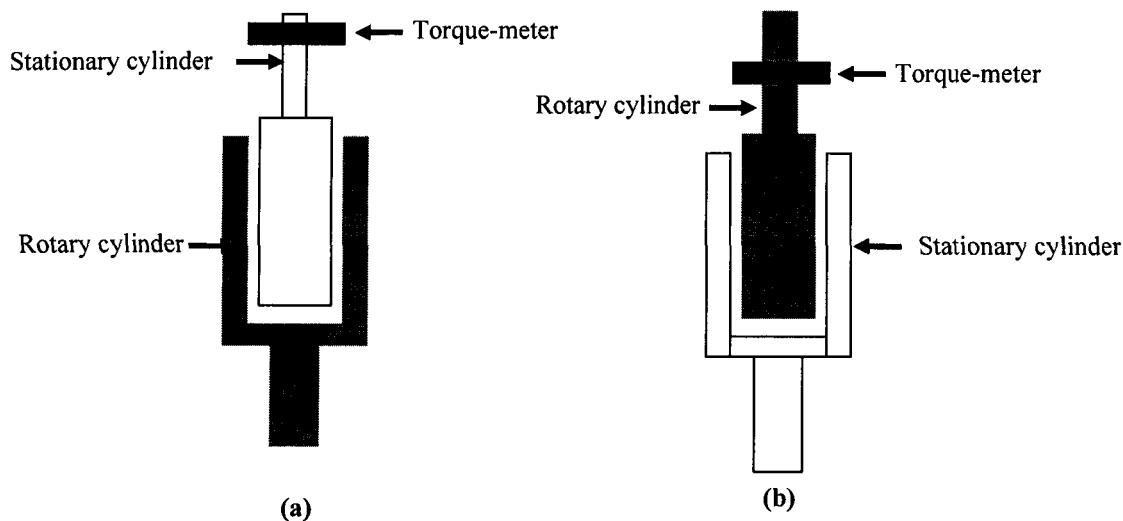
Fig. 3-10: The types of viscometers (a) Couette type with rotary outer cylinder
(b) Searle type with rotary inner cylinder

3.4.1.1 Mathematical treatments

In order to arrive at the fundamental equations for coaxial rotational viscometers, the following assumptions are made [5, 11, 75];

1) The liquid is incompressible

2) The motion of liquid is laminar

3) The streamlines of flow are circles on the horizontal plane perpendicular to the axis of rotation (i.e. the velocity is only a function of radius)

4) The motion is steady

5) There is no relative motion between the surface of the cylinders and the fluid in immediate contact with the cylinders, i.e. no slippage

6) The motion is two dimensional

7) The system is isothermal.

With such assumptions in both methods the apparent viscosity is calculated by a set of equations given below using torque data [5, 11, 75].

$$\tau = \frac{T}{2\pi r^2 L} \qquad (3\text{-}23)$$

$$\overset{o}{\gamma} = \frac{2\Omega}{r^2}(\frac{r_i^2 r_o^2}{r_o^2 - r_i^2}) \qquad (3\text{-}24)$$

$$\eta = \frac{T}{4\pi L\Omega}(\frac{1}{r_i^2} - \frac{1}{r_o^2}) \qquad (3\text{-}25)$$

Where T is the measured torque, L is the liquid altitude inside the cylinder, $\overset{o}{\gamma}$ is shear rate, Ω is angular speed of rotor, η is apparent viscosity, r_i is inner cylinder radius, r_o is outer cylinder radius and r is the actual annular gap radius. There are problems to use co-axial rotating viscometers which are for fluids whose viscosity, is related to the geometry of instrument. This is because of the change of shear rate across the gap from the region of higher stress to that of lower stress. Use of the mean rate of shear is permissible only for Newtonian and plastic fluids. Because there is no set relationship between stress and shear rate for pseudoplastic and dilatant fluids, the actual shear rate, presented at equation 3-24, at any point in the gap cannot be estimated except for extremely small gaps.

Experiments based on torque measurement are useful to investigate the dendritic coherency point during equiaxed/dendritic solidification. The coherency point is determined as the critical point where the torque increases sharply [82].

3.4.2 Parallel plate compression test

For the high solid fraction, self stand, slurries, viscosity is not generally measured by the rotational viscometers. Such slugs is more solid and can only be characterized by other methods including parallel plate compression test [50, 53, 56, 58, 94, 96, 100-103], direct or indirect extrusion [56, 104-106], indentation test, tensile test [28, 107] and cutting tests [108] are some of these methods.

The most popular way to examine rheological behavior of paste like materials is by parallel plate compression test [50, 53, 56, 100]. In this method a dead weight is simply applied on the top surface of SSM slug and its deformation behavior is investigated by analyzing strain variation versus time. The resulting strain-time graph is

further treated mathematically to calculate viscosity and characterize the rheological behavior of tested alloy. The interpretation of results obtained from such graphs can be treated differently depending on the assumption of the SSM slurries behaving as Newtonian or non-Newtonian fluids. In the case of low applied shear rates i.e. less than 0.01 (s^{-1}), the resulting graphs could be treated similar to that of Newtonian fluids [96] with the following equations to calculate the viscosity of the semi-solid cylindrical billets.

Equation 3-6 was rewritten in terms of the applied force, F, for a cylindrical sample squeezed between two parallel plates, and with the assumption of the billet not filling the space between the two plates during the course of deformation, Eq. 3-27 [109]

$$F = -\frac{3\eta V^2}{2\pi h^5}(\frac{dh}{dt})$$
(3-26)

Integrating Eq. 3-26 for $h = h_0$ at $t = 0$ and $h = h$ at $t = t$, (Eq. 3-27), and knowing the initial pressure, $P_o = \frac{Fh_o}{V}$, at the onset of deformation, the viscosity-time relationship is given in Eq. 3-28.

$$\frac{1}{h^4} - \frac{1}{h_o^4} = \frac{8\pi Ft}{3\eta V^2}$$
(3-27)

$$\frac{3Vh_o}{8\pi P_o}(\frac{1}{h^4} - \frac{1}{h_o^4}) = \frac{t}{\eta}$$
(3-28)

The viscosity is calculated as the inverse slope of a graph where the left hand side of Eq. 3-28, $\left[\left(\frac{3Vh_o}{8\pi P_o}\right)\left(\frac{1}{h^4} - \frac{1}{h_o^4}\right)\right]$, is plotted against time, (t). For Newtonian fluids, the average shear rate, $\overset{o}{\gamma}_{av}$, at any instant during compression test is calculated as [109];

$$\overset{o}{\gamma}_{av} = -\sqrt{\frac{V}{\pi}}(\frac{dh/dt}{2h^{2.5}})$$
(3-29)

Where v_x, η, V, h_0, h, F and t are deformation speed (ms^{-1}), viscosity (Pa-s), volume of specimen (mm^3), initial height (mm), instantaneous height (mm), applied dead weight

(N), and deformation time (s) respectively. Appendix A describes the mathematical solutions employed to reach the above-mentioned equations, Eqs. 3-26 to 3-29.

If the SSM billets are treated as non-Newtonian fluids, the solution to the flow equations for cylindrical sample squeezed between two parallel plates is as follows, (see Appendix A):

$$\frac{h_o}{h} = \left\{ 1 + \left(\frac{3n+5}{2n} \right) k h_o^{\frac{n+1}{n}} t \right\}^{\frac{2n}{3n+5}}$$

(3-30)

Where

$$k = \left\{ \left(\frac{2n}{2n+1} \right)^n \left(\frac{4(n+3)}{\pi m d_o^{n+3}} \right) F \right\}^{\frac{1}{n}}$$

(3-31)

Equation 3-30 is only valid for deformation under steady state condition where the engineering strain changes linearly with time. As shown in Appendix A, equation 3-30 could be further treated mathematically to include engineering strain (e) as given in equation 3-32.

$$\log(1-e) = -\left(\frac{2n}{3n+5} \right) \log t - \left(\frac{2n}{3n+5} \right) \log\left(\frac{3n+5}{2n} k h_o^{\frac{n+1}{n}} \right)$$

(3-32)

In order to calculate the values of m and n, the logarithmic of engineering strain, log (1-e), should be plotted against time, log t, and the slope of such graph and its intercept with strain axis should provide the necessary means to calculate m and n [109]. Appendix A presents the details of mathematical treatments for Newtonian and non Newtonian slurries compressed between two parallel plates.

Figure 3-11 shows schematically a parallel plate compression test machine. The current project also requires the design and construction of a large scale parallel plate compression machine [110] to characterize the microstructural evolution of SSM prepared slugs as will be discussed in experimental chapter.

Dead Weight
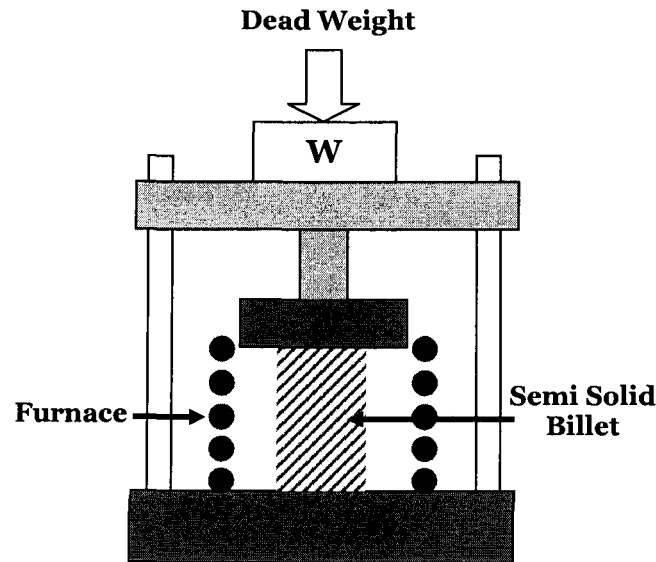
Fig. 3-11: The schematic diagram of a simple parallel plate compression test machine

Drop Forge Viscometer is a special case [53, 58] of parallel plate compression test where similar equations are used to calculate the viscosity. Such instrument is designed to generate a wide range of shear rates for viscometry tests, i.e. 10^{-5} to 10^4 (s^{-1}). Usually the high shear rate tests is performed within thousandth of second and can just investigate the transient part of the viscosity for thixotropic SSM materials. The developed equation used in such manner is given in Eq. 3-33 as a modification in Eq. 3-26:

$$m_p \left(\frac{d^2 h}{dt^2} + g \right) = \frac{-3\eta V^2}{2\pi h^5} \left(\frac{dh}{dt} \right)$$
(3-33)

Where m_p is the mass of upper plate and g is gravitational acceleration. After calculating the derivatives, the variables in equation 3-33 are known; therefore, the viscosity can be calculated as a function of time.

Sherwood et al. [111] have also developed mathematical equations to calculate viscosity of non Newtonian materials squeezed plastically between two parallel plates, where the squeezed material fills the space between two platens. Assuming "σ_f" as the friction stress in plate/work piece interface and "σ_y" as the yield stress of the material, results the following equation which governs deformation behavior of the substance during compression viscometry.

$$F = \frac{2\sigma_f \sigma_y \pi r^3}{3h_o} + \frac{\sqrt{3}\sigma_y \pi r^2}{2} [\sqrt{(1 - \sigma_f^2)} + \frac{1}{\sigma_f} \sin^{-1} \sigma_f]$$
(3-34)

Where F is total force required to compress the material, h_o is initial height and r is the radius of platens, where the squeezed material fills the space between them. The force, F, is independent of the compression rate, $\left(\dfrac{dh}{dt}\right)$, as should be expected from an analysis based upon rate-independent plasticity theory. Kolenda et al. [50] have also used similar equation (as Eq. 3-34) for evaluating the viscosity of two types of ceramic powders blended together as a ceramic paste. The obtained data indicated the ceramic paste behaving as non Newtonian materials.

3.4.3 Direct and indirect extrusion

Extrusion tests may also be used to study die fill-ability of slugs with some information on the viscosity of semi solid material. Figure 3-12 illustrates extrusion tests schematically along with related graphs [105, 107]. More experimental details and suitable theoretical treatments, i.e. mathematical equations, for such methods are accessible in the literature [38, 98, 105, 107].
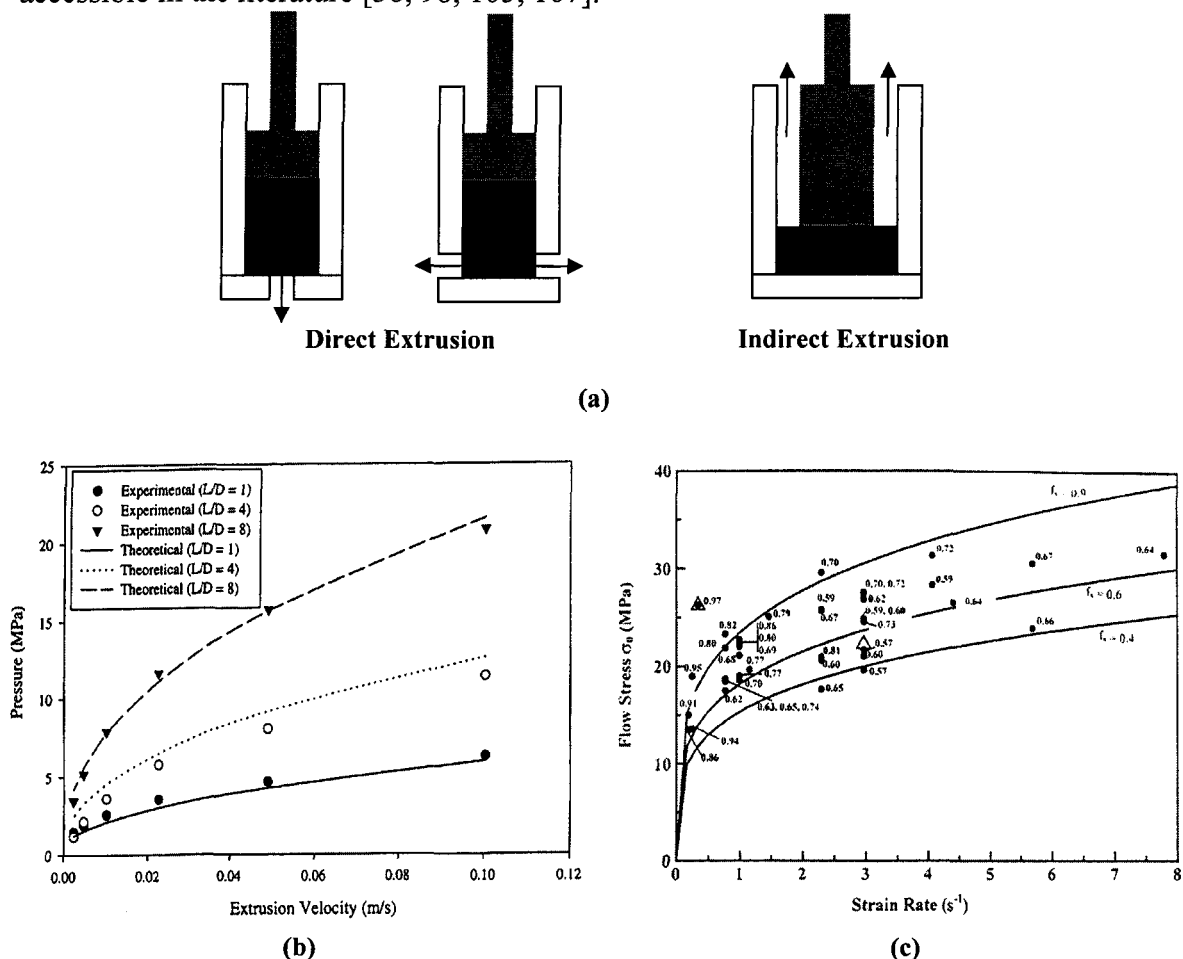
Fig. 3-12: (a) different ways of extrusion viscometry (b) Pressure versus Extrusion velocity graph, comparison of theory and experiments at different dimensions [105] (c) Flow stress versus Strain rate graph at different fraction solid [107]

Indentation test is another simple way to study mechanical properties of slugs [28]. In this method, the depth of penetration of a steel cylinder under a constant pressure in the semi solid billet is taken as an indication of viscosity of the alloy. This is a simple test and can be commercialized for on-line testing of SSM billets. Figure 3-13 shows the effect of testing parameter and fraction solid on the indenter/SSM billets interaction [28]. The following equation was used to calculate the viscosity of SSM specimens during indentation test;

$$\eta = \frac{16\pi^{3/2}[(1-\upsilon^2)F]}{6\sqrt{\pi}r\overset{o}{\varepsilon}} \qquad (3\text{-}35)$$

Where υ is Poisson ratio, F is the applied load, r is the radius of cylindrical indenter and $\overset{o}{\varepsilon}$ is the strain rate. It has been shown the psuedoplastisity behavior of Al-4%Cu alloy around 0.82-0.85 fractions solid and solid like behavior for fractions in excess of 0.85 [28].

Some researchers have also applied the tensile test method for rheological study of semi solid materials [28]. However, both of tensile and indentation tests are not suitable for fraction solid less than about 0.85 [28, 39]. The indentation test is similar to compression tests with more constraints.
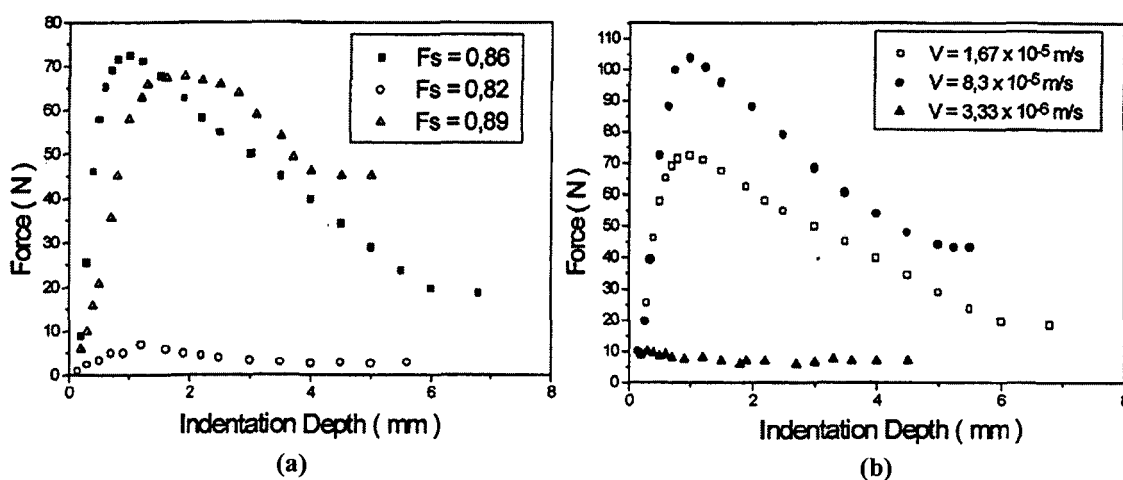
Fig. 3-13: Results of the indentation test for (a) constant penetration speeds and different fractions (b) different penetration speeds and constant 0.86 fractions [28]

Lahaie et al. [112] proposed a physical model to show the relationship between tensile strength and semi solid parameters, Eq. 3-36;

$$\sigma = \frac{\eta\,\overset{o}{\varepsilon}}{9}\left(\frac{f_s^m}{1-f_s^m}\right)^3\left[\left(1-1/2\left(\frac{f_s^m}{1-f_s^m}\right)\varepsilon\right)^{-3} + 2\left(1+\left(\frac{f_s^m}{1-f_s^m}\right)\varepsilon\right)^{-3}\right]$$ (3-36)

Thus from equation 3-36, the mechanical response, i.e. tensile strength (σ), of the semi solid body is dependent on the viscosity of intergranular liquid, η, the applied strain rate, $\overset{o}{\varepsilon}$, the accumulated strain, ε, the solid fraction, f_s, and a microstructural parameter, m, bounded by the values ½ and ⅓, corresponding to columnar and equiaxed microstructure, respectively. A similar equation has also been used by another researcher during compression rheological test [104]

3.5 Rheology Modelling

3.5.1 High shear rate tests

To date the experimental work has demonstrated a strong coupling between the slurry structure and the flow behavior under various external flow conditions [113]. However modeling works on those aspects of the behavior of SSM slurries is far from satisfactory. The existing models are difficult to relate with experiments for further understanding. The rheological models should be linked with microstructural parameters measurable metallographically, because such models are coupled with experimental investigations can result further insight into the mechanics of agglomeration and deagglomeration processes. In this section the progress made on rheological modeling of SSM slurries is briefly reviewed.

3.5.1.1 Modeling of psuedoplastisity

Joly and Mehrabian [77] used a simple power law model to interpret the shear thinning behavior observed during isothermal steady state experiments, i.e. Eq. 3-9. Following this work, other researchers [96] used power law model to consider microstructural effects and to account for visco-plastic deformation of the semi solid phase. There is another model proposed [2] to evaluate energy dissipation during viscoplastic deformation of the semi solid phase. These models are usually referred as a

power law models which are useful for engineering applications such as process simulation. They are however empirical by nature and do not address the origin of psuedoplastisity at microstructural level.

A totally different approach was taken by Fan and Chen [86] to study steady state deformation of semi solid materials. They developed a microstructural model that describes the rheological behavior of liquid like SSM slurries under simple shear flow. In this model, a liquid like SSM slurry is considered as a suspension in which interacting spherical solid particles of low cohesion are dispersed in a liquid matrix. In a simple shear flow field, the dynamic interactions amongst solid particles result in the formation of agglomerates. Under the influence of viscous force, collision between agglomerates lead to new agglomerates of a larger size and at the same time larger agglomerates also break up giving rise to agglomerates of a smaller size. At a particular time, the state of agglomeration is described by a structural parameter, n, which is defined as the average particle number in agglomerates. Through effective solid fraction (f_s^{eff}, defined as the sum of the actual solid fraction and the entrapped liquid fraction) both viscosity η and shear stress τ can be expressed as a function of structural parameter, S.

$$\eta = \eta_o \left(1 - f_s^{eff}\right)^{-5/2}$$ (From eq. 3-16)

$$f_s^{eff} = \left(1 + \frac{S-1}{S} A\right) f_s$$ (From eq. 3-17)

Where η_o is the viscosity of liquid matrix, A is constant related to the packing mode. Eq. 3-17 indicates that the effective solid fraction is affected by the actual solid fraction, agglomerate size, and the packing mode in the agglomerates. It is interesting to note from Eq. 3-16 that the viscosity of semi solid is a direct function of the viscosity of liquid matrix and the effective solid fraction. Theoretical predictions of this model is claimed to be in good agreement with the experimental results.

Under simple shear flow, the steady state represents a dynamic equilibrium between two opposite processes, agglomeration and deagglomeration. At steady state, the microstructure of SSM slurry is characterized by spherical particle morphology, uniform particle size, constant average agglomerate size, and constant effective solid fraction. The theoretical analysis shows that there is a strong dependency between the microstructure and the steady state viscosity [86]. Shear rate affects the viscosity of SSM slurries by

changing the amount of entrapped liquid between solid particles in the agglomerates, and therefore altering the effective solid fraction. The steady state viscosity of SSM slurry decreases with increasing shear rate and approaches an asymptotic viscosity, which is in good agreement with the experimental observation for Pb-15%Sn alloy. The asymptotic viscosity is only a function of solid fraction and corresponds to a microstructure in which there is no particle agglomeration [86].

3.5.1.2 Modeling of thixotropy

The modeling of thixotropic behavior has been performed using predominantly the internal variable framework where structural parameter S is normally used as a scalar measure of the degree of agglomeration in SSM slurry. The parameter S varies between 1 and 0, corresponding to the fully agglomerated state and fully deagglomerated state, respectively. The objective of such thixotropic modeling is to derive the time evolution of the structural parameter S.

Mada and Ajersch [114, 115] used this general framework to model the thixotropic behavior of A356 alloys and the effect of SiC particles on it using Eq. 3-37;

$$\tau = \eta_o \overset{o}{\gamma}(1 - S) + S\tau_o \tag{3-37}$$

η_o, is the liquid matrix viscosity without reinforcing particles. They have further developed the above mentioned equation to obtain the following equation to describe the relationship between the shear stress τ (t) at time t and the shear rate after the shear rate jump where deagglomeration processes are dominant.

$$\tau \ (t) = \tau_e + (\tau_o\text{-}\tau_e) \ exp \left\{ -\frac{\overset{o}{\gamma_f}}{a_1 + b_1 \overset{o}{\gamma_f}} t \right\} \tag{3-38}$$

Where τ_o and τ_e are the isostructural shear stress and the steady state shear stress respectively, and a_1 and b_1 are constants. In the case of reagglomeration during resting the evolution of shear stress with time at rest t_r after resuming shear is given by;

$$\tau \ (t_r) = \tau_\infty - (\tau_\infty \text{-}\tau_e) \ exp \left\{ -\frac{\overset{o}{\gamma_o}}{a_2 + b_2 \overset{o}{\gamma_o}} t_r \right\} \tag{3-39}$$

Where τ_{∞} and τ_e are the shear stresses for the fully agglomerated state and the shear stress when the shear rate is dropped respectively, and a_2 and b_2 are constants.

The structural model developed by Chen and Fan [76] has also been applied to study the transient state behavior [87] of SSM slurries under various deformation conditions. Such as isothermal shearing, transient shear at constant $\overset{o}{\gamma}$, and cyclic shearing. Theoretical prediction of hysteresis loops under various cyclic deformation conditions have revealed that the physical origin of thixotropy lies in the fact that the deagglomeration kinetics is much faster than the agglomeration kinetics with the former being a few seconds and latter a few hundred seconds. In addition the theoretical analysis also shows that, for given SSM slurry, deformation under isostructure condition always results in a constant viscosity showing no shear thickening behavior.

3.5.1.3 Modeling of continuous cooling

In order to explain the experimental results on continuous cooling of Sn-15%Pb alloy, Joly and Mehrabian [77] proposed following equation to correlate the apparent viscosity η to the solid fraction f_s

$$\eta = A \ exp \ \{Bf_s\} \tag{3-40}$$

Where A and B are shear rate dependent coefficients. This equation has also been applied to other alloys. Hirai et al. [99] has also proposed a model for the apparent viscosity in continuous cooling condition.

Nevertheless, the fact that particle morphology has the strong effect on the flow behavior of SSM slurries, the scientific understanding on this subject is limited. The specific surface area or shape factor, have been used to describe the morphological evolution of solid particles during rheological tests or SSM process. Fractal dimension has also been applied by Fan and Chen [84] to quantify the solid particles morphology, Eq. 3-19.

The final results of researchers [84], *shows under constant morphology assumption, the shear thinning effect is much more pronounced for SSM slurries with solid particles of*

lower fractal dimension, i.e. more dendritic morphology, and the degree of thixotropy increases with decreasing fractal dimension of solid particles.

3.5.2 Low shear rate tests

Laxmanan and Flemings [96] modeled the mushy materials empirically under parallel plate compression test condition. Such equation which is limited to fraction solids between 0.3 and 0.6, expresses inter-relationship between viscosity and fraction solid. The authors reported the empirical equation is in good agreement with experimental results within low shear rate ranges.

$$\mu = a\exp(bf_s)\dot{\gamma}_o^{(cf_s+d)} \tag{3-41}$$

Zoqui et al. [34] have also proposed other empirical equation relating viscosity; shear rate and morphology (Rheocast Quality Index, RQI) of the particles, although they have validated such equation just for A356 alloy within low shear rate ranges.

$$\mu = (2.37 + 53.6544e^{(-5.62RQI)})\dot{\gamma}_o^{(-0.5)} \times 10^5 \tag{3-42}$$

Where RQI=0.1 for quasi rosette morphology and RQI=0.9 shows a perfect globular structure.

CHAPTER 4

EXPERIMENTAL PROCEDURES
AND METHODOLOGY

CHAPTER 4
EXPERIMENTAL PROCEDURES
AND METHODOLOGY

4.1 Introduction

The current study is concerned with semi solid metal processing of Al-Si alloys in the framework of a newly patented SSM process, the swirled enthalpy equilibrium device, SEED; where the pouring temperature and swirling intensity as the main process parameters affecting the rheological properties of the SSM prepared billets. These parameters were closely investigated for the conventional cast samples and the SEED prepared billets, in the current research.

4.1.1 Conventional casting

Among the different techniques available for SSM processing, casting at low pouring temperature is regarded as the least expensive alternative to produce thixo/rheo billets. It not only causes the formation of equiaxed grains but also reduces casting defects by lowering gas and shrinkage porosity. The concept of low pouring temperature attracted equally the attention of many researchers and commercial producers by adapting this concept in SSM processes as discussed in chapter 2.

Therefore close control of casting conditions, such as pouring temperature, has been considered to produce the desired microstructures, studying its effect on the viscosity of the SSM billets prepared by conventional casting.

Figure 4-1 shows schematically the sequence of the style test to investigate the effect of pouring temperature on the microstructure of SSM alloys.
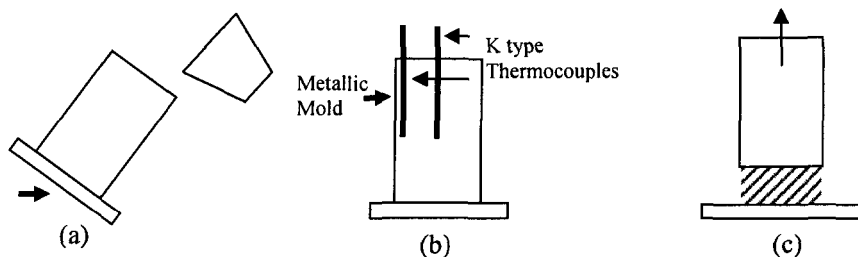
Fig. 4-1: Schematic diagram of the experimental set up;
(a) pouring process (b) resting up to a defined temperature in the mushy zone state, and (c) removal of the billet

4.1.2 SEED process

SEED is a newly developed semi-solid metal processing route, patented by ALCAN international. It is based on off-center swirling of molten metal in a metallic mold within mushy zone, up to a pre-determined fraction solid, and draining of the remaining liquid to reach distinct fractions solid, Figure 4-2. The as-cast billets maybe used as feedstock for high pressure die casting. Amongst different methods of direct semi solid processing, SEED has a distinct feature i.e. swirling, to initiate uniform temperature distribution within the bulk liquid in the mold. The intensity of swirling is an effective parameter in generating a range of structures from dendritic to globular. Pouring temperature has also a distinct effect on microstructural evolution of SEED prepared billets.

(a)

(b)
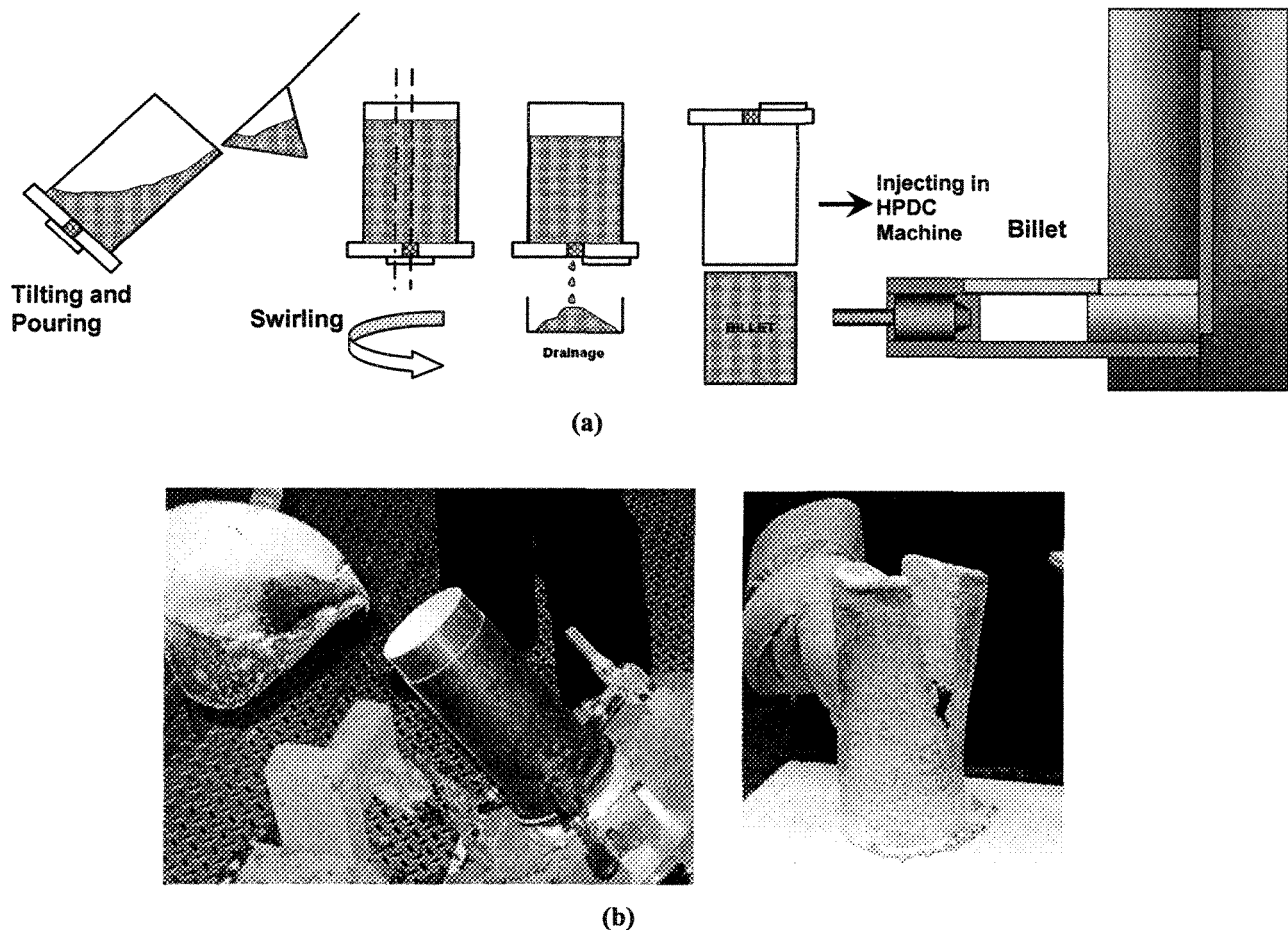
Fig. 4-2: (a) Schematic of SEED Process and high pressure die casting machine,
(b) The actual SEED system and the prepared billet in our laboratory

4.2 Process parameters

As described above SEED is based on two basic parameters, Swirling Intensity and pouring temperature. Manipulation of each parameter brings variety of morphologies within the SSM alloy microstructure. Regarding to the main aspect of the current study (rheological behavior of SSM Al-Si alloys) and close interrelationship between morphology and flowability of matters, these two principal factors were changed to find out the optimum conditions of flow ability for the SEED prepared SSM billets.

Pouring temperatures have been changed amongst 615, 630, 645, 675 and 695°C whilst the swirling intensities have been selected amongst "No swirling", "Low swirling intensities" and "High swirling intensities".

4.3 Melt preparation

The main alloys used in this research are Al-Si binary alloy and A356 commercial alloy. The Al-Si binary alloy was prepared using 99.99% pure aluminum ingots mixed with commercial purity silicon chunks. A356 commercial alloy has been obtained directly from ALCAN. As per requirement of each test, 2, 1.8 or1.2 kg of the ingot were melted in a mica wash coated silicon carbide crucibles using an electric heat resistance furnace. After preparation of the melt the grain refiners and modifiers, per requirement of the test, were added being pursuit by degassing. Degassing process was carried out separately inside each crucible using a graphite lance of 1 inch diameter and by the Argon inert gas by the rate of 0.14 m^3/h for 10 minutes. The temperature of liquid aluminum was set always between 700-710°C just before degassing and was controlled again by a k-type thermocouple just before taking the crucible off.

4.4 Chemical analysis

Specimens for chemical analysis were cast in the standard mold to produce disks of 56 mm diameter and 10 mm thick. The surface of each disk was machined out before being sent to ALCAN-ARDC for optical emission spectrographic analysis. About 6-8 points were analyzed on each disk using THERMO ARL-4460 and averaged to give the chemical composition of the alloys. The standards used in each analysis are manufactured by ALCAN specifically for alloy A356 series. The standards were 356.2-AN and 356.2-

CAK and the reported precision is about 1% depending on the quantity of the elements in the alloy. Table 4-1 shows the chemical analysis of all used alloy in this research.

Table 4-1: Chemical analysis of the melts (wt%)

	Si%	Mg%	Fe%	Mn%	Cu%	Ti%	B%	Sr%	Al%
Al-Si	7.54	0.000	0.00	0.000	0.002	0.000	0.000	0.000	bal.
A356						0.0058	Nil	Nil	
A356 Grain Refined	6.5-6.75	0.36-0.4	0.07-0.08	0.002-0.003	0.001	0.06-0.07	0.010-0.014	Nil	bal.
A356 Modified						0.0058	Nil	0.017-0.018	
A356 Combined						0.06-0.07	0.010-0.014	0.015-0.018	

4.5 Sample preparation

4.5.1 Conventional casting

For conventional casting, where there is no swirling and draining like SEED, about 1.8kg of prepared melt was poured into a cylindrical refractory coated metallic mold of 75 mm diameter and 200 mm long at different superheats, ~ 0-80°C, i.e. 615-695°C. In all experiments, the mold was tilted to reduce turbulence during pouring. Figure 4-1 shows schematically the experimental setup. Two K-type thermocouples were also installed at the mold center and near the wall with their tips at 80mm from the bottom of the mold (Fig. 4-1b) to monitor temperature distribution of the bulk liquid during solidification. The billets were taken out of the mold while still in the mushy zone and either quenched quickly in cold water or transferred into the parallel plate compression viscometer to characterize the microstructure of the billets. The quenching temperature was registered around 595°C, solid fraction of 0.33, for these series.

In order to confirm the reliability of the viscosity values obtained for the large scale billets a series of small size discs were prepared from the water quenched conventional billets as discussed in chapter 8. The above-mentioned billets were

sectioned off transversely at the middle to make a disk of 75 mm diameter and 15 mm thick. These disks were then machined to produce three small disks of 24 mm diameter and 10 mm thick. These discs were placed in a squeezing flow viscometer apparatus, designed and constructed at "Ecole Poly Techniques de Montreal", and reheated to 595°C before being deformed axially. The total reheating time was 15 minutes.

For further rheological studies, 1.2 kg of molten alloy was poured at temperatures of 630 and 675°C to produce the billets with globular and dendritic morphologies at smaller height. The quenching temperatures were registered around 595, 590 and 585±1°C for different solid fractions of 0.33, 0.4 and 0.46 respectively. These billets were used to study the possible correlation amongst fraction solid, shear rate and viscosity as discussed in chapter 7.

4.5.2 SEED process

Two kilos of A356 alloy ingots, Table 4-1, were melted in an electric resistance furnace and degassed with Argon as mentioned before. After degassing, the alloy was poured into the same cylindrical refractory coated steel mentioned for conventional casting, Fig 4-2a. The pouring temperature and swirling intensity varied between 630-695°C and no swirling to high swirling intensities respectively. The mold was initially rotated off-center at different speeds for a specific time, stopped and left to rest for certain duration before opening its bottom enclosure to drain the remaining liquid. However the total process time did not exceed 100 seconds. In all trials, a 0.8 mm diameter thermocouple (K-type) was positioned within the mold centre at a distance 80mm from its bottom to register thermal data. After drainage, i.e. the end of process, the semi-solid slug was quenched in cold water. The billets temperature at the time of quenching varied between 591-600°C depending on the melt temperature at the time of pouring. The microstructure of these billets was characterized using parallel plate compression viscometer as detailed in chapter 6.

In another set of rheological test of the SEED billets, the 1.4 kg of the melt was poured into the same mold at 695°C and swirled at different intensities to produce billets

with different microstructures but similar fraction solid. The final billet temperature was registered at 599±1°C with fraction solid of 0.27 according to Scheil equation. Considering the liquid decanting up to 25% at this temperature, the fraction solid increased to 0.36 according to the following calculation;

$$f_s(after - decanting) = \frac{pri(f_s)}{pri(f_s) + [pri(f_l) - decanted(f_l)]} = \frac{0.27}{0.27 + [0.73 - 0.25]} = 0.36$$

These samples were utilized to establish an empirical relationship amongst morphology (average aspect ratio), shear rate and viscosity, as discussed in chapter 7.

4.6 Equipments for rheological tests

This section introduces the new designed parallel plate compression test machine capable of quality rating of the commercially prepared semi solid slugs. Generally such machine is used in laboratory scale to test the small size disks of 20-30 mm diameter and 10-15 mm thickness. But, industrial requirement for quality rating of the SEED prepared billets of 75 mm diameter and ~ 140 mm height justified the fabrication of a larger scale parallel plate compression test machine. The following section explains the specifications and capabilities of the in-house designed and constructed parallel plate compression test machine used in this study along with the small scale squeezing rheometer used for small discs. It may also be as an on-line quality check tool for Slurry-on-Demand, (SoD), cast houses.

4.6.1 UQAC Parallel plate compression viscometer

Figure 3-11 shows schematically a simple parallel plate compression test machine. It comprises the dead weight, semi solid billet, guide shafts, and the resistance heating furnace. Dead weight is applied on the top of the billet surface by a platen guided trough two/four straight vertical axis. The billet is kept inside a furnace to keep its temperature constant during the course of compression test. The resulting strain-time graph, obtained by registering the displacement of the top platen with time, is treated mathematically to calculate the viscosity of SSM billet. The viscosity is then compared with known viscosity values for billets with dendritic, rosette and globular structure to characterize the structure of the as-cast SSM billet.

The actual fabricated machine can introduce a variety of dead weights, ranging from 1 to 100 kg, onto the billet and could even be increased to 250 kg capacity due to the design of the machine frames. Figure 4-3 shows photographs of the actual machine designed at the University of Québec at Chicoutimi. It consists of four main sections.

1- Pneumatic weight motion control

2- Axle of weight variation

3- Eight roller bearings to control the straightness of motion

4- A cylindrical resistant heating furnace to keep the temperature of billet constant during the course of each test

The installed pneumatic system can carry up to 300 kg weight. This system is controlled by a small switch which changes the motion of weight upward or downward. There are two main switches to allow the operator to move slowly or quickly. Slow motion is useful for introducing the force on the top of the billet at the beginning of the test and the quick motion is used for sudden introduction of force onto the billet. In fact the main part of test will get started after quick releasing of the pre-determined force on the top surface of the billet. Figure 4-4 shows the pneumatic section of the machine.

The axle for the dead weight is placed on the top of the machine. This axle is continued down to the top surface of the furnace compartment. At this point the amount of dead weight can be changed to see the effect of different shear rates on the deformation behavior of the billet and the resulting viscosity number. The magnitude of the dead weight is changed here by moving a plug up and down. The machine is capable of introducing 1kg to 100 kg forces. Figure 4-5 shows the dead weight section.
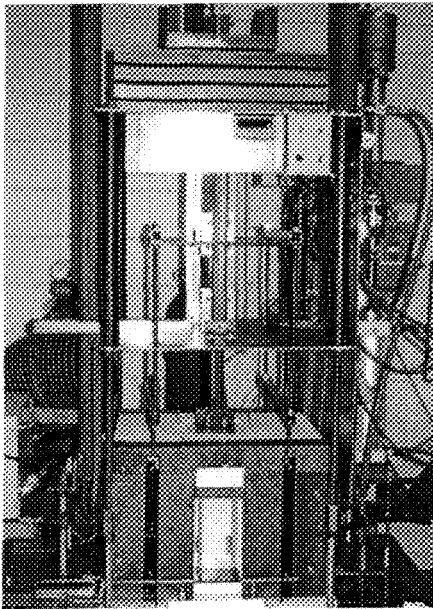
Fig. 4-3: An overview of the fabricated machine
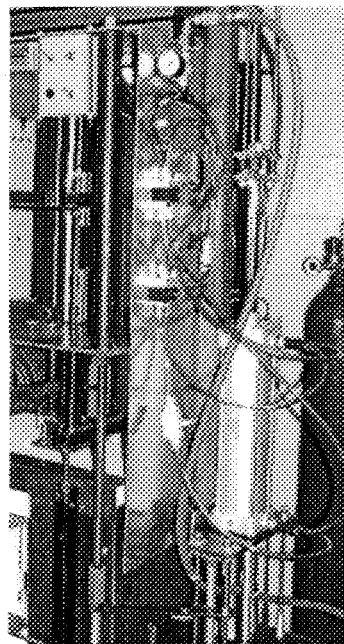
Fig.4-4: Pneumatic section of the machine and control switches

Pulleys

Counter weight
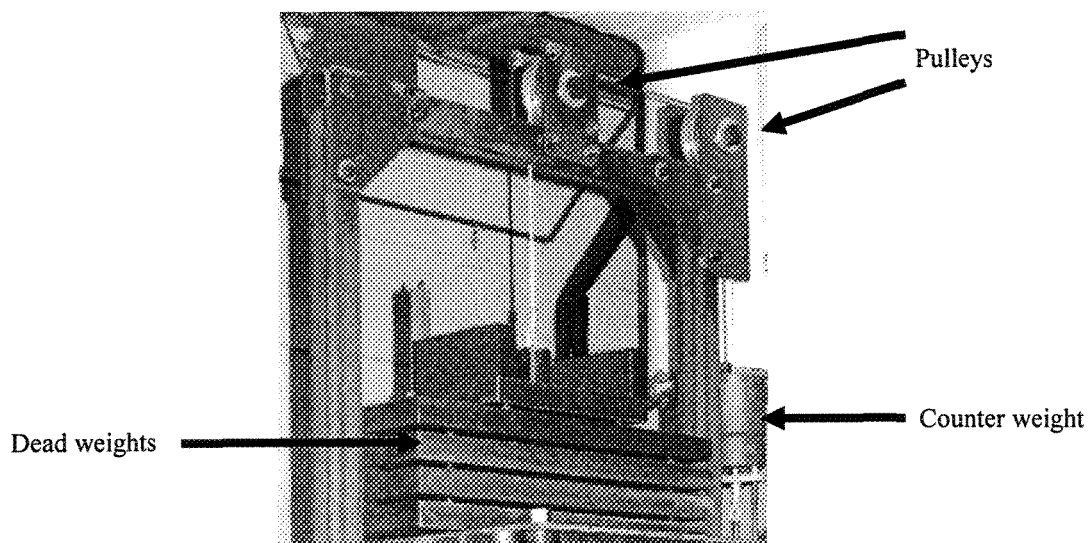
Dead weights

Fig.4-5: Dead weight section

The third main section of the machine is the bearing part where the extension of weight axle passes through this section. There are eight roller bearings installed on two vertical parallel rails to keep the axle motion straight. This is the most important part of the machine and defines the precision of measurement and keeps the stability of vertical motion during the test. Along with the central axle, a potentiometer of 0-255 mm displacement capacity, with precision of ± (0.1-0.2) % full stroke, is installed parallel to

the axle. The displacement values are recorded using a data acquisition system measuring the variation in the billet height during the test.

The fourth section of the machine is a cylindrical resistance heating furnace, Figure 4-6. The furnace is to keep the billet temperature constant during the rheological tests. It is equipped with two quartz heat resistant observation windows for monitoring the billet deformation from the front and back of the furnace. Two thermocouples (type K) were positioned within the furnace to control the hot zone temperature. The furnace is designed to heat up to 650°C having a temperature precision of ±2°C. The central axle of the machine, the moving anvil, is bolted to a refractory alumina plate. This plate enters into the furnace and touches the top surface of the slug with close tolerance to fully insulate the furnace from surrounding environment once the test is in progress.

Furnace controller

Entrance door with heat resistant quartz window

The chariot which carries the slug into the furnace
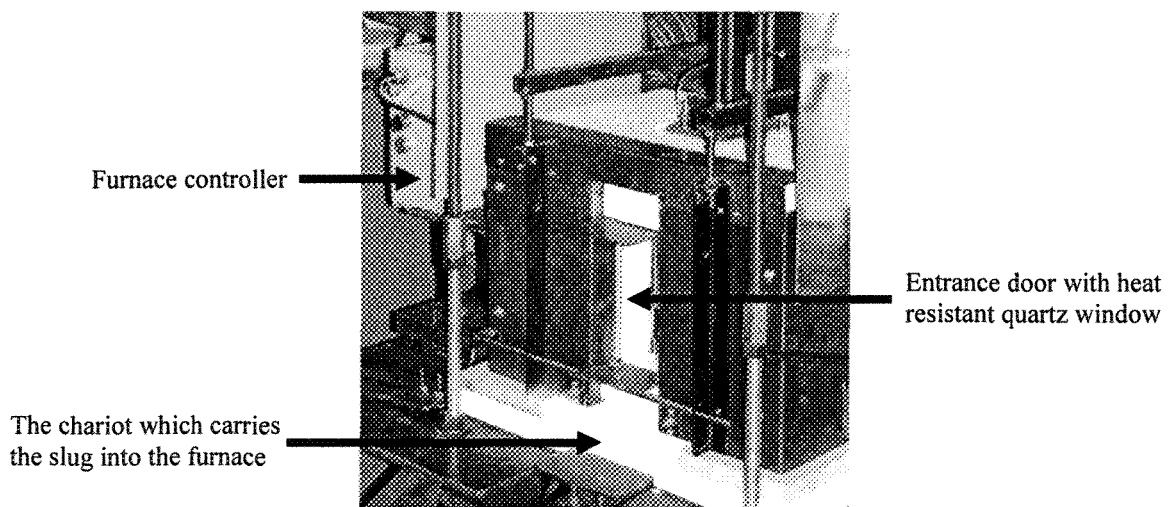
Fig.4-6: Circular heat resistant furnace

As it is seen in Figure 4-6 the bottom side of furnace consists of a sliding chariot. Before commencing a test the chariot is taken out from the furnace and can be tilted up to 90 degrees. The prepared slug along with the mold is put on the surface of the chariot and tilted back ready to enter the furnace. The mold is withdrawn and the chariot with the billet on its surface is pushed into the furnace quickly. The anvil carrying the dead weight is moved down slowly to touch the top surface of the SSM billet and released

quickly after temperature homogenization inside the furnace. This process takes around 30 seconds to be completed.

The applied dead weight is transferred into a data acquisition system, a National instrument data acquisition unit, SCXI-1102, via a load cell with 300 kg maximum capacity and <0.02% precision installed under the chariot. The load cell indicates the actual applied force which may be slightly different to the selected dead weight at the top due to friction or any other factor. Each rheological test depending on the amount of force takes around 2-8 minutes. The variations of billet height and applied load are registered against time and fed into the lap top computer to plot the strain-time graph. The strain-time graph is further treated mathematically using appropriate equations, Eqs. 3-26 to 3-32, to calculate viscosity number of the semi solid billet.

4.6.2 École Polytechnique de Montréal squeezing flow rheometer

This machine comprises almost the same features described for the large scale compression test viscometer, including counter weight axle, roller bearings and two metallic platens, provided for the application of 100-1000 g deadweight. Figure 4-7 schematically shows this simple squeezing flow rheometer. The furnace is the actual metallic platens with embedded heating elements at a depth of 1 mm below the surface. The small disc is placed between these two platens and reheated up to the mushy zone while the specimen is in contact with the platen without any applied load. Both platens are surrounded by refractory plates to ensure temperature uniformity during reheating. The deadweight is applied by putting small weights just on the top of the upper platen as schematically shown in Figure 4-7. The resulting instantaneous height is registered against time using a data acquisition system. The metallic platens are able to cool down rapidly using a water circulation system embedded within the platens. When the deformation of test piece is completed, water circulation is opened to quench the specimens.
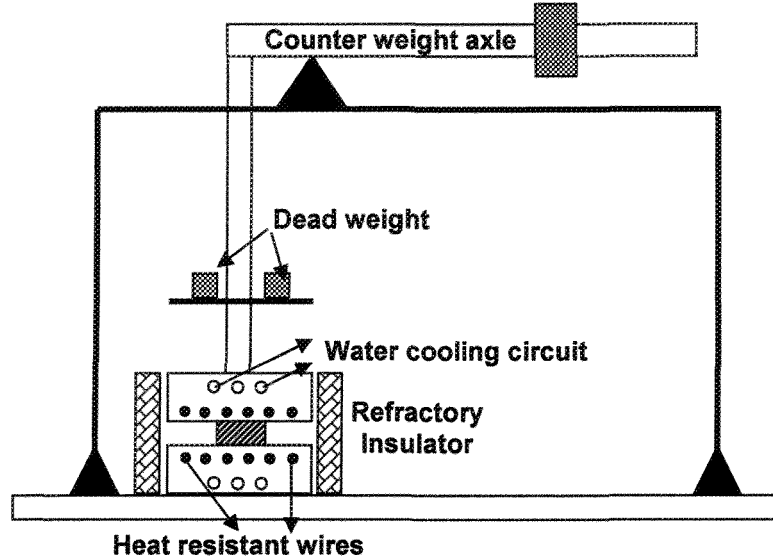
Fig. 4-7: Schematic diagram of the laboratory scale squeezing flow rheometer

4.7 Test Procedure

The prepared billets as the semi solid matters were transferred and compressed uniaxially in a parallel plate compression test machine. The metallic mold containing the SSM billet was handled into the press bed, a mobile chariot, and was situated on the refractory plate of press bed. The chariot was then tilted back and the mold was drawn upward. The free stand SSM billet was transferred within the furnace. The dead weight is applied smoothly up to the top surface of the samples. The test was delayed for 30 seconds to reach the equilibrium thermal condition within the furnace. Then the whole deadweight was applied abruptly on the samples. For the small discs, the prepared samples placed between two platens of squeeze flow rheometer, Figure 4-7. The counter weight axle was balanced to reach the point where the platens are tangent to the samples. The discs were reheated up to the temperature of 595°C for a certain period, 15 minutes in this case, and deformed under different initial applied deadweights. Each compression test took around 2-8 minutes depending on the test condition. The variation of height versus time was registered through the data acquisition system. Further calculation and measurement of engineering strain and viscosity were done upon this primary data. Figure 4-8 shows the SSM prepared billets after deformation for different morphologies,

where the applied pressure kept constant, quenched quickly once taking out of the furnace.
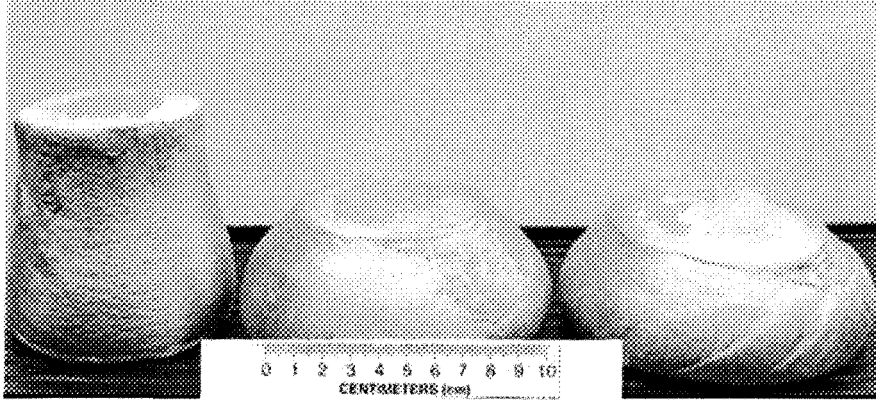
Fig.4-8: Billets after deformation in parallel plate compression test machine

4.8 Microstructural analysis

For both SEED and conventional cast samples, the billets were quenched once the process ends and were used for microstructural studies. The microstructure of the billets was examined on metallographic specimens prepared from regions between the center and mold wall at 80mm from the bottom of each billet. For the deformation tests the as-deformed billets were taken out of the furnace and quenched rapidly in cold water. The microstructure is examined on the regions showing maximum strain. Figure 4-9 illustrates the typical deformed area which were studied during metallographic procedure. For the small discs, the samples were quenched directly between the two water cooled platens of the squeeze flow rheometer, sectioned transversely and prepared conventionally for microstructural analysis. It has to be emphasized that the microstructure was examined on the region with maximum deformation between the center and the edge of the discs, similar to what has been done for seed and conventional billets.
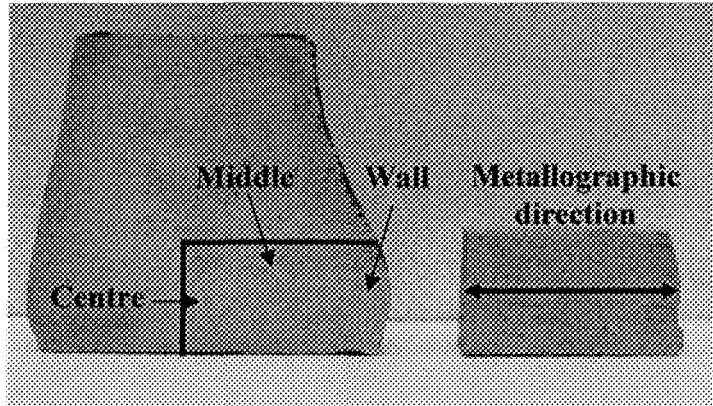
Fig. 4-9: Prepared Metallographic
samples after Deformation

4.8.1 Metallography

All metallographic specimens were prepared conventionally down to 0.05 μm by silicon abrasive solution for microstructural analysis. The samples were chemically etched by HF 5% solution for 30 seconds. Nikon ME 600 optical microscope, Figure 4-10a has been used to see the microstructure of α-Al phases, magnifications of X50 and X25. The system was interfaced to PC through the color video camera Sony DXC-950P, Figure 4-10b. All required photos are taken in black and white format and presented in the next chapters in order to confirm the morphological aspect related to the rheology.

(a)   (b)
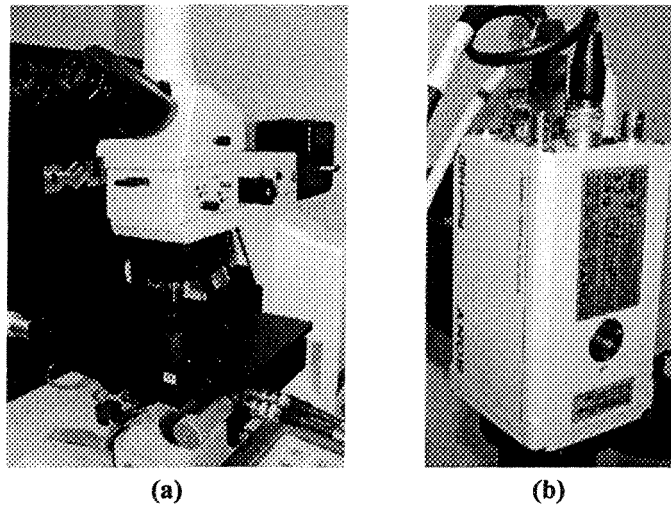
Fig. 4-10: (a) Microscope Nikon ME600 (b) Color Video Camera Sony DXC-950P

4.8.2 Image analysis

A Clemex Image analyzing unit was employed to determine the evolution of primary α-Al phase through measurement of different parameters;

- *Aspect ratio:* longest / shortest feret diameters,

- *Percentage of Aspect ratio more than 2:* number of particles in the structure with aspect ratio more than 2 over all number of particles detected by image system

- *Equivalent circular diameter:* diameter of the smallest line circled around an isolated particle

- *Number Density:* number of primary α-Al particles per unit area

- *Area, A to perimeter, P ratio:* is proportional to inverse of surface area per unit volume, S_V, The lower value of A/P is an indication of more isolated and finer α-Al particles

- $S_v : \dfrac{4}{\pi}\dfrac{P}{A}$, Where, S_v is specific volumetric surface of the particles (an estimation of 3D), P is the perimeter of the liquid-solid interface and A is the total area of primary particles

- *Sphericity:* $\dfrac{4\pi A}{P^2}$ Where A is total area and P is perimeter of liquid-solid interface. The closer the value of sphericity to one (1), the higher the globularity of the particles

For image processing of the resulted microstructure, a total number of 85 randomly selected fields were automatically analyzed, using image analysis system with the total measured area of 255 mm^2 per specimen. The obtained results of image analysis were attributed to the flow behavior of SSM prepared billets during parallel plate compression test.

CHAPTER 5
RESULTS AND DISCUSSIONS

MICROSTRUCTURAL CHARACTERIZATION - METALLOGRAPHY

CHAPTER 5
RESULTS AND DISCUSSIONS
MICROSTRUCTURAL CHARACTERIZATION –
METALLOGRAPHY

5.1 Introduction

Two casting methods, Conventional casting and SEED process, as discussed in chapter 4, were employed to produce different morphologies for primary α-Al phase in A356 alloy. The former, which is simply pouring the melt in the mold and cooling in air to predetermined temperature before quenching in water, affects the microstructure through variation of pouring temperature and thus temperature gradient while solidification proceeds. The latter, as a new patent of ALCAN international for semi solid casting, changes the morphology by introducing rotation into the melt while solidification takes place. In order to investigate the morphological evolution due to the effect of different process parameters, pouring temperature and swirling intensities, the SSM billets prepared by both methods and studied in detail. The results are presented for the Conventional casting and SEED process respectively.

5.2 Conventional casting

Conventional casting is one of the approaches in the current research, where an effort was made to produce different morphologies of primary α-Al phase by variant pouring temperatures. The resulting microstructural evolution, studied by image analysis, is given in this chapter while the related rheological behavior due to different morphologies is presented in the next chapters.

5.2.1 Microstructure

The effect of different pouring temperatures of 615, 630, 645, 675, and 695°C, superheats of ~ 0-80°C, are investigated in collaboration with another Ph.D. student, Sh. Nafisi. The alloy was cooled in air down to 593±2°C and quenched in water to room

temperature. Figure 5-1 represents the cooling curves of the liquid near the mold wall and the center accordingly. There are two different cooling regimes for the wall and center of the mold at the early stages of solidification which eventually reaches to the uniform cooling rates across the billet when solidification proceeds further. The melt temperature at the center is always greater than the mold wall immediately after pouring the melt due to mold chill effect. The following distinct regions are recognized on the cooling curves presented in Figure 5-1:

- Segment-I; the maximum temperature difference between the wall and center of the cast billet, seen at the beginning of solidification.

- Segment-II; part of the primary α-Al phase transformation time placed between the segment I and the point where a uniform cooling rate is established. This is labeled the "metastability period", since the bulk liquid has not yet reached thermal equilibrium.

- Segment-III; the time during which uniform cooling is achieved before quenching time. This is named the "stability period", due to uniform and steady state cooling rate across the bulk liquid.

If the cooling curves in Figure 5-1 are compared to one another it is clear that the maximum temperature rise near the mold wall immediately after pouring occurs in the billets with the lowest pouring temperature, 615°C, which is almost ~10°C in contrast to ~2°C and less than 0.5°C for 645 and 695°C respectively. Such temperature rise may be explained in terms of the released latent heat of fusion at the vicinity of the mold wall resulting from copious nucleation of the primary phase in the bulk liquid. It may also be due to rapid heat flow throughout the melt due to large temperature difference, segment I, established at the early stages of solidification. The magnitude of segment-I is plotted against pouring temperature in Figure 5-2, where there is an inverse relationship between the pouring temperature values and the magnitude of segment I which may be regarded as the driving force for the heat flow across the bulk liquid. Its reduction prolongs the time required to reach to uniform cooling rate within the mold. The metastability period increases while pouring temperature increases, Figure 5-2.

The optical micrographs shown in Figure 5-3 clearly illustrate the effect of pouring temperature on the resulting microstructure. There are different α-Al morphologies of dendrite, rosette and globule depending on the employed pouring temperatures.

According to the above-mentioned observations, two hypotheses proposed to explain microstructural evolution and justify the formation of fine and globular structure, Figure 5-3e. They are based on either nucleation or growth process as the dominant factor on the formation of the primary α-Al particles [27]. It is believed that both hypotheses are active, but in order to identify the main mechanism, further solidification tests are required which is beyond the scope of this research program.

5.2.1.1 Nucleation-based hypothesis

Big bang or copious nucleation is the obvious phenomenon of the highly undercooled melt where a large number of nuclei form near the mold wall at low pouring temperature to reheat the bulk of liquid with the released latent heat of fusion. However as it could be seen in Figure 5-1 the released latent heat of fusion even at very low pouring temperature is not sufficient enough to remelt the primary nuclei, Figure 5-1a, or increase the total heat content of the liquid bulk. It is believed that the higher nucleation frequency is responsible for the greater temperature rise near the mold wall at the lower pouring temperature and thus the shorter times for the metastability period. The central liquid solidifies in normal manner, but comprises the floating nuclei coming from the wall due to fluid flow and natural convection. Decreasing the pouring temperature, results in lower heat content of the melt and increasing the probability of the nuclei to survive. This is assisted by the uniform and multi-directional cooling, due to the geometry of the mold-cylinder, promoting the formation of fine grained equiaxed as-cast structure as clearly detectable in Figure 5-3e for 615°C pouring temperature.

5.2.1.2 Growth-based hypothesis

The growth characteristics of the primary nuclei also have an important effect on the formation of fine grained equiaxed structure at low superheats. It is believed that the rapid heat flow towards the mold wall at low pouring temperature of 615 °C, Figure 5-1a,

is the result of large temperature gap established between the wall and center of mold at the early stages of solidification. In other words the molten alloy near the mold wall could act as a heat sink. Since the mold coating coupled with resulting air gap and assisted by the mold thin wall reduces the rate of heat dissipation into the surrounding environment and therefore increases the melt temperature near the wall. In other words, a uniform temperature occurs at much shorter time at the lower pouring temperature of 615°C within the bulk of liquid i.e. shortest *"metastability period"*.

As a result, the rate of heat flow towards the mold wall diminishes and the growth rate is reduced much sooner for the 615°C pouring temperature. This is coupled with multi-directional heat flow due to mold geometry promotes the formation of equiaxed and globular structure as shown in Figure 5-3e, i.e. 615°C.

With increasing the pouring temperature, the chance of copious nucleation is decreased which eventually results in the formation of a coarser structure. The amplitude of recalescence also decreases which supports the hypothesis of lower nucleation frequency.

It should be noted again that the metastability period at higher temperature, e.g. 695°C Figure 5-1c, takes longer and yields the development of primary α-Al particles in the shape of columnar/dendritic morphology as illustrated in Figure 5-3a and b.
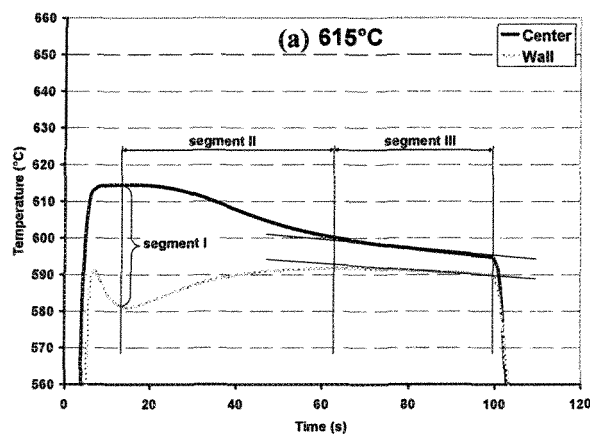
Fig. 5-1: continues
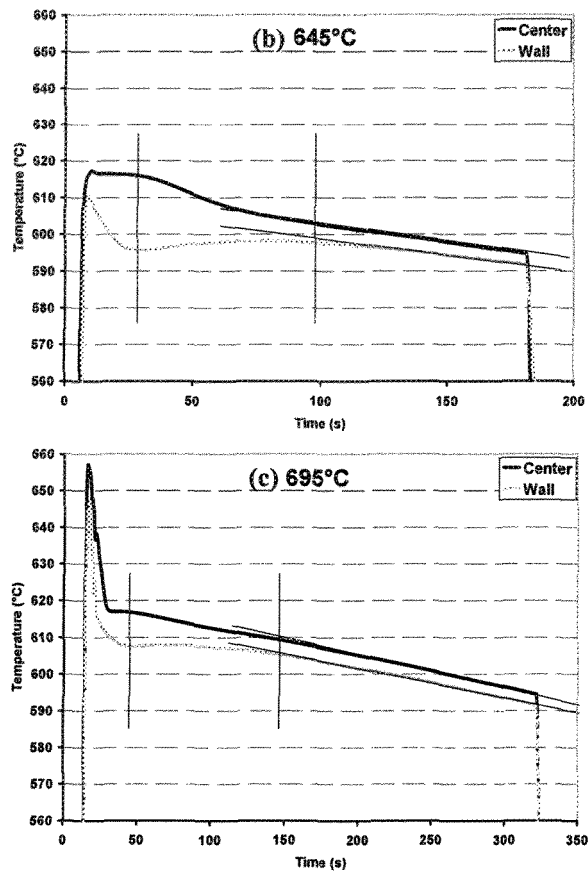
Fig. 5-1: Typical wall and centre cooling curves for (a) 615, (b) 645 and (c) 695°C pouring temperatures
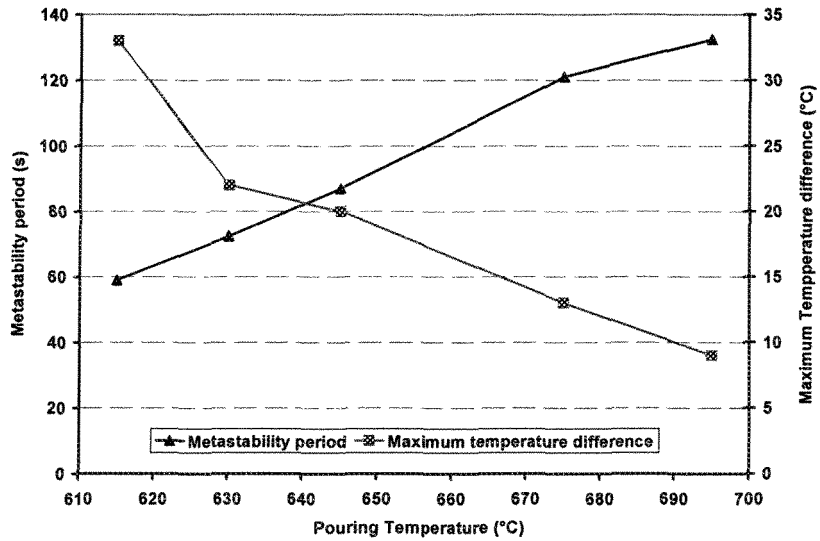
Fig. 5-2: Effect of pouring temperature on the metastability period and temperature variation across the bulk liquid

The results reported here generally support all previous studies [19-22] particularly the findings of Mao et al. [20], but the interpretation and hypotheses put forward in here are different. They have simply attributed the effect of pouring temperature on cooling rate; "faster cooling rate at lower temperature prevents full development of primary α-Al formation" [20].
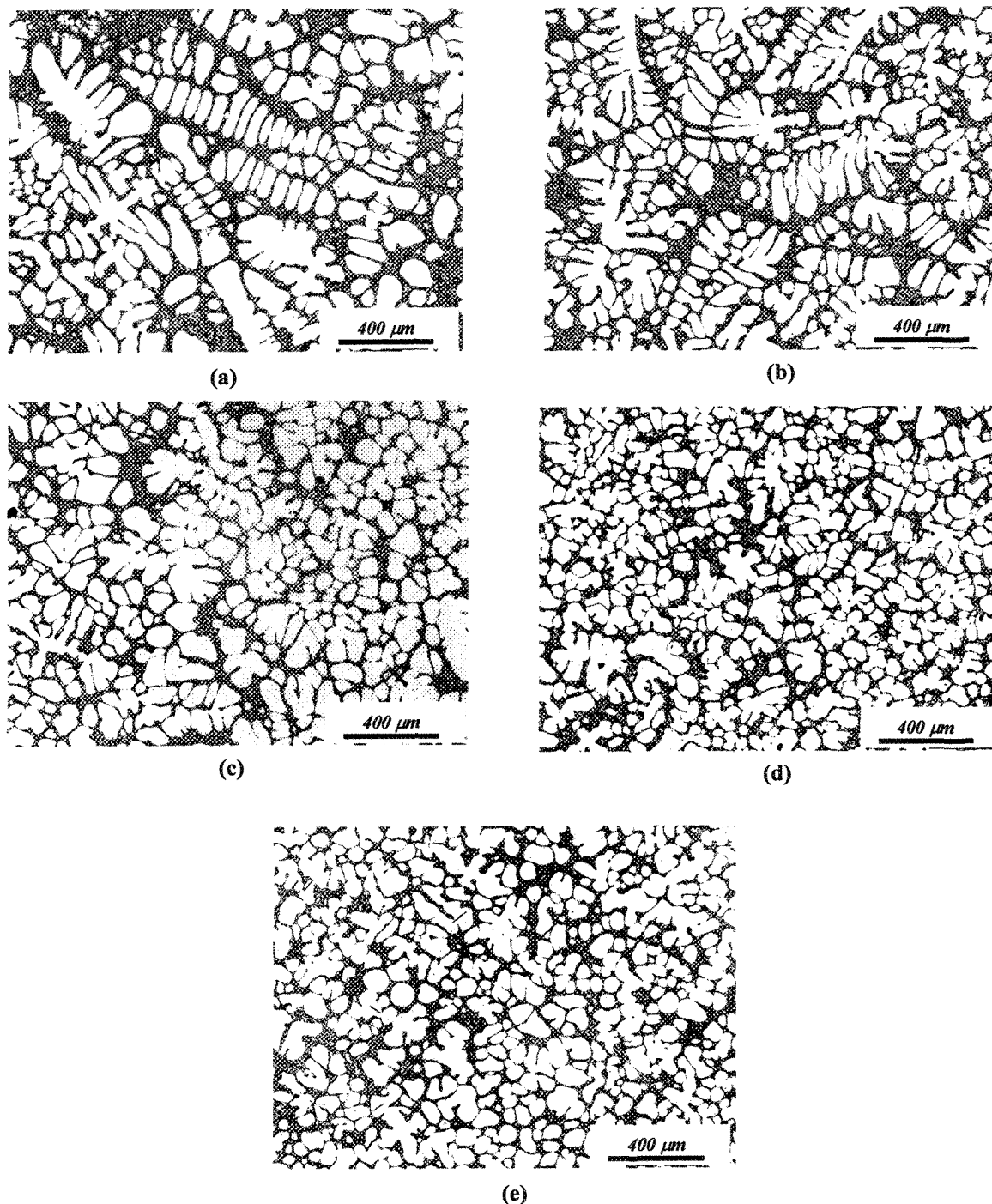
Fig. 5-3: Typical microstructure formed at different pouring temperatures;
(a) 695°C-dendritic, (b) 675°C-dendritic, (c) 645°C-rosette, (d) 630°C mixed rosette and globular, (e) 615°C-globular

5.2.2 Quantitative analysis

Figure 5-4 is the quantitative metallography which is carried out on conventional cast billets to characterize the microstructure and further highlight its inter-relationship with pouring temperature, using automatic image analysis system as previously discussed in chapter 4.

Although the fraction primary α-Al particles is expected to be about ~33% at quenching temperature, $593\pm2°C$, based on equilibrium lever rule and Scheil's equation, there is nearly 66 ± 2 % of primary α-Al phase, Figure 5-4a. Such higher amount of primary α-Al phase was also reported by other investigators [116]. Such discrepancy might be due to the following sources explained briefly.

■ Inefficient quenching (formation of eutectic colonies confirms the ineffectiveness of water quenching to prevent further liquid $\rightarrow$ solid transformation from the quenching temperature). The fact that there is not a duplex structure, i.e. absence of coarse and fine primary α-Al particles formed during pouring and swirling, casting, and quenching respectively, may be due to epitaxial nucleation and growth of quenched-formed α-Al particles on the pre-existing aluminum particles. Otherwise a duplex microstructure should have been observed.

■ Water quenching may have pushed the eutectic line to lower temperatures, expanding mushy zone [27].

■ The Scheil's equation assumptions, such as equilibrium interface, no back diffusion in the solid, homogenous liquid, and equal density for both solid and liquid phases [7].

The image processing results, Figure 5-4, may be summarized as follows;

- Area/perimeter ratio and equivalent circular diameter, Figures 5-4b and c, decreased with decreasing pouring temperature, while number density increased, Figure 5-4d. The findings are in good agreement with optical micrographs, Figure 5-3, where as pouring temperature decreased, the morphology of primary α-Al phase becomes finer and less dendritic.

- The growth in all directions is the obvious result of reduction in pouring temperature as evident by the formation of equiaxed and globular grains, Figure 5-3e and increasing the sphericity percentage shown in Figure 5-4e. The comparison of the percentage of the particles having sphericity greater than 0.9 for both high and low pouring temperatures, presented in Figure 5-5, shows an abrupt shifting for the structure cast at 615°C. This is an indication of more globular structure.

- In order to highlight morphological changes the aspect ratio is a useful tool where increasing in aspect ratio is an indication of a more dendritic microstructure. However, to understand the changes in aspect ratio with pouring temperature the data was presented into two different graphs, Figures 5-4 f and g, where the average aspect ratio and percentage of particles having aspect ratio greater than 2 plotted against pouring temperature. The graphs showed ascending behavior with increasing the pouring temperature to confirm the formation of dendritic microstructure. In other word when the pouring temperature is increased either the aspect ratio or the quantity of primary α-Al particles having aspect ratio greater than 2 is increased.

- One of the disadvantages of image analysis is related to the inability to differentiate between the appearance of dendritic and globular structures on the polished surface. The image analysis only detects the differences between particles and so for example the way a dendrite intersects the surface may be counted as isolated separate particle, see the optical micrographs presented in Figure 5-6, where the particles in the rectangle in Figure 5-6a are counted as isolated separate particles. The more likely isolated are those shown in Figure 5-

6b. However, even with considering this point, the data shows good correlation with increasing the pouring temperature.

(a)

(b)

(c)

(d)

(e)

(f)

(g)
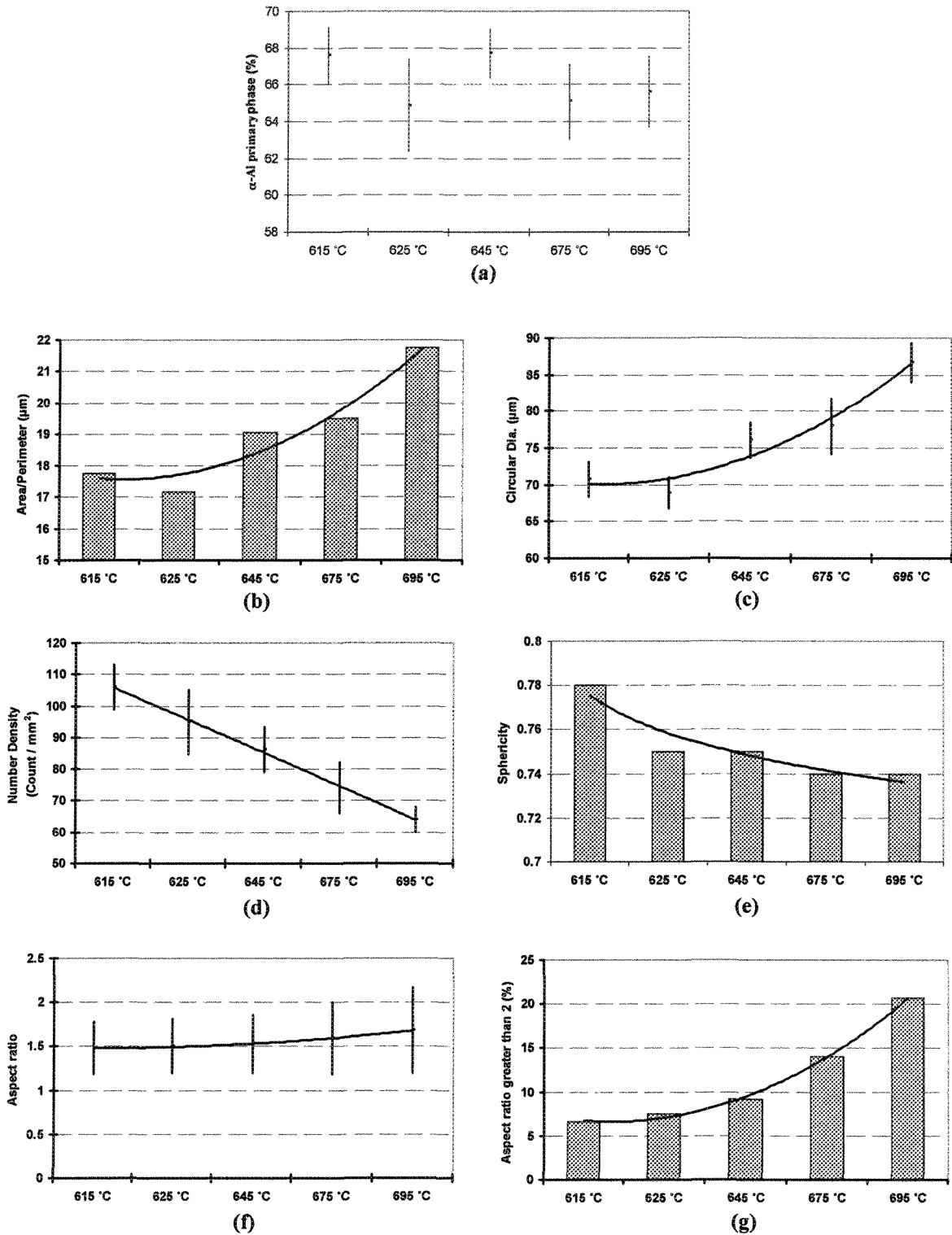
Fig.5-4: Image analysis data obtained from the Conventional cast billets
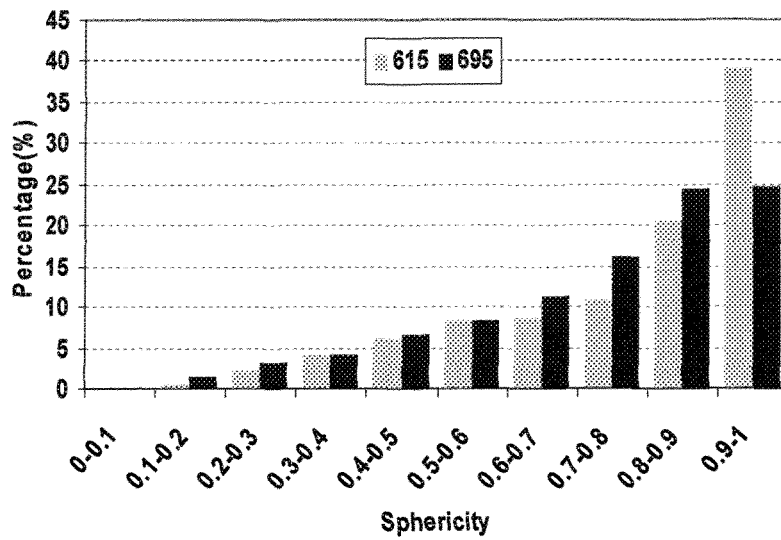
Fig. 5-5: Histogram distribution of particles sphericity for billets cast at 695 °C and 615°C

(a)   (b)
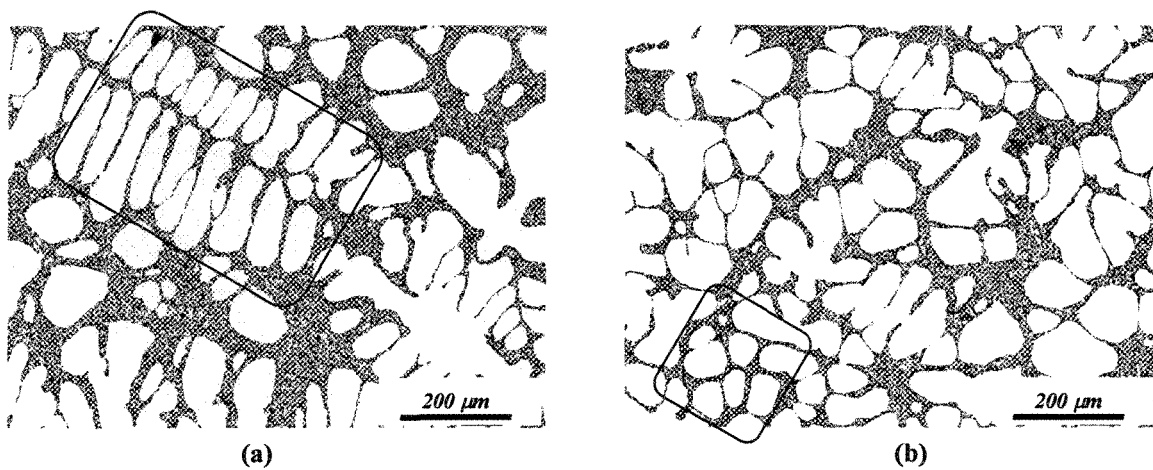
Fig.5-6: Micrographs to show the difference between globules and dendrites branches which are treated as isolated particles by image analysis system; (a) Dendritic morphology (b) Globular morphology

Table 5-1 presents the quantitative metallographic data obtained from image analysis of the resulting structures.

Table 5-1: Average quantitative numbers obtained from the image analysis of the billets cast at different pouring temperatures, all samples are quenched at 593±2°C

°C	Primary α-Al (%)	Circular Diam. (μm)	Aspect ratio	Number Density (count/mm^2)	Sphericity	Area/Perimeter
615	67.59	70.7	1.48	106	0.78	17.77
630	64.86	68.9	1.5	94.9	0.75	17.18
645	67.71	76.1	1.53	86.2	0.75	19.06
675	65.09	78	1.59	74.2	0.74	19.50
695	65.61	86.7	1.68	64	0.74	21.74

5.3 SEED process

5.3.1 Microstructure

In order to proceed with the main objective of the current research program, "The rheological behavior of SSM A356 Al-Si alloy" the as-cast structure of SEED prepared billets needed to be characterized both qualitatively and quantitatively. In this regard a series of structures were produced by changing casting condition. The casting parameters changed, were swirling intensity and pouring temperature which directly affect the morphology of the primary phase in SSM slugs. The effect of swirling speeds, illustrated as no swirling, low swirling and high swirling, and pouring temperatures of 695, 645 and 630°C on the morphology of primary α-Al particles is easily detectable by examining the optical micrographs given in Figures 5-7 to 5-9. As it is evident, with increasing pouring temperature, the structure becomes more dendritic. This may be attributed to steeper temperature gradient within the bulk liquid as a result of higher pouring temperature, melt coming in contact with the cold mold, already discussed for conventional cast billets. As pouring temperature decreased, the reverse trend was established and the shallow temperature gradient coupled with overall low melt temperature encouraged nucleation of the primary α-Al particles within the bulk liquid. Since the heat flow is no longer directional, due to swirling as will be discussed later, the particle growth is multi-directional on further cooling which results in formation of globular particles. This is well demonstrated in Figure 5-9 where the structure is almost fully globular at 630°C pouring temperature.

Swirling also appears to have refined primary α-Al dendrites and promoted the formation of rosette and/or globular α-Al particles with increasing swirling speed. This is similar to what has been seen for lower pouring temperature. The effectiveness of swirling speed may be due to reduction in segregation of alloying elements at the solidification front and better heat transfer between the mold and bulk of liquid to establish a shallow temperature gradient. Shallow temperature gradient coupled with lack of directional heat flow due to swirling are the main recipe for refining and formation of equiaxed as-cast structure. The effect of swirling speed is clearly detectable in optical micrographs taken from the billets cast at 695°C, Figures 5-7. The dendritic structure with no swirling transforms to degenerated dendrites at low swirling intensity and eventually to rosette/globular at high swirling intensity.

It is worth mentioning that in all billets, despite of rotation speed, there was no evidence of entrapped eutectic within the primary α-Al particles. This is one of the advantages of SEED slurry-on-demand technology.

(a)

(b)

(c)
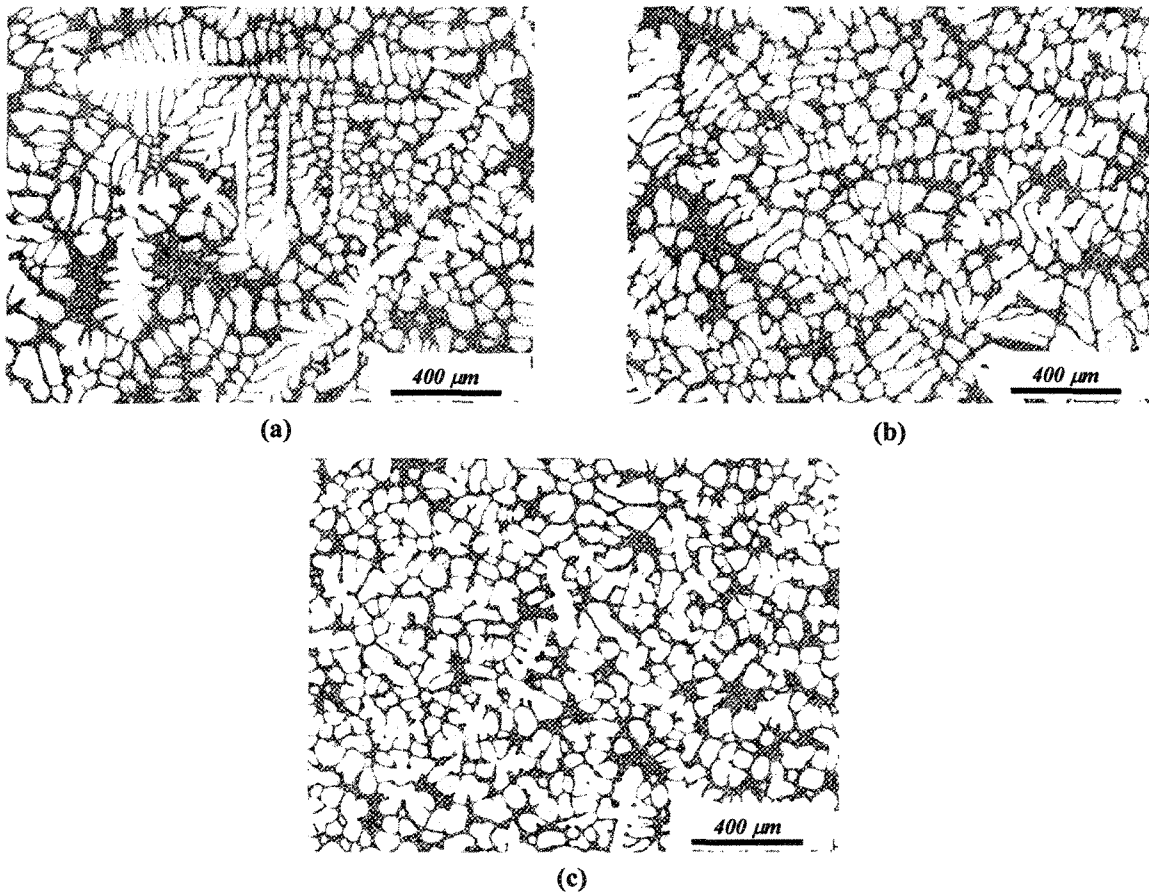
Fig. 5-7: Optical micrographs to show the microstructure of semi solid A356 alloy at 695°C pouring temperature; (a) no swirling, (b) low swirling and (c) high swirling intensities

(a)

(b)

(c)
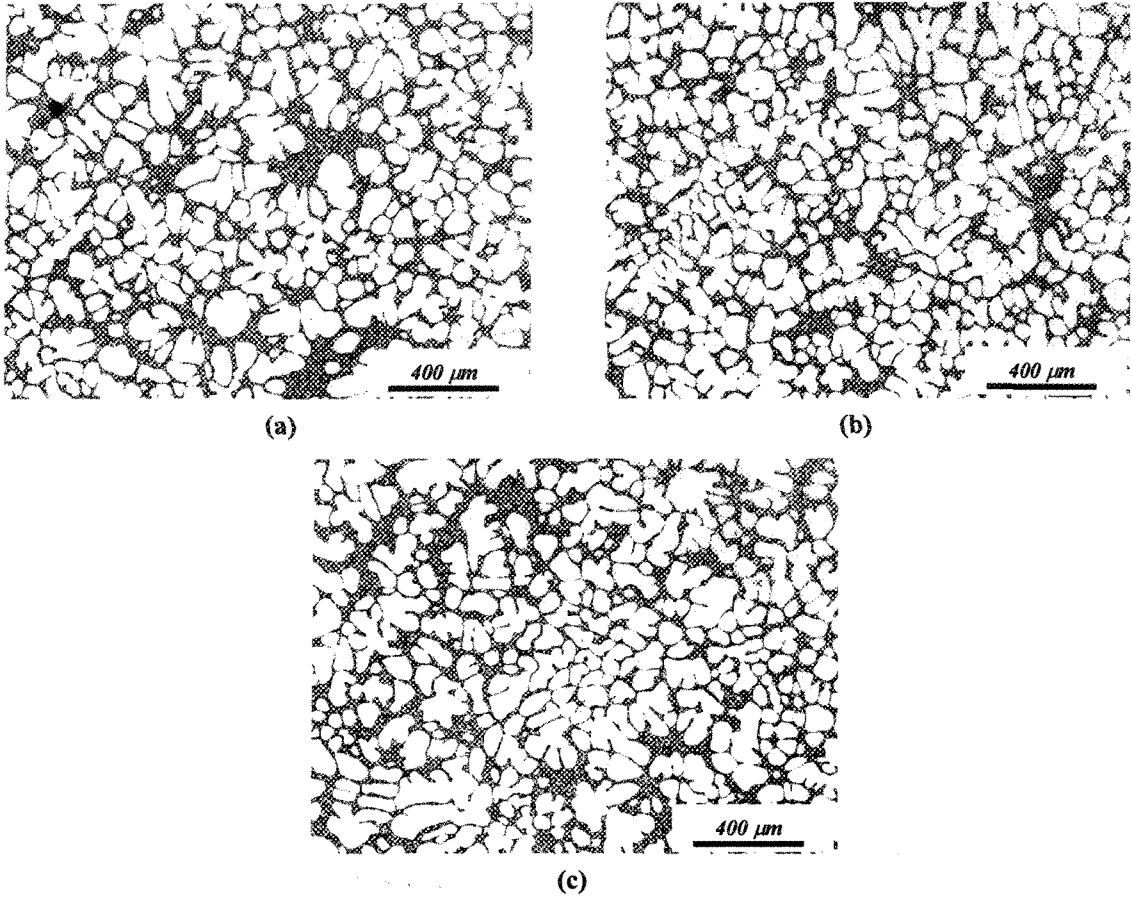
Fig. 5-8: Optical micrographs to show the microstructure of semi solid A356 alloy at 645°C pouring temperature; (a) no swirling, (b) low swirling and (c) high swirling intensities

(a)

(b)

Fig. 5-9: continues

(c)
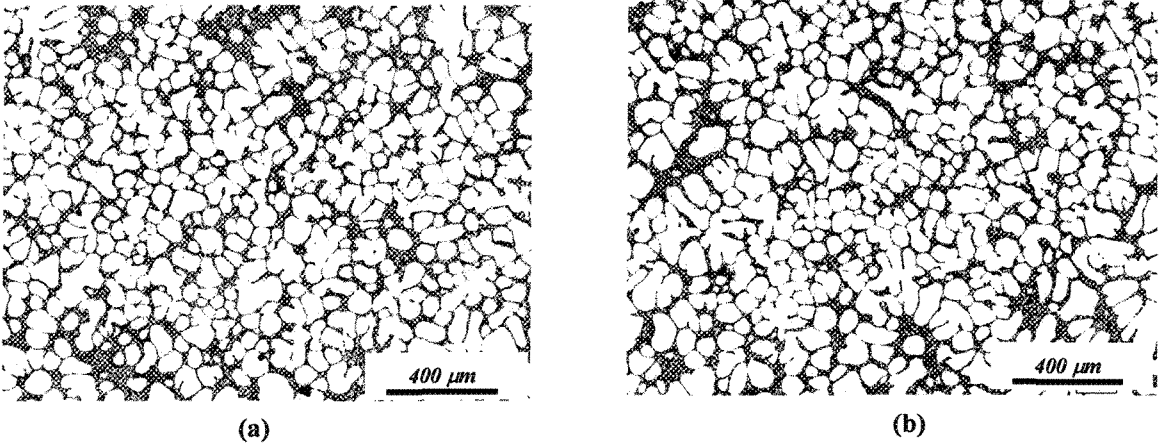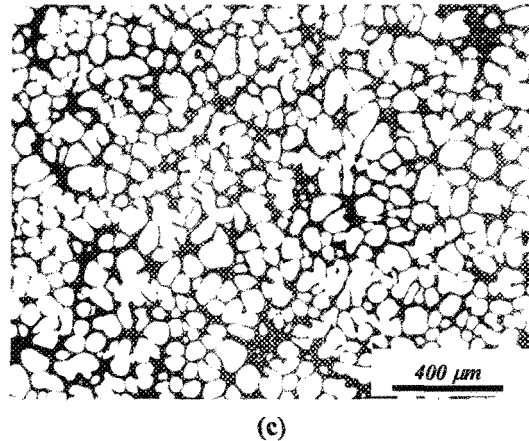
Fig. 5-9: Optical micrographs to show the microstructure of semi solid A356 alloy at 630°C pouring temperature; (a) no swirling, (b) low swirling and (c) high swirling intensities

5.3.2 Quantitative analysis

The microstructure of as-cast SEED billets was examined using the Clemex image analysis system as fully described in chapter 4. The resulting image analysis data are presented in Figures 5-10 to 5-12 for various casting conditions. Figure 5-13, is given to highlight the overall conclusion of changes in microstructure due to changes in casting parameters. It should be emphasized that the interpretation of the data presented here should be carried out in conjunction with the microstructural changes given in Figures 5-7 to5-9. Because of misrepresentation of microstructural feature in the plane of polish, as already discussed and shown in Figure 5-6, it is possible to have the isolated dendrite arms counted as individual globular particles during image analysis; the particles shown in Figure 5-6a (framed) are considered as globules.

Close examination of the image analysis data shows the percentage of primary α-Al particles increases with decreasing the pouring temperature, Figures 5-10a, 5-11a and 5-12a. This is due to the fact that the temperature at which the billet was quenched is lower for lower pouring temperatures, since the time interval between pouring and quenching was kept constant for all trials. Although the predicted value of solid fractions at the quenching temperature range is about 0.32-0.4, using Scheil's equation, the average fraction of primary α-Al phase was more than 66% in all trials. The difference might be due to the sources which are already mentioned for Conventional casting, except the

drainage of the residual liquid as part of SEED process that could be accounted for SEED to increase the fraction of solid;

- The drainage of remaining liquid imbalances the phase ratio and thus should have lifted up the overall percentage of primary α-Al particles.

The percentage of primary α-Al particles for lower pouring temperatures of 630 and 645°C, remains constant (within experimental scatter), regardless of swirling intensity, Figure 5-11a and 5-12a. For higher pouring temperatures of 695°C, Figure 5-10a, there is a slight increase in percentage primary α-Al at the higher swirling intensities. Such behavior may be attributed to improve refinement of the structure and thus lesser capability of refined and disintegrated dendritic microstructure to keep liquid phase within the billet, during drainage step, as clearly seen in drainage graph, Fig. 5-13f. In other words dendrite coherency point (DCP) is postponed with higher swirling speed, since dendrites become less stable and more globular. The solid phase is less intertwined and more open to encourage better fluid flow. The overall solid/liquid ratio is then expected to increase.

Increasing swirling speed at lower superheats has no effect on the amount of drained melt but appears to have slightly increased it at higher superheats. Again, this shows the effect of lower pouring temperature in formation of globular structure to form well packed structure to obstruct liquid flow out of the billet during drainage. However, this subject may be explained better if rheological concepts are employed. This is discussed in detail in the next chapters.

Generally, the equivalent circular diameter decreases with increasing the swirling speed, Figure 5-10b, 5-11b and 5-12b. It should be noted that the definition of circular diameter is ($2\sqrt{area/\pi}$) in the applied image analysis software. Therefore, it is expected to remain unchanged with morphology of the microconstituent, if the area of the respected phase does not change much. For example, for a globule and a dendrite with the same area, equivalent circular diameter should have the same value. For higher pouring temperature, i.e. 695°C, however, the trend is slightly different where after an

initial rise; a decreasing trend is observed with swirling speed. Such behavior may be explained with reference to the optical micrographs in Figure 5-7, where the initial rise could be due to dendritic structure while the reduction in size may be resulted when the globules or rosettes have started to form. Furthermore, the reduction in error bar values for circular diameter, Figures 5-10b, 5-11b and 5-12b, may suggest a more uniform size distribution of primary α-Al particles at lower pouring temperatures, and higher swirling speeds which may be due to better nucleation, and more effective disintegration of primary α-Al phase respectively.
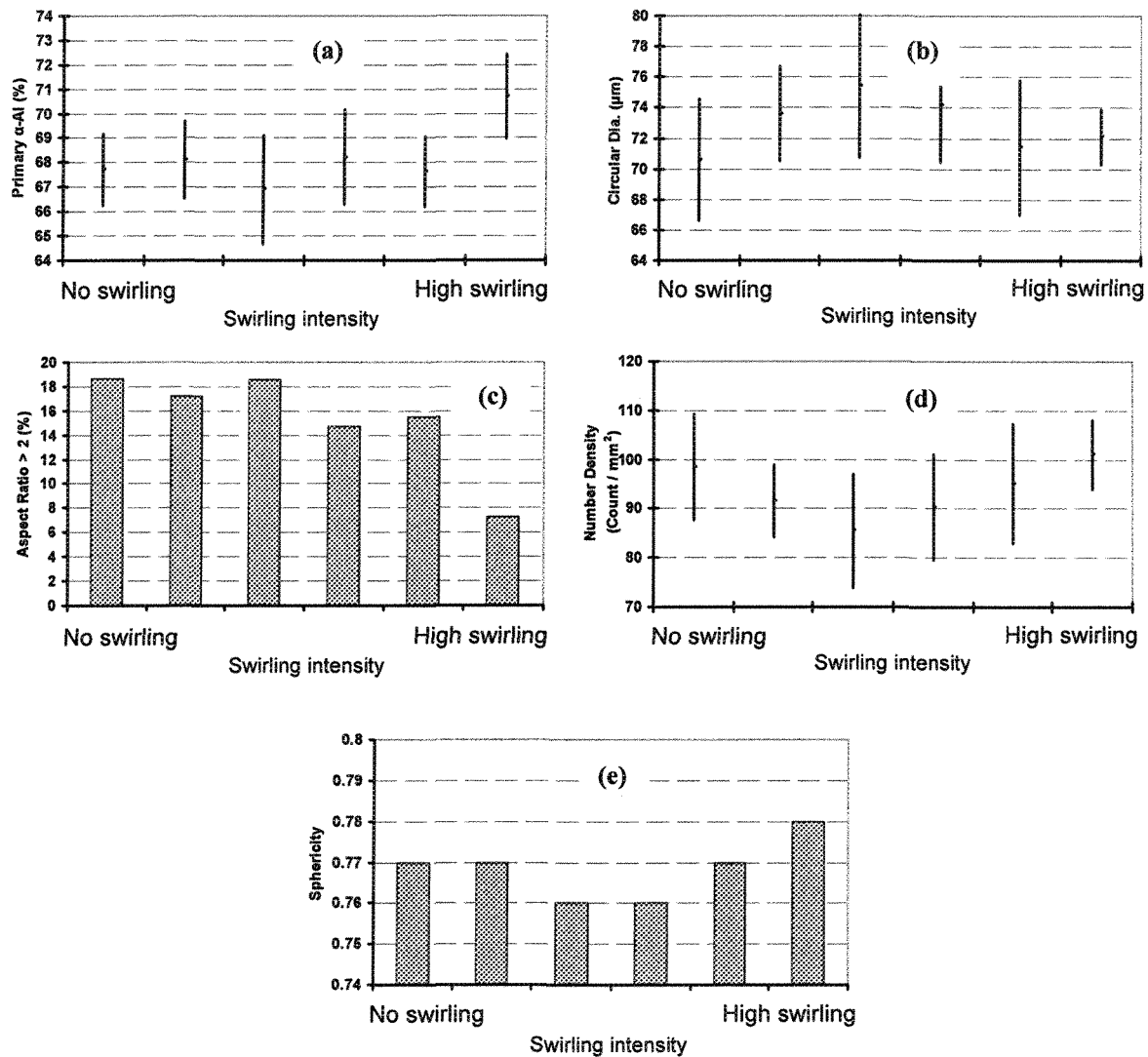
Fig. 5-10: Image analysis data for SSED billets cast at 695 °C
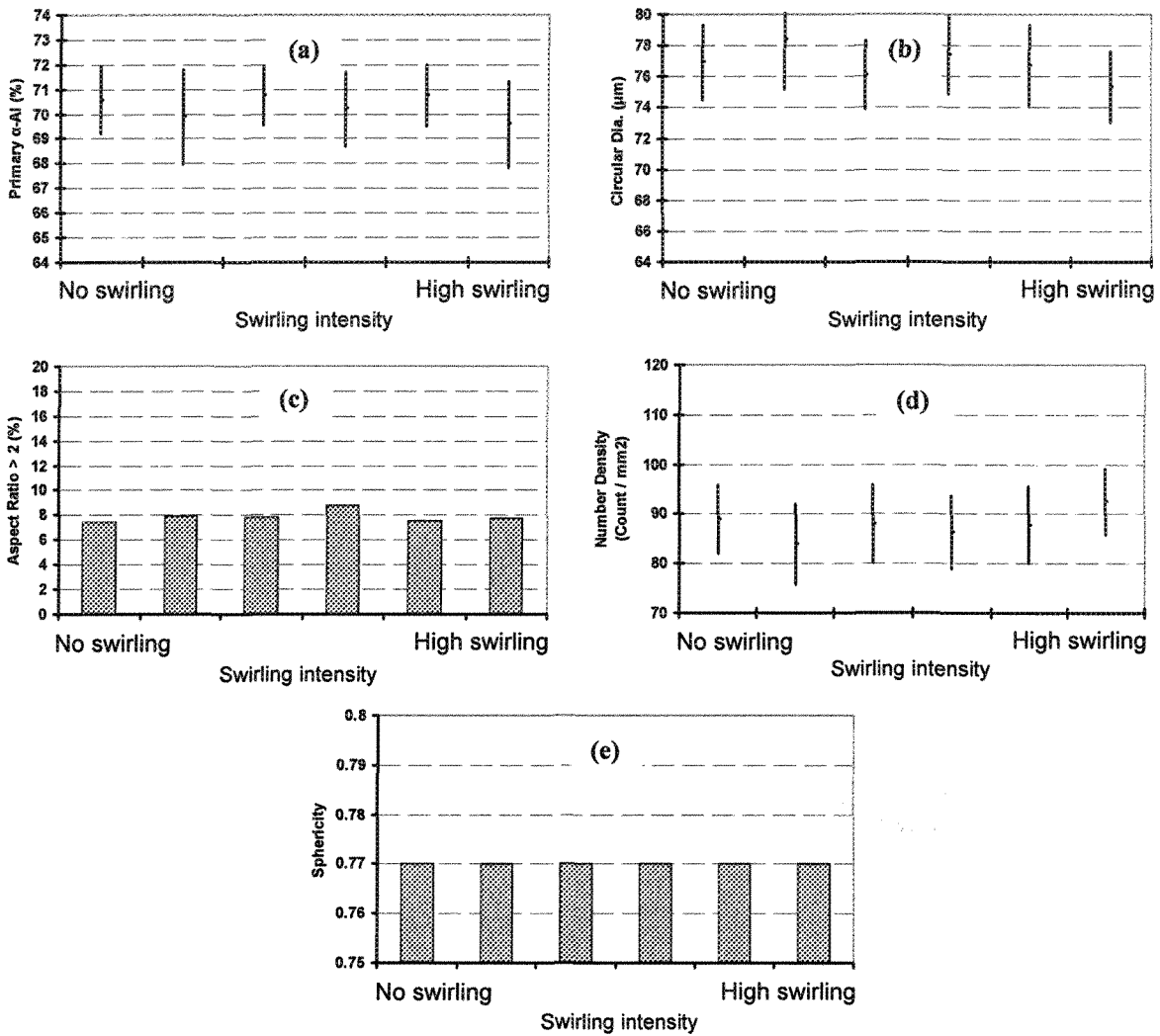
Fig. 5-11: Image analysis data for SEED billets cast at 645 °C
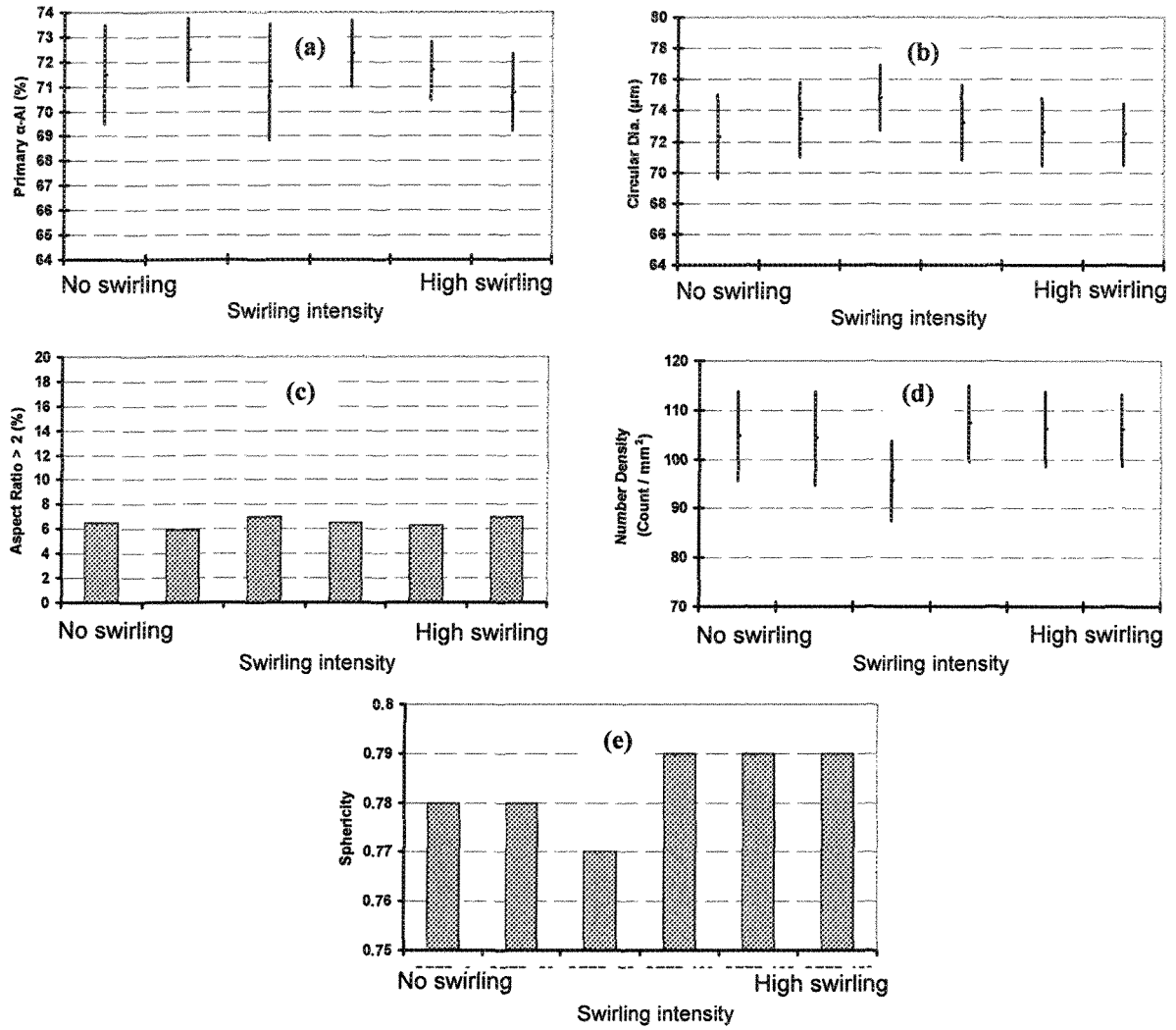
Fig. 5-12: Image analysis data for SEED billets cast at 630 °C
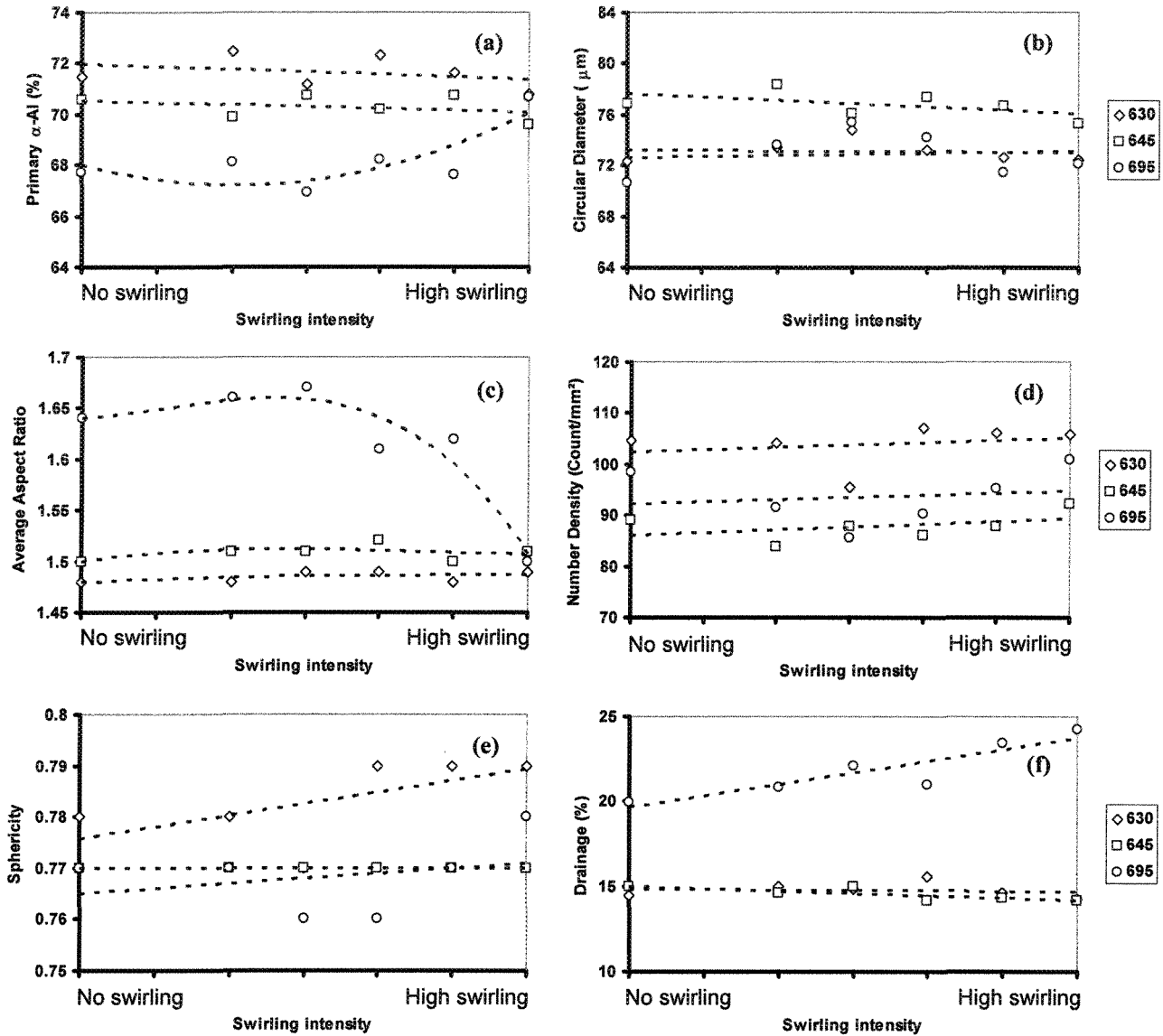
Fig. 5-13: The effect of pouring temperature and swirling intensities on the structural parameters of SEED produced billets

The number of primary α-Al particles per unit area, i.e. number density, increases with decreasing pouring temperature, Figure 5-10d to 5-13d. For higher pouring temperature of 695°C, Figure 5-10d, the trend is the same as for the circular diameter as mentioned before. The important point is the increase in number density values with increasing swirling speed which may suggest more effective disintegration of dendrites with more intense swirling.

The percentage of α-Al particles with aspect-ratio greater than 2 appears to have decreased slightly with increasing swirling speed, more globular particles, but increased with pouring temperature due to the formation of dendrites. The concluding graphs of Fig.5-13c strongly support such effect. Sphericity increases with increasing the swirling speed and decreasing pouring temperature which is again attributed to better globularity and formation of more equiaxed particles, Figure 5-13e.

A common objective of slurry processing routes is the production of metal slurries in which the primary phase particles are fine, preferably less than 100μm diameter, and have globular or rosette structure [117]. As it is evident from the optical micrographs, and the quantitative data, these criteria are easily achieved by SEED.

With higher pouring temperature, the drainage increases because of the greater amount of liquid exist in the mold. However the percentage of molten metal drained increases with increasing swirling speed, Figure 5-13f, which may be due to more uniform distribution of liquid within the mush and less capability of globular microstructure to keep the liquid within the billets. The data presented in Figures 5-10 to 5-12 are tabulated in Table 5-2 for more detailed comparison of results for the SEED billets.

Table 5-2: Average quantitative numbers obtained from the image analysis data within different pouring temperatures and swirling intensities

°C-RPM	Primary α-Al (%)	Circular Diam. (μm)	Aspect ratio > 2 (%)	Number Density (count/mm^2)	Sphericity	Drainage (%)
630-No Swir.	71.48	72.3	6.49	104.68	0.78	14.47
630-Low Swir.	72.32	73.2	6.49	107.22	0.79	15.6
630-High Swir.	70.76	72.4	6.98	105.84	0.79	14.2
645-No Swir.	70.57	76.9	7.48	89	0.77	14.95
645-Low-Swir.	70.2	77.4	8.77	86.2	0.77	14.19
645-High Swir.	69.58	75.3	7.75	92.4	0.77	14.1929
695-No Swir.	67.72	70.6	18.62	98.4	0.77	19.98
695-Low Swir.	68.23	74.2	14.72	90.3	0.76	21
695-High Swir.	70.7	72.1	7.32	101	0.78	24.23

CHAPTER 6
RESULTS AND DISCUSSION

MICROSTRUCTURAL CHARACTERIZATION - VISCOMETRY

CHAPTER 6
RESULTS AND DISCUSSION
MICROSTRUCTURAL CHARACTERIZATION -
VISCOMETRY

6.1 Introduction

In order to investigate the morphological evolution of α-Al primary phase in the SSM A356 alloy irrespective of quantitative metallography (discussed in chapter 5), either for Conventional or SEED billets, the current research proposed an innovative characterization method using parallel plate compression rheometer. Since the viscosity of SSM alloy is dependent on the metallurgical parameters and also is a measure of rheological behavior, rheological tests can be employed to characterize microstructure. Effort was made to correlate between the morphology and the viscosity while other metallurgical parameters kept constant. In fact by introducing the deadweight on top of the billets at very low shear rates and measuring the billets resistance against deformation, engineering strain-time graphs, and further calculation of viscosity assuming Newtonian fluid behavior of SSM billets (detailed explanation given in chapter 3 for equations 3-26 to 3-28), the microstructure of A356 SSM alloy was characterized. This is much faster and less expensive characterization method than quantitative metallography, which is generally employed to characterize the microstructure of SSM billets. This is particularly beneficial if on-line quality checks are required in production of rheo-billets used as feedstock for near net shape manufacturing routes.

In this part, the in-house designed and fabricated compression machine (detailed information given in chapter 4) was employed and before using in principal experiments, had to be verified by testing the materials with known and determined viscosity number, for example plasticine.

The Conventional and SEED billets of 75 mm diameter and ~140 mm height were deformed under different initial pressures and the viscosity values were obtained at

different morphologies. The final viscosity values attributed to the appropriate microstructures. Liquid segregation as a side effect of deformation was also studied.

6.2 Machine verification

The specifications of the parallel plate compression viscometer designed and constructed at CURAL laboratories, have been introduced in the experimental section in chapter 4. Before commencing the principal part of the tests, the verification of the machine was necessary. Normally, the viscometers can be calibrated using materials with determined viscosity numbers at given temperature [68]. Such approach is more applicable for liquid polymers while the paste like materials do not present a precise viscosity value and the viscosity number is always reported within a range concerning different parameters. In the current research, it was attempted to use a paste like material, plasticine or modeling paste, to verify the reliability of the operation for the in-house designed and built machine. The viscosity values reported for plasticine is around 1E10 – 1E14 centi poise (cp) tested at ambient temperature, 20°C [68, 71].

In order to obtain viscosity values it is required to define a strain-time from which the viscosity can be calculated. The engineering strain-time graph (e-t), is the basic graph to evaluate the Rheological behavior of SSM billets and obtained from the initial height-time variation data. The instantaneous changes in the billet height is registered during parallel plate compression test and converted into engineering strain using the simple equation of

$$e = 1 - \frac{h}{h_o} \tag{6-1}$$

Where h_o and h are the initial and instantaneous heights of the specimen during compression respectively. Figure 6-1 shows a typical deformation-time curve. There are three regions recognizable on this graph [27];
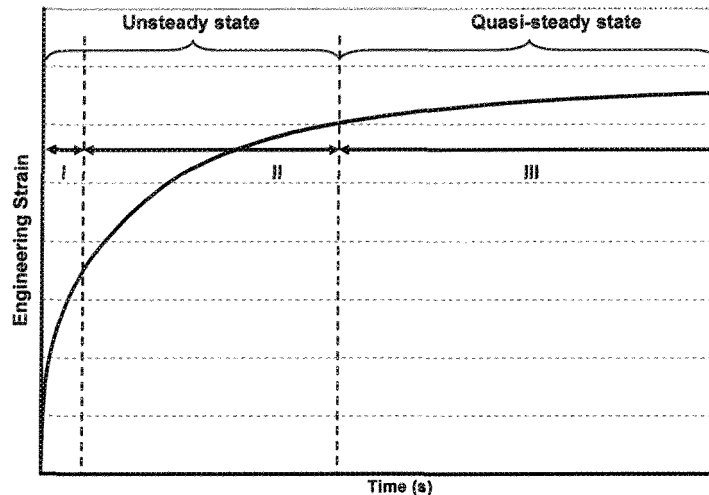
Fig. 6-1: A typical graph expected during parallel plate compression test of SSM billets

1. **Stage-I, unsteady-state,** where the billet flows almost without any resistance to applied pressure. This behavior is attributed to the easy movement of the primary α-Al particles within the residual liquid and without appreciable collision. The extent of this region is dependent on the particle size and applied pressure where it is greater at smaller particle size or higher applied pressure.

2. **Stage-II, unsteady-state,** where there is some degree of resistance to flow due to the collision of solid particles and formation of α-Al agglomerates. The agglomerated chunks are the resisting constituents to billet flow.

Both stages I and II are regarded as non-steady states, since the slope of the graph varies with time, i.e. there is mainly agglomeration. That's why the first two regions are classified as unsteady state segment in Figure 6-1.

3. **Stage-III, Quasi steady-state,** where the billet deforms steadily with a constant slope. It is believed the solid-liquid mixture, "the mush", has reached a state where it deforms as a single phase. The processes of agglomeration and de-agglomeration establish a quasi steady state equilibrium condition in the mush at this stage of deformation.

Such behavior in deformation is almost seen in all Engineering strain-time graphs and will be explained in details later. The quasi steady state segment of the engineering strain-time graph is further developed to calculate viscosity values for different specimens as described in the following paragraph for the verification of parallel plate compression test machine.

The tests to verify the in-house designed and constructed machine were carried out using cylindrical plasticine samples with 75 mm diameter and 100 mm height. The Applied dead weights were 35 and 56 kg. The calculated logarithm of the shear rates $(\log \overset{o}{\gamma})$, using Eq. 3-29, for the samples, were -4.3 and -4 respectively; the very low shear rate allows treating the plasticine as Newtonian fluid. The resulting values were 10^{12} cp for 56 kgf and 5×10^{12} cp for 35 kgf which both are within the expected range [68, 71].

The preliminary tests also confirmed the capability and reliability of the machine to differentiate amongst dendritic, rosette and globular microstructures in a hypoeutectic Al-Si alloy. The effect of billet structure on its ability to deform will be discussed later using strain-time graphs. It will be shown that billets with dendritic morphology have the greatest resistance to flow. It will be further shown that if the billet structure remains unchanged, e.g. globular, the resulting strain-time graphs would be superimposed on one another.

6.3 Conventional Casting

The formation of different microstructures due to changes in pouring temperatures (see Figure 5-3) was examined the flow behavior of the SSM slurries during the application of the external forces. This is because the flow characteristics, as specified by the viscosity, are dependent on the metallurgical parameters including the fraction solid and its morphology, dendritic, rosette or globular [1-3].
This part entirely reports on the effect of pouring temperature, superheat, and the resulting microstructure on the viscosity of SSM billets of hypoeutectic Al-Si alloy prepared by conventional cast method. The rheological test was carried out at constant

solid fraction of 0.33, using cylindrical billets of 75 mm diameter and ~140 mm height where the temperature of the billets during deformation was registered at 594±1°C in all trials.

6.3.1 Strain-time graph

As discussed in chapter 5, the morphology of primary α-Al particles varies with casting condition, pouring temperature for this case. The three morphologies of dendritic, rosette and globular are expected to respond differently to external forces such as compressive forces. The formation of globular microstructure, as for instance shown in chapter 5 for alloy cast at 615°C, Figure 5-3e, has always been the main objective of SSM researchers, since the flowability is rated the best amongst different morphologies. Increasing the temperature gradient within the melt encourages directional growth of primary α-Al phase. Combination of equiaxed and directional growth mode within the pouring temperature range of 630-645°C causes the formation of an intermediate structure, the rosette morphology, with flowability between those of dendritic and globular structure. Such morphology transforms to fully dendritic feature within the melt temperature of 675-695°C which resists against deformation. Formation of the early skeleton structure for the dendritic morphology along with the high dendrite coherency point, DCP, brings about some resistance towards mechanical deformation of the mush. Such resistance governs the flowability of SSM slurries and makes die filling of materials harder. The effect of α-Al morphology on the ability of billets to deform is clearly detectable in strain-time graphs presented in Figure 6-2. As already explained in Figure 6-1, three regions of deformation may be recognized on the strain-time graph of Figure 6-2. It is noticeable that the regions I and II, as the non steady state part of the graphs are less distinct for 675 and 695°C, where the region I is almost non existent. This may be attributed to dendritic morphology and its interlocking nature to inhibit plastic deformation due to the application of external force. The effect of applied pressure on the deformability of different morphologies is also recognizable in Figure 6-2 a-c. The application of higher initial pressure renders easier deformation and greater engineering strain in all trials regardless of the morphology of the primary α-Al particles. However, the maximum and minimum engineering strains are always

obtained at 615°C and 695°C pouring temperatures respectively, irrespective of applied pressure. In other words, the structure at 615°C shows less resistance to plastic deformation and if examined in conjunction with optical micrographs in Figure 5-3e, the obvious conclusion is that, "the more globular and finer microstructure yields more engineering strain, better flow". The engineering strain graphs for 630 and 645°C show moderate deformation behavior which is an indication of becoming less globular and having more rosette morphology of primary α-Al particles as the transitional stage between dendrites and globules, Figure 5-3 c-d. The resulting deformation due to rosette morphology is still considerable when compared to fully dendritic structure; see the graphs for 645 and 695°C in Figure 6-2. As expected the more dendritic structures of 675-695°C, Figure 5-3 a-b, shows greater resistance to deformation. This is not the desirable feature for SSM processing.
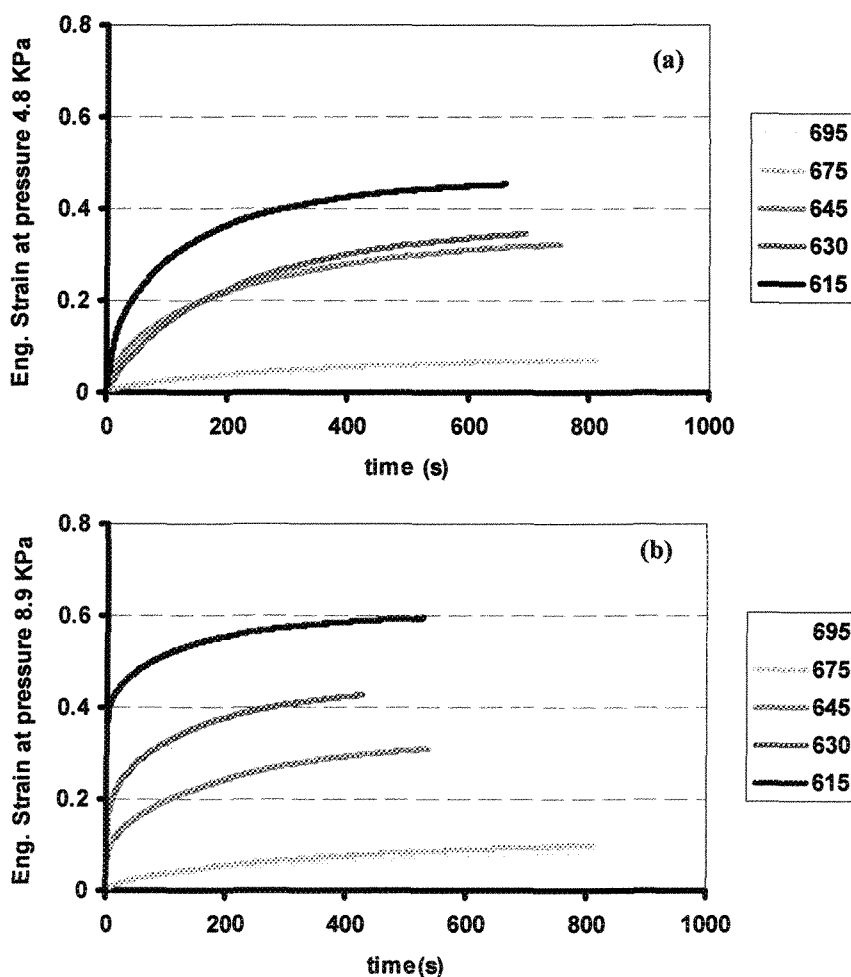
Fig. 6-2: continues
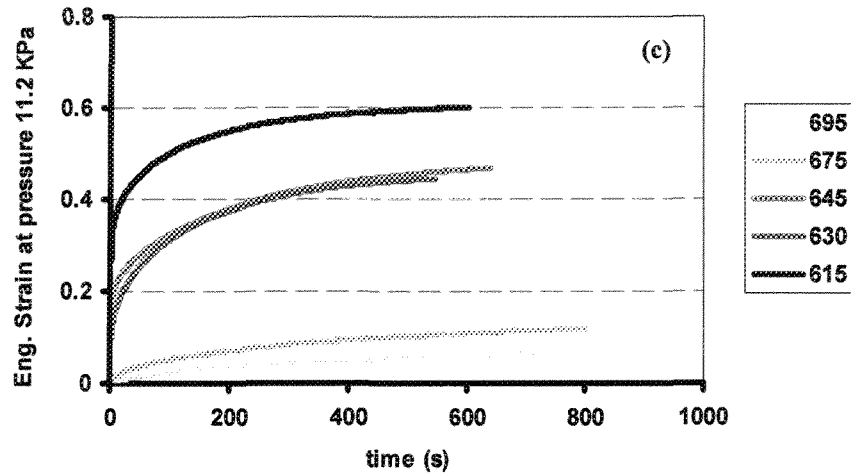
Fig. 6-2: Strain-time graphs obtained at different pouring temperatures and
deformed at 595°C under different applied pressures (a) 4.8 KPa, (b) 8.9 KPa, and
(c) 11.2 KPa

The optical micrographs in Figure 6-3 compare deformation characteristics of SSM billets cast at 695, 630 and 615°C pouring temperatures under a constant applied pressure of 4.8KPa. The flow characteristics of the billet cast at 615°C and 630°C appears to be much better than that cast at 695°C having a fully dendritic structure as discussed in chapter 5, Figure 5-3 a-e.
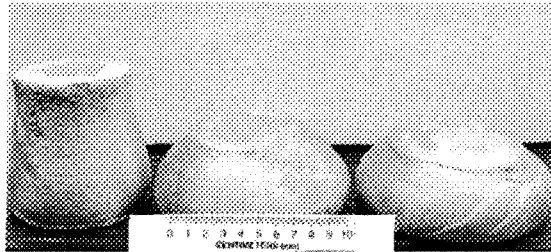
Fig. 6-3: Billets deformed under 4.8 KPa applied pressure, cast at 695, 630&
615°C, from left to right, respectively

6.3.2 Viscosity

Figure 6-4 shows the developed graphs resulting from mathematical treatment of strain-time data and assuming the SSM billets behaving as Newtonian fluid by plotting the left hand side of equation 3-28 versus time. These graphs, obtained from the results for engineering strain-time data during the quasi steady-state deformation period, ~200s after the beginning of each compression test, shows similar trend as the strain-time

graphs of Figure 6-2. The viscosity is calculated through the inverse slope of the graphs in Figure 6-4.

It should be noted that, the treatment of the data, 200 s after the beginning of deformation is related to the size of samples where in the case of large samples, it takes longer time to reach the steady state condition and the suspended solid particles could move easily for longer period of time. This means more spread of segments I and II in Figure 6-1, while this is not the case for small size samples where the steady state is established faster within such billets. As discussed in the next chapters, it is clear that the steady state is developed just about 50 s after the beginning of compression test for the small samples.

The calculated viscosity values are listed in Table 6-1, for all trials. The results support those of the previous reports for semi solid alloys of Sn-15%Pb [96] and A356 [53]. It is evident that, there is almost a three order of magnitude difference between the viscosities for dendritic, 695°C, and globular, 615°C, morphologies and one order of magnitude difference for the case of rosette, 630-645°C, morphology.

This is further confirmation of easier flow of globular structure, shown quantitatively that in contrast to dendritic structure, microstructures with more globular primary α-Al have lower viscosity numbers. Lowering the pouring temperature down to the liquidus point provided appropriate conditions to produce equiaxed α-Al particles within the melt and brought about lower viscosity numbers. The equiaxed grains flow with less resistance as compared to dendrites. This is due to the lack of secondary, tertiary and higher degree branches which impede particle movement as a result of branches' interlocking.

It is further noticeable that the viscosities for each temperature did not change significantly with the applied pressure or shear rate which may confirm the assumption of treating the SSM billets as Newtonian fluid at very low shear rates is not an exaggerated assumption.
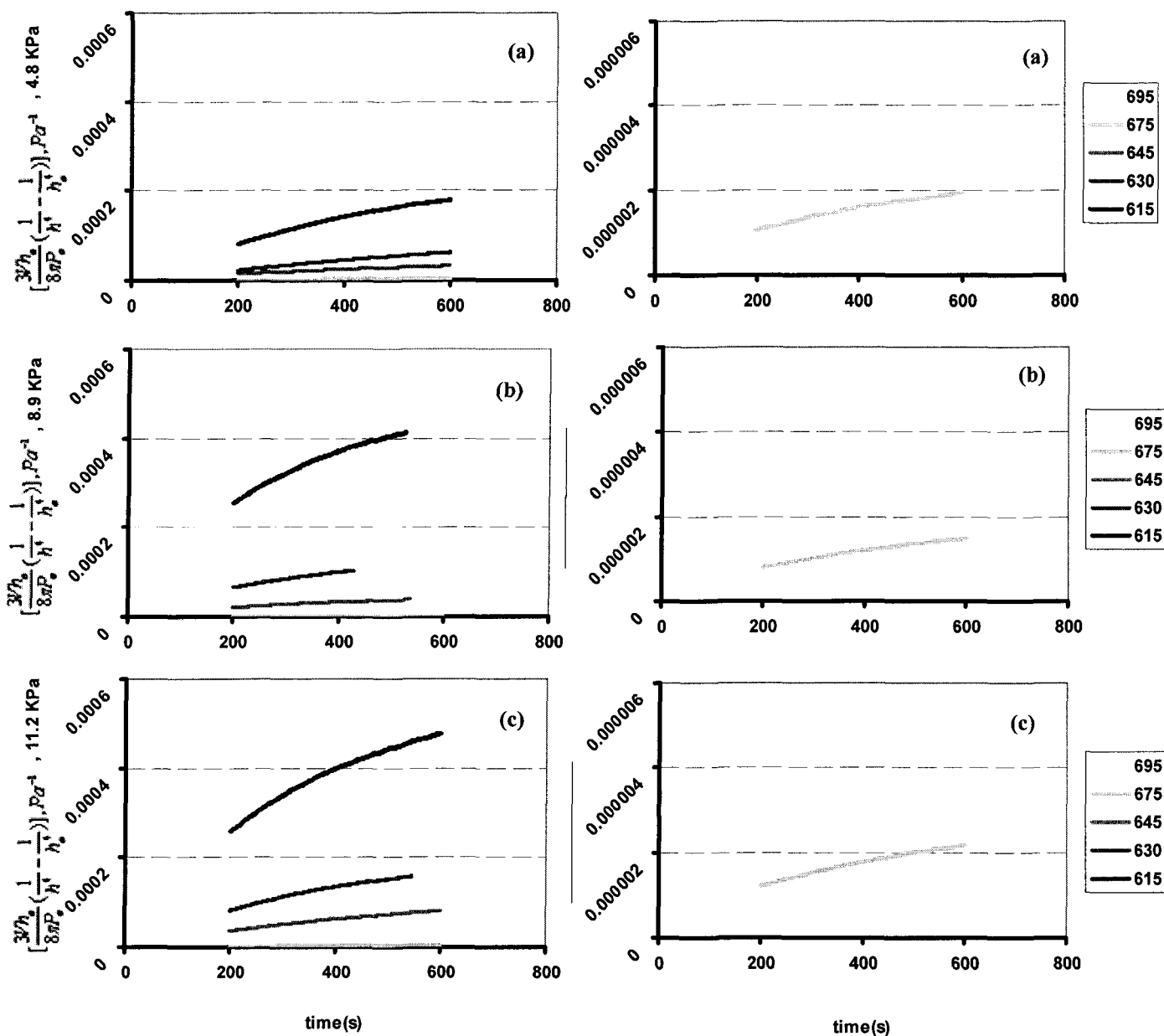
Fig. 6-4: Steady state part of the graphs, equation 3-28 plotted against time, 200 seconds after the beginning of each test to calculate the viscosity at
(a) 4.8 KPa, (b) 8.9 KPa and (c) 11.2 KPa

Table 6-1: Viscosity numbers (Pa-s) at different pressures and pouring temperatures, (Log η), and log shear rate $(\log \overset{o}{\gamma})$, (s^{-1}), Rheocast billets tested at 595°C

Initial pressure, Po	Log η, $[\log \overset{o}{\gamma}]$ (695°C)	Log η, $[\log \overset{o}{\gamma}]$ (675°C)	Log η, $[\log \overset{o}{\gamma}]$ (645°C)	Log η, $[\log \overset{o}{\gamma}]$ (630°C)	Log η, $[\log \overset{o}{\gamma}]$ (615°C)
4.8 KPa	9, [-3.9]	8.6, [-3.95]	7.3, [-3.54]	7, [-3.33]	6.6, [-3.09]
8.9KPa	9, [-3.82]	8.6, [-3.83]	7.3, [-3.18]	6.6, [-2.87]	6.3, [-2.74]
11.2KPa	9, [-3.84]	8.6, [-3.82]	7, [-3.12]	6.6, [-2.86]	6.3, [-2.68]

6.3.3 Liquid segregation

The optical micrographs taken from the central parts of the deformed billets, where deformation is maximum, Figures 6-5 and 6-6, show almost no liquid segregation, dark eutectic mixture, for low superheats and some minor segregation at the higher superheats. The absence of liquid segregation for low pouring temperature billets may be attributed to the globular structure of the billets, white primary α-Al phase, which allows easy glide of the primary α-Al particles over one another, almost at the same speed as the liquid flows within the inter-particle channels. This is further assisted by the fine particle size and the low values of shear rate, $\sim 10^{-3}$ to 10^{-4} (s^{-1}). Low shear rates allows solid particles to move easily without excessive collision to bring about homogenous distribution of α-Al phase. The micrographs presented in Figures 6-5 and 6-6 prove such theory and show almost no segregation of liquid at different applied pressures. Nonetheless minor liquid segregation could be seen near the wall, particularly in the dendritic structure, Figure 6-6, which is due to dendrites interlocking and thus inability to move freely, in contrast to the globules. The reader should be reminded that such segregation within dendritic morphology has taken place just after 0.1 engineering strain, Figure 6-6, against 0.6 strain in the case of globular microstructure, Figure 6-5. This further supports the suitability of globular structure by having lower susceptibility to liquid segregation and better flowability during die casting of SSM billets. The as-cast die-cast parts made from billets with globular morphology should have more uniform structure [88].

The main shortcoming of semi solid materials, the segregation of residual liquid during deformation [9], which is due to the separation of liquid from the solid phase under pressure is therefore mitigated or even overcome by the refinement and globularization of the solid particles and the application of lower applied shear rate.
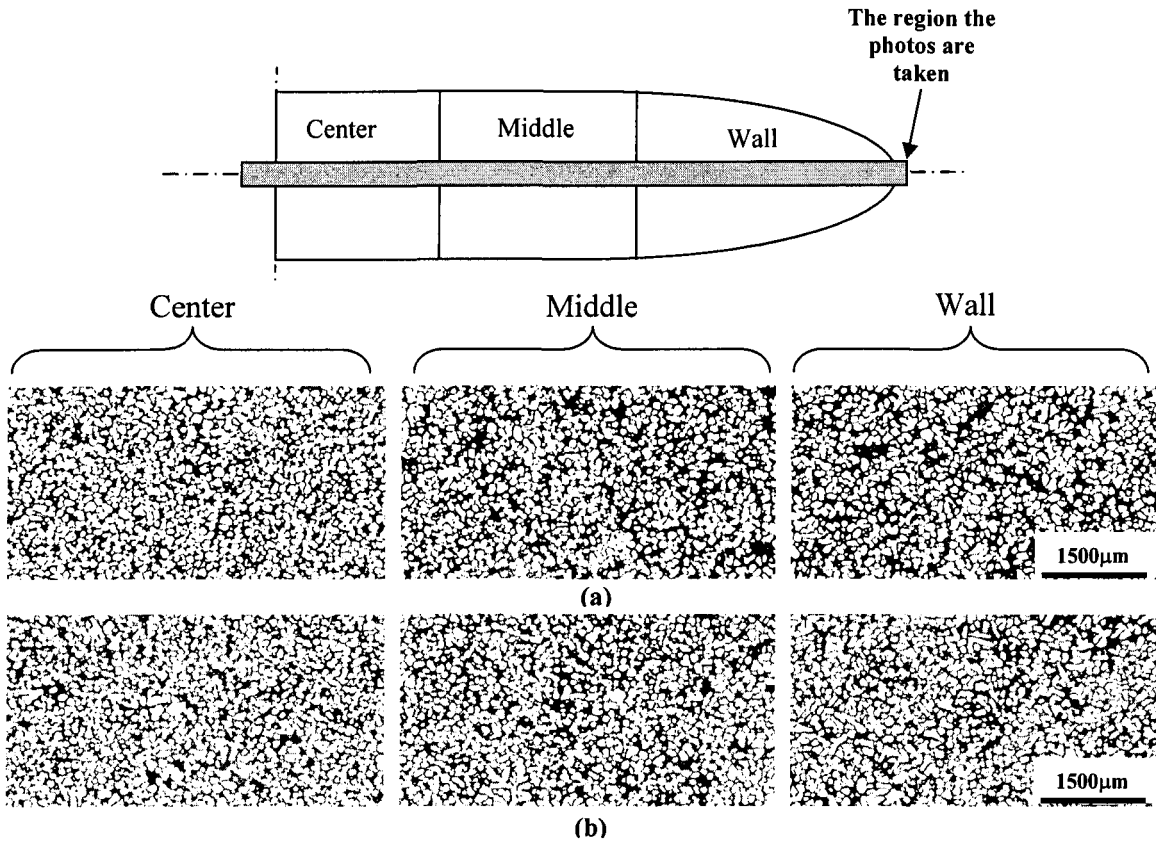
Fig. 6-5: Microstructure of as-deformed SSM billets, maximum strain = 0.6, cast at 615°C;
(a) 8.9 KPa, (b) 11.2 KPa applied pressures, 25X
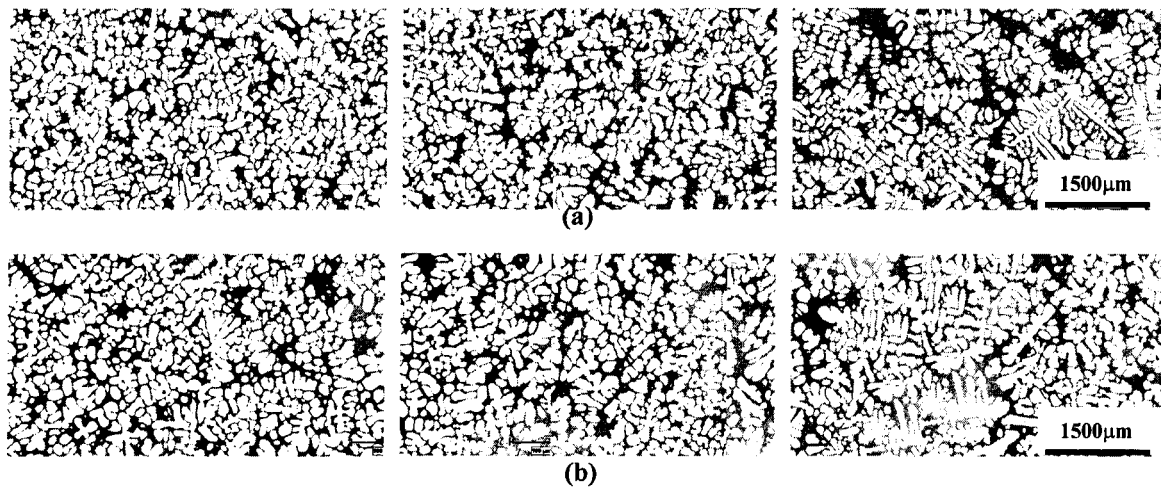
Fig. 6-6: Microstructure of as-deformed SSM billets, maximum strain = 0.1, cast at 695°C,
(a) 8.9 KPa, (b) 11.2 KPa applied pressures, 25X

6.4 SEED process

The microstructure of the SEED billets was characterized using the parallel plate compression viscometer where the swirling intensities and pouring temperatures were chosen the same as those reported in chapter 4. The SSM billets had the final size of 75mm diameter and ~140 mm height produced at no swirling, low swirling and high swirling intensities and the temperatures of the billets during deformation were registered at 591, 594 and 600±1°C for each respective intensity. The pouring temperatures for each set of billets, different swirling intensities, were 630, 645 and 695°C. In order to identify any correlation between the viscosity and resulting microstructure of the billets, the samples were assumed to behave like Newtonian fluid at very low shear rates and the viscosity values were calculated using Equations 3-26 to 3-28. The results confirmed the quantitative metallography data and were in line with the optical micrographs presented in chapter 5, Figures 5-7 to 5-9, where the globular morphology has the lowest viscosity number.

The effort was also made to study the effect of different applied pressures on the deformation behavior and the viscosity of SEED billets where the flowability of the billets becomes almost identical with increasing the applied pressure. In addition a few tests were carried out on the billets treated with grain refiners and modifiers to further highlight the sensitivity of the in house designed and fabricated parallel plate compression machine in distinguishing the effect of minor particle size changes on the viscosity [118].

6.4.1 Pouring temperature and swirling effect

6.4.1.1 Strain-time graph

The effect of different swirling intensities on the deformation behavior of the SEED billets cast at 695°C is presented in Figure 6-7a-c for the different initial applied pressures. The most obvious result of such graphs is the superior deformation of the billets produced at high swirling intensity which if examined in conjunction with the structural analysis presented in chapter 5, Figure 5-7c, is due to the globular structure of the billet rendering better flowability. Decreasing the swirling intensities to low values or

no swirling at all, results in the formation of rosette or dendritic structures as shown in Figure 5-7b and a, respectively, which cause the SSM billets to induce resistance against deformation, harder flow, particularly for the graphs obtained at low applied pressures of 3.55 and 7.54 KPa as seen in Figure 6-7a and b.

Figure 6-8 represents the engineering strains of the billets cast at 645°C where the lower deformation is attributed to the billet produced with no swirling. This is due to the rosette microstructure, as previously described in chapter 5, Figure 5-8a. Once the swirling is applied the engineering strain increases which may be attributed to structural changes resulting from homogeneous distribution of temperature across the billet to induce some degree of globularity in the primary α-Al particles as shown in Figure 5-8b and c. it is interesting to note that swirling has improved the deformability of the billets while the intensity of swirling appears not to be critical since the low and high swirling intensity graphs are almost superimposed on one another. This may be explained with reference to the microstructural analysis where intensity is only effective to improve temperature distribution within the billet but does not improve globularity due to mechanical disintegration as seen for dendritic structure Figure 6-7. In other words further globularization expected due to swirling is almost the same at low and high swirling intensity for the rosette structure; diffusion controlled globularization. Such claim is confirmed if the strain-time graph for 630°C shown in Figure 6-9 is examined closely and in conjunction with the optical micrographs shown in Figure 5-9, where there are no drastic changes in the globular structure due to the application of different swirling intensities. Such phenomenon is the main reason of identical deformation graphs for these billets, Figure 6-9a-c, where the swirling does not dominate the morphological evolution and only the pouring temperature controls the microstructure of the SSM slurry and consequently the flowability of the billets.

The magnitude of applied pressure appears to be an important parameter in differentiating between the structures, especially at low values of 3.55 KPa and 7.54 KPa since the strain-time graphs become almost the same when high applied pressures are employed, 14.32 KPa, Figures 6-7c, 6-8c. This may be attributed to the mechanical

disintegration of primary α-Al particles, dendrites or rosettes, and thus reducing morphological differences. Furthermore the overall strain during steady state deformation is even higher for dendritic or rosette structures, Figures 6-7c and 6-8c, which may be attributed to the formation of finer particles due to mechanical breakdown of secondary or tertiary dendrite arms in the structures which improves flow behavior of the billets. For the SSM billets poured at low pouring temperature of 630°C with globular microstructure, there is no structural changes due to application of high external loads, where all the engineering strains are almost identical and the applied pressure imposes no changes in the flowability of the billets, see Figure 6-9. Table 6-1 shows the maximum engineering strains registered 600s after the beginning of deformation for all trials.
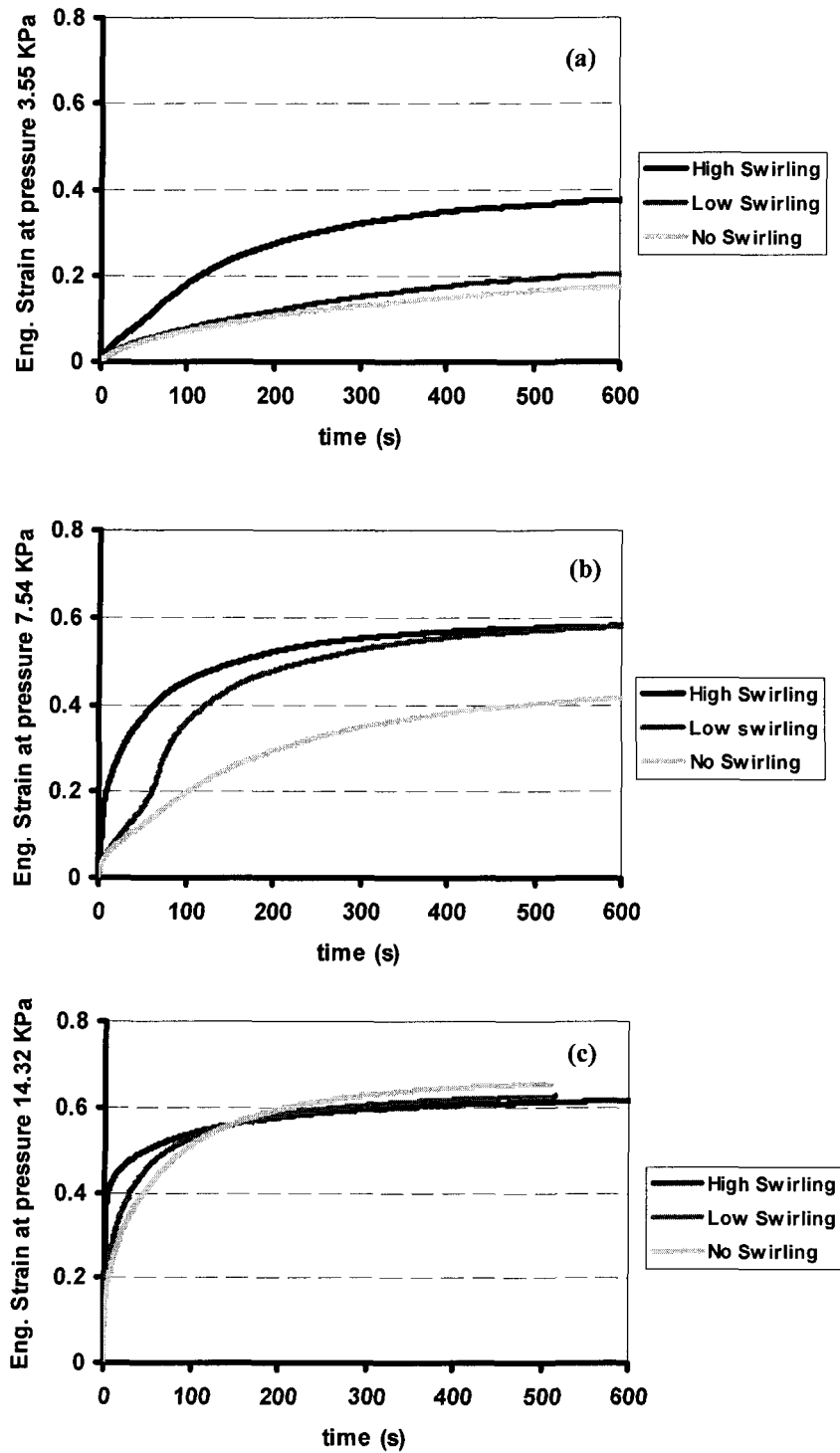
Fig. 6-7: Strain-time graphs for different primary α-Al morphologies and initial pressures at 695°C
(a) 3.55 KPa, (b) 7.54 KPa and (c) 14.32 KPa
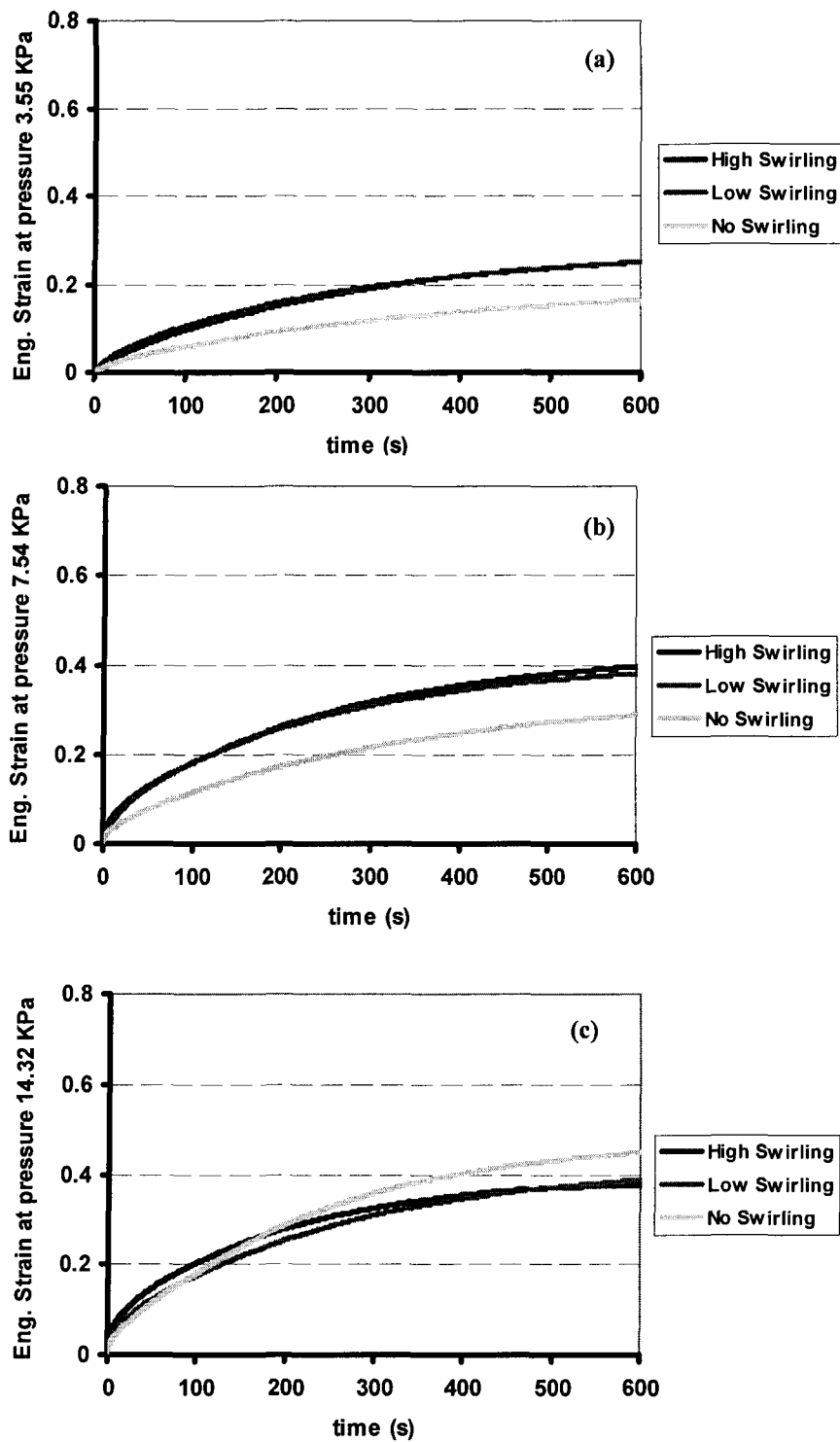
Fig. 6-8: Strain-time graphs for different primary α-Al morphologies and initial pressures at 645°C
(a) 3.55 KPa, (b) 7.54 KPa and (c) 14.32 KPa
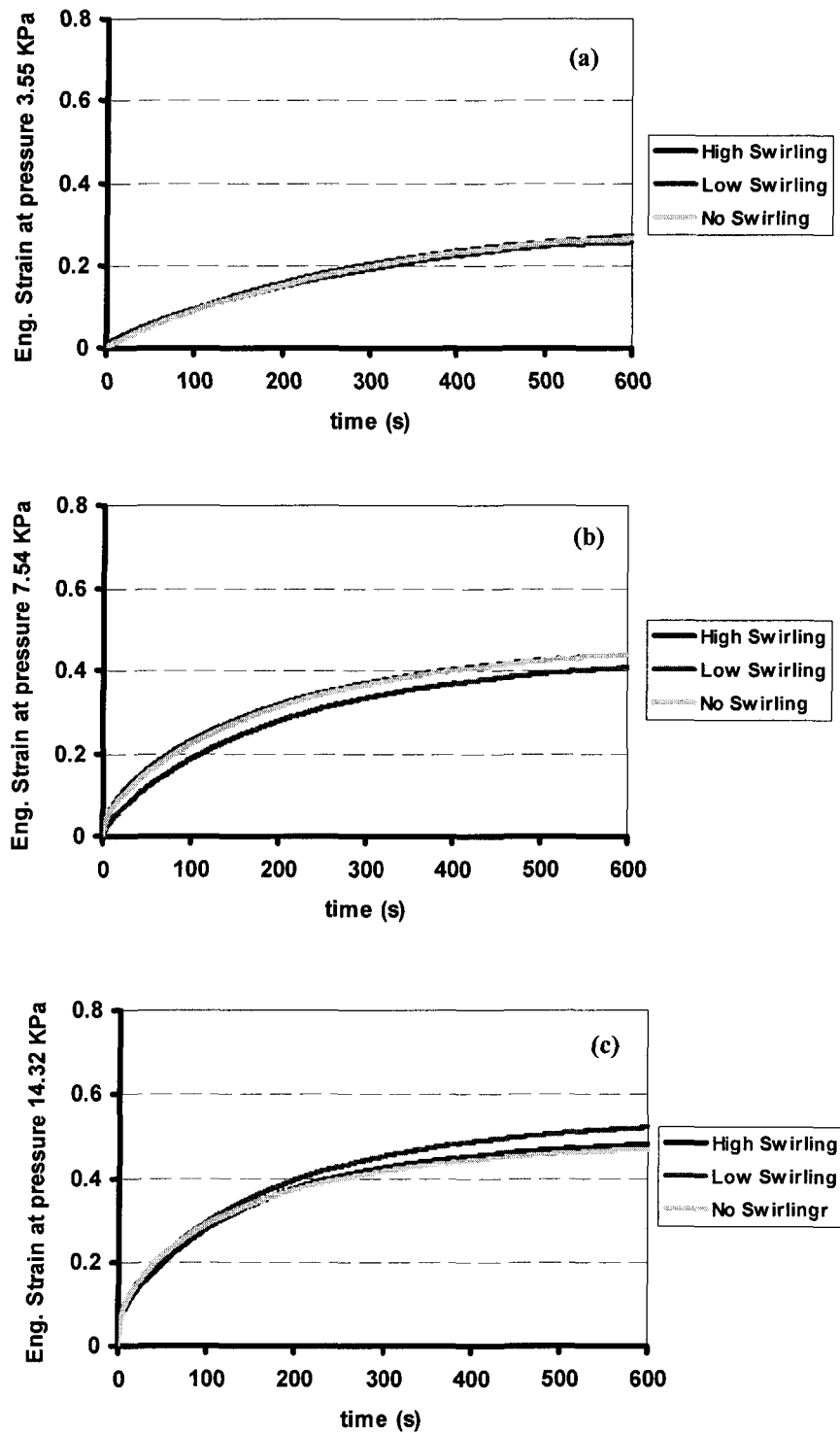
Fig. 6-9: Strain-time graphs for Globular primary α-Al morphology and different initial pressures at 630°C (a) 3.55 KPa, (b) 7.54 KPa and (c) 14.32 KPa

Table 6-2: Maximum engineering strain at different pouring temperatures and pressures after 600 s, Dendritic (D), Rosette (R), Globular (G)

	Applied Pressure	3.55 (KPa)	7.54 (KPa)	14.32 (KPa)		
		Engineering strain				
Pouring Temperature (°C)	695	0.174 D	0.414 D	0.654 D	0	Swirling Intensity
	695	0.204 R	0.577 R	0.626 R	Low	
	695	0.374 G	0.580 G	0.615 G	High	
	645	0.163 R	0.287 R	0.448 R	0	
	645	0.250 G	0.434 G	0.387 G	Low	
	645	0.249 G	0.395 G	0.375 G	High	
	630	0.270 G	0.438 G	0.481 G	0	
	630	0.256 G	0.407 G	0.546 G	Low	
	630	0.265 G	0.439 G	0.469 G	High	

6.4.1.2 Viscosity

Figures 6-10 to 6-12 show the developed graphs based on Newtonian assumption of semi solid slugs, where the left hand side of equation 3-28 is plotted versus time. These graphs, obtained from the results for height changes with time during the quasi-steady state deformation, ~200s after the beginning of each compression test, show the same behavior as the strain-time graphs. The inverse slopes of the lines in these figures are the viscosity values for each structure. The viscosity data is also listed in Table 6-3. These results also support that of the previously reported for semi solid A356 alloy [53]. In all cases, increasing the applied pressure has increased shear rate and caused less viscosity values. Dendritic structure has resisted against pressure and showed higher viscosity values than the globular morphology, at least at lower magnitudes of shear rate, Figure 6-10 a-b. The dendrite disintegration and continuous break down of the particles may be an important factor in reducing the microstructural effect at higher values of shear rate, Figure 6-10c.

Lowering the pouring temperature in SEED process increases the degree of globularity of the microstructure, desirable for SSM processing, but decreases the temperature at which the billets were deformed since as mentioned in chapter 4 the processing time was constant for all pouring temperature and the billets were deformed immediately after casting is completed. Figure 6-11 and 6-12 show that in spite of more globular feature, the SEED prepared billets at lower superheats have higher viscosity

values at the same shear rates when compared with the viscosity numbers presented for the billet prepared at 695°C, Table 6-3.
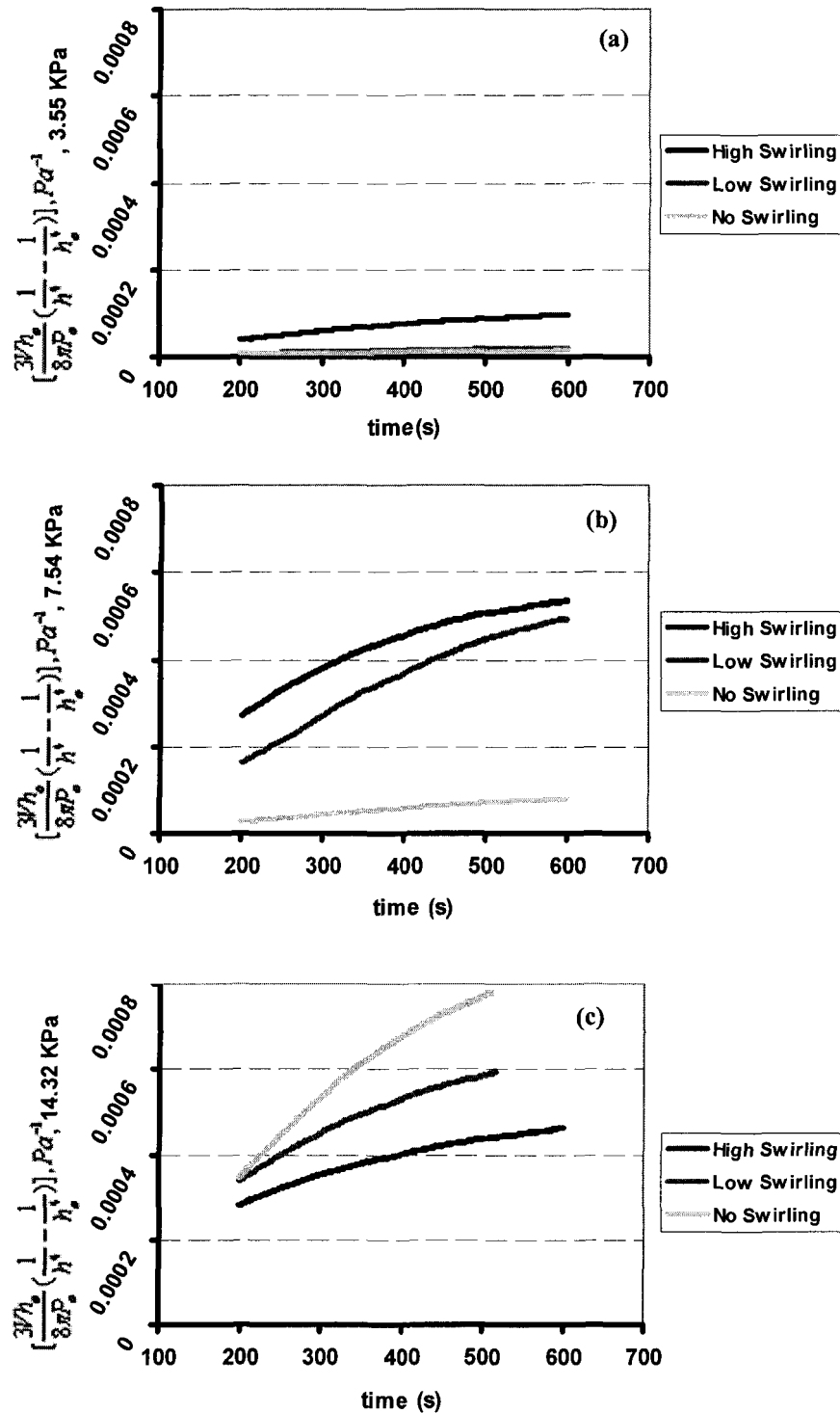
Fig. 6-10: Steady state part of equation 3-28 at 695° C pouring temperature to calculate the viscosity (a) 3.55 KPa, (b) 7.54 KPa and (c) 14.32 KPa
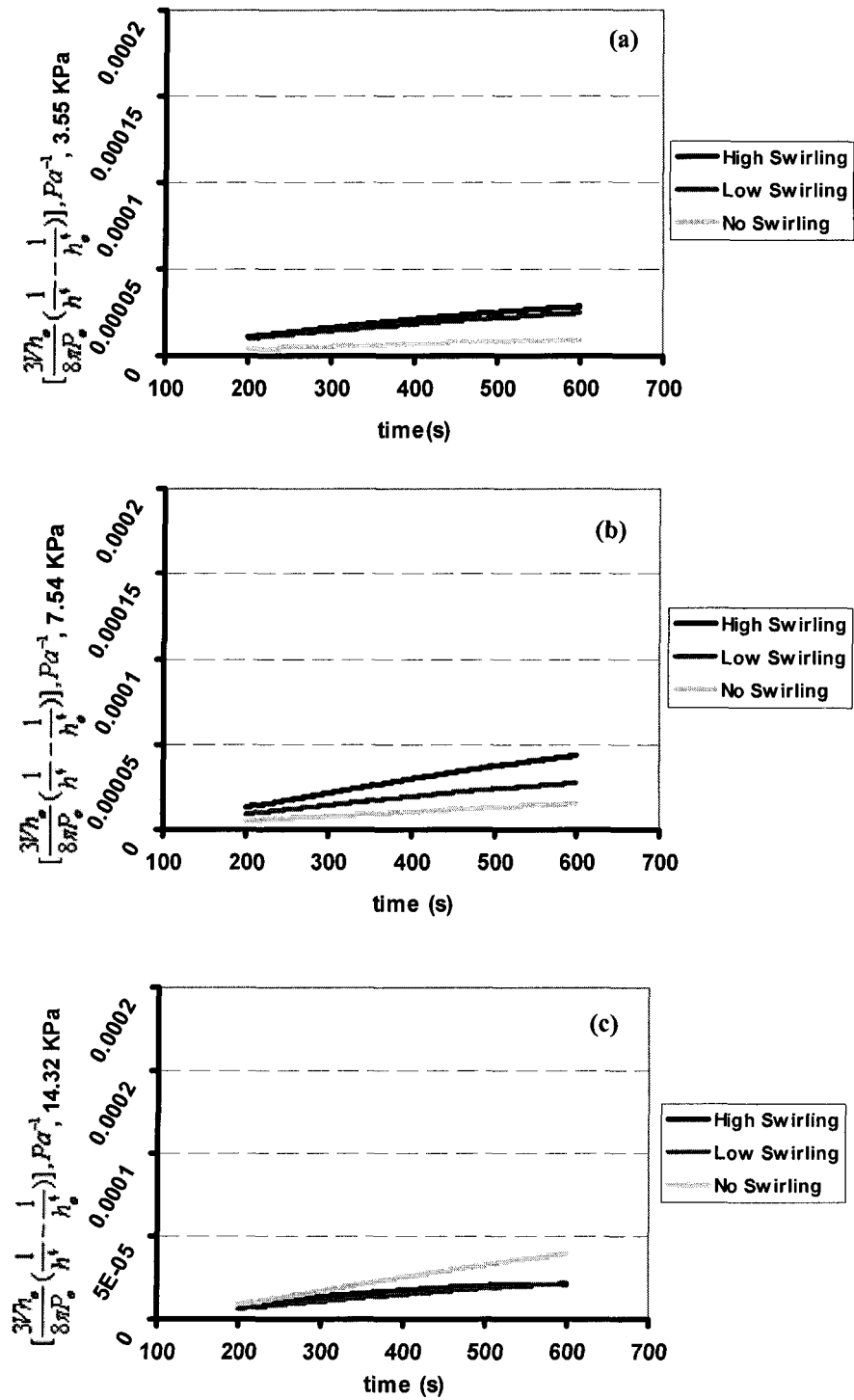
Fig. 6-11: Steady state part of equation 3-28 at 645° C pouring temperature to calculate the viscosity
(a) 3.55 KPa, (b) 7.54 KPa and (c) 14.32 KPa
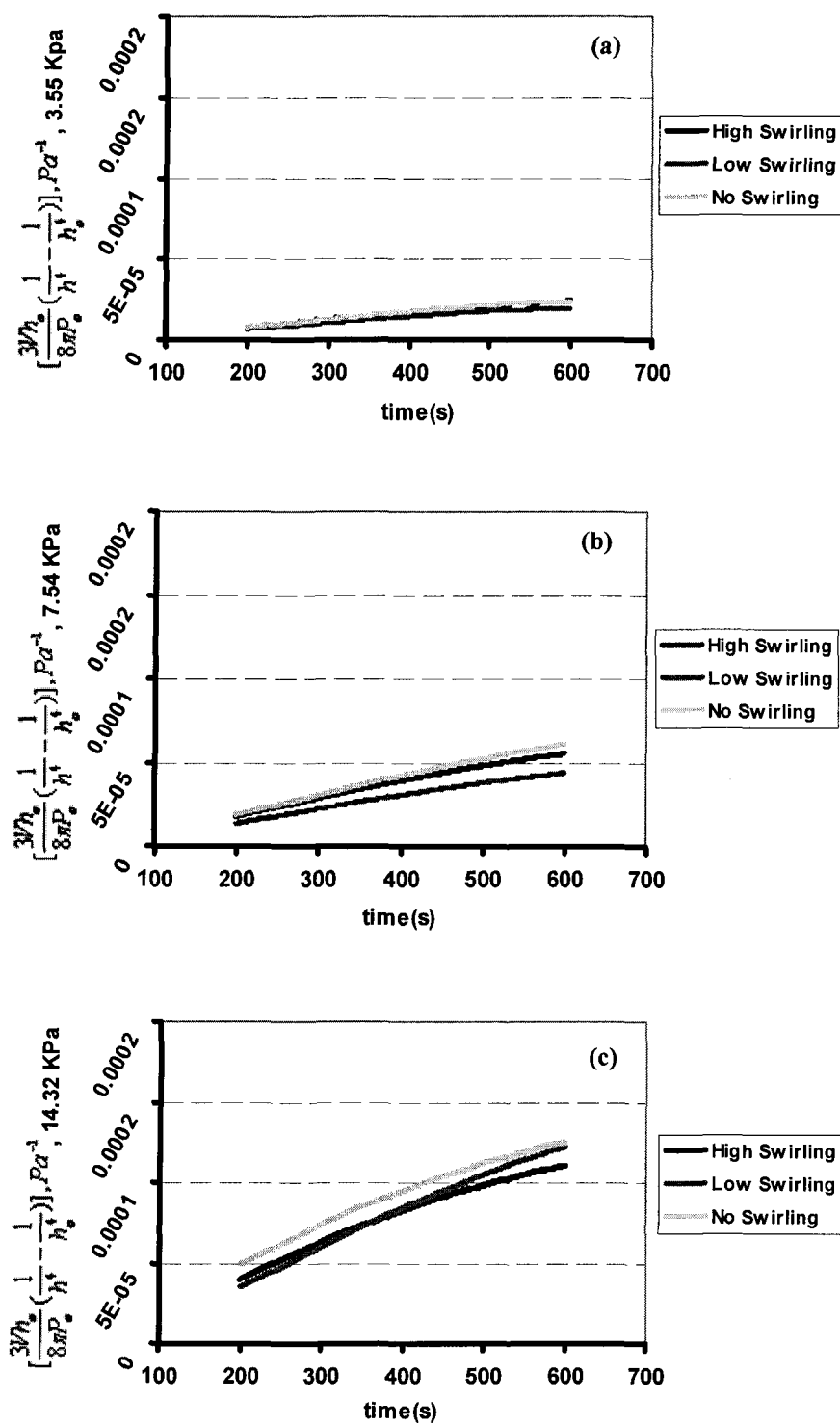
Fig. 6-12: Steady state part of equation 3-28 at 630° C pouring temperature to calculate the viscosity
(a) 3.55 KPa, (b) 7.54 KPa and (c) 14.32 KPa

In conclusion, it is advisable to keep the slug deformation temperature as high as possible by pouring the melt at higher superheat and employing high swirling intensity to have mainly globular structure. Alternatively pour at lower temperatures and application of swirling to benefit homogenous temperature distribution, but reducing the total process time to keep the final temperature of billet as high as possible. It has to be emphasized that the final billet temperature along with the morphology of the primary α-Al are the important parameters which not only affect the viscosity and thus flow characteristics of the SSM billets within the mold, Table 6-3, but also control mechanical properties of the final product [88].

Table 6-3: The calculated viscosity values, (Pa-s), at different pressures and pouring temperatures; Dendritic (D), Rosette (R), Globular (G)

Pouring Temperature (°C)	Applied Pressure	3.55 (KPa)	7.54 (KPa)	14.32 (KPa)		Swirling Intensity
		Logarithm of Viscosity (logη), [log shear rate, $\overset{o}{\gamma}$]				
	695	7.69 D [-3.68]	7.00 D [-3.25]	6 D [-2.62]	0	
	695	7.52 R [-3.6]	6.04 R [-2.89]	6.09 R [-2.63]	Low	
	695	7 G [-3.36]	6.22 G [-2.82]	6.39 G [-2.66]	High	
	645	8 R [-3.83]	7.52 R [-3.62]	7.39 R [-3.34]	0	
	645	7.39 G [-3.65]	7.22 G [-3.28]	7.39 G [-3.46]	Low	
	645	7.3 G [-3.6]	7 G [-3.4]	7.3 G [-3.4]	High	
	630	7.39 G [-3.59]	7.04 G [-3.31]	6.69 G [-2.91]	0	
	630	7.39 G [-3.65]	7.09 G [-3.39]	6.52 G [-2.97]	Low	
	630	7.39 G [-3.61]	7.04 G [-3.32]	6.69 G [-2.98]	High	

6.4.1.3 Liquid segregation

The optical micrograph in Figure 6-13 shows the distribution of α-Al particles from center to the wall of the billet. As it is evident the liquid segregation (dark regions) is not a major problem for the billets with globular morphology, prepared at high swirling intensities and compressed under 3.55-14.32 KPa applied pressures. However there is still some minor segregation of liquid, dark eutectic mixture, near the wall and expected to have no effect during further processing. This is an advantage of SEED process to render SSM billets with superior distribution of solid particles.

Liquid segregation is a problem which can be removed by lowering the viscosity, application of optimum applied force and selection of desired microstructure which can

not be necessarily globular [9, 50, 52]. Current results show no evidence of liquid segregation for the globular morphology within low applied pressure ranges.
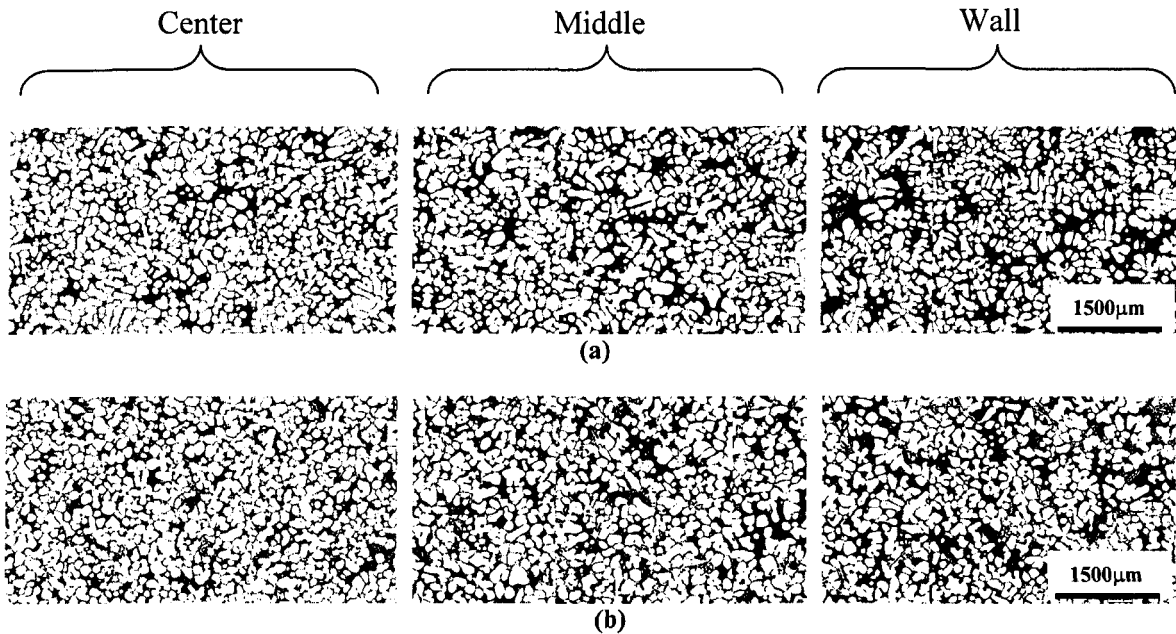
Fig. 6-13: Particle distribution from center to the wall of the samples prepared at (a) 695°C, (b) 645°C at high swirling intensity

6.4.2 Grain refining and modification effect

A comprehensive study was carried out in collaboration with another Ph. D. student Sh. Nafisi [118] to examine the effect of melt treatment, using Ti-B grain refiner and Sr Modifier additions, on the rheological properties and viscosity of A356 aluminum alloy in the semi solid state. Grain refined and Sr modified Al-Si SSM billets were prepared and tested to further highlight the ability of the in-house designed and fabricated parallel plate compression test machine in distinguishing the minor differences in the microstructure of rheocast SSM billets.

6.4.2.1 Strain-time graph

A series of grain refined, modified and combined treated billets were prepared by SEED technology at constant high swirling intensity and pouring temperature of 645°C.

The casting procedure was the same as explained for SEED process previously in chapter 4 and the billet size was 75 mm diameter and 140 mm height.

The effect of melt treatment on the deformation behavior of SEED prepared billets is clearly shown in Figure 6-14, where the base alloy shows the lowest strain values. the higher strain levels obtained for the grain refined and combined treated alloys are due to smaller globule size and lower DCP point as discussed in details elsewhere [118, 119]. Since the deformation behavior of grain-refined and combined treated SSM billets are almost the same, having the same band as shown in Figure 6-14, it is highly desirable to use the combined treated alloy in commercial applications, where in addition to its superior die fill-ability during shaping, it also renders better mechanical properties to the final components. This is because mechanical properties are dependent on both the primary α-Al particles and the morphology of silicon within the eutectic mixture and the combined treatments alters the morphology of eutectic silicon from flake to fibrous as discussed in details elsewhere [118].

The modified alloy lies somewhere between the refined/combined and the base alloy. It has been reported that strontium reduces surface tension of the melt [120,121], and renders better flow to the SSM billets.
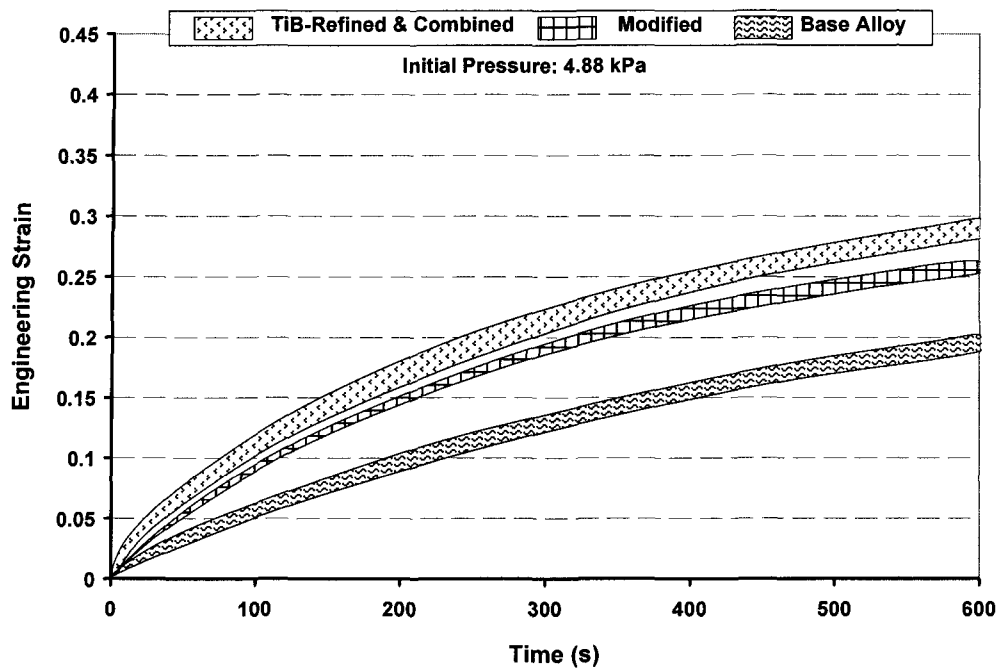
Fig. 6-14: Strain-time graphs for grain refiner and modifier, for SEED prepared billets

6.4.2.2 Viscosity

The graph presented in Figure 6-15 are calculated from the results obtained for height changes with time during the quasi-steady state deformation, as discussed previously in details.

The viscosity is calculated through inverse slope of these graphs and values are listed in Table 6-4. The results are similar to viscosity of semi solid alloys of Sn-15%Pb [96], A356 [53] and Al-SiC composites [100] having globular primary particles at similar solid fraction and shear rate. The working temperature in these series of tests was 598±2°C which according to the thermal analysis and ThermoCalc calculations result in maximum 5% variation of fraction solid [118]. The 5% solid fraction variation is normal in SSM processing and should not be a matter of concern in viscosity measurement. Besides, A356 alloy is a well-researched alloy and has low fraction solid sensitivity to minor temperature variation, which is due to its wide solidification range. This is particularly true for the narrow semisolid window used in this study, 598±2°C.

In all cases where the size of primary α-Al phase was decreased by adding grain refiner or by lowering surface tension using Sr, the viscosity values were found to be lowered. At low values of initial applied pressure, the non- refined structures have shown higher viscosity than grain refined alloys. Normally in a specified alloy, higher primary percentage leads to an increase in the viscosity value which is linked to the larger particles with less liquid percentage (which acts as lubricant). However, this is not the case for refiner addition. By inoculation, the key parameter is the reduction of the globule size with the added bonus of higher sphericity values [118]. Therefore, prevailing factors in the melt treatment procedure are size and sphericity of primaries not the slight rise in α-Al percentage [118].
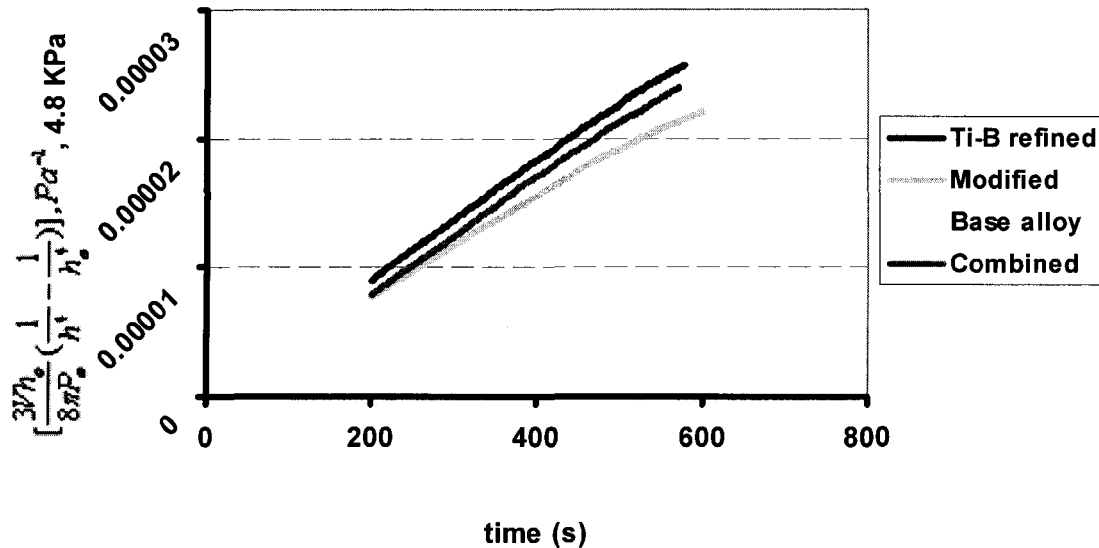
Fig. 6-15: Quasi-steady state part of the strain-time graphs, where the left hand side of equation 3-28 is plotted against time within 200-600 seconds after the beginning of each test to calculate the viscosity

Table 6-4: Viscosity values with different treatments

	Base Alloy	Ti&B-Grain Refined	Modified	Combined
Log η(Pa.s)	8.0-8.1	7.38-7.4	7.39	7.3-7.4

6.4.2.3 Liquid segregation

The main shortcoming of semi solid materials during deformation, liquid segregation, is shown in Figure 6-16 for the differently treated billets, (base, grain refined, modified and combined alloy), and deformed under initial applied pressure of 4.88 KPa. In fact the application of the external axial force causes liquid and solid phases moving in radial direction and increasing the collision amongst solid particles. In such condition the liquid phase tends to run faster than the solid particles to initiate the so-called "liquid segregation", the inhomogeneous distribution of phases in the structure. This phenomenon is exaggerated during the injection of semisolid billets in high pressure die casting due to greater magnitude of applied pressure [88].

The combined treated billets show the least segregation amongst other treated samples which is attributed to the finer and more globular α-Al primary particles along with the better distribution of this phase within the structure. [118]. The ability of fine α-Al solid particles to move easily without excessive collision results in homogenous distribution of primary α-Al phase for the billets with the combined treatment. Figure 6-16d confirms such hypothesis and shows almost no segregation for such billet [118, 119].

Center	Middle	Wall
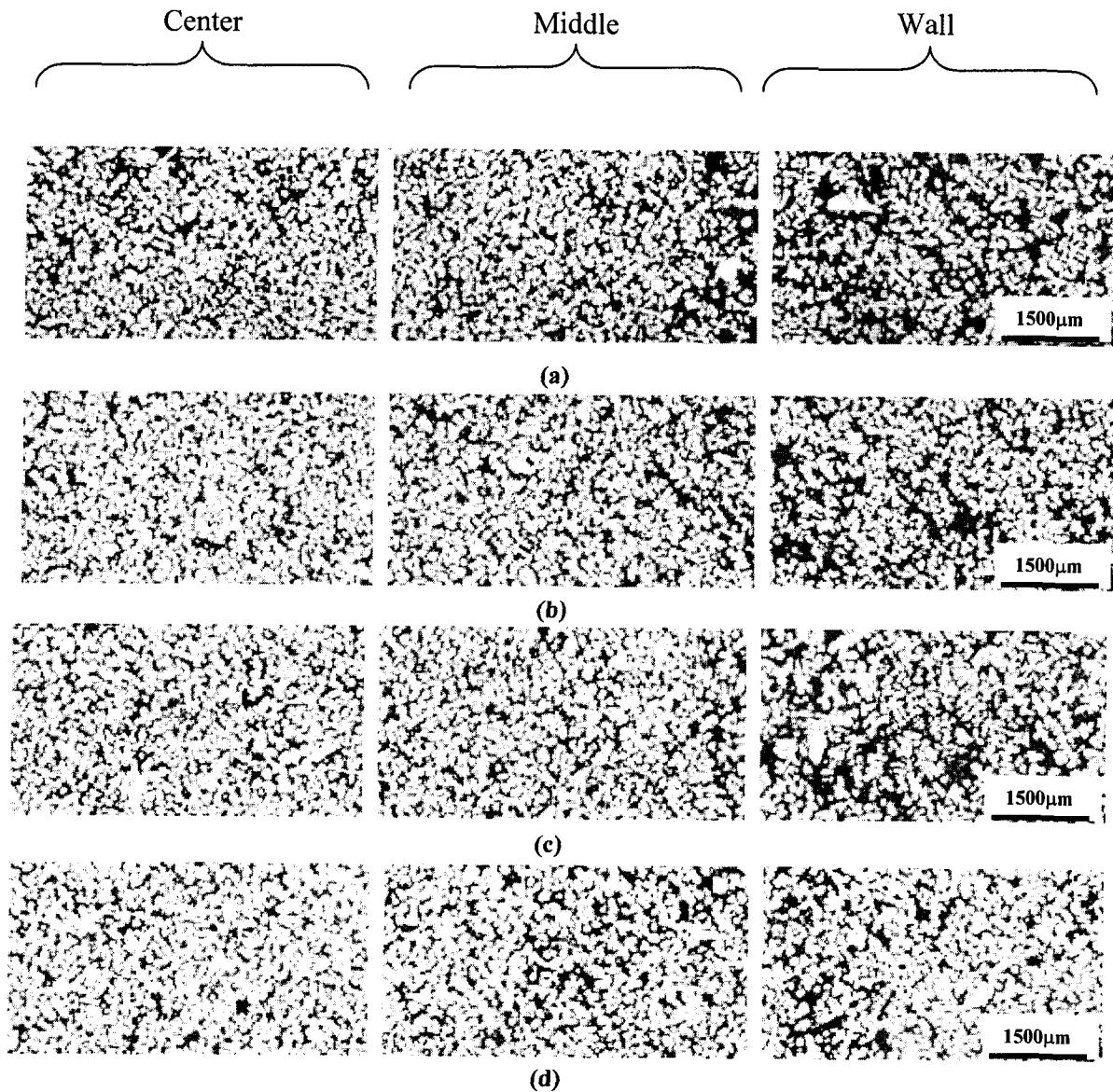
Fig. 6-16: Microstructure of deformed SSM billets from center to the wall, (a) untreated alloy, (b) refined, (c) modified, and (d) combined

CHAPTER 7
RESULTS AND DISCUSSION

RHEOLOGICAL STUDIES

CHAPTER 7
RESULTS AND DISCUSSION
RHEOLOGICAL STUDIES

7.1 Introduction

This section reports the main objective of the current research, on the implication of rheological principles to study the deformation behavior of A356 Al-Si alloy billets cast conventionally at low pouring temperature to produce globular morphology within different fraction of solid, and by the "SEED" process, at high pouring temperature and different swirling intensities, for making various morphologies at a constant solid fraction, while treating both sets of billets as Newtonian and Non-Newtonian fluids to highlight the differences between the two assumptions and to further confirm the reliability of Newtonian fluid assumption for SSM billets at low shear rates, employed in chapter 6 for microstructural characterization. Furthermore, attempts were made to propose empirical relationships to underline the correlation between the viscosity and the material and test parameters such as fraction solid, and morphology (average aspect ratio) of the primary phase and shear rate respectively.

In order to make sure of the uniform barreling of all SSM prepared samples in these series of tests, the billet size of 75 mm diameter and ~100 mm height was employed in all trials, where ~30% reduction in billets height is seen in comparison with the billets employed in chapter 6. For the conventional casting, 1.2 kg of molten alloy was poured at temperature of 630°C. Solidification of the alloy continued down to the billet temperatures of 595±1, 590±1 and 585±1°C at the center of the billets and fraction solid of about 0.33, 0.40 and 0.46, respectively. For the SEED billets, 1.4 kg melt was poured at 695°C within different swirling intensities to produce billets with different microstructures where the fraction solid was registered at 0.36 after decanting the residual liquid, details explained in chapter 4.

The prepared billets were tested using parallel plate compression test and the viscosity values were determined for different solid fractions and morphologies. The time of reaching to the steady state part of the deformation graph for the current sample size of 100 mm height was speeded up, i.e. smaller segments I and II in graph 6-1, where the quasi steady state was assumed to have been reached 50 s after the beginning of each test in this chapter. This matter is discussed in details later.

7.2 Strain-time graph

7.2.1 Fraction solid and Morphology effect

The main objective in this chapter is to study the effect of fraction solid and its morphology of the alloy used here under rheological behavior of the billets prepared conventionally and by the SEED technology.

Figure 7-1, which illustrates the strain changes with time for conventional billets, also shows the effect of solid fraction on the deformability of the billets under a given constant applied pressure. Increasing the fraction solid makes deformation more difficult since there are more collisions expected to take place between the solid particles with increasing solid fraction. Such resistance to deformation may be compensated with increasing the applied pressure, where as shown in Figure 7-2, the engineering strain has increased with, applied pressure. These are further confirmations of the fraction solid effect on the flowability of SSM slurries while an external force is applied, as set forward by the early researches during seventies [5].
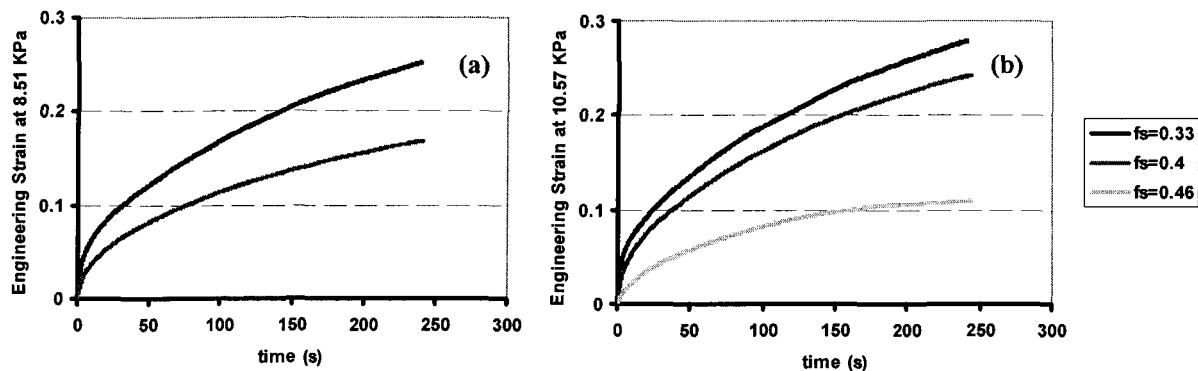
Fig. 7-1: The effect of fraction solid on the engineering strain-time behavior for Conventional cast billets having globular microstructure, i.e. 630°C pouring temperature,
(a) P_o= 8.51 KPa, (b) P_o= 10.57KPa
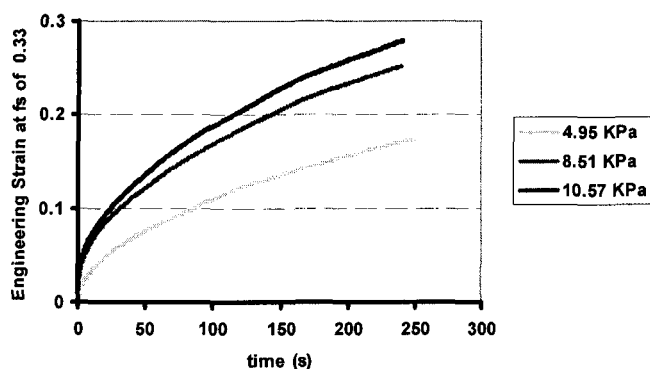
Fig. 7-2: The effect of applied pressure on the engineering strain-time behavior for Conventional cast billets having globular microstructure at fs = 0.33

The graphs presented in Figure 7-3 are typical strain-time behavior of the SEED billets cast at different swirling speeds. The differences in the morphology of primary α-Al particles have distinct effect on the engineering strain. The dendritic structure shows the lowest deformation rate while globular morphology deforms at much higher rate, i.e. easier to flow. The applied pressure appears to be an important parameter in differentiating between structures, since as it was increased from 3.55 KPa to 7.54 KPa, the flow behavior of all structures improved, Figure 7-3. This is also a further confirmation of the results presented in chapter 6 and Figure 6-7.

The overall resulting data for the fraction solid, morphologies, initial pressures and the total engineering strain are presented in Table 7-1 for both Conventional and SEED billets. The fraction solid is calculated at the temperature the billets deformed using Scheil's equation with a constant partition ratio of k = 0.13 [122]. For the SEED the values of fraction solid are calculated by including the 25% drainage of the residual liquid as already explained in experimental procedure in chapter 4.
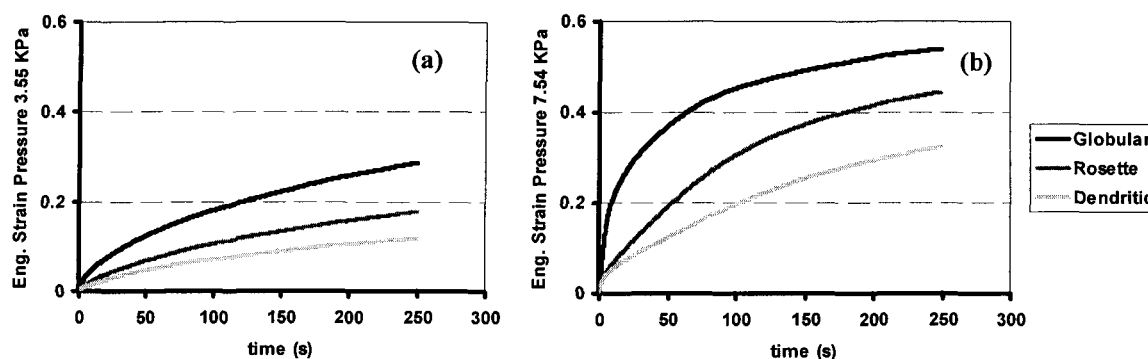
Fig. 7-3: The effect of primary α-Al morphology on the Engineering strain-time behavior for SEED billets poured at 695°C with f_s= 0.36, (a) P_0= 3.55KPa, (b) P_0= 7.54 KPa

Table 7-1: Experimental Data for Conventional and SEED trials,
Dendritic (D), Rosette (R), Globular (G)

Experiment No.	Deformation Temperature °C	Fraction Solid, f_s	Initial Pressure, KPa	Total Strain, e, after 200 s
Globular structure, 630°C, Conventional				
1	595±1	0.33	4.95	0.155
2	595±1	0.33	8.51	0.233
3	595±1	0.33	10.57	0.258
4	590±1	0.4	8.51	0.155
5	590±1	0.4	10.57	0.224
6	590±1	0.4	13.35	0.241
7	585±1	0.46	10.57	0.105
8	585±1	0.46	13.35	0.188
9	585±1	0.46	15	0.21
Different morphology 695°C, SEED		Fraction solid after 25% drainage		
10	599±1	0.36±0.01 D	3.55	0.105
11	599±1	0.36±0.01 R	3.55	0.117
12	599±1	0.36±0.01 G	3.55	0.273
13	599±1	0.36±0.01 D	7.54	0.293
14	599±1	0.36±0.01 R	7.54	0.476
15	599±1	0.36±0.01 G	7.54	0.521
16	599±1	0.36±0.01 G	14.32	0.576
17	599±1	0.36±0.01 G	14.32	0.59
18	599±1	0.36±0.01 G	14.32	0.583

7.3 Viscosity

The viscosity values are calculated for both Conventional and SEED billets, assuming the SSM billets behaving as Newtonian and non-Newtonian fluids, where the effect of solid fraction and its morphology at low shear rates, is studied on the viscosity of so prepared billets.

7.3.1 Newtonian fluid assumption

The simplest way to analyze the results obtained during compression test is to assume the semi solid alloy behaving like a Newtonian fluid. This is a reasonable assumption if the shear rate value is low, less than 0.01 (s^{-1}), and does not vary greatly across the billet during compression. In this case the resulting engineering strain-time graphs could be treated mathematically with the equations 3-26 to 3-28 to calculate the

viscosity of the semi-solid cylindrical billets, as employed for the characterization of microstructure in chapter 6 [96, 102, 103].

Figure 7-4, the developed graphs from Newtonian first law, i.e. equation 3-28, using the instant height values during the steady state condition of deformation which begins at about 50s after the beginning of each compression test in these series, shows the same trend as the strain-time graphs of Figures 7-1 to 7-3. The shorter height of these billets, ~100 mm, in comparison with those reported in chapter 6, ~140 mm, causes shorter period for unsteady state sections of deformation, segments I and II in Figure 6-1, where the easy movement of the primary particles is more restricted and the collision amongst the particles takes place earlier, i.e. quasi steady state deformation approaches faster; after 50 seconds in the present case. Viscosity is calculated through the inverse slope of such graphs. The calculated values of viscosity, and shear rates together with the fractions solid and average aspect ratio ($\overline{AR}$), as an indication of morphology, are listed in Table 7-2. The results obtained for the new billets size also support previous findings for the viscosity of semi solid alloys of A356 [53, 97], Pb-15%Sn [96] and Al-SiC particulate composite [100] having similar fraction solid and globular morphology and tested within the same range of shear rates as plotted in Figure 7-5.

Evidently, the magnitude of viscosity increases with increasing fraction solid, introduction of more dendritic structure or reduction of applied pressure. The reverse trend has been seen for lower fraction solid, globular morphology or higher applied pressure, Figure 7-4. Lowering pouring temperature down to the liquidus point provided appropriate conditions where the formation of equiaxed α-Al particles within the melt brought about lower viscosity numbers. Increasing the pouring temperature induces directional heat flow and encourages the formation of columnar dendritic structure with a resistible character against flow [5]. It is further noticeable that the viscosity numbers have decreased with increasing shear rate, Figure 7-6, which confirms the shear thinning behavior of the semi solid billets tested in this study, i.e. pseudoplastic behavior. Such behavior is also detectable in Figure 7-5, where a range of viscosity values are shown from previous studies. Furthermore, similar behavior was seen for the SSM samples having different morphologies regardless of casting route, Table 7-2. In other words, the

SSM billets are non-Newtonian fluids by nature, i.e. viscosity changes with shear rate. This is treated in more details in the following section.

The average aspect ratio, $\overline{AR}$, is obtained from image analysis measurements and changes from one (1) for fully isolated globular particles and increases slowly depending on the complexity of the morphology and agglomeration of the primary particles. It is important to emphasize that although there may not be much difference in the magnitude of $\overline{AR}$ for dendritic and globular structures as measured by image analysis of as-cast structures, in realty the differences are considerable even with $\overline{AR}$ differing only by one tenth of one. This is because of the nature of image analysis measurement where it only distinguishes between isolated and continuous particles and treats the detached secondary or tertiary dendrite branches, resulting due to sectioning and polishing, as isolated and individual globular particles, detailed explanation is given in chapter 5. The resulting average aspect-ratio values would be quite close for dendritic and globular structure. Therefore, it would be misleading if the $\overline{AR}$ values alone are compared. For instance, the average aspect-ratios measured for the microstructures in Figures 5-3b and 5-3d are 1.5 and 1.7 respectively, while as can be seen there are huge and distinctive differences between the two structures of these billets.
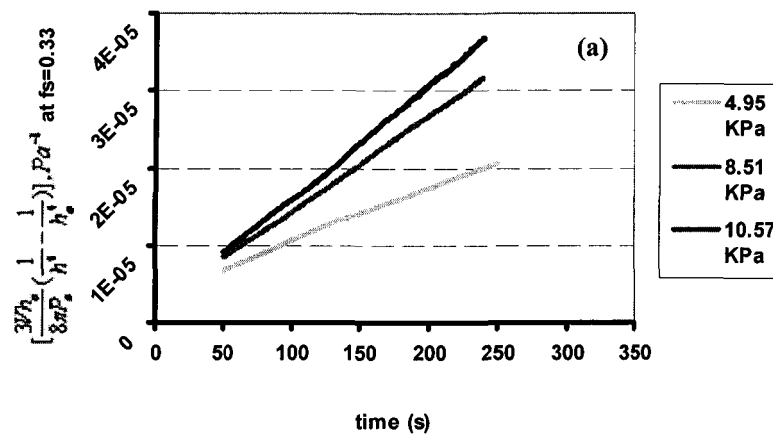
Fig. 7-4: continues
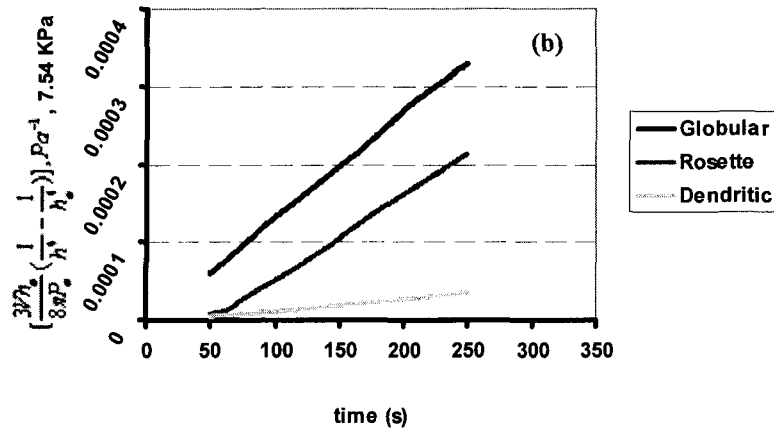
Fig. 7-4: The right hand side of equation 3-28, $[\frac{3Vh_0}{8\pi P_0}(\frac{1}{h^4}-\frac{1}{h_0^4})]$, Pa^{-1}, is plotted against time for the steady-state part of the deformation, to calculate the viscosity at different solid fractions and morphology, (a) Conventional casting, (b) SEED Process

Table 7-2: Logarithm of Viscosity (Pa-s), at different shear rates (s^{-1}), fractions solid and morphology, (Newtonian analysis)

Fraction Solid	$Log \overset{o}{\gamma}$	Log η	$Log \overset{o}{\gamma}$	Log η	$Log \overset{o}{\gamma}$	Log η	$Log \overset{o}{\gamma}$	Log η	$Log \overset{o}{\gamma}$	Log η
f_s=0.33	-3.16	7.11	-3.01	6.95	-2.92	6.82	----	----	----	----
f_s=0.4	----	----	-3.22	7.35	-3.12	7.18	-2.91	6.95	----	----
f_s=0.46	----	----	----	----	-3.35	7.69	-3.09	7.3	-3	7.18

Aspect Ratio	$Log \overset{o}{\gamma}$	Log η	$Log \overset{o}{\gamma}$	Log η	$Log \overset{o}{\gamma}$	Log η
AR=1.5	-3.36	7.09	-2.82	6.5	-2.6	6.3
AR=1.6	-3.6	7.69	-2.89	6.8	----	----
AR=1.7	-3.68	8	-3.25	7.09	----	----
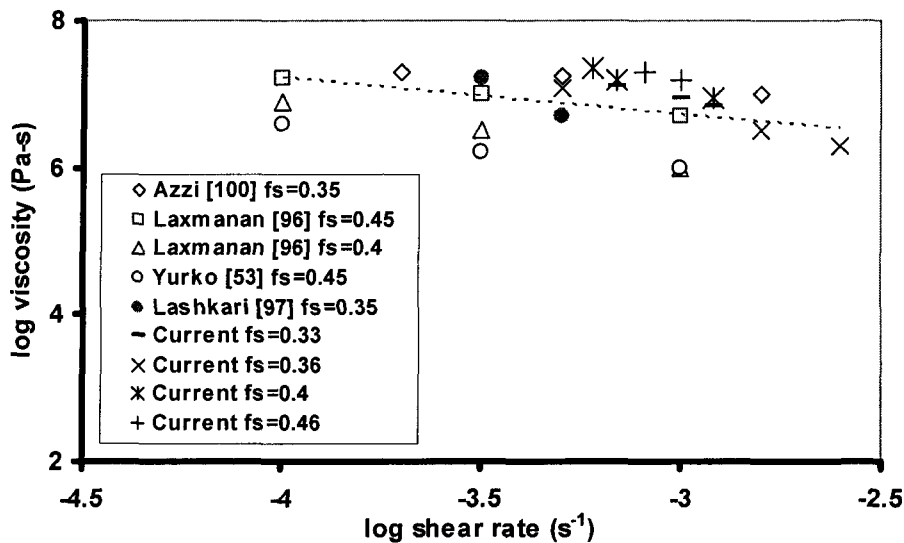
Fig. 7-5: The comparison of the current results with those reported in the literature. The dotted line is just an average value for the collected data
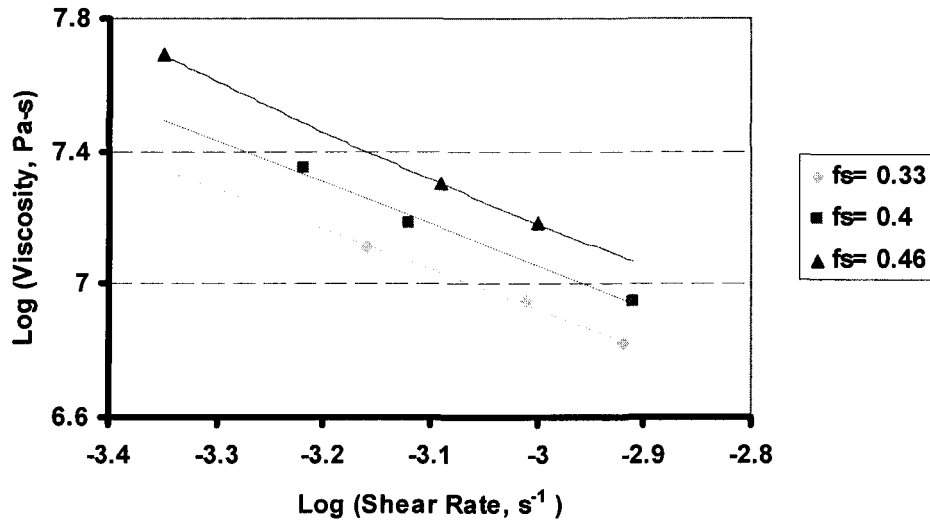
Fig. 7-6: The viscosity versus average shear rates for SSM
samples prepared by Conventional route having different fractions solid

The Figures 7-5 and 7-6 and the results presented in Table 7-2, show the reduction of viscosity logarithm versus shear rate either for different fraction solid or variant average aspect ratios which means shear thinning behavior, psuedoplasticity, of SSM prepared billets. As explained in previous paragraphs, psuedoplasticity is an indication of non Newtonian fluid behavior of semi solid samples. Therefore, efforts have been made to analyze the deformation behavior of the SSM billets through non Newtonian fluid assumption.

7.3.2 Non Newtonian assumption

The non-Newtonian power law model is widely used to study rheological behavior of SSM slurries [53, 96, 100, 102, 103]. The model expresses viscosity changes in terms of applied stress and resulting shear rates, $\eta = m \overset{o}{\gamma}{}^{n-1}$ equation 3-9, where m and n are the consistency and power law index respectively [109]. If the SSM billets are treated as non-Newtonian fluids, the solution to the flow equations for cylindrical sample squeezed between two parallel plates are as equations 3-30 to 3-32 (see Appendix A):

In order to calculate the values of m and n, the logarithmic of engineering strain, log(1-e), should be plotted against time, log t, and the slope of such graph and its intercept with strain axis should provide the necessary means to calculate m and n [109]. This is given in Figure 7-7, plotted for billets prepared by Conventional method having fully globular structure but different fractions solid deformed at different applied pressures. Figure 7-8 is the same as Figure 7-7, but the billets are SEED having different morphologies but equal fraction solid. The graphs are plotted for the steady state deformation i.e. after 50s of deformation commencement in the current tests. The values of m and n, the material constants, were then calculated from these Figures in conjunction with the equations 3-30 to 3-32. The resulting m and n were further substituted in equation 3-9 to calculate viscosity numbers.

The calculated viscosities, shear rates, m and n, are listed in Table 7-3 for different fractions solid and morphologies of the primary α-Al particles. The viscosities of the billets when treated as non-Newtonian fluids are close to those of the results with the Newtonian fluid assumption of the semi solid alloy, Table 7-2. The values of the viscosity for billets tested with the same shear rate, fraction solid and/or morphology are very similar and confirm the validity of Newtonian fluid assumption to simplify the viscosity calculation within low shear rates range.
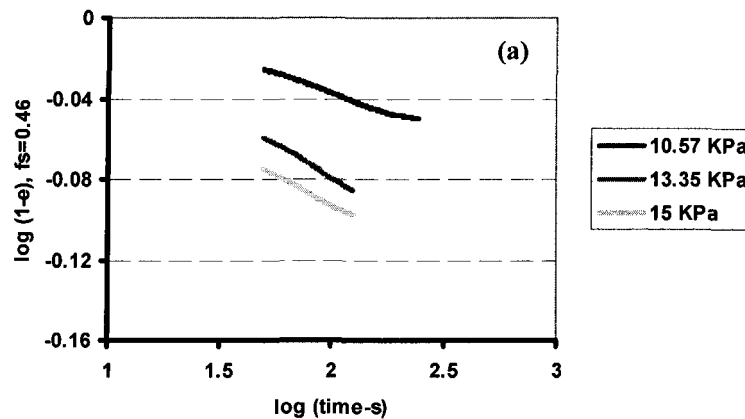
Fig. 7-7: Continues
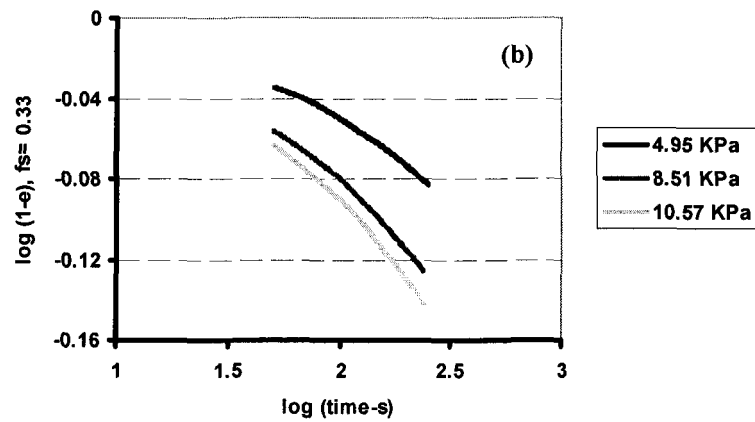
Fig. 7-7: The variation of strain vs time for billets prepared by Conventional having different fractions solid and deformed at different applied pressures (a) fs = 0.46, (b) fs = 0.33
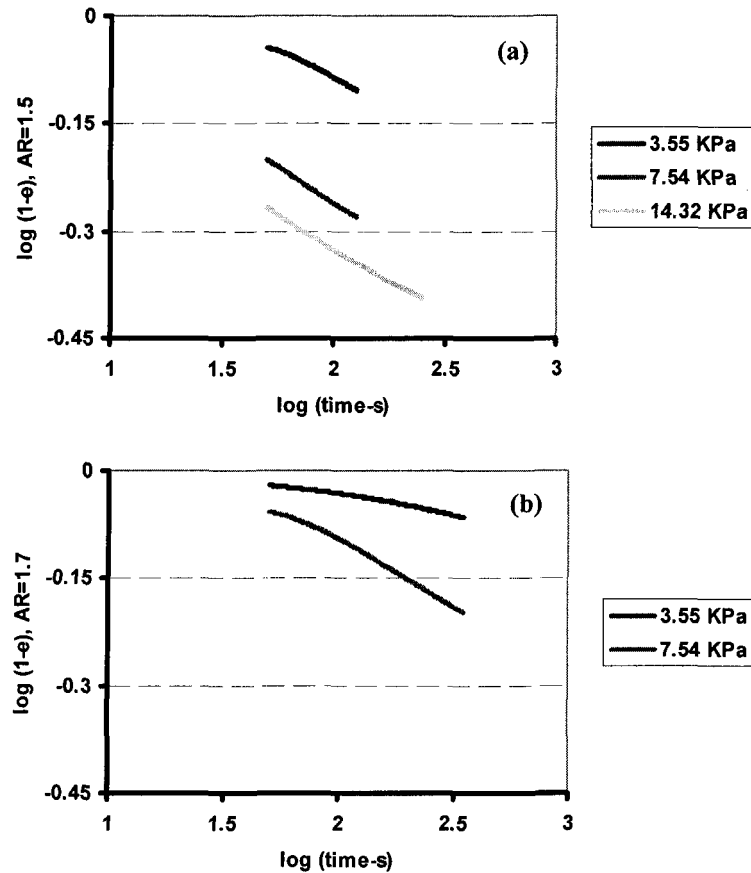
Fig. 7-8: : The variation of strain vs time for billets prepared by SEED having different morphologies but similar fractions solid and deformed at different applied pressures

(a) $\overline{AR}$ =1.5, (b) $\overline{AR}$ =1.7

Table 7-3: Logarithm of Viscosity numbers (Pa-s), n and m at different shear rates (s⁻¹), fractions solid and morphology, Non-Newtonian analysis

Fraction Solid	$Log\,\overset{o}{\gamma}$ Log η	$Log\,\overset{o}{\gamma}$ Log η	$Log\,\overset{o}{\gamma}$ Log η	$Log\,\overset{o}{\gamma}$ Log η	$Log\,\overset{o}{\gamma}$ Log η
f_s=0.33	-3.16 7.19	-3.01 7.14	-2.92 7.09	---- ----	---- ----
f_s=0.4	---- ----	-3.22 7.47	-3.12 7.24	-2.91 6.88	---- ----
f_s=0.46	---- ----	---- ----	-3.35 7.78	-3.09 7.39	-3 7.39
f_s=0.33	n=0.313, log m=5.02	n=0.332, log m=5.06	n=0.379, log m=5.20	----	----
f_s=0.4	----	n=0.230, log m=4.99	n=0.268, log m=5.109	n=0.280, log m=5.181	----
f_s=0.46	----	----	n=0.098, log m=4.8	n=0.134, log m=4.872	n=0.182, log m=5.025

Average Aspect ratio	$Log\,\overset{o}{\gamma}$ Log η	$Log\,\overset{o}{\gamma}$ Log η	$Log\,\overset{o}{\gamma}$ Log η
$\overline{AR}$=1.5	-3.36 7.10	-2.82 6.39	-2.6 6.20
$\overline{AR}$=1.6	-3.6 7.62	-2.89 6.64	---- ----
$\overline{AR}$=1.7	-3.68 7.72	-3.25 7.09	---- ----
$\overline{AR}$=1.5	n=0.410, log m=5.12	n=0.593, log m=5.53	n=0.634, log m=5.22
$\overline{AR}$=1.6	n=0.350, log m=5.3	n=0.553, log m=5.93	----
$\overline{AR}$=1.7	n=0.332, log m=6	n=0.542, log m=6.51	----

Figures 7-9 and 7-10 are plotted to highlight the effect of structural parameters, fraction solid and its morphology, on the materials constants m and n. Equations 7-1 to 7-4 show the resulting relationships for n and m obtained from the trend fitted to these Figures;

$$m = 10^{(5.56-1.39f_s)} \qquad 0.33 < f_s < 0.46 \qquad (7\text{-}1)$$

$$n = 0.87 - 1.56\ f_s \qquad 0.33 < f_s < 0.46 \qquad (7\text{-}2)$$

$$m = 10^{(1.85-4.9\overline{AR})} \qquad \text{for } 1.5 < \overline{AR} < 1.7 \qquad (7\text{-}3)$$

$$n = 0.97 - 0.255\ (\overline{AR}) \qquad \text{for } 1.5 < \overline{AR} < 1.7 \qquad (7\text{-}4)$$

It should be noted that the equations for m and n do not include the applied pressure and the resulting shear rate. This is because of the negligible effect that applied

pressure has on *m* and *n* values as seen in Figures 7-9 and 7-10 where the points, each representing a specific applied pressure for each fraction solid, do not vary much.

The effect of structural parameters on materials constants, *m* and *n*, is only reported for fraction solid [53, 96, 100, 102, 103], but not for morphology.

The graphs in Figure 7-9 show the descending behavior of *m* and *n* with increasing fraction solid within fs = 0.33-0.46 range calculated from equations 7.1 and 7.2. The current results for *m* are in good agreement with several previous reports [102-103] but contradict others [53, 100] where an ascending trend is reported for *m* with fraction solid. For *n* however, the reported data is quite dispersed [53, 100, 102, 103] with no particular trend detected or reported when *n* plotted against fraction solid. Such controversy could be attributed to different rheological properties of the alloys used here and in the reported literature as well as the morphological disparity between primary phases in each respective alloy. Regardless of the disparity within the reported results for the trends of *n* and *m*, the values of *m* and *n* in the current research and those of others [53, 96, 100, 102, 103] are within the same range and have similar magnitudes.

As for the effect of primary phase morphology, the graphs in Figure 7-10 together with the related equations 7-3 and 7-4 show the reducing and increasing trends for *n* and *m* respectively with increasing the average aspect ratio at a constant fraction solid, 0.36. The effect of morphology is not reported before; probably due to the fact that all tested SSM slurries were fully globular. The validity of equations 7-3 and 7-4 is therefore verified using the results of Conventional casting [97] for SEED and visa-versa as discussed later for viscosity numbers.
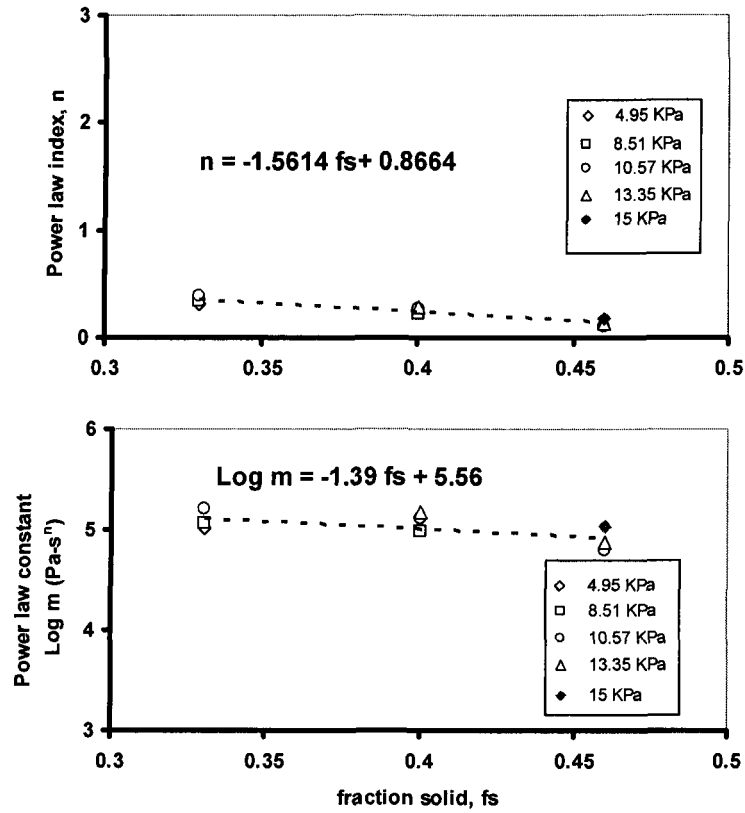
Fig. 7-9: Effect of solid fraction on the power law index, (*n*) and constant, (*m*)
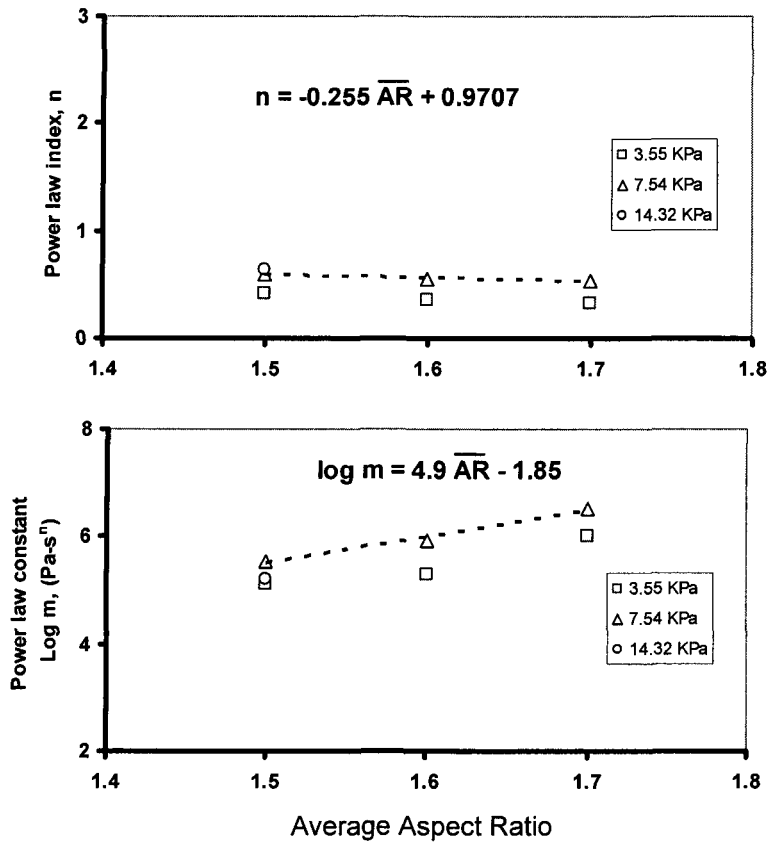
Fig. 7-10: Effect of primary α-Al particle aspect ratio on the power law index, (*n*) and constant, (*m*)

Having established the effect of solid fraction and morphology on the material constants, they are then substituted (equations 7-1 to 7-4) in the equation 3-9 for the calculation of m and n, and to generate empirical relationships for the power law model incorporating fraction solid and morphology of the primary α-Al particles. Such equations, 7-5 and 7-6, are useful to predict the viscosity of semi solid materials within a specific fraction solid range and morphology, i.e. average aspect ratio.

$$\log \eta = 5.56 - 1.39 f_s - (1.56 f_s + 0.14) \log \overset{o}{\gamma} \tag{7-5}$$

$$\log \eta = -1.85 + 4.9 \overline{AR} - (0.255 \overline{AR} + 0.03) \log \overset{o}{\gamma} \tag{7-6}$$

The empirical relationship of equation 7-5 expresses the direct effect of fraction solid on the viscosity of semi solid billets and if fraction solid kept constant, the viscosity varies inversely with the shear rate. This is in good agreement with the previous reports [5, 96]. The decreasing trend for the viscosity with increasing the applied pressure and resulting shear rate, in both sets of experiments, confirms once again the pseudoplastic behavior of SSM A356 alloy, at least within the shear rates reported in the current study, less than 0.01 s^{-1}.

In order to further confirm the validity of equation 7-5, the viscosity is plotted against shear rate in Figure 7-11 for different fractions solid and the values from literature are superimposed on these graphs. There is a good agreement between the predicted values, equation 7-5, and the previously reported results [96, 97, 100]. In spite of good agreement at low shear rate, equation 7-5 appears to be less reliable when the shear rate is beyond 10^{-1} s^{-1}. This is presented in Figure 7-12, where the predicted value for viscosity at shear rate of 10^{3}s^{-1} is almost three orders of magnitude greater than those reported for A356 SSM alloy in the literature [11]. The calculated viscosity number from equation 7-5 at a shear rate of $\overset{o}{\gamma}$=10^3, is around 10^4-10^5 Pa-s while the reported values [11] are about 100 Pa-s.

This is an indication of the fact that shear rate plays an important role on the viscosity value of SSM slurries and the empirical equations are only valid for certain range of shear rates.
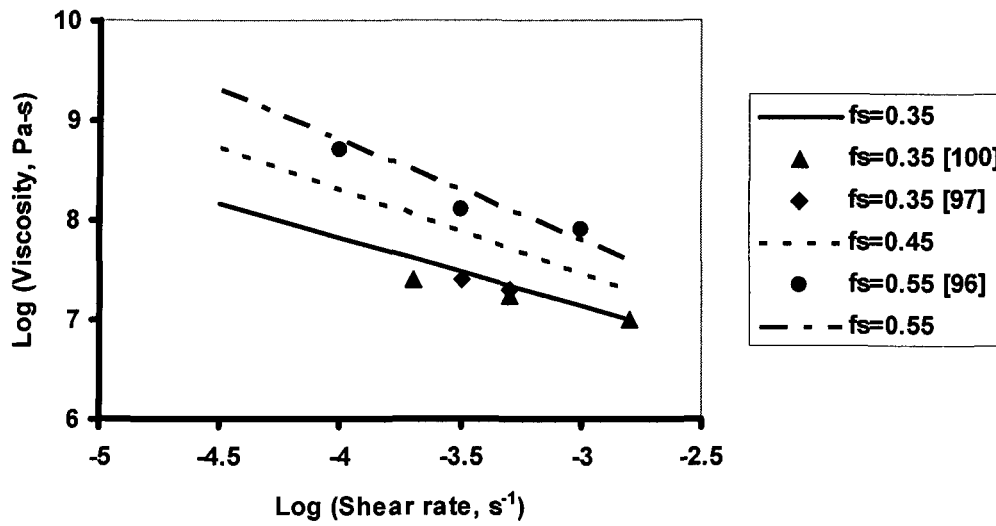
Fig. 7-11: The predicted effect of shear rate on the viscosity of SSM billets at different fraction solid obtained from equation 7-5, (lines). The points are values reported by other investigators
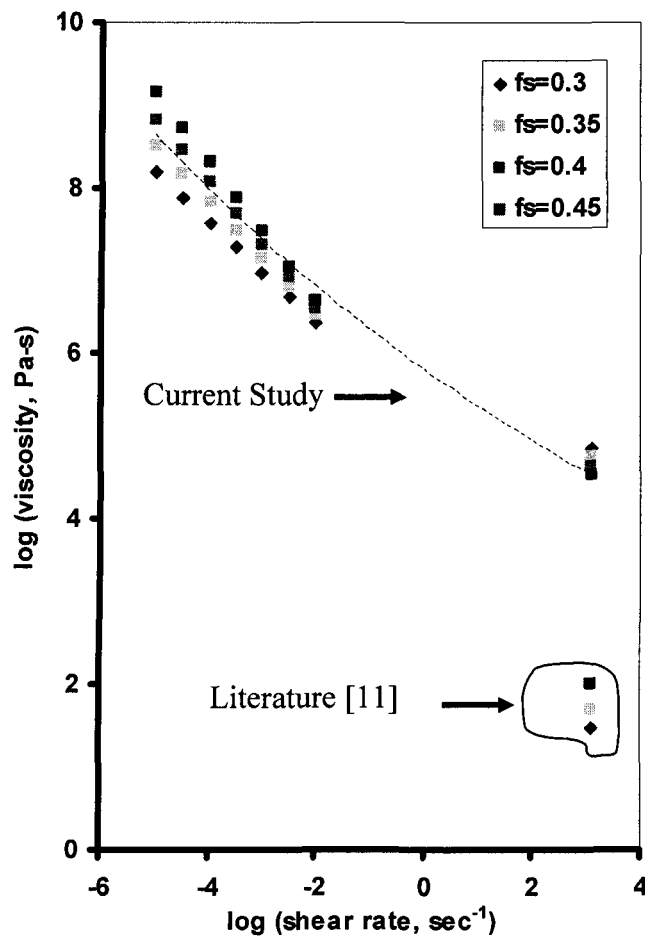
Fig.7-12: The effect of shear rate on the viscosity of SSM billets according to equation 7-5 to highlight the importance of shear rate

A similar approach to that of fraction solid was used to highlight the effect of morphology on the viscosity by incorporating the average aspect-ratio in the empirical equation for viscosity, i.e. combining equations 7-3, 7-4 and 3-9. The resulting equation 7-6 was plotted in Figure 7-13 to emphasize the importance of solid phase morphology on the viscosity number. Such equation also justifies the concept of rheology, where the viscosity of slurries could be altered by changing the morphology of solid phase [5, 53]. In contrast to fraction solid, other reports could not be found to substantiate the validity of the empirical relationship given here, equation 7-6. This is because of the lack of an effective method to quantify the particle morphology and associated theoretical model to account for the effect of particle morphology. To the best of author's knowledge, Fan and Chen [84] and Zoqui et al. [34] who have recently reported the effect of morphology on the rheology of SSM alloys, used fractal dimension and rheocast quality index respectively, explained in chapter 3, not aspect-ratio. In other words, there is not any report where aspect-ratio is correlated to viscosity.

Therefore, equation 7-6 is plotted for SEED billets having different morphologies but substantiated with the results of Conventional tests having globular, $\overline{AR}$ =1.4 or dendritic, $\overline{AR}$ = 1.8, morphologies [97]. Figure 7-13 further shows the psuedoplastisity of the SEED prepared SSM A356 billets within low shear rates range, where the viscosity decreases with increasing shear rate.
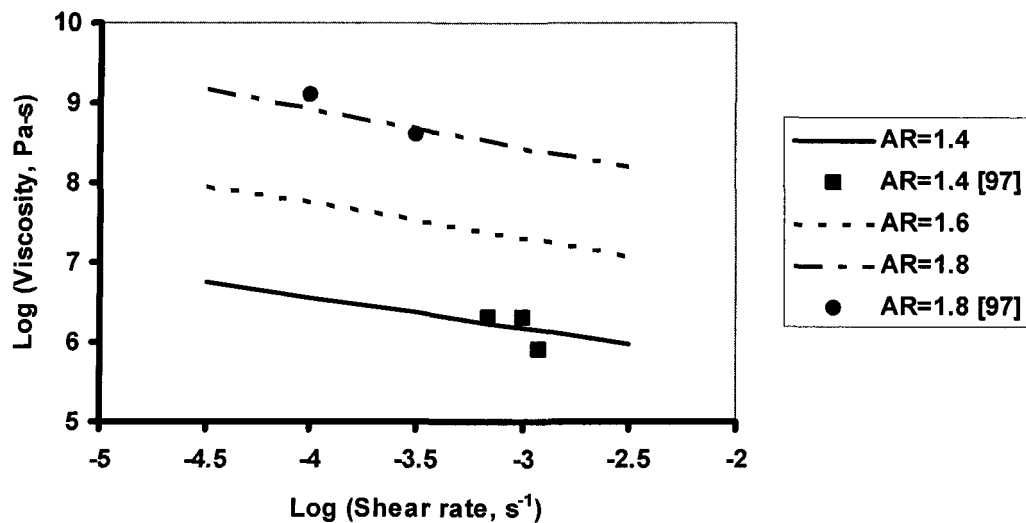
Fig. 7-13: The predicted effect of shear rate on the viscosity of SEED prepared SSM billets for different morphologies of the solid particles, equation 7-6, (lines). The points are values from Conventional tests and those reported in literature [97]

CHAPTER 8
RESULTS AND DISCUSSION

RHEOLOGICAL STUDIES -
SAMPLE SIZE EFFECT

CHAPTER 8
RESULTS AND DISCUSSION
RHEOLOGICAL STUDIES -
SAMPLE SIZE EFFECT

8.1 Introduction

Generally the sample size effect on the rheological behavior of materials is not a matter of concern if the homogeneity of temperature and shear rate within the sample is maintained. Nonetheless it is preferred to perform tests on small size specimens to reduce the cost of testing, since for larger specimens more powerful machines are needed. In the case of parallel plate compression viscometry [96, 100] the small size discs of aspect ratio less than 1 (h<<d) are used which refers back to the mathematical calculation of viscosity for cylindrical samples based on the assumption that there is negligible deformation in the direction parallel to the applied load axes to reduce mathematical complexity.

Current research employed the same mathematical treatments, presented in chapter 3, to calculate the viscosity within the large scale billets, as discussed within previous chapters of 6 and 7, and the obtained data in all trials were in good agreement with other results reported in literature. But in order to further confirm the reliability of the obtained results in this research and to highlight that the sample size has no effect on the final deformation and viscosity values, a new series of tests were designed and performed. This section as a supplementary part of Rheological studies attempts to compare the viscosity values coming from conventional cast billets of 75mm diameter and 140 mm height, presented in chapter6, and small discs of 25mm diameter and 10mm height prepared from the same original large size billets. The SSM samples were assumed once again to behave as Newtonian fluid, where the compression tests carried out at very low shear rates

8.2 Sample size effect

Rheo-route, conventional casting, and Thixo-route, explained in chapter 2, approaches were used to study the effect of semi solid processing on the deformation behavior of SSM A356 alloy by testing cylindrical samples with two height/diameter (h/d) ratios of 0.4 and 1.8.

Conventional casting was employed to produce different morphologies for the primary α-Al phase within the rheocast billets of 75mm diameter and 140 mm height. The prepared billets were transferred onto the parallel plate compression test machine to deform under different initial applied pressures of 5-11 KPa and temperature of 595°C where the fraction of α-Al phase is 0.33 according to lever rule and Scheil equation discussed before. The detailed information for the conventional cast billets is presented in chapter 6.

The compression test was also performed on the small size discs, 10 mm thickness and 25 mm diameter, machined from conventional cast-water quenched billets, reheated to 595°C and compressed with the same initial pressures of 5-11 KPa. The small discs, hereafter, are referred to thixocast discs

8.3 Microstructure

8.3.1 Rheocast

Figure 5-3 shows the effect of pouring temperature on the microstructural features of A356 alloy. Details microstructural examinations of these billets are given in chapter 5.

8.3.2 Thixocast

Figure 8-1 shows the effect of reheating on the microstructure of the small thixo-disks machined out of the quenched rheo-billets, Figure 5-3. The main differences between the two structures are the formation of entrapped liquid, minor disintegration of dendrites, Figure 8-1a, and coarsening of the primary α-Al particles regardless of pouring temperatures as shown in Figures 8-1a, b and c. This is the natural consequence of reheating the small disks to the compression test temperature, 595°C, resulting in better

diffusion of alloy constituents to encourage dendrite disintegration, mainly due to dendrite branch root necking and remelting and coarsening by Ostwald ripening and particle coalescence mechanisms.

However, the differences in the microstructure are not significant and it is acceptable to assume the structures of both rheo-billets and thixo-disks are almost the same, as shown in Figures 5-3 and 8-1, just before deformation. Quantitative metallography results in Figure 8-2 further support such assumption. One of the distinct features of reheating of thixo-disks to the deformation temperature is the formation of small quantities of entrapped eutectic, liquid, as seen in Figure 8-1a which have negligible effect on the viscosity. Therefore, if there is any considerable discrepancy in the viscosity values, it could be mainly attributed to the sample size for each respective morphology, since both the testing parameters, including applied pressure, temperature and shear rate, and metallurgical parameters, morphology, size and distribution of primary α-Al particles, are almost identical for the two sets of specimens.

(a)

(b)

(c)
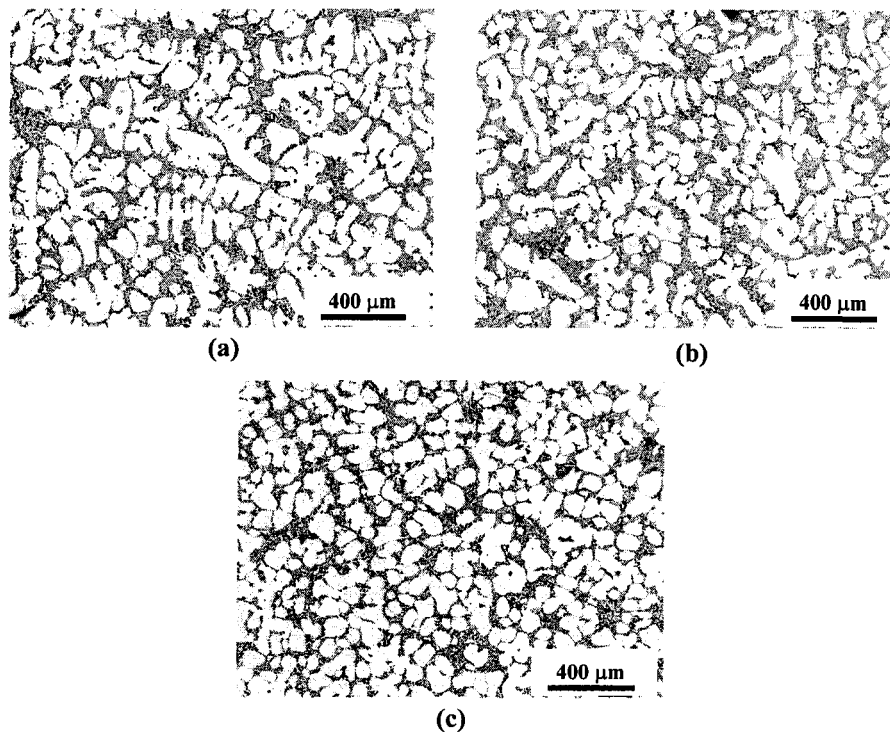
Fig. 8-1: Typical microstructure formed after 15 minutes reheating to 595°C of the thixo-disks initially cast at different pouring temperatures;
(a) 675°C-dendritic, (b) 630°C -rosette, (c) 615°C-globular

159
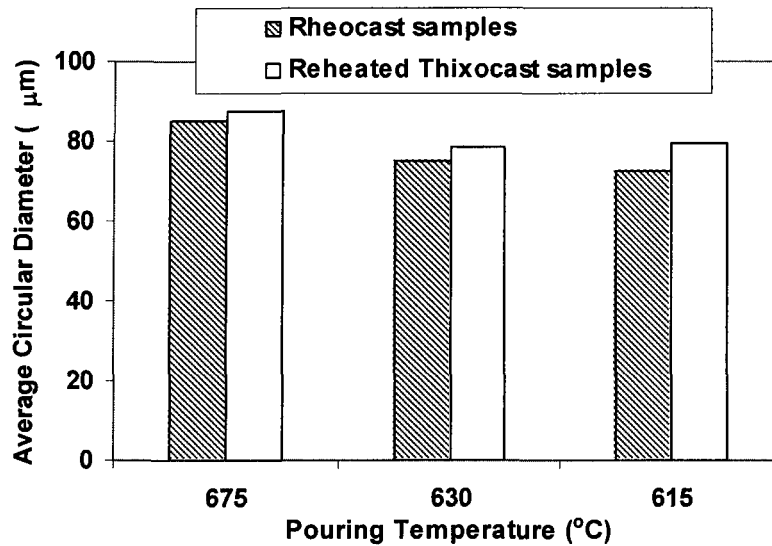
Fig.8-2: Average equivalent circular diameter of the primary α-Al particles just before deformation for both rheo-billets and thixo-disks

8.3.2.1 Isothermal deformation

The microstructural evolution of the primary α-Al particles after 5 minutes isothermal deformation at 595°C for the rheo-billets and thixo-disks is presented in Figure 8-3. The optical micrographs were taken from the samples prepared from the most deformed region of the rheo-billets and thixo-disks, Figure 8-3 (a and b). The distinct feature of the microstructures in Figure 8-3 is the general coarsening of the primary α-Al particles when compared with those of Figures 5-3 and 8-1. The disintegration of the dendritic structure into rosette-globular morphology is due to a series of processes active during isothermal deformation including break down, either mechanically or diffusion controlled mechanisms such as dendrite arm root necking and remelting, and general coarsening dominated by Ostwald ripening. For rheo-billets the process of coarsening is uniform across the bulk structure since the primary α-Al particles are dispersed within the residual liquid matrix and therefore solute distribution due to diffusion and convection is uniform. This is also the case for the thixo-disks where the localized liquid pools, formed during reheating beyond solidus, are negligible, Figure 8-3 (d and f), and thus not expected to impart any significant changes. In both cases, the primary α-Al particles have spheroidized and coarsened when deformed isothermally, but the structure of thixo-disks appears to be more prone to globularization and coarsening than the rheo-

billets. This is probably due to reheating stage, where spheroidization and coarsening were active even before the start of deformation.

The effect of applied external pressure is also the same in both cases where the residual liquid in the rheo-billets and thixo-disks acted as lubricant to enhance the movement of solid phase particles during deformation and at its worst case to induce liquid segregation. The fact that the thixocast disks have larger particle size than the rheo-billets goes back to the coarsening effect during reheating which could have resulted in imposing a larger particle size gradient across the structure to eventually improve the kinetics of coarsening process, Ostwald ripening mechanism. This is particularly true for dendritic structure, if Figures 8-3 c and d are compared.

Figure 8-4 shows the primary α-Al particles sizes of rheo-billets and thixo-disks before and after 5 minutes isothermal deformation. The quantitative results are in good agreement with the micrographs in Figures 5-3, 8-1 and 8-3, where the thixo-disks comprise larger primary α-Al particles. Furthermore, the higher the pouring temperature, the greater is the particle size, since there are lower isolated particles at higher pouring temperature due to dominance of dendritic morphology.

(a)   **(b)**

Schematic diagrams of (a) Rheo- billets, and (b) Thixo-disks, to show the areas
where microstructural analysis performed

(c)   **(d)**

(e)   **(f)**
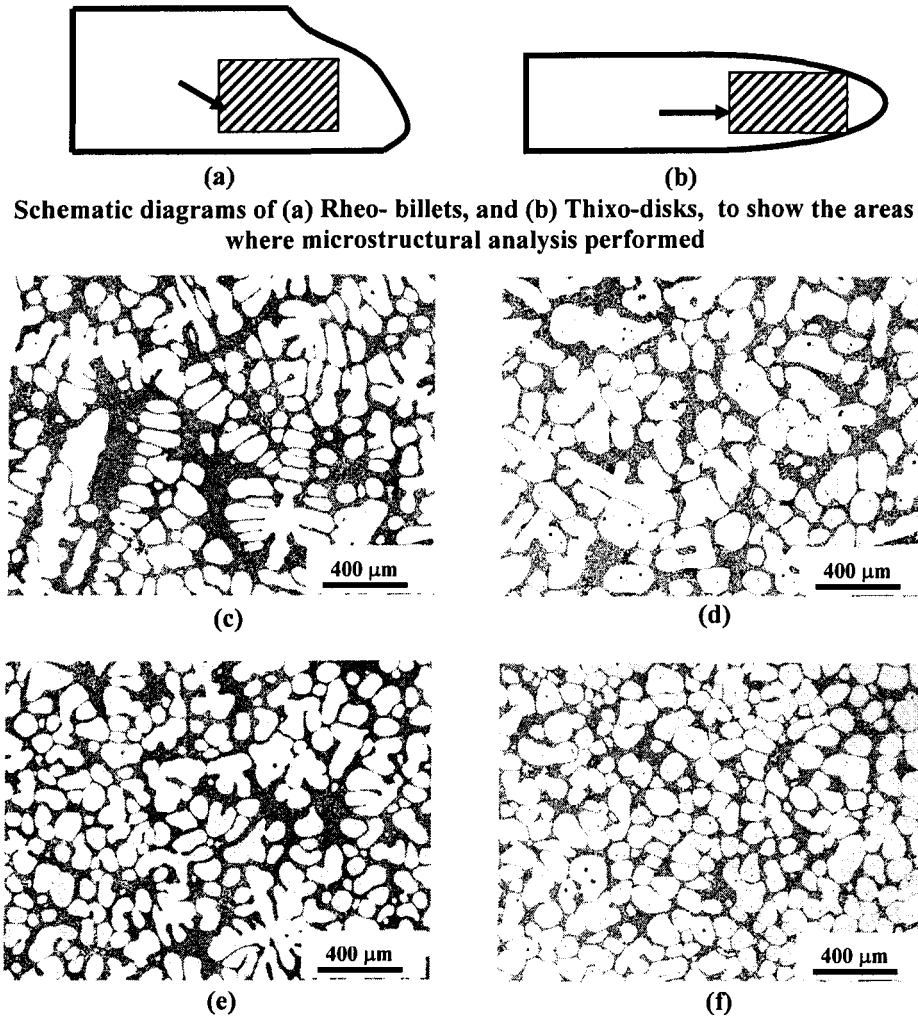
Fig. 8-3: Typical microstructure after 5 minutes of isothermal deformation at 8.9 KPa
initial pressure at 595°C for specimens cast at different pouring temperatures;
(c) Rheo-billet, 675°C, (d) Thixo-disk, 675°C, (e) Rheo-billet, 630°C, (f) Thixo-disk, 630°C
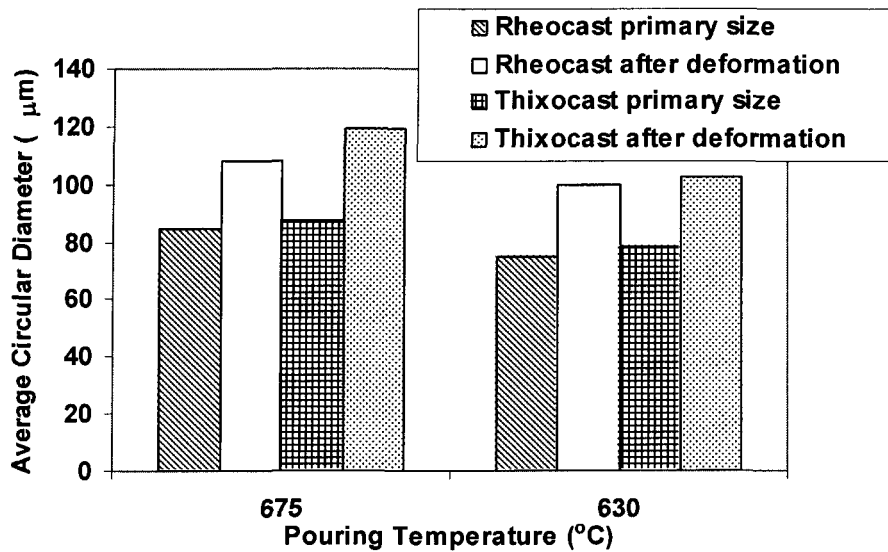
Fig. 8-4: Average equivalent circular diameter of the primary α-Al particles just before deformation
and after 5 minutes isothermal compression for both rheo-billets and thixo-disks

8.4 Strain-time graph

Figure 8-5 is plotted to highlight the differences between the rheo-billets and thixo-disks having dendritic and rosette/globular structures respectively. It has to be reiterated here that the sample size is the main variant, since as shown in Figures 5-3 and 8-1, the microstructure of rheo-billets and thixo-disks are almost the same for each respective pouring temperature especially for the rosette/globular structures, see Figures 5-3b, 8-1b, 8-3e and 8-3f. The differences between the strain-time graphs for the rosette/globular morphology, Figure 8-5b, is less pronounced and considering the experimental scatter including minor size changes of the primary α-Al particles due to coarsening during reheating of thixo-disks, both rheo-billets and thixo-disks show similar flow behavior irrespective of huge sample size differences. For the dendritic microstructure, the differences between the strain-time graphs of the rheo-billets and thixo-disks, Figure 8-5a, are greater than those of rosette/globular. It is believed the morphological changes including coarsening effect is more pronounced for dendritic structures than rosette/globular morphology, if the optical micrographs of Figure 5-3a, 8-1a, 8-3c and 8-3d are examined closely. Table 8-1 gives the engineering strain values of all trials after 200 s of the beginning of deformation. It is quite clear that the pouring temperature, which is the main parameter to alter the microstructure, controls the engineering strain values, not the sample size. This is further discussed when the viscosity values are reported in the next section.
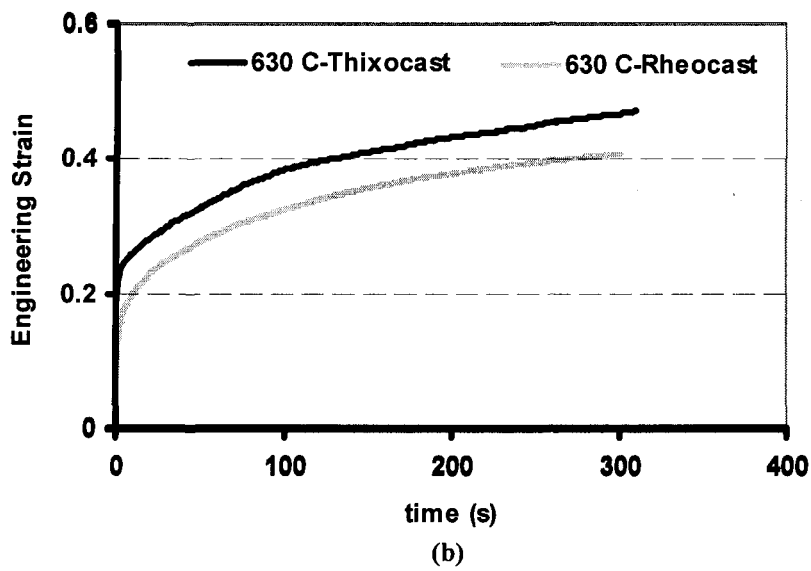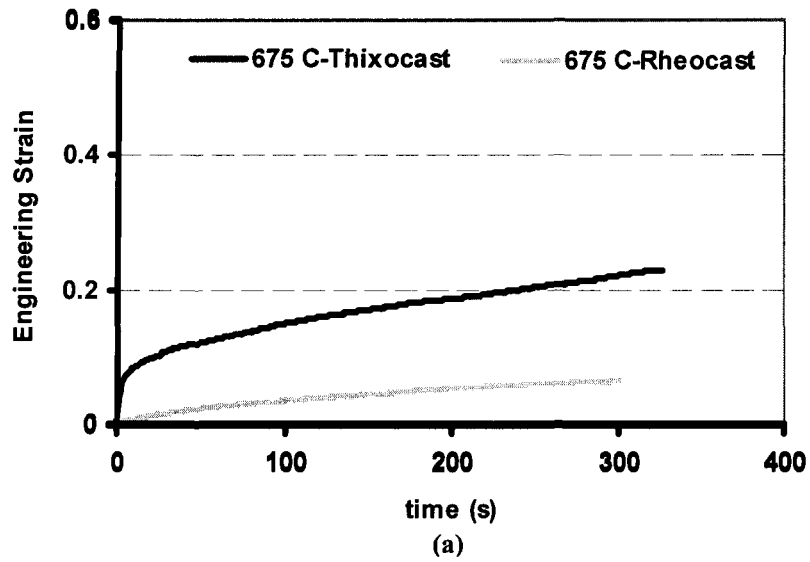
Fig. 8-5: Strain-time graphs obtained at different routes and different microstructures for the pouring temperature of (a) 675°C, (b) 630°C, (applied pressure = 8.9 KPa)

Table 8-1: Engineering strain Data for Rheocast and Thixocast trials deformed at 595±1°C,
Dendritic (D), Rosette (R), Globular (G)

Experiment No.	Pouring Temperature °C	Fraction Solid, f_s	Initial Pressure, KPa	Total Strain, e, after 200 s
Rheocast Samples				
1	695 D	0.33	4.8	0.03
2	695 D	0.33	8.9	0.03
3	695 D	0.33	11.2	0.04
4	675 D	0.33	4.8	0.03
5	675 D	0.33	8.9	0.05
6	675 D	0.33	11.2	0.07
7	645 R	0.33	4.8	0.21
8	645 R	0.33	8.9	0.24
9	645R	0.33	11.2	0.37
10	630 G	0.33	4.8	0.22
11	630 G	0.33	8.9	0.37
12	630 G	0.33	11.2	0.45
13	615 G	0.33	4.8	0.36
14	615 G	0.33	8.9	0.55
15	615 G	0.33	11.2	0.6
Thixocast Samples				
1	695 D-R	0.33	4.8	0.06
2	695 D-R	0.33	8.9	0.08
3	695 D-R	0.33	11.2	0.12
4	675 D-R	0.33	4.8	0.09
5	675 D-R	0.33	8.9	0.18
6	675 D-R	0.33	11.2	0.22
7	645 R-G	0.33	4.8	0.23
8	645 R-G	0.33	8.9	0.26
9	645 R-G	0.33	11.2	0.35
10	630 G	0.33	4.8	0.33
11	630 G	0.33	8.9	0.43
12	630 G	0.33	11.2	0.53
13	615 G	0.33	4.8	0.35
14	615 G	0.33	8.9	0.54
15	615 G	0.33	11.2	0.58

8.5 Viscosity

The resulting strain-time graphs were further treated mathematically to calculate the viscosity of the tested alloys, equation 3-28. The interpretation of results obtained from the strain-time graphs are based on the assumption of the SSM slurries behaving like Newtonian fluids, Figure 8-6.
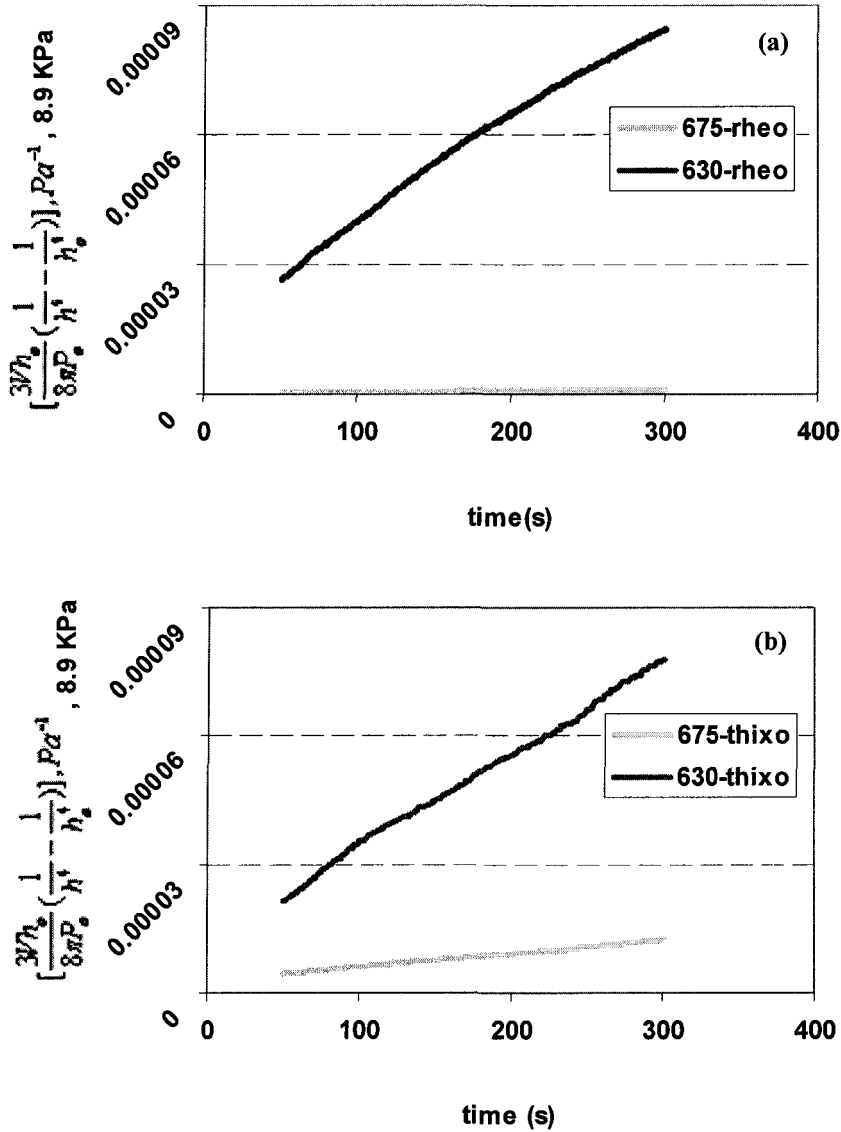
Figure 8-6: Steady state part of the graph, where $[\frac{3Vh_0}{8\pi P_0}(\frac{1}{h^4}-\frac{1}{h_0^4})]$, Pa^{-1} is plotted against time, to calculate the viscosity for; (a) Rheocast billets (b) Thixocast discs

Table 6-1 lists the calculated values of viscosity for the rheocast billets ($\frac{h}{d} > 1$) obtained from Newtonian model, using equation 3-28, during the quasi-steady-state part of deformation graphs, ~200 s after the beginning of each compression test in the current study. The results support previous findings for the viscosity of semi solid alloys as mentioned in the previous sections of the current thesis. It is evident that, there is an

almost three order of magnitude difference between the viscosity of dendritic, 695°C, and globular, 615°C, morphologies. This difference reduces to one order of magnitude when rosette morphology, 630-645°C, is compared to globular.

Table 8-2 shows the calculated viscosity data for the thixo-disks ($h \langle \langle d$) which were compressed under the same pressure and temperature as the rheo-billets but the quasi-steady-state is reached at ~50 s after the beginning of each test.

The fact that the calculation of viscosity were conducted after 200 s for the rheo-billets and 50 s for thixo-disks is based on the size of specimens where the smaller thixo-disks reached quasi-steady-state at shorter time after the beginning of deformation. In other words, the slope of strain time graphs remains constant after 50 seconds for thixo-disks and 200 s for the rheo-billets. as already mentioned in chapter 7.

These results also support previous findings for the viscosity of semi solid alloys [53, 96, 100]. In contrast to rheo-billets, the difference between the viscosity values for the globular and dendritic microstructures in the thixo-disks reduced to one order of magnitude. This is attributed to partial spheroidization and coarsening of dendrites, Figure 8-3c, during the course of reheating the disks to deformation temperature. This is not the case for the disks with original rosette and globular morphologies where no disparity between the viscosity values was seen rheo-billets and thixo-disks. This is further confirmation of the morphology of the primary α-Al particles being the main parameter to control viscosity values and sample size is not critical as proposed before, provided that the viscosity calculations are carried out from the steady-state region of strain-time graphs. It also justifies the reliability of the parallel plate compression test to calculate the viscosity of SSM slurries.

Table 8-2: Viscosities (Pa-s) at different pressures and pouring temperatures, (Log η), and log shear

rate (log $\overset{o}{\gamma}$), (s^{-1}), for thixocast discs, reheated up to 595°C

Initial pressure, Po	Log η, $[\log\overset{o}{\gamma}]$ (695°C)	Log η, $[\log\overset{o}{\gamma}]$ (675°C)	Log η, $[\log\overset{o}{\gamma}]$ (645°C)	Log η, $[\log\overset{o}{\gamma}]$ (630°C)	Log η, $[\log\overset{o}{\gamma}]$ (615°C)
4.8 KPa	7.85, [-4.15]	7.52, [-4.1]	7.2, [-3.61]	7, [-3.31]	6.6, [-3.1]
8.9 KPa	7.69, [-3.90]	7.52, [-3.86]	7.1, [-3.26]	6.6, [-2.95]	6.4, [-2.85]
11.2 KPa	7.63, [-3.68]	7.2, [-3.75]	7, [-3.08]	6.69, [-2.81]	6.5, [-2.7]

Figure 8-7 shows the trends for the variations of the average viscosity values for both sets of samples. It is interesting to note that the viscosity values are almost the same for the globular structure regardless of sample size to once again emphasize the irrelevance of h⟨⟨d criterion proposed by Stephen [109] and employed by other researchers such as Laxmanan et. al.[96]. The more pronounced difference between the viscosity of the dendritic microstructures is due to changes in the morphology of α-Al primary during reheating and formation of degenerated dendrites as shown in Figure 8-3c and 8-3d. This is also further evidence to emphasize the importance of the microstructural feature on the viscosity and flowability of SSM materials. The formation of globular morphology as a result of applying low pouring temperature of 615-630°C, had the greatest effect on the viscosity.
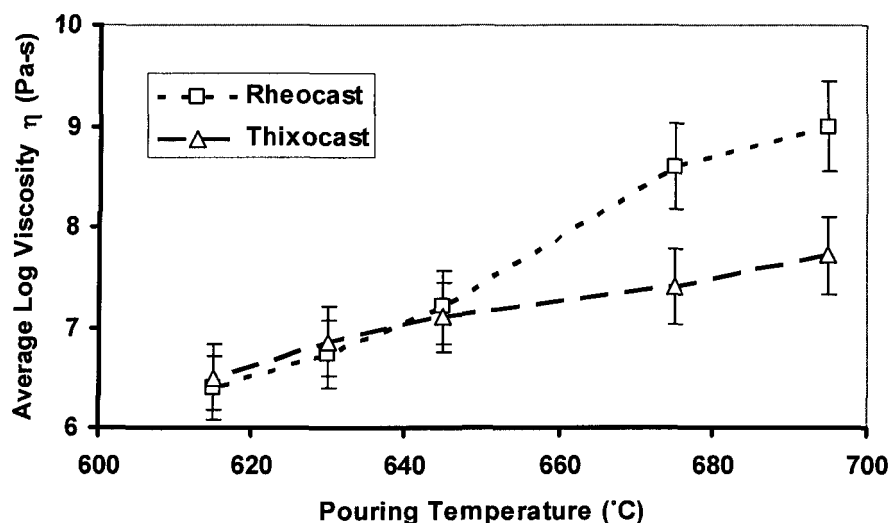
Fig. 8-7: Average values of viscosity reported in table 6-1 & 8-2, showing the big difference between the rheocast and thixocast dendritic morphology and almost no difference in the globular morphology case

CHAPTER 9

**CONCLUSIONS AND
FURTHER SUGGESTIONS**

CHAPTER 9
CONCLUSIONS AND
FURTHER SUGGESTIONS

9.1 Introduction

The current research was mainly concerned with a newly patented rheocasting route semi-solid metal (SSM) processing, SEED, by ALCAN international. This work was further complemented by Conventional casting. There are several process parameters that directly affect the final billet microstructure prepared by SEED process including swirling speed or intensity of swirling and pouring temperature or superheat. For the conventional casting, the pouring temperature as an effective parameter to fabricate the optimum microstructure was considered.

In addition to the preliminary studies on the interrelationships between the SEED process parameters and the resulting microstructure, reports prepared in confidence and submitted to ALCAN, the main objective of the current research was the rheological behavior of SSM billets prepared by SEED and Conventional casting routes employing parallel plate compression test viscometry. The concluding remarks presented in this chapter are divided into the following sections in line with result and discussions, chapters of 5, 6, 7 and 8 respectively:

9.2 Microstructure

1. It was found that conventional billets cast at low pouring temperature of 615°C comprise fine and equiaxed grains while the billets cast at high pouring temperature of 695°C shows dendritic structure. In order to explain such behavior, two proposals were put forward based on nucleation and growth respectively;

    - The highly undercooled melt near the mold wall explodes with a large number of nuclei, big bang or copious nucleation, which rises the melt temperature with the released latent heat of fusion near the wall. The floating of these nuclei towards the central regions establishes a uniform

cooling rate through out the mold. The uniform cooling rate coupled with multi-directional cooling, promotes the formation of fine grained equiaxed as-cast structure.

- The very large temperature gap between the wall and central region of the mold during the early stage of solidification encourages faster heat flow towards the mold wall at lower pouring temperatures. The mold coating, air gap and mold thickness, reduce the rate of heat dissipation from the mold wall to establish a low temperature gradient within shorter time. Such low temperature gradient (G), coupled with multi-directional heat flow, encourage multi-directional growth of primary α-Al nuclei within the melt, i.e. formation of equiaxed and eventually globular structure.

2. For SEED billets, swirling refined the primary α-Al dendrites and promoted the formation of rosette and/or globular α-Al particles with increasing swirling speed. This is similar to what has been seen for conventional billets cast at lower pouring temperature. The effectiveness of swirling speed may be due to reduction in segregation of alloying elements at the solidification front and better heat transfer between the mold and bulk of liquid to establish a shallow temperature gradient. Shallow temperature gradient coupled with lack of directional heat flow due to swirling and mold geometry are the main recipe for refining and formation of equiaxed as-cast structure. There was no evidence of entrapped eutectic within the primary α-Al particles. This is one of the advantages of SEED slurry-on-demand technology.

3. Quantitative metallography, image analysis, of the as-cast billet is an effective tool to characterize SSM structures. Number density, circular diameter, and aspect ratio are the most suitable parameters to show the refinement of microstructure. Aspect ratio is an important parameter to characterize the globularity of the particles. The percentage of the particles with aspect ratio greater than two is a

useful means to highlight the progress of globularization, degree of globularity, in the structure.

4. Based on the micrographs and image analysis data, SEED process is a simple, capable, and cost effective method for producing high quality rheocast billets, comprising homogenous distribution of primary α-Al particles with almost unique size and morphology in all parts of the billet from center to the wall.

9.3 Microstructural characterization - Viscometry

1. The current research proposed an innovative method for microstructural characterization using parallel plate compression rheometer. Since the viscosity of SSM alloy is dependent on the metallurgical parameters and also is a measure of rheological behavior, rheological tests were employed to characterize microstructure. Effort was made to correlate between the morphology and the viscosity through measuring the billets resistance against deformation and further calculation of the viscosity assuming Newtonian fluid behavior. This method is much faster and less expensive than quantitative metallography, which is generally employed to characterize the microstructure of SSM billets. This is particularly beneficial, if on-line quality checks are required in production of rheo-billets, used as feedstock for near net shape manufacturing routes, in cast shops.

2. The reduction of pouring temperature down to liquidus point, 615°C, brings about globular microstructure with improved flow characteristics of the billets. The calculated viscosity for the billets with globular primary α-Al particles prepared at 615°C and compressed at a given temperature of 595°C are almost three orders of magnitude less than that for the fully dendritic structure cast at 695°C. The difference reduces to one order of the magnitude in the case of rosette morphology compared to that of globular. The actual viscosity value plays an important role during die filling of such billets.

3. Application of swirling during solidification has an obvious effect on the deformability and viscosity of the SEED prepared SSM billets. For the billets cast at 695°C, the results show superior deformation and lower viscosity number at high swirling intensity due to the globular structure of the billet. Decreasing the swirling intensity brings some degree of resistance against deformation, higher viscosity, due to presence of rosette or dendritic morphology. For the billets cast at 645°C, once the swirling is applied the engineering strain increases due to structural changes resulting from homogeneous distribution of temperature across the billet to induce some degree of globularity in the primary α-Al particles. In the case of 630°C, swirling is important to induce uniform temperature distribution across the bulk liquid where the resulting globular structure renders better deformability. However, there is not drastic changes in the globular morphology due to the application of various swirling intensities as for instance seen for the billets cast at 695°C.

4. The magnitude of applied pressure is also an important parameter in differentiating between the structures. Application of higher applied pressure results in the mechanical disintegration of primary α-Al particles, dendrites or rosettes, and thus reducing morphological differences. Furthermore the overall strain during steady state deformation is even higher for dendritic or rosette structures deformed at the highest pressure used in this study, 14.55 KPa, due to the formation of broken and finer particles which improves flow behavior and viscosity of the billets.

5. For SEED process, it is advisable to keep the slug deformation temperature as high as possible by pouring the melt at higher superheat and employing high swirling intensity to produce globular morphology or alternatively pour at lower temperatures and application of swirling to benefit homogenous temperature distribution, but reducing the total process time to keep the final temperature of billet as high as possible.

6. It was concluded that grain refining and modification treatments improve flow characteristics of SSM billets and reduce the viscosity values. The refinement of the grains has been identified as the main factor for better deformability of the billets. Modification also plays an important role on alloy deformability through reduction of the residual liquid surface tension which reduces the apparent viscosity of the billets.

7. The liquid segregation within the SSM structures is dependent on the applied shear force and size and morphology of primary α-Al particles. It is reduced at lower shear rates and with finer and globular primary α-Al particles. Microstructural analysis of the deformed area showed less segregation of liquid for the combined and over refined semisolid billets than other billets. This is attributed to the smaller particles size and lower viscosity of the billets.

8. The parallel plate compression test is simple, fast and effective method to characterize SSM microstructure. It is also capable of differentiating amongst the globular, rosette and dendritic morphologies of the primary α-Al particles in Al-alloys.

9.4 Rheological studies

1. The effect of structural parameters of solid fraction and its morphology on the viscosity of A356 SSM billets was studied for the billets cast conventionally and by SEED technology. It was confirmed at low shear rate values, the SSM billets can be treated as Newtonian fluid even though the two phase fluids are basically non-Newtonian. However, the billets showed pseudoplastic behavior where the viscosity decreased with increasing applied pressure (increasing $\overset{o}{\gamma}$).

2. when the SSM billets were treated as Non-Newtonian fluids, the materials constant m and n were calculated and presented as empirical relationships for different fractions solid and morphologies using a power law relationship;

$$m = 10^{(5.56-1.39f_s)} \qquad 0.33<f_s<0.46$$

$$n = 0.87 -1.56 \text{ fs} \qquad 0.33<f_s<0.46$$

$$m = 10^{(1.85-4.9\overline{AR})} \qquad \text{for } 1.5<\overline{AR}<1.7$$

$$n = 0.97-0.255\,(\overline{AR}) \qquad \text{for } 1.5<\overline{AR}<1.7$$

3. And the respected viscosities were presented as;

$$\log\eta = 5.56-1.39f_s -(1.56f_s +0.14)\log\overset{o}{\gamma}$$

$$\log\eta = -1.85+4.9\overline{AR}-(0.255\overline{AR}+0.03)\log\overset{o}{\gamma}$$

4. These empirical relationships express the direct effect of solid fraction and morphology on the viscosity of semi solid billets and if the solid fraction or average aspect ratio kept constant, the viscosity varies inversely with the shear rate. The decreasing trend for the viscosity with increasing the applied pressure and resulting shear rate, in both sets of experiments, confirms once again the psuedoplastic behavior of SSM A356 alloy, at least within the shear rates less than 0.01 s^{-1}, reported in the current study. The validity of these equations was further confirmed with plotting log viscosity against shear rate for different fractions solid and morphology and a good agreement was found between the predicted values and the previously reported results in the literature. In spite of good agreement at low shear rates, the proposed equation for fraction solid appeared to be less reliable when the shear rate was beyond 10^{-1} s^{-1}, where the predicted value for viscosity at shear rate of 10^{3} s^{-1} was almost three orders of magnitude greater than those reported for A356 SSM alloy in the literature.

9.5 Rheological studies - Sample size effect

1. One of the most important findings of the current research is the negligible effect of sample size on the viscosity of SSM billets. As described, two different sample

sizes with the aspect ratios 0.4 (10 mm height 24 mm diameter) and 1.8 (140 mm height 75 mm diameter) were employed to be compressed under the same initial pressures and holding temperature, 595°C. Based on the mathematical solution of the equation 3-28, such relationship could be reliable if the "axial flow is negligible against the radial flow". This assumption is realized by many researchers using the low aspect ratios samples. The current study implemented such condition by considering engineering strain-time results after a certain period of time where the steady state deformation is established.. The current thesis reported that using large scale samples, the axial movement of the billets could be neglected against the radial flow during the steady state deformation stage, where the magnitude of viscosity values, are within the same range for both the rheocast

$(\dfrac{h}{d} > 1)$ and thixocast ($h \langle\langle d$) samples.

2. Reheating of the thixocast disks brings about minor morphological and size changes in the primary α-Al particles which may affect the viscosity value. This is particularly true for dendritic morphology while for rosette and globular morphologies the changes in viscosity value due to reheating was negligible.

3. The viscosity for the conventional billets with globular morphology prepared at low pouring temperatures of 615-630°C were almost the same in both thixocast and rheocast specimens which confirms the irrelevance of $h \langle\langle d$ criterion and the reliability of parallel plate compression test to determine viscosity of SSM slurries.

4. The most important parameter to influence the flow characteristics of SSM slurries is the morphology of the primary phase, not the sample size.

9.6 FURTHER SUGGESTIONS

A comprehensive study was performed on the effect of morphology and fraction solid on the rheological behavior of SSM billets prepared via conventional casting and SEED technology. However, there are still some studies needed to be done to compliment the current study. These are suggested in the following paragraphs.

1. The in-house designed and fabricated machine in this project could be further developed to use in forging or extrusion applications. This may help the researchers to investigate the forgability of the SSM billets in commercial scale or the rheological behavior of the alloy using other rheological methods such as direct/indirect extrusion.

2. Application of high shear rate ranges during parallel plate compression test is advised to put the theoretical data in practice and to simulate processes where the SSM billets are shaped at high deformation rates such as high pressure die casting or closed die forging.

3. It is proposed to study the effect of solid particles morphology on the viscosity of SSM billets by introducing other parameters to specify morphology than that used in this investigation, aspect-ratio. This is useful since there is a lack of published results on the effect of morphology on the SSM viscosity values.

4. A theoretical approach to model rheological behavior of the SSM billets including the effect of morphology and solid fraction should be the logical continuation of the current study using the findings reported in this document.

5. A comprehensive study on the formability and viscosity of the Semi Solid aluminum composites is highly advisable, to understand the feasibility of near net shape forming of aluminum composites.

REFERENCES:

1- M. C. Flemings, "Behavior of metal alloys in the semi-solid state", Metal. Trans. A, Vol.22A, 1991, pp.957-981

2- Z. Fan, "Semisolid metal processing", Inter. Mater. Rev., Vol.47, No.2, 2002, pp.49-85

3- D. H. Kirkwood, "Semisolid metal processing", Inter. Mater. Rev., Vol.39, No.5, 1994, pp.173-189

4- M.C. Flemings, R.G. Riek, K.P. Young, "Rheocasting Processes", AFS Inter. Cast Metal Journal, September 1976, pp.11-22

5- D.B. Spencer, R. Mehrabian, M.C. Flemings, "Rheological behavior of Sn-15 Pct Pb in the crystallization range", Metal. Trans., Vol. 3, 1972, pp.1925-1932

6- R. Mehrabian, D.R. Geiger, M.C. Flemings, "Refining by partial solidification", Metal. Trans., Vol. 5, 1974, pp.785-787

7- "Solidification processing", M.C. Flemings, Mc Graw Hill Pub., 1974

8- D. Brabazon, D.J. Browne, A.J. Carr, "Mechanical stir casting of aluminum alloys from the mushy state: process, microstructure and mechanical properties" Mater. Sci. Eng. A, Vol. A326, 2002, pp.370-381

9- A. Beaulieu, L. Azzi, F. Ajersch, S. Turenne, F. Pineau, C.A. Loong, "Numerical Modeling and Experimental analysis of die cast Semi-Solid A356 Alloy", Proceeding of M. C. Flemings on solidification and materials processing, edited by R. Abbaschian, H. Brody, A. Mortensen, TMS 2001, pp.261-265

10- C. Edwards, S.B. Palmer, M.J. Hornsby, "Ultrasonic monitoring of the partial melting of Al-Si alloys", Proceeding of 2nd inter. Conf. on Semi-Solid processing of alloys and composites, 1992, pp.22-32

11- D. Brabazon, D.J. Browne, A.J. Carr, "Experimental investigation of the transient and steady state rheological behavior of Al-Si alloys in the mushy state", Mater. Sci. Eng. A, Vol. A356, 2003, pp.69-80

12- L. Arnberg, A. Bardal, H. Sund, "Agglomeration in two semisolid type 6082 aluminum alloys", Mater. Sci. Eng. A, Vol. A262, 1999, pp.300-303

13- K. Ishikawa, Y. Kinoshita, "Microstructural control of intermetallics CuAl-based and hypereutectic Al-Si alloys by stirring synthesis method", Mater. Trans., JIM, Vol. 34, No. 5, 1993, pp.467-473

14- S. Mohan, V. Agarwala, S. Ray, "Hypereutectic Al-Si rheocast alloys, part1. Microstructural features", Z. Metallkde., Vol. 79, 1988, pp.403-406

15- Sh. Nafisi, D. Emadi, M.T. Shehata, R. Ghomashchi, A. Charette, "Semi-Solid processing of aluminum silicon alloys, effect of stirring on iron based intermetallics", S2P 2004, 8th international conference of semi solid processing, Limassol Cyprus,

16- Sh. Nafisi, R. Ghomashchi, D. Emadi, M.T. Shehata, "Effect of stirring on the silicon morphological evolution in hypoeutectic aluminum silicon alloys", Light Metal, TMS 2005, Edited by H. Kvande, pp. 1111-1116

17- A. Das, S. Ji, Z. Fan, "Morphological development of solidification structures under forced fluid flow: a Monte-Carlo simulation", Acta Mater., Vol. 50, 2002, pp.4571-4585

18- S.C. Bergsma, M.E. Kassner, "The optimized tensile and fatigue properties of semi-solid modified 319 aluminum alloys", Light Metals Conference, COM1999, Edited by M. Bouchard, A. Faucher, 1999, pp. 375-382

19- H. Wang, C.J. Davidson, J.A. Taylor, D.H. StJohn, "Semisolid casting of AlSi7Mg0.35 Alloy produced by low temperature pouring", Mater. Sci. Forum, Vols. 396-402, 2002, pp.143-148

20- W. Mao, C. Cui, A. Zhao, J. Yang, X. Zhong, "Effect of pouring process on the microstructure of semi solid AlSi7Mg alloy", J. Mater. Sci. Tech. , Vol.17, No.6, 2001, pp.615-619

21- K. Xia, G. Tausig, "Liquidus casting of a wrought aluminum alloy 2618 for thixoforming", Mater. Sci. Eng. A, Vol. A246, 1998, pp.1-10

22- S. Midson, K. Young, "Impact of casting temperature on the quality of components semi-solid metal cast form alloys 319 and 356", 5th AFS International Conference of Molten Aluminum, 1998, pp.409-422

23- R. Zehe, "First production machine for rheocasting", Light Metal Age, Oct. 1999, pp. 62-66

24- UBE Industries, European Patent EP 0 745 694 A1, Dec. 4, 1996

25- R. Martinez, A. Figueredo, J.A. Yurko, M.C. Flemings, "Efficient Formation of Structures Suitable for Semi-Solid Forming", Transactions of the 21st International Die Casting Congress, 2001, pp.47-54

26- J.L. Jorstad, M. Thieman, R. Kamm, "SLC, the Newest and Most Economical Approach to Semi-Solid Metal (SSM) Casting", 7th International Conference on Semi-Solid Processing of Alloys and Composites, Tsukuba, Japan, 2002, pp. 701-706

27- O. Lashkari, Sh. Nafisi, R. Ghomashchi, "Microstructural Characterization of Rheo-cast Billets Prepared by Variant Pouring Temperatures", Accepted for publication, Mater. Sci. Eng. A. March 2006

28- M. Ferrante, E. de Freitas, "Rheology and microstructural development of Al-4wt%Cu alloy in the semi solid state", Mater. Sci. Eng. A, Vol. A271, 1999, pp.172-180

29- Y. Uetani, H. Takagi, K. Matsuda, S. Ikeno, "Semi-continuous casting of mechanically stirred A2014 and A390 aluminum alloy billets", COM 2001, Light Metals Conference, Edited by M. Sahoo, T.J. Lewis, 2001, pp. 509-520

30- "Science and technology of semisolid metal processing", A. Figueredo, North American Die Casting Association pub., 2001

31- K. Ichikawa, M. Katoh, F. Asuke, "Continuous rheocasting for aluminum-copper alloys", Mater. Trans., Vol. 43, No. 9, 2202, pp.2285-2291

32- M. Kiuchi, S. Sugiyama, "A new process to manufacture semi-solid alloys", ISIJ inter., Vol. 35, No. 6, 1995, pp.790-797

33- C. Pluchon, W. Loué, M. Garat, "Production of thixotropic aluminum alloy billets", Casting plant and Tech. Inter., Vol. 2, 1998, pp.24-28

34- E.J. Zoqui, M. Paes, M.H. Robert, "effect of macrostructure and microstructure on the viscosity of the A356 alloy in the semi-solid state", J. Mater. Process. Tech., Vol. 153-154, 2004, pp.300-306

35- E.J. Zoqui, M.T. Shehata, M. Paes, V. Kao, E. Es-Sadiqi, "Morphological evolution of SSM A356 during partial remelting", Mater. Sci. Eng. A, Vol. A325, 2002, pp.38-53

36- B.I. Jung, C.H. Jung, T.K. Han, Y.H. Kim, "electromagnetic stirring and Sr modification in A356 alloy", J. Mater. Processing Tech., Vol. 111, 2001, pp.69-73

37- Y. Zhang, K. Zhang, G. Liu, J. Xu, L. Shi, D. Cui, X. Wu, B. Cui, "The formation of rosette α phase, structural evolution during the reheating and semi-solid casting AlSi7Mg alloy", J. Mater. Processing, Tech., Vol. 137, 2003, pp.195-200

38- J.P. Gabathuler, "Evaluation of various processes for the production of billets with thixotropic properties", Proceeding of 2nd conference of Semi solid materials, 1992, pp.33-46

39- "Mise en forme des alliages métalliques à l'état semi solide", M. Suéry, Hermès Science Pub. Lavoisier, 2002, ISBN : 2-7462-0453-3

40- V.O. Abramov, O.V. Abramov, B.B. Straumal, W. Gust, "Hypereutectic Al-Si based alloys with a thixotropic microstructure produced by ultrasonic treatment", Mater. Design, Vol.18, Nos. 4-6, 1997, pp.323-326

41- D. Doutre, G. Hay, "semi-solid concentration processing of metallic alloys", U.S. patent, No. US 6428636 B2, Aug 2002

42- D. Doutre, G. Hay, P. Wales, J.P. Gabathuler, "SEED: A new process for semi solid forming", Light Metals Conference., COM 2003, Ed. J. Masounave, G. Dufour, Vancouver, Canada, pp.293-306

43- D. Bouchard, F. Pineau, D. Doutre, P. Wales, J. Langlais, "Heat transfer analysis of swirl enthalpy equilibration device for the production of semi-solid aluminum", Light Metals Conference, COM 2003, Ed. J. Masounave, G. Dufour, Vancouver, Canada, pp.229-241

44- O. Lashkari, Sh. Nafisi, R. Ghomashchi, A. Charette, J. Langlais, B. Kulunk, "Impact of superheat on the microstructural evolution of 356 alloy in SEED slurry on demand process", Light Metals Conference, COM 2004, ed. D. Gallienne, R. Ghomashchi, Hamilton, Canada, pp.315-322

45- A.C. Fonseca, M. Prates, "Rheocasting techniques applied to grain refinement of aluminum alloys", The Metals Society, Proceeding of Inter. Conf., Solidification technology in foundry and cast house, 1983, Warwick, UK, pp.143-146

46- E. Tzimas, A. Zavaliangos, "Evolution of near-equiaxed microstructure in the semi solid state", Mater. Sci. Eng. A, Vol. A289, 2000, pp.228-240

47- E. Tzimas, A. Zavaliangos, "A comparative characterization of near-equiaxed microstructures as produced by spray casting, magneto hydrodynamic casting and the stress induced, melt activated process", Mater. Sci. Eng. A, Vol. A289, 2000, pp.217-227

48- T. Motegi, F. Tanabe, E. Sugiura, "Continuous casting of semisolid aluminum alloys", Mater. Sci. Forum, Vols. 396-402, 2002, pp.203-208

49- T. Haga, P. Kapranos, "simple rheocasting processes", J. Mater. Processing Tech., Vol. 130-131, 2002, pp.594-598

50- F. Kolenda, P. Retana, G. Racineux, A. Poitou, "Identification of Rheological parameters by the squeezing test", Powder Tech. Vol. 130, 2003, pp.56-62

51- R. Mehrabian, R.G. Riek, M.C. Flemings, "Prepartion and casting of metal-particulate non-metal composites", Metal. Trans., Vol. 5, 1974, pp.1899-1905

52- M. Modigell, J. Koke, "Rheological modelling on semi-solid metal alloys and simulation of thixocasting processes", J. Mater. Processing Tech., Vol. 111, 2001, pp.53-58

53- J.A. Yurko, M.C. Flemings, "Rheology and microstructure of semi-solid aluminum alloys compressed in the drop forge viscometer", Metal. Trans. A, Vol. 33A, 2002, pp.2737-2746

54- C.A. Loong, C.Q. Zheng, A. Beaulieu, F. Ajersch, "Semi-solid casting of A356 alloy billets re-heated by high frequency induction system", Light Metals Conf., COM 2001, Edited by M. Sahoo, T.J. Lewis, 2001, pp.501-508

55- C.G. Kang, J.H. Yoon, Y.H. Seo, "The upsetting behavior of semi-solid aluminum material fabricated by a mechanical stirring process", J. Mater. Processing Tech., Vol. 66, 1997, pp.30-38

56- M. Suéry, M.C. Flemings, "Effect of strain rate on deformation behavior of semi-solid dendritic alloys", Metal. Trans. A, Vol. 13A, 1982, pp.1809-1819

57- L.A. Lalli, "A model for deformation and segregation of solid-liquid mixtures", Metal. Trans. A, Vol. 16A, 1985, pp.1393-1403

58- P. Kapranos, H.V. Atkinson, D.H. Kirkwood, "Rapid compression testing of semi solid alloy slugs", Mater. Sci. Forum, Vols. 329-330, 2000, pp.525-530

59- S.Y. Lee, S. Oh, "Thixoforming characteristics of thermo-mechanically treated AA 6061 alloy for suspension parts of electric vehicles", J. Mater. Processing Tech., Vols. 130-131, 2002, pp.587-593

60- P.R. Prasad, S. Ray, L. Gaindhar, M.L. Kapoor, "Relation between processing, microstructure and mechanical properties of rheocast Al-Cu alloys", J. Mater. Sci., Vol. 23, 1988, pp.823-829

61- S. Mohan, V. Agarwala, S. Ray, "Hypereutectic Al-Si rheocast alloys, part2. Mechanical properties", Z. Metallkde., Vol. 79, 1988, pp.407-409

62- E. Cerri, E. Evangelista, S. Spigarelli, P. Cavaliere, F. DeRiccardis, "Effect of thermal treatments on microstructure and mechanical properties in a thixocast 319 aluminum alloy", Mater. Sci. Eng. A, Vol. A284, 2000, pp.254-260

63- T. Mori, H. Iwasaki, M. Kodama, "Mechanical properties of rheocasting aluminum alloy at elevated temperatures", Proceeding of 4th inter. Conf. on Semi-Solid processing of alloys and composites, Sheffield, 1996, pp.347-351

64- Y.B. Yu, P.Y. Song, S.S. Kim, J.H. Lee, "Possibility of improving tensile strength of semi solid processed A356 alloy by a post heat treatment at an extremely high temperature", Scripta Mater., Vol. 41, No. 7, 1999, pp.767-771

65- E.R. De Freitas, M. Ferrante, "Rheological behavior and deformation characteristics of a commercial and a laboratory-cast Al-4%Cu alloy in the semi-solid state", Acta Mater., Vol. 49, 2001, pp.3839-3847

66- N. Hayat, H. Toda, T. Kobayashi, N. Wade, "Experimental investigations of fatigue characteristics of AC4CH cast aluminum alloys fabricated through rheocast and squeeze cast methods", Mater. Sci. Forum, Vols. 396-402, 2002, pp.1353-1358

67- W.R. Loué and M. Suéry, "Microstructural evolution during partial remelting of AlSi7Mg alloys", Mater. Sci. Eng. A, Vol. A203, 1995, pp. 1-13

68- "Viscosity and flow measurement", V. Wazer, L. K. Colwell, John Wiley Pub., 1966

69- "Rheology for chemists, an introduction", J. W. Goodwin, R. W. Hughes, Royal society of chemistry Pub., UK, 2000

70- "Viscoelastic properties of polymers", J.D. Ferry, John Wiley Pub., 1970

71- "Transport phenomena in materials processing", D.R. Poirier, G.H. Geiger, TMS Pub., 1994

72- X. Yang, Y. Jing, J. Liu, "The rheological behavior for thixocasting of semi-solid aluminum alloy (A356)", J. Mater. Processing Tech., Vols. 130-131, 2002, pp.569-573

73- W. Nan, S. Guangji, Y. Hanguo, "Rheological study of partially solidified Tin-Lead and Aluminum-Zinc alloys for stir casting", Mater. Trans. JIM, Vol. 31, No. 8, 1990, pp.715-722

74- "Rheology of solids and the earth", S.E. Karato, M. Toriumi, Oxford Science Pub., 1989

75- T.Z. Kattamis, T.J. Piccone, "Rheology of Semi solid Al-4.5%Cu-1.5%Mg Alloy", Mater. Sci. Eng., Vol. A131, 1991, pp.265-272

76- J.Y. Chen, Z. Fan, "Modeling of rheological behavior of semisolid metal slurries, part1 – Theory", Mater. Sci. Tech., Vol. 18, 2002, pp.237-242

77- P.A. Joly, R. Mehrabian, "The Rheology of partial solid alloys", J. Mater. Sci., Vol. 11, 1976, pp.1393-1403

78- C.L. Martin, P. Kumar, S. Brown, "Constitutive modeling and characterization of the flow behavior of semi-solid metal alloy slurries-II. Structural evolution under shear formation", Acta metall. mater., Vol. 42, No. 11, 1994, pp.3603-3614

79- M. Perez, J.C. Barbe, Z. Neda, Y. Brechet, L. Salvo, M. Suery, "Investigation of the microstructure and rheology of semi-solid alloys by computer simulation", J. Phys. IV France, Vol. 11, 2001, pp.93-100

80- E. Tzimas, A. Zavaliangos, "Evaluation of volume fraction of solid in alloys formed by semisolid processing", J. Mater. Sci., Vol. 35, 2000, pp.5319-5329

81- Y. Zhu, J. Tang, Y. Xiong, Z. Wu, C. Wang, D. Zeng, "The influence of the microstructure morphology of A356 alloy on its rheological behavior in the semisolid state", Sci. Tech. Adv. Mater. Vol. 2, 2001, pp. 219-223

82- G. Chai, T. Roland, L. Arnberg, L. Backerud, "Studies of dendrite coherency in solidifying aluminum alloy melts by rheological measurements", 2nd inter. conf. of semisolid material processing, 1992, pp.193-201

83- O. Lashkari, R. Ghomashchi, "The Implication of Rheological principles for Characterization of Semi-Solid Aluminum Cast billets" Internal report, NSERC-ALCAN-UQAC Industrial Chair, Grant Number: IRCPJ268528-01, University of Quebec at Chicoutimi, Feb. 2005

84- Z. Fan, J.Y. Chen, "Modelling of rheological behavior of semisolid metal slurries, Part4 – Effects of particle morphology", Mater. Sci. Tech., Vol. 18, 2002, pp.258-267

85- S. Jabrane, B. Clement, S. Ajersch, "Evolution of primary particle morphology during Rheoprocessing of Al-5.2%Si Alloy", 2nd Inter. Conf., Semi-Solid processing of alloys and composites, Cambridge, Massachusetts, 1992, pp.223-236

86- Z. Fan, J.Y. Chen, "Modeling of rheological behavior of semisolid metal slurries, part2 – Steady state behavior", Mater. Sci. Tech., Vol.18, March2002, pp.243-249

87- J.Y. Chen, Z. Fan, "Modeling of rheological behavior of semisolid metal slurries, part3 – Transient state behavior", Mater. Sci. Tech., Vol.18, March2002, pp.250-257

88- Sh. Nafisi, , O. Lashkari, R. Ghomashchi, J. Langlais, B. Kulunk, "The SEED Technology: A New Generation in Rheocasting", Light Metals Conference, COM 2005, Ed: J.P. Martin, Calgary, Canada, 2005, pp.359-371

89- R.J. Kissling, J.F. Wallace, "Grain Refinement of Aluminum Castings", Foundry, 1963, pp.78-82

90- M. Hirai, K. Takebayashi, Y. Yoshikawa, "Effect of chemical composition on apparent viscosity of Semi-solid alloys", ISIJ Inter., Vol. 33, No. 11, 1993, pp.1182-1189

91- O. Lashkari, Sh. Nafisi, R. Ghomashchi "The Implication of Solidification Principles during Semi Solid Processing of Al-Si alloys: Effect of Pouring Temperature", Internal report, NSERC-ALCAN-UQAC Industrial Chair, Grant Number: IRCPJ268528-01, University of Quebec at Chicoutimi, Jan. 2005

92- H.I. Lee, R.D. Doherty, E.A. Feest, J.M. Titchmarsh, "Structure and segregation of stir-cast aluminum alloys", The Metals Society, Proceeding of Inter. Conf., Solidification technology in foundry and cast house, 1983, UK, pp.119-125

93- C.S. Sivaramakrishnan, R.K. Mahanti, R. Kumar, "Stir cast morphology of aluminum-silicon alloys", Aluminum, Vol.57, No.12, 1981, pp.820-821

94- O. Lashkari, R. Ghomashchi, F. Ajersch, "Rheological study of 356 Al-Si foundry alloy prepared by a new innovative SSM process", EPD congress, Edited by Mark E. Schlesinger, TMS 2005, pp.149-156

95- P.R. Prasad, A. Prasad, C.B. Singh, "Calculation of primary particle size in rheocast slurry", J. Mater Sci. Letters, Vol. 14, 1995, pp.861-863

96- V. Laxmanan, M.C. Flemings, "Deformation of semi-solid Sn-15 Pct Pb alloy", Metal. Trans. A, Vol. 11A, 1980, pp.1927-1937

97- O. Lashkari, R. Ghomashchi, "The Implication of Rheological principles for Characterization of Semi-Solid Aluminum Cast billets" accepted for publication, Journal of Materials Science, October 2005

98- E.A. Vieira, A.M. Kliauga, M. Ferrante, "Microstructural evolution and rheological behavior of aluminum alloys A356, and A356 + 0.5% Sn designed for thixocasting", J. Mater. Processing Tech., Vols. 155-156, 2004, pp.1623-1628

99- M. Hirai, K. Takebayashi, Y. Yoshikawa, R. Yamaguchi, "Apparent viscosity of Al-10mass%Cu semi-solid alloys", ISIJ Inert., Vol. 33, No. 3, 1993, pp.405-412

100- L. Azzi, F. Ajersch, "Development of aluminum-base alloys for forming in semi solid state", TransAl conference, Lyon, France, 2002, pp.23-33

101- J.H. Han, D. Feng, C.C. Feng, C.D. Han, "Effect of sample preparation and flow geometry on the rheological behavior and morphology of micro phase-separated block copolymers: comparison of cone-and-plate and capillary data", Polymer, Vol. 36, 1995, pp.155-167

102-W.M. Gearhart, W.D. Kennedy, "Cellulose acetate butyrate plastics", Industrial Eng. Chemistry, Vol. 41, No. 4, 1949, pp.695-701

103-G.H. Dienes, H.F. Klemm, "Theory and Application of the Parallel Plate Plastometer", J. Applied Phys., 1946, Vol. 17, pp.458-464

104-A. Wahlen, "Modelling the processing of aluminum alloys in the semi-solid state", Mater. Sci. Forum, Vols. 396-402, 2002, pp.185-190

105-O. Draper, S. Blackburn, G. Dolman, K. Smalley, A. Griffiths, "A comparison of paste rheology and extrudate strength with respect to binder formulation and forming technique", J. Mater. Proc. Tech., Vols.92-93, 1999, pp.141-146

106-S. Turenne, N. Legros, S. Laplante, F. Ajersch, "Mechanical behavior of Aluminum matrix composite during extrusion in the semisolid state", Metal. Mater. Trans. A, Vol. 30A, 1999, pp.1137-1146

107-M. Ferrante, E. de Freitas, M. Bonilha, V. Sinka, "Rheological properties and microstructural evolution of semi-solid aluminum alloys inoculated with Mischmetal and with Titanium", 5th Inter. Conf. Semisolid processing of alloys and composites, 1998, pp.35-42

108-Hugues Blanchette. M.Eng. Research Project, University of Quebec at Chicoutimi, 2005

109-J. F. Stefan, Versuche Uber Die Scheinbare Adhasion Sitzber M th. Naturw. Kl. Bagar Akad. Wiss Munchen, 1974, vol. 69, part 2

110-O. Lashkari, R. Ghomashchi, "A New Machine to Characterize Microstructural Evolution of Semi Solid Metal Billets through Viscometry", Accepted for publication, Materials & Design, January 2006

111-J.D. Sherwood, D. Durban, "Squeeze flow of a power-law viscoplastic solid", J. Non Newtonian Fluid Mech., Vol.62, 1992, pp.35-54

112-D.J. Lahaie, M. Bouchard, "Physical modeling of the deformation mechanisms of semisolid bodies and a mechanical criterion for hot tearing", Metal. Mater. Trans. B, Vol. 32B, 2001, pp.697-705

113-C.G. Kang, Y.I. Son, S.W. Youn, "Experimental investigation of semi-solid casting and die design by thermal fluid-solidification analysis", J. Mater. Processing Tech., Vol. 113, 2001, pp.251-256

114-M. Mada, F. Ajersch, "Rheological model of semi-solid A356-SiC composite alloys. Part I: Dissociation of agglomerate structures during shear", Mater. Sci. Eng. A, Vol. A212, 1996, pp. 157-170

115-M. Mada, F. Ajersch, "Rheological model of semi-solid A356-SiC composite alloys Part II: Reconstitution of agglomerate structures at rest", Mater. Sci. Eng. A, Vol. A212, 1996, pp. 171-177

116-A.M. Figueredo, Y. Sumartha, M.C. Flemings, "Measurement and Calculation of Solid Fraction in Quenched Semi-Solid Melts of Rheocast Aluminium Alloy A357", Light Metals, TMS Publication, 1998, pp.1103-1106

117-D. Apelian "Semi-Solid Processing Routes and Microstructure Evolution", 7th International Conference on Semi-Solid Processing of Alloys and Composites, Tsukuba, Japan, 2002, pp.25-30

118-Sh. Nafisi, "Effect of grain refining and modification on the microstructural evolution of semi solid A356 alloy", Ph.D. project, UQAC, Chicoutimi, QC, Canada, 2006

119-Sh. Nafisi, O. Lashkari, R. Ghomashchi, F. Ajersch, A. Charette, "Microstructure and Rheological Behavior of Grain Refined and Modified Semi-Solid A356 Al-Si Slurries", Accepted for publication, Acta Mater., 2006

120-D.Emadi, J.E.Gruzleski, J.M.Toguri, "The Effect of Na and Sr Modification on Surface Tension and Volumetric Shrinkage of A356 Alloy and Their Influence on Porosity Formation", Metallurgical Transactions, Vol.24B, 1993, pp.1055-1063

121-J.P.Anson, J.E.Gruzleski, M.Stucky, "Effect of Strontium Concentration on Microporosity in A356 Aluminum Alloy", AFS Transactions, 2001, pp.01-09

122-M. Easton, D. StJohn, "Grain refinement of aluminum alloys: part 1, the nucleant and solute paradigms-a review of the literature", Metal. Mater. Trans. A, Vol. 30A, 1999, pp.1613-1623

APPENDIX:

The deformation behavior of non-Newtonian fluids squeezed between two large parallel plates when considered in cylindrical coordinates, are expressed by the following equation [109]:

$$\tau_{rz} = -m \left| \frac{\partial v_r}{\partial z} \right|^{n-1} \left(\frac{\partial v_r}{\partial z} \right)$$ (1)

Where v_r is the radial velocity and m and n are the material constants. Assuming steady state deformation, $\frac{\partial v_z}{\partial t} = 0$, and the fact that the reduction in height is rather negligible during steady state deformation in contrast to deformation in radial direction, the normal velocity of flow v_z, can be neglected in comparison with the radial velocity, v_r. Also assuming circular symmetry, v_θ is zero. With these assumptions, the basic equations for the flow field become,

Continuity $\qquad\qquad \frac{1}{r}\frac{\partial}{\partial r}(rv_r) + \frac{\partial v_z}{\partial z} = 0$ (2)

Momentum $\qquad\qquad \frac{\partial P}{\partial r} = -m\frac{\partial}{\partial z}\left(-\frac{\partial v_r}{\partial z}\right)^n$ (3)

$$\frac{\partial P}{\partial z} = 0$$ (4)

With the boundary conditions

$z = 0:$ $\qquad\qquad \partial v_r / \partial z(r, o) = 0$ (5)

$z = \dfrac{h}{2}:$ $\qquad\qquad v_z\left(r, \dfrac{h}{2}\right) = \dfrac{dh}{dt}$, $v_r\left(r, \dfrac{h}{2}\right) = 0$ (6)

$r = 0:$ $\qquad\qquad v_r(o, z) = 0$ (7)

$r = R$ $\qquad\qquad p(R) = p_0$ (8)

Equation 4 means that P is independent of z. Hence integrating equation 3 twice with respect to z, yields:

$$v_r = (-1)^{1/n}\left(\frac{n}{n+1}\right)\left(\frac{1}{m}\frac{dp}{dr}\right)^{1/n} \times \left[\left(\frac{h}{2}\right)^{n+1/n} - z^{(n+1)/n}\right]$$ (9)

With integrating the continuity equation (2) over z:

$$\frac{dh}{dt} = -\frac{2}{r}\frac{\partial}{\partial r}\left(r\int_0^{h/2}v_r dz\right) \qquad (10)$$

Integrating equation 10 over (r), results:

$$\frac{r}{2}\frac{dh}{dt} = -2\int_0^{h/2}v_r dz \qquad (11)$$

Substituting equation 9 in 11 and integrating the pressure gradient so obtained gives,

$$p - p_0 = \left(\frac{m}{n+1}\right)(-1)^{n+1}\times\left\{\left(\frac{2n+1}{4n}\right)\left(\frac{h}{2}\right)^{-[(2n+1)/n]}\frac{dh}{dt}\right\}^n(r^{n+1}-R^{n+1}) \qquad (12)$$

Here R is radius of the specimen at time, t. integrating over the surface of the plates gives:

$$F = (-1)^n\left(\frac{m}{n+3}\right)\pi R^{n+3}\times\left\{\left(\frac{2n+1}{4n}\right)\left(\frac{h}{2}\right)^{-[(2n+1)/n]}\frac{dh}{dt}\right\}^n \qquad (13)$$

Since the fluid does not completely fill the space between the plates, R varies with time, t. However since the volume of the work piece remains unchanged during deformation i.e. $R^2h = R_0^2h_0$, and letting $d_0=2R_0$, equation 13 may be rewritten;

$$-\frac{dh}{dt} = \left\{\left(\frac{2n}{2n+1}\right)^n\frac{4F}{\pi d_0^{n+3}m}(n+3)\right\}^{1/n}h_0^{-[(n+3)/2n]}h^{[5(n+1)/2n]} \qquad (14)$$

If
$$k = \left\{\left(\frac{2n}{2n+1}\right)^n\frac{4F}{\pi d_0^{n+3}m}(n+3)\right\}^{1/n} \qquad (15)$$

Thus:

$$-\frac{dh}{dt} = kh_0^{-[(n+3)/2n]}h^{[5(n+1)/2n]} \qquad (16)$$

Integrating from $h=h_0$ at $t=0$

$$\left(\frac{1}{h}\right)^{(3n+5)/2n} - \left(\frac{1}{h_0}\right)^{(3n+5)/2n} = \left(\frac{3n+5}{2n}\right)kh_0^{-[(n+3)/2n]}t \qquad (17)$$

If $n=1$, m becomes equal to η according to the power law equation and equation 17 reduces to equation 3-27 in the text.

Rewriting equation 17 yields:

$$\frac{h_o}{h} = \left\{ 1 + \left(\frac{3n+5}{2n}\right) h_o^{(n+1)/n} kt \right\}^{2n/(3n+5)}$$ (18)

This is a modified form of the condition where the fluid does not fill the space between the plates.

Assuming the engineering strain $e = \left(1 - \frac{h}{h_o}\right)$ results:

$$e = 1 - \left\{ 1 + \left(\frac{3n+5}{2n}\right) h_o^{(n+1)/n} kt \right\}^{-[2n/(3n+5)]}$$ (19)

Equation 19 is the theoretical strain-time curve for a power law fluid. From this equation the following achieved:

$$\log(1-e) = -\left(\frac{2n}{3n+5}\right) \times \log\left\{ 1 + \left(\frac{3n+5}{2n}\right) h_o^{(n+1)/n} kt \right\}$$ (20)

For $1 << \left(\frac{3n+5}{2n}\right) h_o^{(n+1)/n} kt$, i.e. at steady state deformation; after appreciable deformation-long times, the equation 3-32 in the text is given:

$$\log(1-e) = -\left(\frac{2n}{3n+5}\right) \log t - \left(\frac{2n}{3n+5}\right) \log\left(\frac{3n+5}{2n} h_o^{(n+1)/n} k\right)$$ (21)

The shear rate, $\overset{o}{\gamma}$, at any point (r,z) within the fluid is given by [109] :

$$\overset{o}{\gamma} = -\frac{\partial v_r}{\partial z} = -\frac{2(dh/dt)}{h^2}\left(\frac{2n+1}{2n}\right)\left(\frac{z}{h/2}\right)^{1/n} r$$ (22)

For $n=1$, this reduces to the following:

$$\overset{o}{\gamma} = -\frac{6rz}{h^3}\frac{dh}{dt}$$ (23)

The average shear rate, $\overset{o}{\gamma_{av}}$, obtained by integrating throughout the volume is:

$$\overset{0}{\gamma}_{av} = \frac{2\pi}{V} \int_{0}^{R} \int_{0}^{h/2} \overset{0}{\gamma} \, r \, dr \, dz \tag{24}$$

Combining equations 23 and 24 yields:

$$\overset{0}{\gamma}_{av} = -\frac{R}{2h^2} \frac{dh}{dt} \tag{25}$$

Rewriting equation 25, using $V = \pi R^2 h$ gives the average shear rate quoted in the text, equation 3-29.

$$\overset{o}{\gamma}_{av} = -\sqrt{\frac{V}{\pi}} (\frac{dh/dt}{2h^{2.5}}) \tag{26}$$